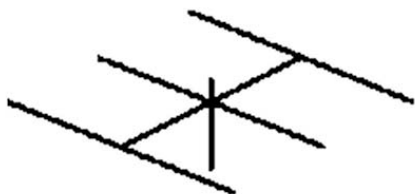
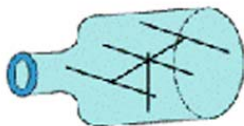


# Antenna Modeling Notes



Volume 6



L. B. Cebik, W4RNL

---

# **Antenna Modeling Notes**

**Volume 6**

**L. B. Cebik, W4RNL**

---

---

***Published by  
antenneX Online Magazine***

**<http://www.antennex.com/>**

**POB 271229**

**Corpus Christi, Texas 78427-1229 USA**

---

---

Copyright 2010 by ***antenneX Online Magazine***. All rights reserved. No part of this book may be reproduced or transmitted in any form, by any means (electronic, photocopying, recording, or otherwise) without the prior written permission of the publisher.

ISBN: 1-877992-57-7

---

## Table of Contents

Preface-----	5
Chapter 118: Modeling Odd Structures: the Gamma Match I-----	7
Chapter 119: Modeling Odd Structures: the Gamma Match II-----	24
Chapter 120: Back on the Ground-----	43
Chapter 121: Radiation Patterns and Propagation-----	60
Chapter 122: Reciprocity: Home on the Range-----	80
Chapter 123: Radiating and Transmission-Line Currents-----	109
Chapter 124: Modeling (with) Parabolic Reflectors-----	135
Chapter 125: When to Worry and When to Not: a Case Study-----	155
Chapter 126: "Ideal" Polar Plots-----	171
Chapter 127: A Potpourri of Modeler Miscellanea-----	193
Chapter 128: When Not to Use NEC for Antenna Modeling-----	216
Chapter 129: Some Rudiments of Receiving Pattern Modeling-----	234
Chapter 130: Models vs. Prototypes-----	256
Chapter 131: AM BC Modeling with NEC I-----	278
Chapter 132: AM BC Modeling with NEC II-----	298
Other Publications-----	323

## Preface

This collection of antenna modeling notes continues the compilation of the series that I began in 1998 in *antenneX*. This Volume 6 contains numbers 118 through 132 of the long-running series that continues even today. The time came to collect these columns into a more convenient form for the reader. There is just too much material for a single volume, so the collection is broken into numerous units. I have reviewed the text and graphics for each column to ensure as much accuracy as I can muster. I have also reviewed the sample models used in each column. That process permitted me to add something to these volumes that is not available in *antenneX* or at my own web site. Some models require elements of the command set not included in entry-level programs such as EZNEC. Others require NEC-4

At the time of writing some of the columns, reference was made to the use of NEC-Win Plus for some of the models presented. However, since then, software maker Nittany-Scientific appears to have drifted into a state of instability and with an unknown future. The reader should not rely on the use of that software referred to herein. The software was written for MS Win95, but appeared to work okay through MS Win2k. MS operating systems later than Win2k are known to have issues with NSI software. It is not compatible with VISTA at all as of this writing and has not been tested with the recent Windows 7.

Along the way, we shall explore some basic NEC calculations, including electric fields at a distance. We shall also learn how to supplement NEC calculations by using its output data to arrive at circular gain. Finally, we shall explore the relationship between the EX command and the PT command for special receiving-mode models. The NEC-2 and NEC-4 manuals provide fundamental collections of sample models designed to illustrate in the most compact way possible as many NEC features as possible. These models appear only in print form. In this volume, we shall examine the models, and the model collection will include them in .NEC format.

The adequacy of our models is, as it should be, a continuing challenge. Therefore, we shall revisit the convergence test with particular reference to its use with NEC. In addition, we shall take a look at some of the correctives that we use to work around some of the core's limitations. However, finding limitations and faults is not our goal. Rather, the goal is to make effective use of the program. Toward that end, we shall look at a techniques that will let us in NEC-2 handle insulated wires in a way that is comparable to the IS command in NEC-4. We shall also examine the various ground calculation systems that appear in NEC (and MININEC) software.

Although the list of topics seems to grow more advanced and complete, the appearance is an illusion. The command set is far too large for full coverage even in 4 volumes. As well, good antenna simulations depend as much on the ingenuity of modelers as they do on simply knowing how to apply various commands. Hence, the list of techniques by which to improve our models may well be endless. Mastering antenna modeling software has a further benefit: the use of the software to educate ourselves on the capabilities of various types of antennas. If we add this dimension of the use of NEC and MININEC to further mastery of the command structures and additional modeling techniques, then we may fairly predict that the series is far from its final episode.

***ED: L.B. Passed away in April 2008, but is immortalized in his writings.***

## Chapter 118: Modeling Odd Structures: the Gamma Match

### Part 1. Gamma Modeling Basics

**N**ewer modelers often carry into the enterprise a number of presumptions about antenna structures or geometries. One of them is that small appurtenances on an antenna generally make no difference and thus we may ignore them, thus simplifying the model. In many cases, the presumption works, but sometimes it does not.

The presumption toward simplification combines with an urge that the newer modeler should try to overcome. The urge is to create a single model for a given antenna. After all, we have only one subject antenna, and a single model should correspond to it. Along that road the modeler will eventually discover that he or she is blocking a host of information that might be acquired about the antenna's performance.

In this episode, we shall explore what we can learn both by overcoming the presumption underlying simplification of models and by setting aside the urge to encapsulate everything in a single model. Our example will be the gamma-match assembly used by so many Yagi beams. However, the general ideas surrounding our exploration will have applications elsewhere. It may seem at times that we are discussing gamma matches, but our real subject matter is careful modeling.

## Why the Gamma Match Is So Hard to Model

Let's suppose that a particular Yagi design uses a gamma match. We often encounter such assemblies when the manufacturer chooses to connect the antenna elements directly to the conductive boom. **Fig. 1** shows one such assembly.



The assembly has several features that automatically make it difficult to model. First, the connector plate and the shorting bar are

not round wires. Second, the series capacitor takes the form of concentric tubes with a dielectric lining between them. Third, the gamma rod may extend beyond the shorting bar, although that extension is minimal in the photo. Fourth, the gamma rod is very often not the same diameter as the element. **Fig. 2** summarizes in outline form the differences between the physical gamma match assembly and the model that we are likely to make.

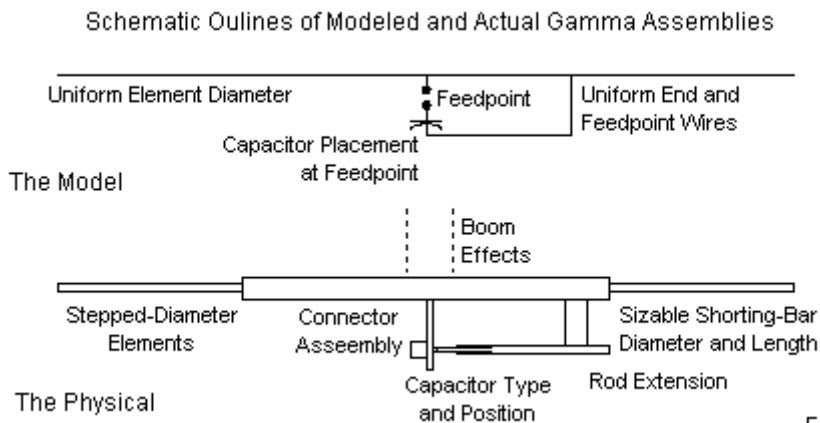


Fig. 2

If we choose to model the gamma match, we are likely to add the minimal number of wires needed to do the job. As well, we are likely to place the series capacitor at the feedpoint to simplify the compensation for the usual inductive reactance at the feedpoint.

These two measures assume that we are inclined to model the gamma match at all. Some modelers shrug off the match as being

"simply a match," akin to beta and series matching systems, and they model the antenna without the match in place. Of course, beta matches and series matching systems add transmission lines or lumped components at the feedpoint and do not change the fundamental driven-element geometry. In contrast, the gamma match adds wires in the feedpoint region and thereby changes the geometry of the element. Short of extensive field-testing, we cannot know in the absence of an adequate model whether the driven element changes result in any pattern changes for the beam relative to the patterns without the match. Therefore, let's assume that modeling a gamma match is a worthy task, even if it creates a more complex model.

We can only model a gamma match if the modeling software is capable of handling the task. NEC (both -2 and -4) faces some major challenges in this regard. If the gamma rod is not the same diameter as the main element, then we shall have from 2 to 4 angular junctions of wires with dissimilar diameters, depending on the diameter that we assign to the gamma connector plate and the shorting bar. In addition, NEC shows limitations when we bring into close proximity parallel wires of different diameters, even if we carefully align the segment junctions. In garden-variety cases, NEC will show average gain test (AGT) scores in the region 0.9 when 1.000 is the ideal. Hence, we may expect gain errors greater than 0.4 dB and impedance errors about 10% off the mark. For these reasons, many NEC modelers give up altogether trying to model gamma matches.

Raw MININEC 3.13 has equal or greater difficulties. First, the core shows considerable error at corners unless we use a very high number of segments. Second, the uncorrected core has difficulties with closely spaced wires. Third, the core exhibits a frequency drift that leads to various degrees of inaccuracy as we raise the modeling frequency higher. One problem that MININEC does not have is handling junctions of wires with dissimilar diameters. However, if we compare the gamma structure to the listed problems, we might also disqualify MININEC as an appropriate modeling core. Seemingly we are left with nothing to use--at least within an economic price range.

However, the development of MININEC has seen numerous correctives that largely overcome the flaws in the raw core. Perhaps the most refined version is part of the Antenna Model package, with correctives for corners, frequency, and closely spaced wires. In addition, Antenna Model has added the AGT test to the user-accessible outputs for running model assessments. Therefore, if we are willing to take the time to model a gamma match assembly, we may be able to learn something.

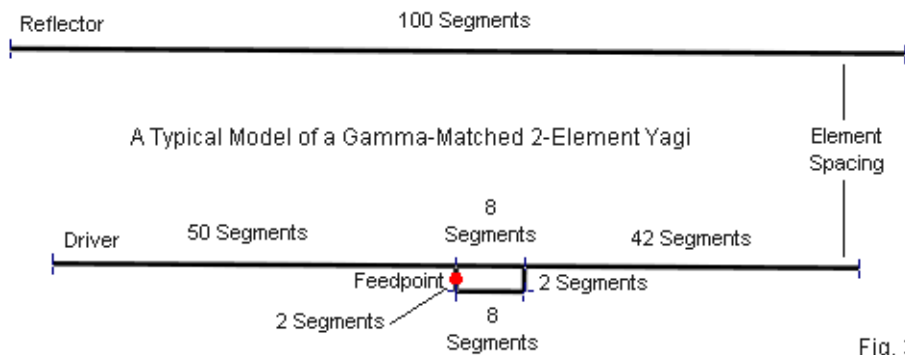
## Basic Modeling Requirements

Let's begin with a 2-element 28-MHz beam for which we might use a gamma match. We shall specify the use of 0.5"-diameter elements. The driver will be 190.7" long, while the reflector will be 211.9" long. The spacing will be about 0.12-wavelength or 50.58". Without a gamma match, Antenna Model reports the feedpoint

impedance as 29.84-j25.73 Ohms. The AGT score is 0.9997, which is exceedingly close to ideal.

One limitation that is inherent to both NEC and MININEC is that neither core will reveal boom effects in the event that we wish to connect the element directly to the boom. However, that fact does not prevent us from using a gamma match; it only means that the results will not precisely reflect a real situation.

We provided a modeling report, but omitted one critical fact: the level or density of segmentation. For the pre-gamma model, the level makes no difference, and we might use any value from about 10 segments per element upward. However, the segmentation density will make a considerable difference when we create the gamma model. Therefore, we use 100 segments per element for both the pre-gamma and the gamma model. **Fig. 3** helps us explain why.



At 28 MHz, each segment will be about 2" long. With the 0.5"-diameter elements, this segment length allows a 4:1 segment-length-to-diameter ratio, well above the limits for either NEC or MININEC. Next we shall construct a gamma match, as shown on the driver element in the outline. The main-element-to-gamma-rod spacing is 4" center-to-center. Note that we need to place the feedpoint or source at the connecting wire center, that is, on a pulse or segment junction. A 2-segment wire gives us the source position that we need and also allows for segments that are roughly equal in length with the segments on the other parts of the overall driver assembly.

Note that the driver element itself now consists of 3 wires. The non-gamma side has 50 segments. We divide the gamma side into two parts such that the gamma section has N segments, and the remainder has 50-N segments. N is based on the length that we eventually assign to the gamma rod. Given the driver length, the final gamma rod requires 9.7 segments. Since we can only assign segments in integers, we give both the short main element section and the gamma rod 10 segments each, with the remainder of the main element receiving 40 segments. **Fig. 4** provides a look at the Antenna Model Wire table that describes the geometry that we have just created.

Fig. 4		End 1			End 2			Wire Properties			
Wire	Segments	X	Y	Z	X	Y	Z	Diameter	Material	Conductivity	Permeability
1	50	0.0000000	-95.35020	0.0000000	0.0000000	0.0000000	0.0000000	0.5000000	Perfect	(Infinite)	1.000000
2	10	0.0000000	0.0000000	0.0000000	0.0000000	18.47000	0.0000000	0.5000000	Perfect	(Infinite)	1.000000
3	40	0.0000000	18.47000	0.0000000	0.0000000	95.35020	0.0000000	0.5000000	Perfect	(Infinite)	1.000000
4	2	0.0000000	0.0000000	0.0000000	4.000000	0.0000000	0.0000000	0.5000000	Perfect	(Infinite)	1.000000
5	10	4.000000	0.0000000	0.0000000	4.000000	18.47000	0.0000000	0.3750000	Perfect	(Infinite)	1.000000
6	2	4.000000	18.47000	0.0000000	0.0000000	18.47000	0.0000000	0.5000000	Perfect	(Infinite)	1.000000
7	100	-50.58370	-105.9310	0.0000000	-50.58370	105.9310	0.0000000	0.5000000	Perfect	(Infinite)	1.000000

Several additional facts present themselves in the table. Foremost is the fact that our model uses a 0.375" diameter gamma rod. However, the 2-segment connecting wires use that same diameter as the main element. Although this initial strategy reflects the relatively "beefy" structure that we saw in **Fig. 1**, it does leave us with a future question about the affect of connecting wire diameter on gamma performance. In addition, the model has no gamma rod extension beyond the limit of the far-end connecting wire. Hence, we acquire a second question for future exploration. The wire table itself does not show the position of the source, which is at the center of the connecting wire at the element center. The series capacitor in the form of a load is also missing from this table. As a starting point, we place it at the same pulse as the source.

With a gamma rod that is 18.47" long and a series capacitance of 38.32 pF, we obtain a gamma-match feedpoint impedance of  $50.04 + j0.07$  Ohms. You may use any set of limits that you desire in setting the gamma assembly. Since I do a good bit of systematic modeling, I used very tight tolerances: 0.1 Ohm for either resistance or reactance relative to the 50-Ohm target value. The AGT score for this model is 1.0005, once more very close to ideal.

With so many open questions, we cannot claim that this model is yet a good building guide. However, it does provide us with an internally consistent and adequate model of a gamma match for an element that is electrically independent of any supporting boom. Thus, we have a starting point for further exploration.

## The NEC Question

We may construct the same model of a gamma-matched beam using NEC. I shall use NEC-4 (single-precision), as provided in the EZNEC Pro/4 package for the exercise. **Fig. 5** shows the EZNEC wire table for ready comparison with the corresponding Antenna Model table in **Fig. 4**.

No.	End 1				End 2				Diameter (in)	Segs
	X (in)	Y (in)	Z (in)	Conn	X (in)	Y (in)	Z (in)	Conn		
1	0	-95.3502	0		0	0	0	w2E1	0.5	50
2	0	0	0	w4E1	0	18.47	0	w3E1	0.5	10
3	0	18.47	0	w5E2	0	95.3502	0		0.5	40
4	0	0	0	w1E2	4	0	0	w6E1	0.5	3
5	4	18.47	0	w6E2	0	18.47	0	w2E2	0.5	3
6	4	0	0	w4E2	4	18.47	0	w5E1	0.375	10
7	-50.5837	-105.931	0		-50.5837	105.931	0		0.5	100

For most linear elements with a center feedpoint we must use an odd number of segments in at least the driven element. However, the gamma match element is not on the main element, but on the connecting wire. Hence, we can replicate the MININEC segmentation--with one exception. Centered NEC sources require an odd number of segments. Therefore, I increased the segments in the connecting wires to 3. Having shorter segments in the connecting wires is the better option, since it allows the source to have a segment on either side of the source segment that is the

same length as the source segment. NEC tends to be most accurate under this condition.

If we use the same 18.47" gamma rod that we used in the earlier model, but change the series capacitor to 37.15 pF, we obtain a feedpoint impedance of 55.30-j0.06 Ohms. The NEC result is 5 Ohms off the target 50-Ohm value. If we check the AGT score for the model, NEC-4 returns a value of 0.902, a considerable distance from the ideal value. We would expect the forward gain of the antenna to be about 6.25 dBi, but the NEC report is a gain value of 5.80 dBi. NEC appears to be considerably off the mark with such numbers.

In order to obtain a 50-Ohm feedpoint impedance within the prescribed limits for this exercise, we must change the modeled gamma rod length and the value of series capacitance. If we reduce the gamma rod length to 17.56" and use a 39.36-pF capacitance value, we can obtain 50.07-j0.01 Ohms. However, the trustworthiness of this report is cast in doubt by the 0.904 AGT score for the revised model. As well, we can find some further fluctuations that are interesting. For example, changing the ratio of gamma segments to remainder segments between 9-41 and 10-40 yields a 0.3" change in the required gamma-rod length--not much but noticeable. As well, single-precision and double-precision versions of NEC-4 yield slightly different values, a very unusual situation in more adequate (higher-AGT-score) models.

All is not necessarily lost in terms of using NEC as a preliminary guide to gamma matching. The AGT scores can help us provide

some correctives to the data. For example, we may translate a basic AGT score into a value in dB by taking 10 times the log of the AGT score. For the 0.902 value, we obtain  $-0.45$  dB. If we add this value to the gain report (5.80 dBi), we obtain the pre-gamma-match beam gain of 6.25 dBi, which coincides with the Antenna Model reports for both the pre-gamma and the gamma models.

For a normal feedpoint that is close to resonant, we may generally correct the reported feedpoint impedance by multiply the basic AGT value times the report of the resistive component.  $55.30 * 0.902 = 49.88$  Ohms, very close to our target value. Therefore, we can employ the following strategy to model a gamma match. First, develop an approximate model using the required wire diameters. Actually, the only approximation will be the gamma-rod length. Obtain an AGT score. Divide the target impedance (in these examples, 50 Ohms) by the AGT to obtain a new target value. Redesign the gamma assembly to obtain the revised target impedance.

Alternatively, you may design the gamma match for 50 Ohms. Divide the modeled gamma rod length by the square root of the AGT to obtain the actual value. The revised model had an AGT score of 0.904 and produced a 50-Ohm impedance with a gamma-rod length of 17.56". Applying this technique yields a revised gamma-rod length of 18.49", very close to the value produced by the Antenna Model version of the assembly.

Both techniques are approximate and may vary as we change the precise ratio of gamma-rod segments to remainder segments. As

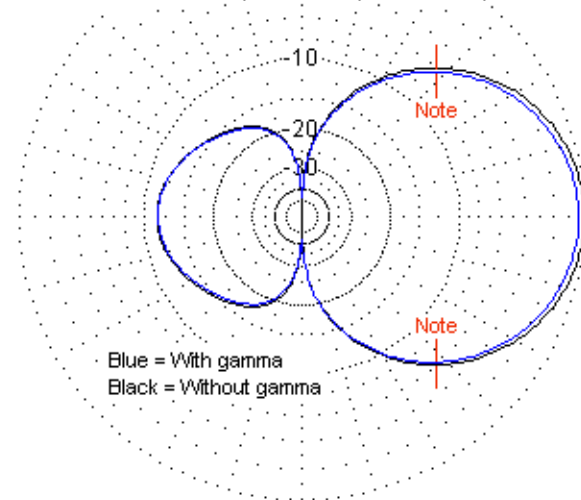
well, the series capacitance will likely hold only within about +/-1pF. Nevertheless, they may prove useful if one only has a NEC program with which to work.

## Some Additional Questions and Additional Modeling

For any gamma-matched beam, whatever the size, learning to construct such structures can be useful in more ways than just trying to model the gamma assembly itself. For example, the modeling technique is useful in seeing whether the assembly yields a significant distortion to the normal beam pattern. The gamma matches constructed for the sample models extend forward of the main element by the 4" spacing value that we selected. We may ask whether the gamma assembly in any way disturbs the pattern that we might obtain from the antenna without the gamma match in place.

By means that may vary with the specific software that we use, we can compare the patterns of a pre-gamma and a gamma-matched model (understanding that the comparison will not account for any boom effects). For the sample models that we have used so far, **Fig. 6** provides two sorts of comparison. For this exercise, I selected the EZNEC models precisely because the gamma-model shows a reduced gain. As a consequence, the forward lobes of the two beam patterns are fairly distinct. (A moderately poor AGT score ordinarily does not disrupt a radiation pattern shape.)

Overlaid Free-Space Patterns  
 28-MHz 2-Element Yagi . . . 0 dB  
 Without and With  
 Gamma Match



Blue = With gamma  
 Black = Without gamma

Note = Asymmetries or  
 Differences

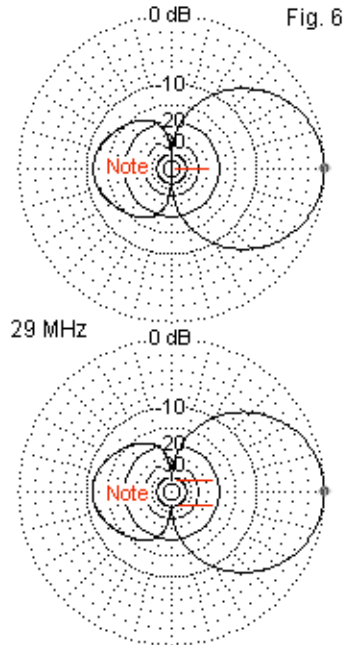


Fig. 6

The overlaid patterns show the degree to which the gamma assembly tilts the radiation pattern in the X-Y plane (ordinarily the azimuth plane). The amount is detectable, but minuscule, far below the level that we could notice in operation and likely below the level that we could measure. The smaller patterns to the right compare the degree to which the gamma match assembly might disturb the side nulls. For a match-less beam, the nulls exceed NEC's ability to record them in a finite number of digits. However, the side nulls in the gamma model have a limited depth--perhaps -40 dB relative to

forward gain of the array. Although numerically detectable, the difference between -40-dB nulls and indefinitely large nulls is completely insignificant.

On the basis of a single 2-element Yagi design that does not show boom effects, we cannot reach the conclusion that gamma matches do not distort beam patterns. The point of the example is not the conclusion, but the use of modeling to reach a preliminary conclusion on a case-by-case basis relative to an antenna design under analysis.

In addition to examining the question of pattern distortion, we can also and easily perform some systematic modeling to answer "what-if" questions. Perhaps the first question is what happens when we change the diameter of the gamma rod. We may keep all of the model parameters as we began, using the same pre-gamma model. We shall also retain the connecting wires at the 0.5" main-element diameter and revise only the diameter of the gamma rod. In fact, for simplicity in this exercise, we shall keep the same ratio of segments on the gamma side: 10 segments for the gamma length and 40 for the remainder of the half elements. For each new gamma rod diameter, we shall record the gamma rod length and the series capacitance required to bring the feedpoint impedance to 50 Ohms within the tolerances that we previously used. The results will resemble those in **Table 1**.

Test Series at 28 MHz: Changing Gamma Rod				
		Diameter for a 50-Ohm Match		
Dimensions		Dr. Len	Ref Len	EI Space
Non-Resonant		190.7	211.9	50.58
		EI Dia	Pre-R	Pre-jX
		0.5	29.84	-25.73
Gamma Match		Modeled Values		
Spacing	Rod Dia	Length	Cap pF	AGT
4	0.125	18.60	33.80	0.9999
	0.25	18.53	36.50	1.0002
	0.375	18.47	38.32	1.0005
	0.5	18.41	39.70	1.0010
	0.625	18.35	40.85	1.0015
Change		-0.25	7.05	
All Dimensions in Inches				Table 1

Those who are familiar with some of the algebraic methods of calculating gamma matches may be surprised by the very small change in the length of the gamma rod as we vary the rod diameter over a 5:1 range. The difference is a mere 0.25". The change in the required capacitance is larger (about 7 pF), but still small.

The exact numbers in the table are less important than what they can tell us about the probable behavior of a gamma match. The models suggest that a gamma match is not especially sensitive to changes in the gamma rod diameter. We may easily perform a similar systematic investigation beginning with any main element diameter and any value for the spacing between the gamma rod and the main element. Therefore, we need not treat the results of this test as generally true. Instead, we can perform the requisite

test for ourselves using the materials and test frequency for virtually any beam.

## Unfinished Business

In the course of our exploration of the basic modeling techniques needed for the gamma match as an example of an "odd structure," we did not strive to develop a gamma match that we can build. Instead, we strove to assemble a model that we can rely upon, at least internally to the modeling enterprise. Unfortunately, all forms of gamma-match calculation have undergone only spot checks. Hence, we cannot determine which of the numerous systems of gamma design is the most accurate to physical reality. Nevertheless, we can examine the trends suggested by the models in anticipation of actual building experiences.

We did encounter a number of questions left unanswered by our initial attempts to formulate and analyze gamma-match models. For example, we may wish to know the consequences of varying the spacing between the main element and the gamma rod. We may wish to understand the effects of leaving a gamma rod extension beyond the shorting bar. Do variations in the connecting-wire diameters have significant effects on the gamma-rod length or the series capacitance? Finally, what are the consequences of moving the series capacitor position from its ideal modeling position?

Therefore, we may usefully spend another episode on this topic. Our goal will not be to come up with definitive answers. Instead, we

shall examine the nature of the models that can provide those answers, at least within the limits of the modeling enterprise.

## Chapter 119: Modeling Odd Structures: the Gamma Match Part 2. Gamma Assembly Variables

In the preceding episode, we began an exploration of modeling "odd" structures that we find within the geometry of some antennas, using the gamma match as a good example. The gamma match has both basic and additional properties that are worth modeling in order to discover what effect a number of structural variables may have on the performance of the antenna. Because the gamma match assembly is primarily an impedance transformer, we have been less interested in such antenna performance properties as forward gain and front-to-back ratio than we have in the structure necessary to arrive at a desired feedpoint impedance.

We began with a "pre-gamma" model to arrive at the antenna source impedance prior to adding the gamma-match structure. Our basic subject model used a test frequency of 28 MHz with 0.5" elements in a 2-element driver-reflector Yagi configuration. The driver was 190.7" long, while the reflector was 211.9" long. The spacing was about 0.12-wavelength or 50.58". Without a gamma match, Antenna Model reports the feedpoint impedance as 29.84-j25.73 Ohms. The AGT score for the basic or pre-gamma model was 0.9997, where the ideal value is 1.0000.

Our decision to use Antenna Model software, a highly corrected version of MININEC 3.13, rested on its ability to handle--so far as tests internal to modeling can tell--accurate models of elements within a gamma-match assembly. NEC is subject to systematic

errors that make its use difficult and potentially questionable. Less corrected versions of MININEC may yield equally erroneous results. Although Antenna Model may produce the most trustworthy models within the collection of extant wire antenna simulation programs, we must remember that our exercises lack one important step: the calibration of the simulation results with physical antennas. However, our goal in tracking these exercises has not been to yield a building guide. Rather, we have been concerned to explore what counts as good modeling practice for structures as "odd" as the gamma-match assembly.

Our initial gamma-match model employed a basic structure consisting of several new wires and some modifications to the main driver element. As shown in the upper portion of **Fig. 1**, the main element now has 3 sections. We selected 100 segments as the total of the segments on all three element sections, with 50 assigned to the non-gamma side of the element. The ratio of segments on the gamma side, divided between the gamma assembly section and the remainder of the element, rests on equalizing to the degree possible the lengths of segments along the element. We assigned 2 segments to the source wire and to the shorting bar wire both to equalize segment lengths throughout the model and to place the source at the center of its wire. The latter consideration rests on the need to place MININEC sources (and loads) on a pulse or segment junction. Our initial spacing between the main element and the gamma bar was 4", yielding 2" segments that roughly correspond to the length of segments in the main element.

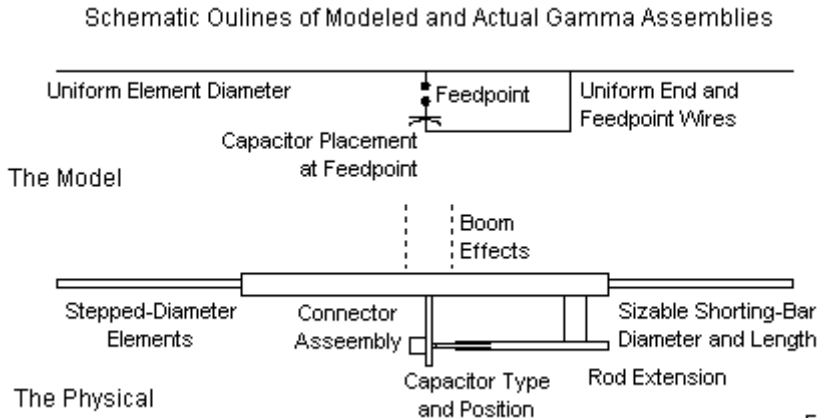


Fig. 1

The goal of the modeling was to produce a model that gave us a 50-Ohm feedpoint impedance, the value that corresponds to general amateur practice for the use of main feedlines. For the exercise, we arbitrarily set a close tolerance limit of 0.1 Ohm in the resistive and the reactive components. For many purposes, this limit is too fine, although it is useful for some systematic modeling exercises. We also began with a gamma-rod diameter of 0.375", although we left the end wires at the same 0.5"-diameter as the main wire. With a gamma rod that is 18.47" long and a series capacitance of 38.32 pF, we obtained a gamma-match feedpoint impedance of 50.04+j0.07 Ohms.

The lower portion of **Fig. 1** shows us a number of ways in which an actual gamma match may differ from the idealized model that we have been using. The variations fall into two general categories that

we might call simple and complex variations. Simple variations involve selected modifications of single changes to one of the initial dimensions of the ideal gamma-match model. For example, before we closed the preceding episode, we explored the effects of changing the diameter of only the gamma rod, Wire 5 on the basic model wire table. **Fig. 2** replicates that table from Antenna Model so that we may identify both the change that we have so far made and changes yet to come.

Fig. 2		End 1			End 2			Wire Properties			
Wire	Segments	X	Y	Z	X	Y	Z	Diameter	Material	Conductivity	Permeability
1	50	0.0000000	-95.35020	0.0000000	0.0000000	0.0000000	0.0000000	0.5000000	Perfect	(Infinite)	1.000000
2	10	0.0000000	0.0000000	0.0000000	0.0000000	18.47000	0.0000000	0.5000000	Perfect	(Infinite)	1.000000
3	40	0.0000000	18.47000	0.0000000	0.0000000	95.35020	0.0000000	0.5000000	Perfect	(Infinite)	1.000000
4	2	0.0000000	0.0000000	0.0000000	4.000000	0.0000000	0.0000000	0.5000000	Perfect	(Infinite)	1.000000
5	10	4.000000	0.0000000	0.0000000	4.000000	18.47000	0.0000000	0.3750000 *	Perfect	(Infinite)	1.000000
6	2	4.000000	18.47000	0.0000000	0.0000000	18.47000	0.0000000	0.5000000	Perfect	(Infinite)	1.000000
7	100	-50.58370	-105.9310	0.0000000	-50.58370	105.9310	0.0000000	0.5000000	Perfect	(Infinite)	1.000000

The starred entry shows the entry with which we were concerned in our first foray into systematic modeling with the gamma-match assembly. As we changed the gamma rod diameter from 0.125" to 0.625" in 0.125" increments, we adjusted the gamma-rod length to arrive at a 50-Ohm impedance. This process involved changes to the wire-table entry wherever the initial wire-table shows 18.47. Because the source and the series capacitance load are on the same pulse, we could independently arrive at the desired source resistance and then modify the load capacitance value to remove any remnant reactance. **Table 1** shows the results of our efforts.

Test Series at 28 MHz: Changing Gamma Rod				
Diameter for a 50-Ohm Match				
Dimensions		Dr. Len	Ref Len	EI Space
Non-Resonant		190.7	211.9	50.58
		EI Dia	Pre-R	Pre-jX
		0.5	29.84	-25.73
Gamma Match		Modeled Values		
Spacing	Rod Dia	Length	Cap pF	AGT
4	0.125	18.60	33.80	0.9999
	0.25	18.53	36.50	1.0002
	0.375	18.47	38.32	1.0005
	0.5	18.41	39.70	1.0010
	0.625	18.35	40.85	1.0015
Change		-0.25	7.05	
All Dimensions in Inches				Table 1

During our model modifications, we kept a close eye on the amount by which the gamma rod length changed in order to assure ourselves that the segment lengths on the main element remained stable. In this case, the total length change from the thinnest to the thickest gamma rod was about 0.25", so we could maintain the 10:40 segment division on the gamma side of the element. Of course, the gamma rod and the gamma section of the main element will have the same number of segments, and the two values on the gamma side of the element will add up to 50.

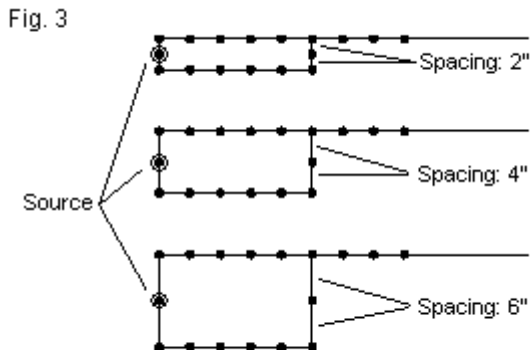
The initial exercise left us with a number of unanswered questions that we might pose to the model, based on normal gamma construction methods and on the lower portion of **Fig. 1.** For example, we may wish to know the consequences of varying the spacing between the main element and the gamma rod. We may

wish to understand the effects of leaving a gamma rod extension beyond the shorting bar. Do variations in the connecting-wire diameters have significant effects on the gamma-rod length or the series capacitance? Finally, what are the consequences of moving the series capacitor position from its ideal modeling position? Some of these questions involve equally simple modifications to our initial gamma match model, while others may involve more complex modifications.

### The Gamma Spacing Question and Its Models

The systematic testing of various gamma-rod diameters is only one of many such tests that we may perform to obtain a general idea of the properties of a gamma-match assembly. We may perform a similar test of gamma-rod-to-main-element spacing. Our basic model used a 4" center-to-center spacing between the rod and the element. We might wish to know something about what happens with narrower and wider spacing values.

As a sample, we might specify alternative spacing values--perhaps 2" and 6"--in order to bracket our initial design. We shall retain the 0.5" main element and the original 0.375" rod diameters. **Fig. 3** shows preliminary outlines of the three modeling situations and alerts us to some modeling cautions.



The Effects of Changing Element-to-Rod Spacing

The first caution concerns the change in the segment length for the connecting wires. A 2" spacing value will reduce the segment length to 1", while the 6" spacing value will increase the segment length to 3". Because we wish to keep the source centered in its connecting wire, we have no practical way to obtain exact 2" segment lengths. Therefore, we shall have to pay closer attention to the AGT scores for each model to assure ourselves that the results are reasonably reliable. The initial model with a 4" spacing value achieved a score of 1.0005, very close to ideal. We shall be interested in the scores for the alternative spacing values.

The second caution concerns the segment length within the gamma rod. Casual modelers likely would simply try the new spacing and then adjust the gamma rod length (and the series capacitance), forgetting to be certain that the segment lengths throughout the entire driver element are as equal as feasible. However, we have

already noted that unequal segment lengths among the sections of the driver may result in deviant source impedance reports. Hence, we shall reset the relative segmentation between the gamma section and the remainder in order to achieve the most ideal AGT score possible by obtaining the most equal segment lengths feasible.

If we attend to these cautions, then we might obtain results such as those in **Table 2**.

Test Series at 28 MHz: Changing Gamma Rod					
		Spacing for a 50-Ohm Match			
Dimensions		Dr. Len	Ref Len	EI Space	
Non-Resonant		190.7	211.9	50.58	
		EI Dia	Pre-R	Pre-jX	
		0.5	29.84	-25.73	
Gamma Match		Modeled Values			
Spacing	Rod Dia	Length	Cap pF	AGT	Segment
2	0.375	23.87	40.60	0.9966	12:38
4		18.47	38.32	1.0005	10:40
6		16.27	36.30	0.9971	8:42
Change		7.60	4.30		
All Dimensions in Inches					Table 2

The table suggests a number of modeled gamma-assembly properties. First, despite the changes that we made in the relative segmentation, the models for the alternative spacing values are farther from the ideal score than the original model. Nevertheless, the probable accuracy of our 50-Ohm source impedance is within 1%. Therefore, the general trends shown by the length and

capacitance numbers are reasonably reliable. Second, the gamma-rod length grows shorter as we increase rod spacing. Although not precise, the trend suggests that length changes linearly as the ratio of one spacing value to the next. Third, the required series capacitance decreases with increased spacing, although the amount is small and likely within the adjustment range of any type of capacitor used for this function.

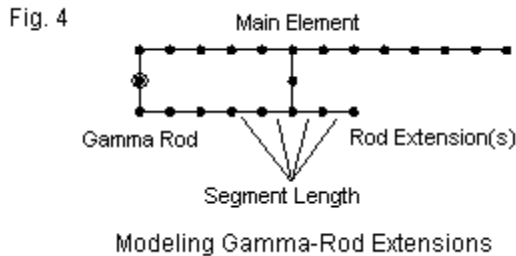
Note that these trends apply so far only to the particular initial feedpoint impedance of the pre-gamma model. For a truly systematic exploration of gamma behavior, we might wish to construct alternative models using a variety of pre-gamma feedpoint impedances. These impedances should not only include several resistance values, but as well a number of reactance values. From such a systematic survey, we might glean a wider view of gamma assembly trends and develop some rational expectations of gamma-assembly behavior at interpolated values for gamma spacing and rod diameter.

## Other Model Variations

Let's return to our basic gamma model with the 0.5" and 0.375" diameter assembly elements. **Fig. 2** showed us two conditions that might or might not have a significant impact on the assembly final dimensions. One factor is the extension of the gamma rod beyond the shorting bar. The second is the diameter that we assign to the two connecting wires to simulate the plates and bars that we might use to connect the gamma rod to the main element at each end. To

ensure that we do not confuse potential effects, we should treat each case separately.

Let's first add extensions to the gamma rod to simulate what might happen if the shorting bar does not come close to the end of the rod that we construct. The rod extensions will use the same 0.375" diameter as the main section of the rod. The extension lengths will consist of a new wire that we add to the model. The wire joins the junction of the shorting bar and the main section of the rod and runs parallel to the main element. **Fig. 4** shows the outline of the construct, and points to a caution that we should observe.



We have striven to equalize to the degree possible the lengths of all segments in the model. The average segment length is close to 2". Therefore, we should add gamma rod extensions in 2" increments, using 1 segment per each 2" of extension. Within these restrictions, we might usefully test 2", 4", and 6" extensions.

For this test, we might bypass the earlier procedure of carefully adjusting the rod length and the series capacitance until we see if

such a tedious procedure is necessary. Instead, let's retain the 18.47" rod length and the 38.32-pF series capacitance. What we shall observe is the effect of the extensions on the reported feedpoint impedance. The results appear in **Table 3**.

Test Series at 28 MHz: Adding a Gamma-Rod Extension					
Dimensions		Dr. Len	Ref Len	EI Space	
Non-Resonant		190.7	211.9	50.58	
		EI Dia	Pre-R	Pre-jX	
		0.5	29.84	-25.73	
Gamma Assembly		Rod Len	Cap pF		
		18.47	38.32		
Ext Len	0	2	4	6	
R	50.05	50.44	51.02	51.63	
X	0.07	0.06	0.05	0.01	
AGT	1.0005	1.0005	1.0005	1.0005	
All Dimensions in Inches					Table 3

We had set 0.1-Ohm limits on the initial search for the proper gamma rod and series capacitance for a 50-Ohm match. With no extensions, the source impedance values fall within the limits. As we add successively longer extensions, the reactance does not change in any way that drives it outside the initial limits. Hence, for any reasonable rod extension, the existence of that extension is not likely to require a series capacitor adjustment. The extensions do have a small affect on the source resistance. However, a full 6" extension displaces the match impedance by only about 1.6 Ohms. This change is likely to be well within the field adjustment variables. Hence, it appears not to be a significant factor. For the initial pre-

gamma beam, at least, one might cut off the extension or to leave it according to non-electronic reasons.

We should perform an additional test after returning the model to its initial gamma configuration. Let's explore what happens if we vary the 4" connecting wire diameters. We initially set them at 0.5", the same diameter as the main element. We might see what happens with connecting wires ranging from 0.125" to 1.0" in 0.125" increments. To simplify the exercise, we shall change both connecting wires at the same time.

Because we shall be creating some radical differences in the wire diameters at gamma-assembly junctions, we shall pay close attention to the AGT scores to ensure that we do not exceed program limits. Because we might have to adjust both the gamma length and the series capacitance to obtain source impedance values within our limits, we can expect this exercise to be somewhat tedious. However, this feature of systematic modeling is unavoidable. The results of our survey appear in **Table 4**.

Test Series at 28 MHz: Changing the Connecting-Wire Diameter						
		for a 50-Ohm Match				
Dimensions		Dr. Len	Ref Len	EI Space		
Non-Resonant		190.7	211.9	50.58		
Spacing	Rod Dia	EI Dia	Pre-R	Pre-jX		
4	0.375	0.5	29.84	-25.73		
C-W Dia	Rod Len	Cap pF	R	X	AGT	
0.125	18.53	36.35	49.99	-0.02	1.0004	
0.25	18.51	37.30	49.96	-0.07	1.0005	
0.375	18.49	37.90	49.97	0.02	1.0005	
0.5	18.47	38.32	50.05	0.07	1.0005	
0.625	18.43	38.65	50.05	-0.05	1.0006	
0.75	18.39	38.95	50.05	-0.05	1.0007	
0.875	18.34	39.25	50.01	0.02	1.0008	
1	18.29	39.50	49.99	0.02	1.0009	
Change	-0.24	3.15				
All Dimensions in Inches						
						Table 4

Note that this and all other tables try to include all of the information about the starting points. After several exercises in systematic modeling, scratch pads notes and incomplete table data can obscure the initial model to which the new table's information may apply. Not every modeling caution applies to something that we enter into the software program--some apply to our record keeping procedures.

The table shows that for the initial model, changing the size of the connecting wires by an 8:1 ratio creates only a quarter-inch change in the required gamma length. The required series capacitance changes by only about 3 pF. Some sources suggest that the connecting wire effects are much greater. However, for the present

initial gamma model, we do not find significant effects from connecting wires ranging from very thin to very thick, relative to the element and rod diameters. The consistency of the AGT scores suggests that nothing in the modeling itself artificially washes out the anticipated effects. Hence, we now have a real question that we might pose to reality: are the supposed effects as great as some sources assume?

## Series Capacitor Placement

The final part of our survey of gamma properties concerns the placement of the gamma capacitor. **Fig. 1** shows a concentric capacitor installed on the gamma line. The capacitance is distributed along the section of line in which the two tubes overlap (with a dielectric between them). Hence, we have two difficulties at first sight. One is the changing diameter of the gamma rod. However, as we saw in one of our earlier surveys, the likely increment of diameter change is unlikely to create any significant difference in performance.

The second potential problem concerns the capacitor position. At best, a model can only approximate the distributed capacitance. The version of MININEC in the Antenna Model implementation further limits the potential position of a gamma capacitor to the end of a wire or at its center--assuming that we have an even number of segments on the wire. **Fig. 5** shows the relevant positions. The numbered dots represent not only available positions, but also the most popular positions for series capacitors in actual gamma-match construction.

Fig. 5



Possible Modeled Capacitor Locations

Position 1, which we seldom find in practice, is the ideal position on the same pulse as the source. All of our previous models have used this capacitor position. Builders tend to favor position 2 when using a standard variable capacitor (which they sometimes replace after adjustment with a fixed capacitor having the closest value). Position 3 approximates the position of a concentric tubular capacitor. Although not precise, it is useful for tracking the trends in gamma dimensions as we move the capacitor from one position to the next.

Test Series at 28 MHz: Changing the Capacitor Position for a 50-Ohm Match							
Dimensions		Dr. Len	Ref Len	EI Space			
Non-Resonant		190.7	211.9	50.58			
Spacing	Rod Dia	EI Dia	Pre-R	Pre-jX			
4	0.375	0.5	29.84	-25.73			
Capacitor Position		Rod Len	Cap pF	R	X	AGT	
1. At the source		18.47	38.32	50.05	0.07	1.0005	
2. On rod corner		18.89	37.58	50.02	0.02	0.9995	
3. Rod mid-point		20.50	35.60	50.01	-0.05	0.9968	
Change		2.03	2.72				
for a 50-Ohm Match						Table 5	

**Table 5** tracks the effects of the change of capacitor position, using the ideal position as the starting point. The required capacitance goes down as we move the capacitor away from the source, but not by enough to exceed construction variables in most cases. The major change lies in the required gamma rod length to achieve a 50-Ohm resonant feedpoint. The simple 2" move to the corner (position 2) requires an additional half-inch of gamma rod. Moving the capacitor to midway along the gamma rod calls for a further 1.5" increase in rod length. The 2" total exceeds 10% of the originally modeled gamma rod length--a significant amount.

One further aspect of moving the series capacitor position does not show up in tabular results, but does appear as we work with the model trying to obtain the correct gamma rod length and the correct capacitor value. When the capacitor is on the same pulse as the source, the resistive and reactive components of the source impedance are independent. We adjust the rod length for an

acceptable resistive component. Then we adjust the capacitor value for an acceptable reactive component. However, when we move the capacitor away from the ideal position, we discover that the rod length and the capacitor value interact in the model. Changing the value of the capacitor at position 3 alters both the reactance and the resistance at the source. In many cases, the resistance may not change enough to require a change in rod length, but occasionally, we may need to adjust both components until we find the correct values to yield the desired feedpoint impedance. Indeed, under these conditions, model adjustment reflects what we encounter when making field adjustments on a gamma match.

## Conclusion

Although we may now conclude this exercise, we are far from concluding the modeling explorations that may go into understanding and designing a gamma match for a given antenna. Our model used a sample antenna that showed a moderate resistance and a considerable reactance at the source relative to the final gamma-match impedance. The trends that we observed apply to this situation. We have not explored other beam feedpoint impedance values, both resonant and non-resonant. We should not presume in advance of modeling that all trends applicable to our subject antenna would hold true of all antenna designs. Even if the trends are generally applicable, the rates of change may vary with the initial feedpoint values prior to adding the gamma assembly. Hence, other initial impedance values may show different levels of sensitivity to small changes than we found within the example.

For each test, we also froze all but one dimension in order to explore systematically a single variable. In many cases, you may need to perform multiple explorations in order to determine for a given test frequency, initial impedance, and main element diameter the most promising gamma rod diameter, capacitor position, and rod length. One additional situation that we have not examined at all is modeling for boom effects. One technique often used to simulate boom effects is to install at the element center a short wire having a large diameter. Such a wire often creates a large difference in diameter within the main element in the gamma area, thus changing the surface-to-surface spacing between the main element and the gamma rod along the rod's length. As well, the short fat wire that compensates for the NEC and MININEC inability to handle transverse boom currents may also make it more difficult to maintain element length equality along the main element. Indeed, the diameter values often used for such exercises may exceed the segment-length limits that we imposed on our models to obtain adequate segmentation of the connecting wires and proper source placement. In all such cases, we need to keep a close eye on the AGT scores to assure ourselves of a reasonably adequate model.

In fact, this episode and the preceding one have not aimed to provide a complete analysis of the gamma match--not even for the beam design used as our focal sample. Rather, the two-part series has tried to show many--but not all--of the modeling challenges that may go into modeling the gamma match as an example of an odd structure relative to normal or simple antenna construction. We varied our efforts along the way as we took into account as many of

the physical aspects of the structure that may form variables in the overall element geometry. In the process, we showed a few ways in which we might evaluate whether the structure was relatively sensitive or relatively insensitive to changes in each variable. Even for the single beam example that we selected as a starting point, there is considerably more--and sometimes tedious--work ahead before we complete the portrait of the assembly. Systematic modeling is not a synonym for tedium, but the latter is at least the second cousin of the former.

The fundamental principles involved in modeling odd structures are themselves simple. We need to take into account every physical aspect possible for the structure. We need to devise models that permit systematic variation of each significant aspect of the physical structure while remaining within the limits of the software to yield reliable models. Finally, we need to be as systematic as possible both in obtaining model reports and in recording them so that we produce reliable data--if not to the last numeric place, at least in terms of trends that will likely appear in the physical antenna.

## Chapter 120: Back on the Ground

Our modeling notes have been looking up for many episodes. Perhaps it is time to look down for a change. In Chapter 11, we looked at the basics of using the ground-entry commands, mostly as implemented in entry-level software. However, the goal was to create some realistic expectations of the models that we make when the ground is involved. In episode 34, we looked at the GN and GD commands to see both the opportunities and the limitations of giving a NEC model a second medium. One limitation of the second medium was the need to place it either at the same level or below the inner ground medium. A second limitation was the restriction to specifying either a perfect circle (relative to the coordinate system origin) or a straight line at some distance along the X-axis and extending indefinitely parallel to the +/-Y-axis for the boundary between ground media. Hence, NEC cannot directly replicate most rooftop or mountainside antenna locations.

NEC offers us 4 basic ground selection options. Of course, there is free space, which eliminates the ground altogether from field calculations. Next, we may select a perfect ground, which engineers like to call by one or two abbreviations (to prove to one another that they have read the text and know how to talk "engineer-eze"). The NEC method of handling a perfect ground is to use image calculations that are almost as fast as free-space calculations. We may also select between two "real" ground calculation systems. The Reflection Coefficient Approximation (RCA or "fast") system uses a simplified set of calculations that we

once widely used to speed NEC calculations on slow computers. The alternate selection is the Sommerfeld-Norton (SN) or "high accuracy" system that evaluates integrals developed and modified by the individuals after whom the method is named. The process is slower, and in the earlier days of NEC, modelers often saved the results for re-use to conserve computation time. The modern generation of desktop and laptop computers is fast enough to make the RCA method unnecessary, and one NEC implementation had dropped it as an option. Another implementation has by-passed the search for a usable SN result file and now calculates the SN ground anew for each model run. Users cannot tell the difference in run time.

The RCA ground calculation system or method has a second cause of relative demise. Below about 0.2-wavelength, the results are no longer reliable. For horizontal wires, the RCA system shares this problem with the ground calculation system in MININEC, but shows variance curves (relative to SN calculations) that differ from the MININEC ground. The RCA method does have a provision that allows an approximation for a system of buried radials without having to model the radials, but it is not especially accurate. Likewise, the MININEC ground allows a vertical monopole to reach ground without introducing errors (by always presenting the source impedance over perfect ground), but it also shows significant deviations from models that create buried radials (in NEC-4) using the SN method for ground calculations. In "olden times" when computers worked at the speed of ox-carts, even a modest radial field might require the completion of a few chores or a lunch break during the core run. However, the current "interstate" speeds of

computers allow very rapid calculation of large radial fields for multiple monopoles using the SN calculation methods that yield the highest accuracy available to modelers.

## What is NEC Doing When It Calculates Ground Influences?

Whenever we invoke a non-free-space environment, NEC establishes a ground in the X-Y plane at  $Z=0$ . The program employs a flat earth, in contrast to the shallow curve of the real earth's surface. The ground surface at  $Z=0$  is not an absolute limit on all NEC calculation functions. For example, if we invoke a second ground medium, we may place it below (but not above)  $Z=0$  by specifying an increment in meters below the inner medium. A sample GN command with a circular boundary might look like the following entry (without the extra spaces used to separate entries).

GN	2	0	0	0	13	.005	81	5	10.7	10.7
Card	Gnd	Nr of	Zeros		D.C.	Cond.	D.C.	Cond.	Boundary	Neg.
Type	Type	Radials			[Inner Med.]		[Outer Med.]		Radius	Outer Hgt

This card specifies two media, an inner and an outer, with the inner medium having average soil values and the outer one having salt water values. The boundary radius tells us how far (in meters) from the coordinate system origin that the outer medium begins. Note that boundaries are always specified in terms of distance from the 0, 0, 0 point of the coordinate system, not necessarily from the antenna. Since we can alter the coordinates of the antenna's elements, we can place it anywhere in the inner medium region.

The final number (again in meters, even if user interface entry is in other units) represents the distance by which the outer medium surface is below the inner medium surface. A commercial program might call for a negative number as an input to remind the user that the outer medium can never be higher than the inner medium. However, the NEC card requires that this value of lower ground be entered in the command as a positive distance downward. 10.7 meters is about 1 wavelength at the 28 MHz test frequency for the model we are using.

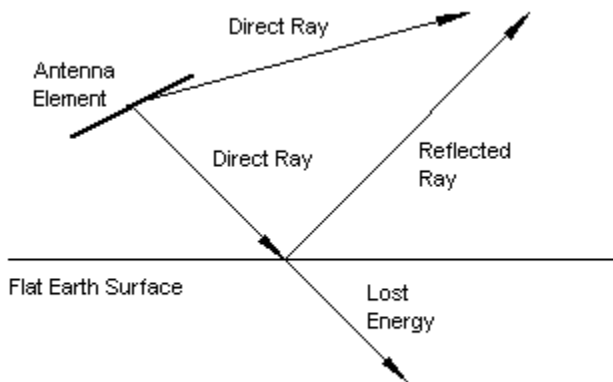
We may also specify the second medium using the GD command in order to free the GN command for alternative uses. For further details on entering GN and GD commands, see episode 34 of this series. The setting of a second medium affects only the calculations for the radiated field. It does not affect the calculation of near fields or currents, even if the antenna geometry extends into the outer medium. As well, the second medium specification has no effect on the ground-wave calculations, which require an infinite flat ground and the primary ground parameters (conductivity and relative permittivity).

The second facet of calculations that involve the region below  $Z=0$ , even when an SN ground has been specified, involves buried wires. A wire that penetrates the surface must have at least a segment junction at  $Z=0$ . NEC-4 will calculate the currents in buried wires, with suitable modifications of the segment lengths for these calculations based upon the medium specified for the primary ground parameters. Therefore, in the NEC output report, expect to

see a difference in the segment information between the initial geometry portion of the report and the current calculation section.

Many modelers observe a difference in the take-off (TO) angle (or theta/elevation angle of maximum field strength) when changing the ground parameters. The explanation for this phenomenon is straightforward, if we examine **Fig. 1**.

Fig. 1



The General Situation for Modeled Ground

If we take any antenna, its radiation will initially consist of direct rays in all elevation directions from the structure. Rays that intercept the earth's flat surface will divide into two components. One component will be a portion of the energy reflected upward. The second portion will be energy dissipated within the earth's surface. The figure only points to the division of energy and not to

the complex manner in which energy penetrates the surface before being reflected (or refracted) upward.

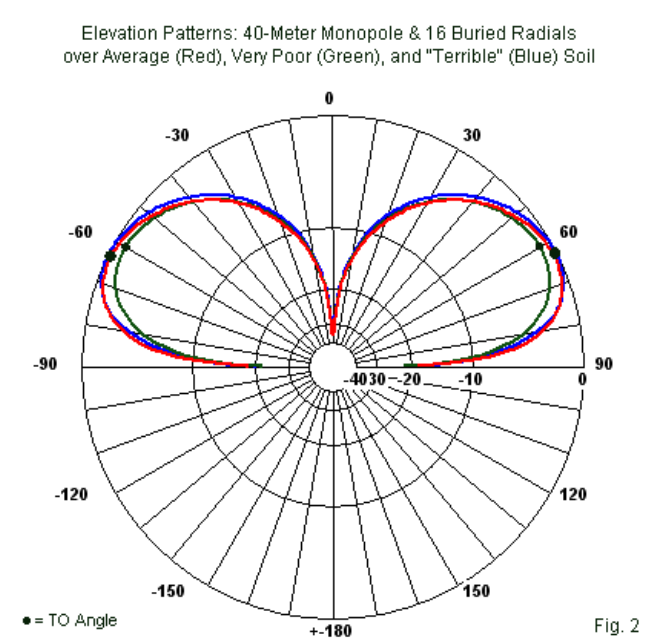
The elevation or theta angle of maximum field strength results from the combination of direct and reflected rays, taking due note of their strength and their relative phases. However, differing ground parameters yield not only differing level of energy loss, but as well, differing depths of penetration, resulting in differences in the reflected rays that parallel the direct rays in phase. The result is a different TO angle.

Within the range of normal values for conductivity and permittivity, lower values of either or both terms normally results in higher TO angle. However, it is possible to specify values of conductivity and permittivity so low that the earth beneath the antenna becomes nearly RF transparent. Let's consider three (for the moment) arbitrary soil qualities called "average," "very poor," and "terrible." If we model a 40-meter 1/4-wavelength monopole with 16 radials buried about 0.1 m below ground, the three soil qualities listed produce the results shown in **Table A**. The TO Angle column lists the theta angle followed by the elevation angle.

Table A. NEC-4 modeling reports for a 40-meter monopole and 16 buried radials with three soil qualities

Quality Name	Conductivity S/m	Permittivity	Maximum Gain dBi	TO Angle degrees
Average	0.005	13	-0.73	63/27
Very Poor	0.001	5	-1.31	60/30
"Terrible"	0.0001	1.2	-0.49	63/27

The hypothetical soil labeled "terrible" uses a conductivity value that appears within the original charts from which we draw the more usual soil types. However, the permittivity is approaching the absolute limit of 1 (relative to free space) and is a value not found for any existing soil. Nevertheless, as we enter these values into NEC, we obtain a slight rise in gain and a drop in the TO angle toward the horizon. Both values run counter to anticipated curves for a soil that is approaching the status of a reasonably good insulator. **Fig. 2** overlays the modeled elevation patterns of the antenna under the three soil conditions.



We enter values of conductivity and permittivity, but for many modelers, these values are strictly conventions. We tend to encounter conductivity in the arena of antenna materials. The basic term, *sigma*, describes conventional current due to electron motion. Tabular values of permittivity, *epsilon*, are actually the relative permittivity, *epsilon<sub>r</sub>*, which is the dielectric constant that we associate with materials used between capacitor plate. At root, the term represents displacement current. Relative permittivity derives from the absolute permittivity (*epsilon*) divided by the permittivity of free space (*epsilon<sub>0</sub>*), or

$$\epsilon_r = \frac{\epsilon}{\epsilon_0} = \frac{\epsilon}{8.87(pF/m)}$$

Since absolute permittivity is also in pF/m, relative permittivity has no units.

We enter separate values for conductivity and permittivity because we can measure each independently and because one may vary while the other remains constant. See "Practical RF Soil Testing" by Eric von Valtier, K8LV, in *QEX* for July/August, 2006, pp. 46-49, for a good summary of basic soil terms and concepts, as well as a technique for measurement.

For use in SN calculations, NEC employs one of two formulations of complex permittivity ( $\epsilon_g$ ), according to how the modeler enters the value of  $\sigma$ . If the entry is positive, as is normally the case, then

$$\epsilon_g = \epsilon_r - j \frac{\sigma}{\omega \epsilon_0}$$

$\Omega$  is the familiar  $2 \text{ Pi } f$  function. If the user enters  $\sigma$  as a negative number, then

$$\epsilon_g = \epsilon_r - j|\sigma|$$

without regard for frequency. Since most users derive values from tables, the normal form is usually the form of choice.

## Expanding Our Appreciation of Soils

The most common table of soil values from which modelers draw values is actually very old. **Table 1** represents an adaptation of values found in *The ARRL Antenna Book*, 20th Edition (p. 3-13), which are themselves an adaptation of the table presented by Terman in *Radio Engineer's Handbook* (p. 709), taken from "Standards of Good Engineering Practice Concerning Standard Broadcast Stations," *Federal Register* (July 8, 1939), p. 2862. Terman's value for the conductivity of the worst soil listed is an order of magnitude lower than the value shown here. Sharp eyes will immediately spot the categories of average and very poor soil,

although there is no such thing as "terrible" soil in the listing. The list shown is from Intermediate Antenna Modeling: A Hands-On Tutorial, published now by *antenneX* at:

[http://www.antennex.com/Sshack/tutorials/model\\_books.html](http://www.antennex.com/Sshack/tutorials/model_books.html) .

I have put this table and the next one in the form of graphics so that--if you do not have some other convenient reference--you may download and print these tables on 1 or 2 sheets..

### ***Conductivity and Permittivity of Common Ground Conditions***

A Standard Table

Table 1

The following soil descriptions are commonly used in antenna modeling. Always substitute more precise values wherever known. The table represents an adaptation of values found in *The ARRL Antenna Book* (p. 3-6), which are themselves an adaptation of the table presented by Terman in *Radio Engineer's Handbook* (p. 709), taken from "Standards of Good Engineering Practice Concerning Standard Broadcast Stations," *Federal Register* (July 8, 1939), p. 2862. Terman's value for the conductivity of the worst soil listed is an order of magnitude lower than the value shown here.

<b>Soil Description</b>	<b>Conductivity in S/m <math>\sigma</math></b>	<b>Permittivity (Dielectric Constant) <math>\epsilon</math></b>	<b>Relative Quality</b>
Fresh water	0.001	80	
Salt water	5.0	81	
Pastoral, low hills, rich soil, typical from Dallas, TX, to Lincoln, NE	0.0303	20	Very Good
Pastoral, low hills, rich soil, typical of OH and IL	0.01	14	Good
Flat country, marshy, densely wooded, typical of LA near the Mississippi River	0.0075	12	
Pastoral, medium hills, and forestation, typical of MD, PA, NY (exclusive of mountains and coastline)	0.006	13	
Pastoral, medium hills, and forestation, heavy clay soils, typical of central VA	0.005	13	Average
Rocky soil, steep hills, typically mountainous	0.002	12 - 14	Poor
Sandy, dry, flat, coastal	0.002	10	
Cities, industrial areas	0.001	5	Very Poor
Cities, heavy industrial areas, high buildings	0.001	3	Extremely Poor

In the absence of a need for a soil quality applicable to a particular location, most modelers opt to place antennas above average soil. Alternatively, they may select a range of soils over which to run a model, ranging from very good down to very poor. *The ARRL Antenna Book* does allow the modeler to regionalize--but not to localize--soil conductivity through the U. S. map that it presents in Fig. 19 on page 3-14 of the 20th edition. True localization would require measurements, such as those described by K8LV.

Between 1939 and the present day, numerous measurements of soil conditions have occurred--where soil also covers various waters and ices.

The lists in the tables differ somewhat in the extremes of non-water values. The traditional list shows a maximum conductivity (in very good soil) that is about 3 times higher than the highest land conductivity in the newer list. The highest values of relative permittivity also differ (20 vs. 30), but above about 20, higher permittivity values tend to show no significant performance increases. Note that the entry a "City industrial area" uses the same conductivity value as our contrived terrible soil, lower than the lowest conductivity in the traditional list by a factor of 10. Both lists show a minimum permittivity value of 3, which is considerably higher than the arbitrary value assigned to terrible soil.

### **Conductivity and Permittivity of Common Ground Conditions**

*The Table Used in NEC-Win Pro and GNEC*

*Table 2*

The following list of conductivity and permittivity values is drawn from many recent sources and is used as a set of user-selectable entries for ground conditions in GN and GD entries in NSI programs. Users may also enter custom values wherever information on the actual soil conditions is available.

<b>Soil Description</b>	<b>Conductivity in S/m <math>\sigma</math></b>	<b>Permittivity (Dielectric Constant) <math>\epsilon</math></b>
Poor	0.001	4.5
Moderate	0.003	4
Average	0.005	13
Good	0.01	4
Dry, sandy, coastal	0.001	10
Pastoral hills, rich soil	0.007	17
Pastoral medium hills and forestation	0.004	13
Fertile land	0.002	10
Rich agricultural land, low hills	0.01	15
Rocky, steep hills	0.002	15
Marshy land, densely wooded	0.0075	12
Marshy, forested, flat	0.008	12
Mountainous, hilly (up to about 1000 m)	0.002	5
Highly moist ground	0.005	30
City industrial of average attenuation	0.001	5
City industrial of maximal attenuation	0.0004	3
City industrial area	0.0001	3
Fresh water	0.001	80
Fresh water @ 10° C and 100 MHz	0.001	84
Fresh water @ 20° C and 100 MHz	0.005	80
Sea water	5.0	81
Sea water @ 10° C up to 1 GHz	4.0	80
Sea water @ 20° C up to 1 GHz	4.0	73
Sea ice	0.001	4
Polar ice	0.0003	3
Polar ice cap	0.0001	1
Arctic land	0.0005	3

Perhaps the greatest contribution of the expanded table is the detailed listing of water and ice values. However, for any critical modeling, the modeler himself remains responsible for the figures

entered. In all cases, any account that makes use of the model should not only present the values of conductivity and permittivity used with the model, but should also provide a good reason for using them. I have seen a few cases in which antennas have claimed some advantage over other designs, where the advantage rested mostly on an unproclaimed use of better soil conditions.

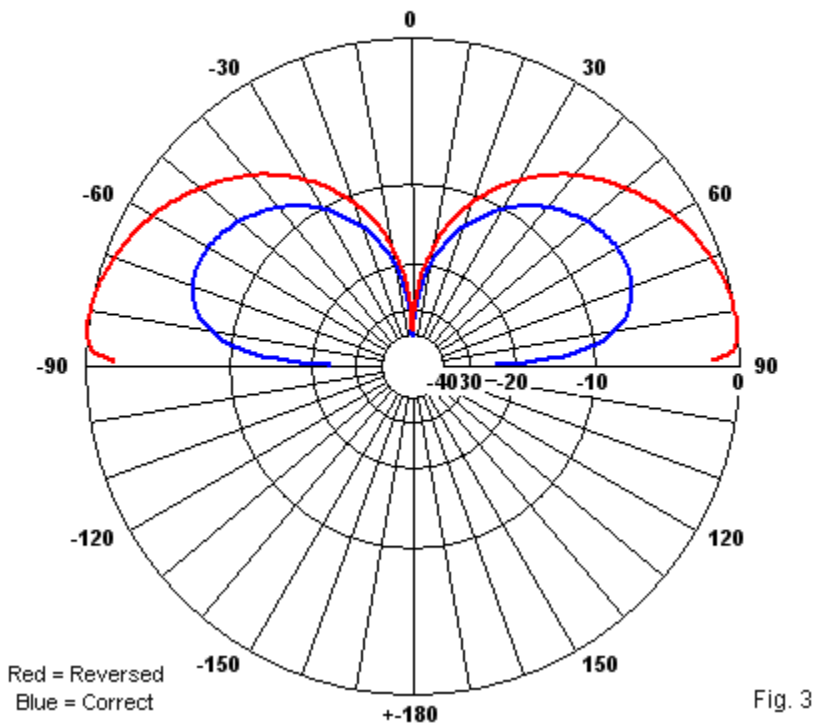
In any writing that makes use of antenna models over soil, there are two errors to avoid. One is suddenly to change the soil quality while still making non-soil-related comparisons. The second is inadvertently to reverse the conductivity and permittivity entries for an intended level of soil quality. **Table B** shows what happens to our 40-meter monopole with 16 buried radials over average ground with correct and with reversed entries.

Table B. NEC-4 modeling reports for a 40-meter monopole and 16 buried radials over average ground

Entry	Conductivity S/m	Permittivity	Maximum Gain dBi	TO Angle degrees
Correct	0.005	13	-0.73	63/27
Reversed	13	0.005	4.79	82/08

However implausible the error sounds, it is far more common than most people wish to believe, according to models that I have reviewed over the years. (I withhold the modeler names to protect the embarrassed.)

Overlapping Elevation Patterns: 40-Meter Monopole and 16 Radials  
with Correct and with Reversed Conductivity and Permittivity Entries



**Fig 3** shows the radical difference in patterns. Note that a 40-meter monopole over perfect ground would show a maximum gain of about 5.2 dBi, with maximum gain along the horizon. The unreal value of conductivity (2.5 times the value of salt water) tends to override the very low value of permittivity. The value that we

plugged in is in fact lower than the minimum relative value (1), but the program dutifully calculated a set of results.

## Conclusion

These notes will supplement previous episodes concerning NEC's ground entry system for real ground values of conductivity and permittivity. However, the potpourri of ideas by no means counts as completing the story of ground as it applies to antennas.

Researchers continue to search for calculation methods even more accurate than the SN system, which has proven quite trustworthy for a large class of cases. As well, experimenters continue to refine methods of measuring both conductivity and permittivity to allow more antenna users to obtain truly local information. (Of course, we must use an extended sense of what is truly local, since we are interested not only in the ground immediately beneath an antenna, but as well for a considerable number of wavelengths away in the region in which ground reflections occur in the formation of the far field.)

We have not mentioned MININEC extensively in these notes, since the standard MININEC ground calculation system uses a truncated method that is generally inaccurate for antennas having any horizontal component that is less than 0.2-wavelength above ground. However, one implementation of MININEC, Antenna Model, has grafted the SN calculation system onto the MININEC core, with very good results down to virtually the same limits that the system has with NEC. However, the MININEC core does not

permit buried wires. Hence, monopoles with radial systems must lie totally above ground.

Those who wish to look more deeply into the SN ground calculation methods may consult the NEC-2 and NEC-4 manuals. The lists of references in those volumes will lead to seminal books and papers at least through the appearance of the programs.

## Chapter 121: Radiation Patterns and Propagation

**A** number of statements that we might correctly make about the far-field radiation patterns produced by NEC tend to strike a dull chord among newer modelers--if my e-mail over the years has been any kind of indicator. Many of these statements seem to run counter to experience or reports of experience in one or more ways. Most of the answers to the quandaries lie in the realm of distinguishing antenna phenomena as NEC models than from what happens to HF signals as they propagate via the ionosphere toward and from a communications target. Therefore, I shall devote this episode to seeing the differences that are crucial to understanding NEC's reports and communications reports without conflict.

In the process of developing these notes, we shall encounter a number of highly simplified sketches--along with the usual collection of NEC-based graphics. The sketches are not designed to capture all of the nuances of propagation, but only to focus on certain features. However, ionospheric propagation is a very complex phenomenon (or collection of phenomena). Hence, for every detail that I include, I shall omit dozens of others that occur simultaneously.

*Are antennas truly reciprocal?*

Our first question seems to arise because when we communicate, we often find that reciprocity over a communications path seems not to apply as often as it does apply. We call stations that do not

hear us, and we receive reports from third parties that another station is calling us although we cannot hear him. Even when we do manage to communicate in the HF range, the signal strengths may differ at each end of the line. As a result of these situations, one may naturally ask whether antennas are reciprocal.

Note that we are addressing this question in very broad terms. Many a theoretical debate arises from time to time as to whether antennas are "really" capable of being reciprocal. However, we shall not in these notes engage the question at such a theoretical level.

The entry-level software used by most modelers gives no clue to a proper answer to the question. Most entry-level software restricts the user to only one of the excitation possibilities, the direct voltage source (EX0) (or an indirect current source). For example, we might encounter a 6-element Yagi modeled in free space. The following lines define the model in ASCII format.

```
CM 6-el 2M Yagi
CE
GW 1 21 -.514604 0. 0. .514604 0. 0. .0024
GW 2 21 -.5075174 .257302 0. .5075174 .257302 0. .0024
GW 3 21 -.4746752 .3637788 0. .4746752 .3637788 0. .0024
GW 4 21 -.461137 .6585204 0. .461137 .6585204 0. .0024
GW 5 21 -.461137 .9469628 0. .461137 .9469628 0. .0024
GW 6 21 -.443992 1.377137 0. .443992 1.377137 0. .0024
GE 0
LD 5 0 0 0 2.5E+07 1.
FR 0 1 0 0 146. 0
GN -1
EX 0 2 11 0 1 0.
RP 0 1 361 1500 90. 0. 1.00000 1.00000 0.
EN
```

The EX command line specifies that we apply a voltage source to the center segment of wire 2. In most entry-level programs, we then request a radiation pattern (RP0). Since the antenna is in free space, we request an azimuth pattern, which is technically an E-plane pattern. The result appears in **Fig. 1**. Note that the wire entries place the element spacing values in the Y columns, while the elements extend in the +X and -X directions. The conventions of the software used here (NSI's GNEC) place 0-degrees at the top of the polar plot. The pattern is a phi pattern (where a true azimuth pattern would increase the degree values clockwise). Hence, the main lobe of the antenna points to the left at 90 degrees phi.

E-Plane Pattern of a 6-Element 146-MHz Yagi with Data

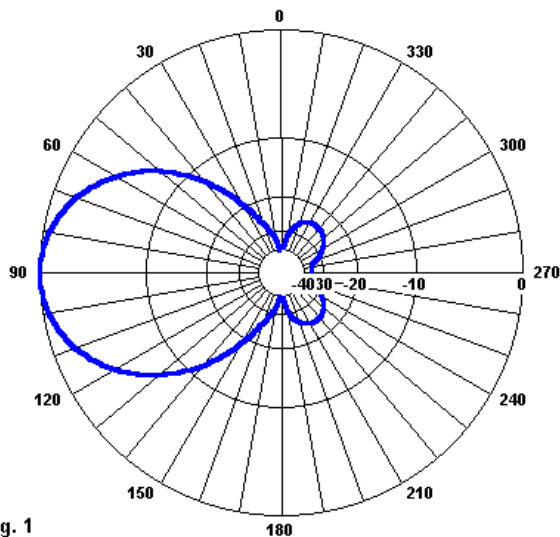
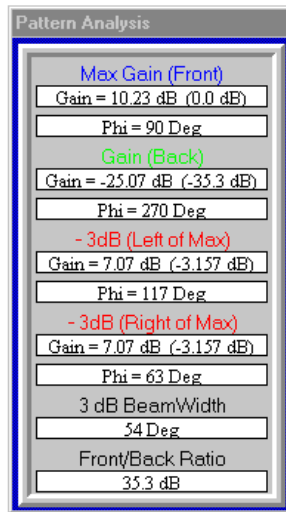
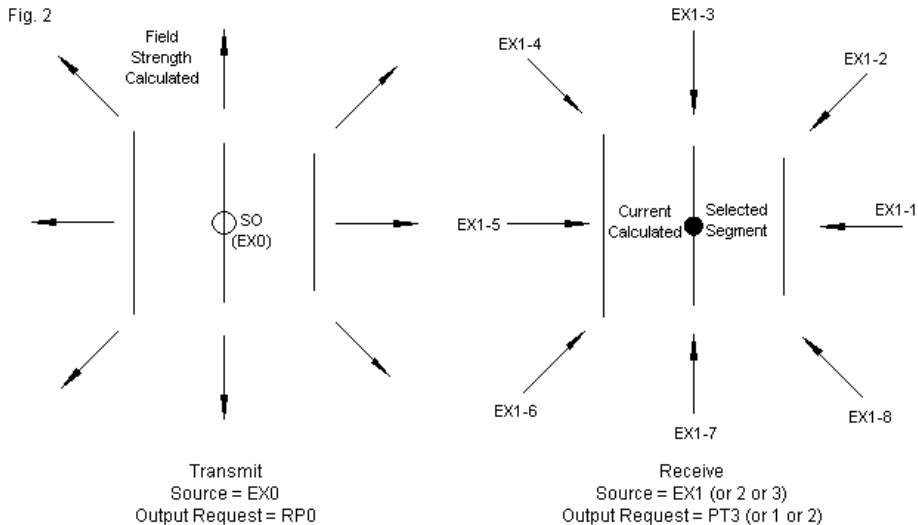


Fig. 1



The side panel in the figure provides the analytical data to accompany the normalized plot on a logarithmic scale. One reason that I selected this antenna was its free-space gain value of just over 10 dBi. For data-gathering purposes, the XNDA specification in the RP0 command is 1500. When  $N=5$ , the radiation pattern portion of the NEC output file produces an additional table. It lists for each value of phi and theta the antenna gain normalized to the peak gain of the antenna. The bearing of peak gain will read 0 dB, and all other gain values will be negative, indicating how much below the peak gain they are, as recording in dB. However, even a pattern like this one does not show why the antenna is or is not reciprocal, or even what reciprocity might mean.

An antenna is reciprocal if its receiving pattern and its transmitting pattern are the same. We ordinarily record the transmitting pattern in dBi, or dB relative to an isotropic source. Normalized, the gain appears relative to a peak value of 0 dB. The counterpart to transmitting gain would be receiving sensitivity. More advanced versions of NEC offer a number of options for deriving receiving patterns. They involve the EX1 command for linear antennas, that is, providing the antenna with external excitation in the form of linear plane waves. We systematically rotate the excitation around the antenna in a series of steps. Then we invoke the PT command to record the relative current at a selected point--our former feedpoint. **Fig. 2** shows in simplified form with only 8 positions for the EX1 command how the development of receiving patterns differs from the development of transmit patterns.



Simplified View of How NEC Handles Transmit and Receive Analyses

A typical model might have the following appearance. Note that NEC has a limitation in how large a receiving matrix may be. Therefore, the data generation has two parts, one from  $-90$  to  $+90$  degrees, the other from  $90$  to  $270$  degrees. **Fig. 1** tells us why we selected the division of the work. Since we shall request normalized data, each section of data must contain a peak gain/current point, which occurs at  $90$  degrees  $\phi$ . The program then normalizes the data against this value. The PT3 command allows us to capture only the normalized current in dB at a selected segment, in this case, the same segment that we formerly used as the transmit source or feedpoint.

```

CM 6-el 2M Yagi
CE
GW 1 21 -.514604 0. 0. .514604 0. 0. .0024
GW 2 21 -.5075174 .257302 0. .5075174 .257302 0. .0024
GW 3 21 -.4746752 .3637788 0. .4746752 .3637788 0. .0024
GW 4 21 -.461137 .6585204 0. .461137 .6585204 0. .0024
GW 5 21 -.461137 .9469628 0. .461137 .9469628 0. .0024
GW 6 21 -.443992 1.377137 0. .443992 1.377137 0. .0024
GE 0
LD 5 0 0 0 2.5E+07 1.
PT 3 2 11 11
EX 1 1 181 0 90 0 90 0 1 0 0
XQ
PT 3 2 11 11
EX 1 1 181 0 -90 180 90 0 1 0 0
XQ
EN

```

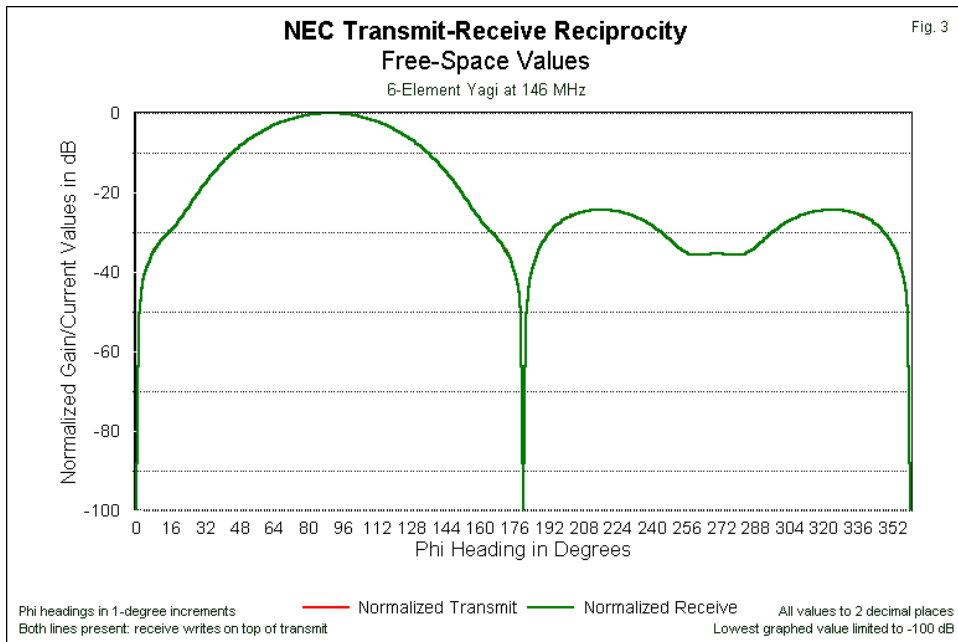
The data for both the transmitting pattern and the receiving pattern can be transferred to a spreadsheet for graphing. For both sets of data, we have 361 data points (from 0 to 360 degrees phi). **Table 1** provides a glimpse of the data from 0 to 120 degrees for the 6-element Yagi in free space at 146 MHz. Three data points call for attention: 0, 180, and 360 degrees. Each of these points represents a free-space side null. Values for these nulls have two properties that are problematical for graphing. First, they may have very large negative values. Graphing such values may result in severe compression of the upper part of the graph. Second, the values are subject to large variations with very small differences in the rounded values of numbers that go into their development. For the sake of graphing, I have set these numbers to an artificially high value of -100 dB.

Phi	Norm Xmt	Norm Rcv	Phi	Norm Xmt	Norm Rcv	Phi	Norm Xmt	Norm Rcv	Phi	Norm Xmt	Norm Rcv
0	-100	-100	<i>Note: actual values at 0, 180, and 360 degrees leveled at -100 dB for graphing.</i>								
1	-51.58	-51.59	31	-18.05	-18.05	61	-3.67	-3.67	91	0	0
2	-45.66	-45.67	32	-17.31	-17.32	62	-3.41	-3.41	92	-0.02	-0.02
3	-42.25	-42.26	33	-16.6	-16.6	63	-3.16	-3.16	93	-0.04	-0.04
4	-39.88	-39.89	34	-15.9	-15.91	64	-2.92	-2.92	94	-0.07	-0.07
5	-38.08	-38.09	35	-15.23	-15.23	65	-2.69	-2.69	95	-0.1	-0.1
6	-36.64	-36.65	36	-14.57	-14.58	66	-2.47	-2.47	96	-0.15	-0.15
7	-35.45	-35.46	37	-13.94	-13.94	67	-2.26	-2.26	97	-0.2	-0.2
8	-34.44	-34.45	38	-13.32	-13.32	68	-2.06	-2.07	98	-0.27	-0.27
9	-33.57	-33.58	39	-12.72	-12.73	69	-1.88	-1.88	99	-0.34	-0.34
10	-32.81	-32.82	40	-12.15	-12.15	70	-1.7	-1.7	100	-0.42	-0.42
11	-32.12	-32.13	41	-11.59	-11.59	71	-1.53	-1.53	101	-0.5	-0.51
12	-31.49	-31.5	42	-11.05	-11.05	72	-1.37	-1.37	102	-0.6	-0.6
13	-30.9	-30.91	43	-10.52	-10.53	73	-1.22	-1.22	103	-0.71	-0.71
14	-30.32	-30.33	44	-10.02	-10.02	74	-1.08	-1.08	104	-0.82	-0.82
15	-29.75	-29.76	45	-9.53	-9.53	75	-0.94	-0.95	105	-0.94	-0.95
16	-29.17	-29.18	46	-9.05	-9.06	76	-0.82	-0.82	106	-1.08	-1.08
17	-28.57	-28.58	47	-8.6	-8.6	77	-0.71	-0.71	107	-1.22	-1.22
18	-27.95	-27.95	48	-8.16	-8.16	78	-0.6	-0.6	108	-1.37	-1.37
19	-27.29	-27.29	49	-7.73	-7.73	79	-0.5	-0.51	109	-1.53	-1.53
20	-26.59	-26.6	50	-7.32	-7.32	80	-0.42	-0.42	110	-1.7	-1.7
21	-25.87	-25.87	51	-6.92	-6.93	81	-0.34	-0.34	111	-1.88	-1.88
22	-25.11	-25.12	52	-6.54	-6.54	82	-0.27	-0.27	112	-2.06	-2.07
23	-24.34	-24.34	53	-6.17	-6.17	83	-0.2	-0.2	113	-2.26	-2.26
24	-23.55	-23.55	54	-5.81	-5.82	84	-0.15	-0.15	114	-2.47	-2.47
25	-22.75	-22.75	55	-5.47	-5.47	85	-0.1	-0.1	115	-2.69	-2.69
26	-21.94	-21.95	56	-5.14	-5.14	86	-0.07	-0.07	116	-2.92	-2.92
27	-21.14	-21.15	57	-4.82	-4.82	87	-0.04	-0.04	117	-3.16	-3.16
28	-20.35	-20.35	58	-4.52	-4.52	88	-0.02	-0.02	118	-3.41	-3.41
29	-19.57	-19.57	59	-4.22	-4.22	89	0	0	119	-3.67	-3.67
30	-18.8	-18.8	60	-3.94	-3.94	90	0	0	120	-3.94	-3.94

Normalized Transmit Gain and Received Currents for 0 to 120 Degrees in 1-Degree Increments  
6-Element Yagi at 146 MHz in Free Space

Table 1

If we conjoined the two graphs--one for the transmitting pattern and one for the receiving pattern--we obtain a result like **Fig. 3**.



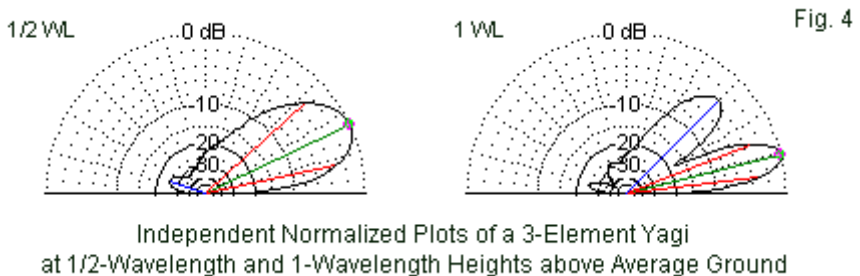
Computer-generated graphs "write" the curve for one color and then overwrite it with the second color line. The result for our test case is the nearly complete disappearance of the red line beneath the green. A few red "dots" appear as verification that the line is present. However, as both the graph and the table suggest, the normalized pattern graphs are as identical as one might find in any data generation system. In short, within the limits of our ability to calculate and present the results, the patterns for transmitting gain and for receiving sensitivity are the same. From the perspective of

NEC, the antenna performance is reciprocal with respect to transmitting and receiving.

For further information on the use of the EX command in conjunction with the PT command to develop receiving patterns and information, see episode 88 of this series.

*Why do we continue to claim that a horizontal antenna performs better as we increase height? When we increase the height of an antenna from 1/2-wavelength to 1-wavelength, we find a high-angle lobe that simply wastes power.*

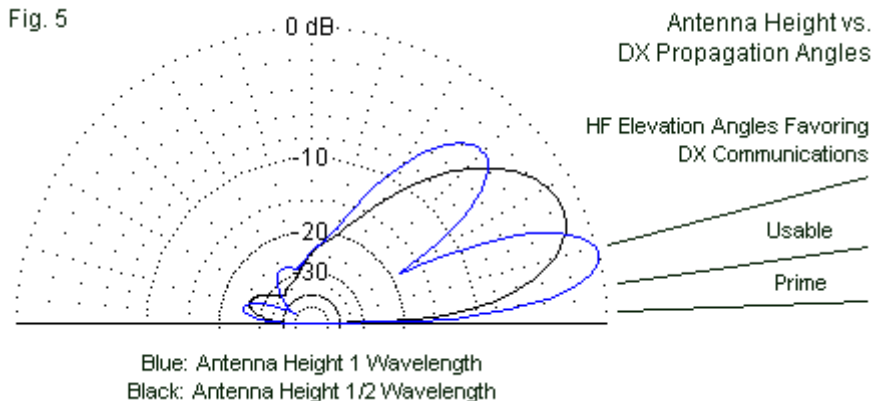
The question arises from looking at independent normalized elevation patterns for the same antenna at different heights. **Fig. 4** captures the situation, so let's us see what might mislead a novice pattern reader.



If we examine the patterns without reference to the numerical data and without some important external data, we might easily reach

the same conclusion that prompted the question. The elevation plot for the Yagi at a height of 1/2-wavelength seems to contain more energy, and the forward pattern forms a continuous whole. Hence, more energy seems to be concentrated at lower elevation angles. In contrast, the pattern for a height of 1-wavelength contains two lobes with a very deep null between them. The upper lobe has a center angle of about 45 degrees, well above the elevation angles at which we find skip except under the most unusual conditions. The lower lobe has a narrower vertical beamwidth than we find in the forward lobe for the pattern at a height of 1/2-wavelength. In the abstract, then, the pattern for a height of 1-wavelength appears to be distinctly inferior.

To determine if appearances are true or deceiving, we can do one of two things--or both. We can refer to the numerical data. Or, we may overlay the pattern so that their relative strengths become apparent. **Fig. 5** provides the overlaid patterns (using EZNEC software) along with some supplementary data that NEC does not and cannot calculate.



The portion of the figure that NEC does calculate shows the relative proportions of the two patterns. If we assume that the azimuth patterns for the two heights are similar to each other (and we may always check by looking at those patterns), the energy within the cross-sections of the elevation patterns is about the same. However, most of the energy in the pattern for the lower height is directed at higher angles relative to the lower of the two lobes that form the pattern for the upper height. Below about 15 degrees elevation, the higher antenna shows a significantly stronger radiation pattern (and by virtue of our earlier discussion, a more sensitive receiving pattern).

At this point, we must combine the data from NEC with information derived from other sources. For example, extensive studies by Dean Straw, N6BV, have shown that most long-distance (DX) HF signals arrive at very low levels, as suggested in the additions to

the patterns at the far right of **Fig. 5**. (The N6BV information is included with recent editions of *The ARRL Antenna Book*.) Despite the seeming waste of energy in the elevation region around 45 degrees, the higher antenna's lower lobe better intercepts the propagation angles at which much, if not most, long-distance HF energy arrives and departs. Indeed, the prime angles might even favor raising the horizontal antenna further.

We have reached a certain "interface." NEC calculations produce patterns based on a set of constant conditions in the far-field region of the antenna, that is, from several wavelengths beyond the limits of the antenna outward. However, it says nothing about what occurs to either radiated or incoming energy that is a function of variables within the far field region. Moreover, NEC says nothing about nearer influences unless we expressly model them.

*Why can I sometimes hear a station but not be heard by them--and vice versa--at both HF and VHF frequencies?*

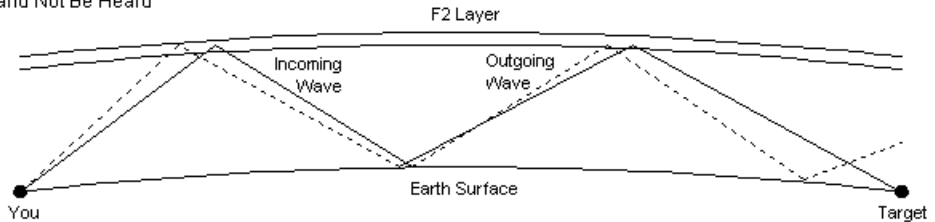
At HF, the vast majority of signals that we receive (and our return transmitted signals) undergo ionospheric refraction so long as the ionosphere is sufficiently ionized to allow refraction. This simple statement involves us in the very complex field of propagation. On an average day--depending on the time of day, the month of the year, and the strength of the sun's ionizing UV radiation--we find many ionized layers. Many monthly columns exist in journals that go into various details about the actions of these layers under the many combinations of influences. We shall not try to replicate those studies here. Indeed, if you wish to predict ionospheric conditions to

assist your own operation, you may find considerable benefit in obtaining one of the programs that use VOACAP or similar calculation engines to develop profiles of the most probable propagation conditions for paths that you specify.

Here, we can concentrate on the daytime F2 layer, which has perhaps the greatest influence on the path of long-distance HF signals. **Fig. 6** provides a partial answer to our question of why HF signals have different strengths in each direction. They simply take slightly different elevation paths over the distance between two stations. It is possible for the two stations to have equal strengths, to have unequal strengths, or for one to be on target while the other is wholly off target.

Why You Can Sometimes Hear  
and Not Be Heard

Fig. 6



What the figure does not show is one of the reasons for the condition shown. The position of the sun relative to the path determines the strength of ionization all along the path. The strength of ionization influences the angle of refraction and how far through the ionized layer that energy travels before departing downward. (The strength of ionization also determines how much

energy passes through the ionosphere to be lost into outer space and at what angles relative to the two stations and to the intermediate ground-reflection region. The ground reflection region near the center of the figure may also show differences in losses depending on whether the region is over dry land or salt water.)

On a "normal" morning in the U.S., one might expect to hear first stations from Eastern Europe. As the morning moves onward (or as the European afternoon moves onward), the strongest stations appear to come from western European areas. Very often, however, the western European stations could hear my U.S. signals earlier in the day (from various inland locations, such as Tennessee or Nebraska), but would call in vain for a reply. Their transmitted skip was landing somewhere other than at my location. However, as the sun moved, those signals began intercepting my antenna, while the more eastern stations in Europe faded.

All of these phenomena occur beyond the limits of what NEC calculates as the antenna pattern. At best, we can arrange our models to produce patterns that are most likely to transmit and intercept signals at the most favored angles--or to understand why the limitations of our feasible installation will fall short of the ideal elevation angles. However, NEC will not take propagation effects into account.

Even at VHF and UHF, there are a myriad of influences that NEC usually does not take into account. Some of these factors we may model and some fall outside of feasible modeling. For example, the antenna support structure may affect performance, and we may

(often with some difficulty) model this structure. At a slightly larger distance from the antenna, but still close by, we find a myriad of objects that we often refer to as "clutter." The ground clutter may include power line, poles, trees, buildings, and other items too varied to list. If we view these objects as significant, we may always try to model them. However, the level of conductivity and the actual structure of the most conductive parts may not be visible.

Modeling objects at a distance is standard engineering practice in some enterprises. For example, the potential of cell towers for distorting AM BC radiation patterns requires careful analysis within which modeling both the broadcast tower and the somewhat distant cell-phone tower plays a significant role.

VHF and UHF line-of-sight communications often encounters terrain and building effects at further distances than we might use for counting ground clutter. Edge diffraction that "bends" radio waves into otherwise dark areas by a wall-like or knife-edge object may not appear in both directions for an intended communications path. In fact, diffraction may also affect the elevation patterns of HF antennas. For further information on these optically-related wave phenomena, see Chapters 3 and 23 of the most recent edition of *The ARRL Antenna Book*. One passage in Chapter 3 refers to the analysis of these phenomena as a limitation of NEC's flat-ground mode of analysis. The point being made is that NEC does not model everything. In some cases, we may incorporate some distant objects within the model, but often a wire grid stand-in--with the wires assigned a general conductivity that reflects the materials of the object--fails to act like the real object within the radiation pattern

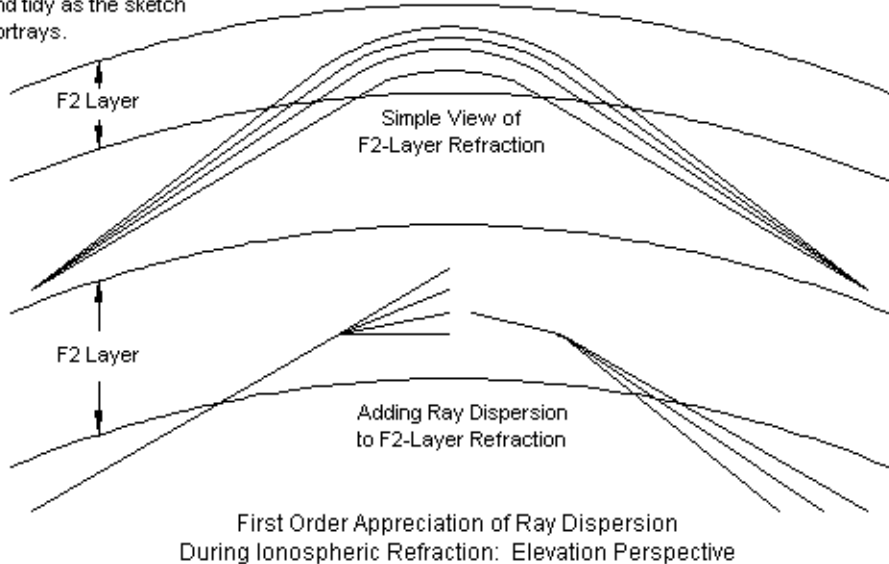
field. When it comes to propagation, there is no practical way to model its effects within NEC.

*When I communicate with stations along a coastline, I often acquire stronger signals with my antenna pointed somewhat off shore than when I align it with the station's geographic location? Is the NEC radiation pattern in error?*

Although this question seems unrelated to the ones that we have been addressing, it is actually a variation of the earlier questions. Once more, the effect is not a part of what NEC can calculate, but is instead a function of propagation phenomena. One term that we have used is the idea of a "ray," a representation of radiated energy as a straight line. In the ionosphere, we find that the ray is refracted in some kind of arc--if the angle is not too severe and the ionization is not either too weak or too strong--so that it re-emerges on a downward slope toward a communications target. The simplified portrait of rays appears in the upper portion of **Fig. 7**.

Note: The ionosphere is not as neat and tidy as the sketch portrays.

Fig. 7



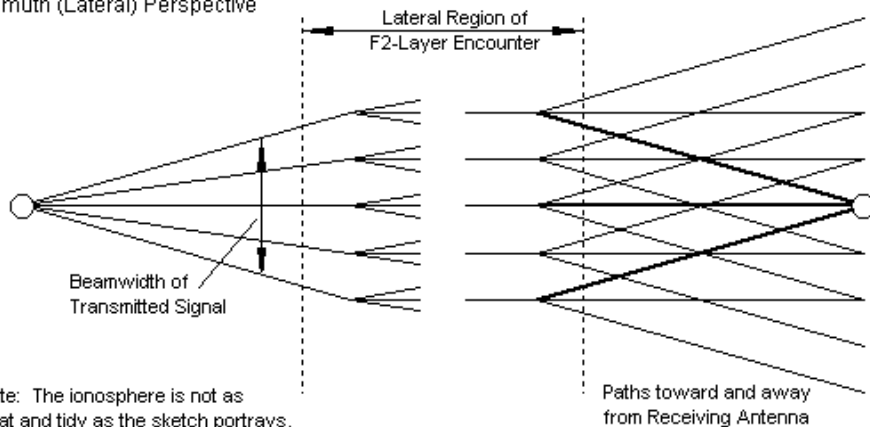
The lower portion of the figure is also an oversimplification, but may be good enough to get across a general idea of some importance. Rays are not like bullets, although we often portray them that way. When the energy reaches the ionosphere, it disperses. Some is lost. Some is absorbed. Some proceeds along one of several directions that would support refraction for re-entry downward. Any single component may undergo many dispersions, usually continuously along the path through the ionosphere. The result is a downward "spray" of energy. The actual signal that we receive is the statistical sum of all of the effects. If that sum is strong enough

at the reception site, then we have at least half the conditions needed for successful communications. (For a broadcast station, this one-way analysis may be all that we need, since the only goal is reception.)

Dispersion effects are not only elevation phenomena. They also occur laterally, as suggested by **Fig. 8**. Once more, I have oversimplified the sketch so as not to lose the lines in a uniform gray mass. The actual dispersion effects are relatively continuous, rather than being stepped as shown in the sketch. Once more, what emerges as the downward energy will be--with respect to the target location--a statistical sum of all of the effects at work.

First Order Appreciation of Ray Dispersion  
During Ionospheric Refraction:  
Azimuth (Lateral) Perspective

Fig. 8



Note that from a lateral perspective, the received signal may come from directions that have diverse azimuth bearings from the target location. Now let us suppose that at least some of the energy had to use two "hops" to reach the target. Reflections from dry ground tend to be lossier than reflections from salt water. Hence, we may find, at least on some occasions that an off-shore antenna direction may produce stronger signals (in one or both directions) than a straight-line or great-circle bearing. The NEC radiation pattern would be correct in indicating the direction of the strongest signal. However, propagation effects would place the direction of the signal at a bearing that might not coincide with the actual target station location. Indeed, I am not aware that current propagation software takes this effect into account. Like NEC itself, propagation software has its calculating limitations.

## Conclusion

These simple notes are no substitute for a proper study of the propagation of radio waves in any frequency region of interest. Rather, the notes have been designed to show in a somewhat rudimentary way what the NEC radiation patterns can and cannot tell us. With a flat ground and an ideal medium above ground, they give an accurate portrayal of both transmitting and receiving patterns for the class of antennas that we may model on the software.

However, those patterns cannot tell us anything about phenomena that modify the patterns once energy leaves the antenna on transmission or before it arrives at the antenna on reception. We

have distinguished two general categories of modification. One set includes objects that we might attempt to include within the model, whatever the difficulty we may have in arriving at adequate models of those structures. The other set of modifying phenomena we have no hope of capturing with NEC, namely, all of the possible influences of propagation. Our survey of propagation effects is both over-simplified and incomplete. We only examined a few facets of propagation that have a relationship to questions often raised by newer modelers as they try to connect NEC radiation patterns with communications experience. Understanding propagation may be more complex than understanding antenna modeling. Hence, these notes are not suitable for conversion into sound bites that may easily mislead you when you take them out of context. Rather, the notes form a suggestion for the study of a set of phenomena that play the major role in what goes on between antennas.

The bottom line is that NEC radiation patterns give us useful information about a subject antenna. However, there is much in the use of that antenna that NEC cannot (and was never designed to) tell us.

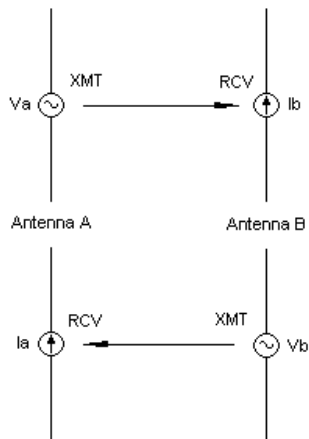
## Chapter 122: Reciprocity: Home on the Range

The *ARRL Antenna Book* (20th Ed., p. 2-1) contains a beginner's discursive explanation of reciprocity. "In the same fashion that a loudspeaker can act as a microphone, a radio antenna also follows the principle of reciprocity. In other words, an antenna can transmit as well as receive signals." This brief extract follows an explanation of an antenna as a "special transducer" capable of converting RF current into propagating electromagnetic waves and converting intercepted waves into electrical current. The context is the very beginning of a chapter called "Antenna Fundamentals." Hence, we should not expect mathematical sophistication.

More mathematically inclined readers may wish to consult various college-level antenna texts. I keep a small number on my shelf as references, for example, Stutzman and Thiele, *Antenna Theory and Design* (2nd Ed., pp. 404-409), and Balanis, *Antenna Theory: Analysis and Design* (2nd Ed., pp. 127-132). I have listed the most relevant pages of each text for a reason. Balanis discusses reciprocity early in the text's development, but Stutzman and Thiele defer the treatment until late in the text. We shall have occasion to note the Stutzman and Thiele placement later. Both treatments share a common kernel, the development of antenna reciprocity from the Lorentz reciprocity theorem, which itself derives from Maxwell's equations. (Those comfortable with calculus may wish to compare the Stutzman and Thiele equation 9-36 with Balanis' equation 3-66.)

A better-known text among amateur radio operators is Kraus, *Antennas* (2nd Ed., pp. 410-413). One interesting aspect of the Kraus treatment is that he uses a different starting point for his development of reciprocity. He begins with the Rayleigh-Helmholtz reciprocity theorem as generalized in the 1920s by J. R. Carson. (Rayleigh's initial context of sound is not unrelated to the ARRL basic analogy between antennas and loudspeakers.) Without ado, Kraus expresses the theorem in the following terms: "If an emf is applied to the terminals of an antenna A and the current measured at the terminals of another antenna B, then an equal current (in both amplitude and phase) will be obtained at the terminals of antenna A if the same emf is applied to the terminals of antenna B." (p.411) **Fig. 1** provides a graphic representation of the terms of the theorem.

Fig. 1



Carson's Formulation of the Reciprocity Theorem

Kraus goes on to note some of the limiting conditions in which the theorem applies. Of course, the frequency of the applied emf (or voltage) must be the same, and the media must be "linear, passive and also isotropic." For our purposes in evaluating whether NEC honors reciprocity, the following note is critical: "An important consequence of this theorem is the fact that under these conditions the transmitting and receiving patterns of an antenna are the same."

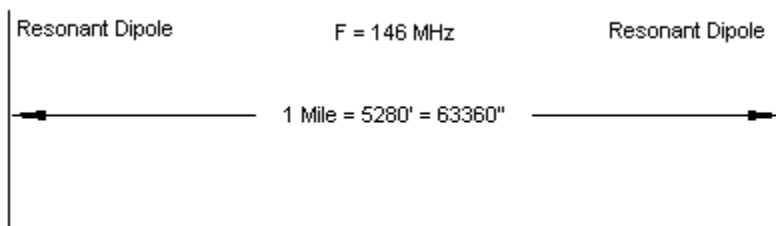
Kraus' statement gave us something that we could test and demonstrate within NEC, as we did in episodes 88 and 121 of this series. By using plane wave excitation (EX1) and checking the current magnitude at the wire segment that would serve as the source in a transmitted pattern, we were able to develop a receiving pattern. When we normalize both the transmit and the receive patterns, they formed a virtually perfect overlay. However, the demonstration required us to use portions of the NEC command set that are not generally available in entry-level software, such as basic EZNEC and NEC-Win Plus. These programs generally require us to use a voltage source (or an indirect current source) and they yield transmit patterns, that is, far-field data.

The question for this episode is whether we can achieve the same goal of demonstrating reciprocity within NEC using only the tools generally available in entry-level software. With a little ingenuity, we can arrive at comparable results. In the process, we may also come to appreciate better the terms of reciprocity within NEC calculations.

## Home on the Range with Dipoles in Free Space

We may model the Carson version of the reciprocity theorem simply by using two antennas and separating them by a considerable distance. Our basic models will use a number of simplifying conditions to prevent potential confusions introduced by intervening variables. For example, we shall use lossless or perfect wire in the models. Our first examples will use a free-space environment so that ground reflections and losses do not play a role in the development of data. Because the frequency is convenient for later purposes, we shall set the test antennas at 146 MHz, although any frequency will do as well. The initial two test antennas will be resonant (technically, near-resonant) dipoles. Each dipole is 38.3" long with a 0.1875" diameter. So long as the distance between the dipoles places them in the far field of each other, it would be adequate. Arbitrarily, I selected a distance of 1 mile (5280', 63360", 1609.344 m, 783.7366 wavelengths). Distance will affect the numbers that we gather, but not the principles involved. **Fig. 2** shows the general outline of the modeling set-up.

Fig. 2



The First-Stage Test Model

The following model in ASCII format shows the basic set-up. The dimensions are in meters.

```
CM dpl-dpl 1 mile fs
CE
GW 1,21,0.,-.48641,0.,0.,.48641,0.,.0023813
GW 2,21,1609.344,-.48641,0.,1609.344,.48641,0.,.0023813
GE 0
FR 0,1,0,0,146.
GN -1
EX 0,1,11,0,200,0.
RP 0,1,361,1000,90.,0.,0.,1.,0.
EN
```

For reference only, **Fig. 3** shows the dipole pattern. The analysis panel provides the transmit performance data with one exception. The source impedance is  $71.941 + j0.515$  Ohms. Both antennas shown in **Fig. 2** will be identical dipoles. As the pattern suggests, the NEC runs occurred on NSI software, specifically GNEC and NEC-4. However, for this and all following steps, any version of NEC will do.

Reference Free-Space  
E-Plane Pattern:  
Dipole

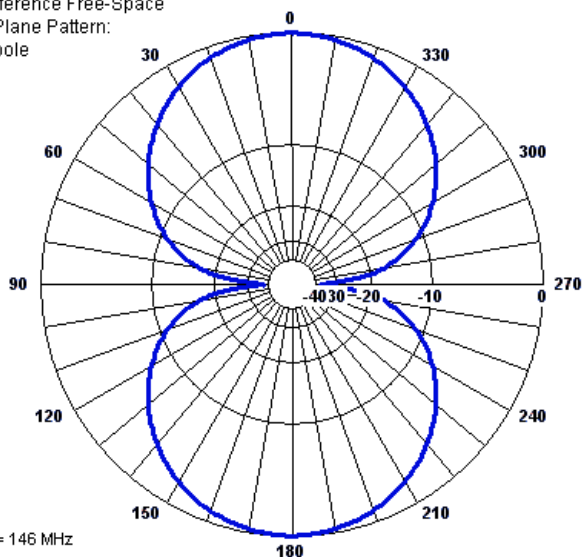


Fig. 3

### Pattern Analysis

#### Max Gain (Front)

Gain = 2.13 dB (0.0 dB)

Phi = 0 Deg

#### Gain (Back)

Gain = 2.13 dB (0 dB)

Phi = 180 Deg

#### -3dB (Left of Max)

Gain = -1. dB (-3.13 dB)

Phi = 40 Deg

#### -3dB (Right of Max)

Gain = -1. dB (-3.13 dB)

Phi = 320 Deg

#### 3 dB BeamWidth

80 Deg

#### Front/Back Ratio

0 dB

The transmit pattern is only background information for our real goal, the reading of the reported current on the center segment of the un-excited dipole. In terms of the model shown, we shall be interested in GW 2, segment 11. The NEC output report provides a table of current values for each segment within a model (unless the user selects a specific command to suppress printing them). We shall be using data for which most NEC implementations do not provide graphing capabilities, so we may expect to use alternative means to present the information.

*Special Note about EZNEC:* NEC makes use of input and output voltage and current peak values. EZNEC uses RMS values for

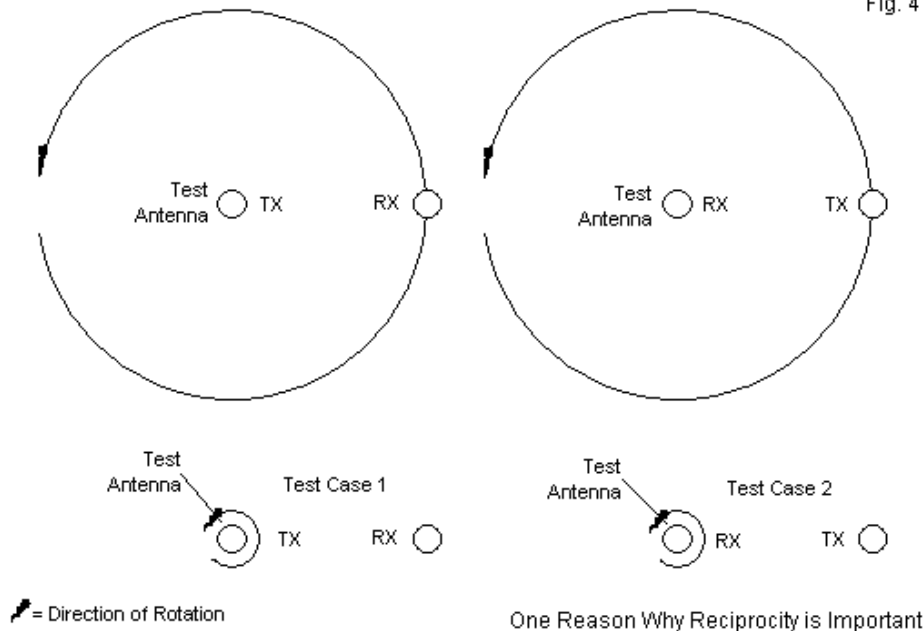
input and output voltages and currents. If we assign a specific numeric voltage value to an EZNEC source, we shall receive a certain numeric value for any segment current in its current table. These numeric values will coincide with those that NEC produces in other software if we remember that EZNEC up-converts to peak value at the start of the core run and then down-converts back to RMS in its output files.

We are now prepared to look at some interesting cases involving reciprocity.

### *Assessing the Receiving Pattern Shape*

In our initial notes on reciprocity, we noted that Stutzman and Thiele defer their account until late in the text, specifically in a chapter devoted to antenna testing and measurement. If reciprocity is correct, then we may test an antenna on a proper range using any of the 4 systems shown in **Fig. 4**. The top two versions of the test are complex and inconvenient. However, a version of the system at the upper left is commonly used with fixed broadcast towers by taking periodic field-strength readings at ground level and specified distances from the installation. The lower two versions of the test are more common for range tests used by manufacturers.

Fig. 4



We may evaluate the pattern of the dipoles in the model shown earlier by rotating either the excited or the un-excited antenna in useful increments. In fact, we may do both in succession and compare results. We might use 10-degree increments and confine the range of rotation to 90 degrees, since we expect two orders of symmetry in the pattern. A range would likely rotate one of the antennas through a complete cycle and perhaps trace the pattern continuously rather than using our stepped procedure.

Since the two antennas are 1 mile apart in the model, I have arbitrarily raised the excitation voltage to 200 V pk, or a power level of 278 watts. (We shall shortly examine the question of the source voltage.) For pattern evaluation, we need not concern ourselves with the fact that the receiving antenna does not have a load that represents the feedpoint impedance. Instead, we shall concern ourselves with accurately rotating each antenna (in turn) in 10-degree increments and recording the magnitude and phase of the current on the center segment of the receiving antenna. **Table 1** records the results of our rotational tests. NEC, of course, reports using engineering notation to maximize the number of significant digits in the smallest possible printing space. Indeed, an 8-unit printing space for any report value is standard in NEC tables.

Dipole-Dipole-Free-Space			Table 1		
	XMT Rotates		RCV Rotates		
Rotation	Current		Current		
Angle	Mag	Phase	Mag	Phase	
0	9.2326E-04	-3.117	9.2326E-04	-3.117	
10	9.0311E-04	-3.104	9.0311E-04	-3.104	
20	8.4506E-04	-3.066	8.4506E-04	-3.066	
30	7.5567E-04	-3.007	7.5567E-04	-3.007	
40	6.4393E-04	-2.932	6.4393E-04	-2.932	
50	5.1903E-04	-2.849	5.1903E-04	-2.849	
60	3.8860E-04	-2.768	3.8860E-04	-2.768	
70	2.5759E-04	-2.699	2.5759E-04	-2.699	
80	1.2810E-04	-2.653	1.2810E-04	-2.653	
90	3.4709E-07	177.089	3.4709E-07	177.091	
Notes:	Excitation voltage 200				
	0-degrees = broadside to the other antenna				
	Non-rotating antenna is broadside to the center of the rotating antenna				

As the table shows, it does not matter whether we rotate the transmitting dipole or the receiving dipole, since we obtain identical results in both cases. (The deep null at 90 degrees is the only place where we find a minuscule difference in the calculated phase angle of the current.) The values appear plausible as reflections of the transmit pattern for the dipole. Since appearances may sometimes deceive, we should likely see if we can confirm the actual pattern shape. The pattern in **Fig. 3** is a normalized pattern given in decibels. It has a convenient checkpoint in the pattern analysis information: at 40 degrees, the pattern should show a deficit of 3.13 dB relative to maximum gain.

At this point, we may introduce the only significant external calculation that we need to make throughout these proceedings. We may convert ratios of current into gain values in dB by reference to the following common equation"

$$\text{Gain}_{dB} = 20 \log \left( \frac{I_1}{I_2} \right) = 10 \log \left( \frac{P_1}{P_2} \right)$$

If we let the current at 0 degrees be  $I_1$  and the current at 40 degrees be  $I_2$ , we obtain a gain differential of 3.1297 dB. Since the half-power points coincide between the transmit radiation pattern and the receive patterns using either method of rotation, we can satisfy ourselves that the dipole patterns are the same in both modes of use. If we still have doubts, we may trace the normalized gain of the transmit radiation pattern at 10-degree increments and perform the same calculation at every one of them.

### *Transmit Voltage and Receive Current*

Newer modelers are very often relatively new students to antennas. Therefore, it may be useful to employ the double-dipole range model in a second way. Let's allow the two dipoles to face each other, that is, be broadside to broadside. In this test or demonstration, we shall be paying close attention to the terms in which Carson expresses reciprocity: "If an emf is applied to the terminals of an antenna A and the current measured at the terminals of another antenna B, then an equal current (in both

amplitude and phase) will be obtained at the terminals of antenna A if the same emf is applied to the terminals of antenna B."

A common misunderstanding of antennas is that the current at the receiving antenna will be proportional to the power applied to the transmit antenna, assuming that we have an unchanging set of antennas in an equally unchanging environment. However, as noted in the reciprocity theorem, the received current, as sampled at the erstwhile feedpoint of the receiving antenna, will be proportional to the feedpoint voltage at the transmitting antenna. Therefore, according to the theorem (and, of course, a good bit of other basic antenna theory), if we halve the transmitting antenna voltage, we should also halve the receiving current. We may measure (or model) the current in two ways. One way is to continue to use no load at the feedpoint segment of the receiving dipole. The other method is to use a matched load on the feedpoint segment. From our transmitting model, we know that the feedpoint impedance is  $72.941 + j0.515$  Ohms. We may introduce this load to the receiving dipole model by adding one line to the model itself. The LD 4 complex load command provides all that we need.

```
CM dpl-dpl 1 mile fs with receiving antenna load
CE
GW 1,21,0.,-.48641,0.,0.,.48641,0.,.0023813
GW 2,21,1609.344,-.48641,0.,1609.344,.48641,0.,.0023813
GE 0
LD 4,2,11,11,71.941,.515
FR 0,1,0,0,146.
GN -1
EX 0,1,11,0,200,0.
RP 0,1,361,1000,90.,0.,0.,1.,0.
EN
```

Let's use source (EX 0) peak voltages of 200, 100, and 50 volts to see what we obtain at the receiving antenna under both conditions. The NEC output file provides the current values as two sets: one pair of values providing real and imaginary numbers, the other pair of values listing the magnitude and phase angle. **Table 2** shows what the model reports.

Dipole-Dipole-Free-Space						Table 2
A. RCV Antenna with No Load						
XMT Ant		RCV Ant				
Epeak	Power	Ireal	Imag	Imag	Iphase	
200	2.7799E+02	9.2190E-04	-5.0199E-05	9.2326E-04	-3.117	
100	6.9490E+01	4.6095E-04	-2.5099E-05	4.6163E-04	-3.117	
50	1.7374E+01	2.3047E-04	-1.2550E-05	2.3082E-04	-3.117	
B. RCV Antenna with 71.941+j0.515-Ohm Load						
XMT Ant		RCV Ant				
Epeak	Power	Ireal	Imag	Imag	Iphase	
200	2.7799E+02	4.6095E-04	-2.5099E-05	4.6163E-04	-3.117	
100	6.9490E+01	2.3047E-04	-1.2550E-05	2.3081E-04	-3.117	
50	1.7374E+01	1.1524E-04	-6.2748E-06	1.1541E-04	-3.117	
Notes:	Epeak = peak excitation voltage at source					
	Receive antenna currents lists as peak values in both real/imaginary terms and in magnitude/phase angle terms					

In my table transcriptions, I have also recorded the NEC report of the antenna input power. For each halving of the source voltage, the resulting power is 1/4 the previous value. In contrast, the receiving current progressions are exactly in step with the applied transmitting voltage. Halving the voltage value produces half the peak current in each of the report columns. Of course, in the model

set-up, proportional changes of the real and imaginary components of the current result in the same phase angle throughout.

In a number of e-mails that I have received regarding test-range models, the writer will inquire whether the receive antenna requires a load. The two sections of the table suggest one sort of answer. Installing a perfect load on the receiving antenna, that is, a load that matches the impedance of the antenna at that segment, results in current values that are exactly 1/2 the values recorded without the load. In this case, we obtained the load value by examining a transmitting version of the model and noting the source impedance. In some cases, one may wish to use a standard load, regardless of the feedpoint impedance. 50 Ohms is a common value. Unless the antenna happens to have a feedpoint impedance of 50 Ohms, expect a different set of current values.

## **Home on the Range with Monopoles over Perfect Ground**

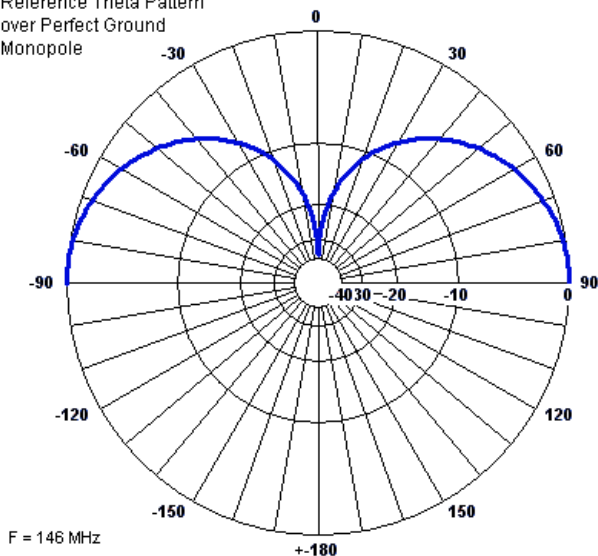
We may replicate the model set-up using monopoles over perfect ground instead of dipoles in free space. Since perfect ground pattern calculations use standard image techniques, we do not create any intervening variables to disturb the basic NEC processes. In fact, we may set up a resonant monopole using the same materials (19.15" of 3/16" diameter lossless wire) that we used for the dipoles. The following lines record a reference monopole in .NEC format.

```
CM monopole perfect ground
CE
GW 1,21,0.,0.,0.,0.,0.,.48641,.0023813
GE 1
FR 0,1,0,0,146.
GN 1
EX 0 1 1 0 200.00000 0.00000
RP 0 181 1 1000 -90 90 1.00000 1.00000
EN
```

**Fig. 5** shows the standard theta radiation pattern, while the side-bar provides most of the reference data that we may need. We may bypass an analysis of the received pattern shape by noting its near identity to one-half of a free-space dipole pattern. If you compare **Fig. 5** to **Fig. 3**, you will find that the half power point is 40 degrees away from the angle of maximum gain in both cases. The reported impedance for the monopole is  $36.146 + j0.833$  Ohms. The value is very close to but not exactly half the dipole value. The dipole feedpoint occurs at the exact center of the antenna. The corresponding point on the monopole would be where the wire intersects ground level ( $Z=0$ ). Since that position is not available, the monopole's feedpoint is on the closest segment (of the 21 segments on the wire) to ground, which places it very slightly off the virtual center point.

Fig. 5

Reference Theta Pattern  
over Perfect Ground  
Monopole



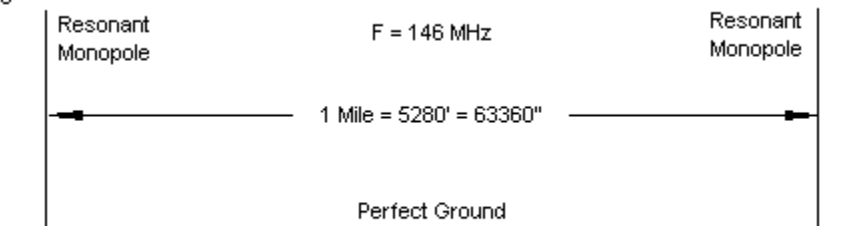
### Pattern Analysis

Max Gain (Front)	Gain = 5.15 dB (0 dB)
Theta = 90 Deg	
Gain (Back)	Gain = 5.15 dB (0 dB)
Theta = -90 Deg	
- 3dB (Left of Max)	Gain = 2.01 dB (-3.133 dB)
Theta = 50 Deg	
- 3dB (Right of Max)	N / A
	N / A
3 dB BeamWidth	N / A
Front/Back Ratio	N / A

## Transmit Voltage and Receive Current

Although we have introduced a perfect ground and shrunk the antennas into monopoles, we may otherwise use the same basic "range" model used for the dipoles. **Fig. 6** outlines its basic dimensions. Since a monopole's phi pattern will be circular, we may ignore the pattern analysis step that we used with the dipole and turn directly to an examination of transmitted voltages and received currents.

Fig. 6



The Monopole Test Model

The test uses the same procedures invoked earlier. We shall begin with no load on the receive monopole feedpoint and later add a matched load of  $36.146 + j0.833$  Ohms. Within each data set, we shall begin with a source voltage of 200 volts peak and reduce it to 100 and then to 50 volts. **Table 3** supplies the data from the NEC output report current tables.

Monopole-Monopole-Perfect Ground						Table 3
A. RCV Antenna with No Load						
XMT Ant		RCV Ant				
Epeak	Power	Ireal	Imag	Imag	Iphase	
200	5.5302E+02	1.8306E-03	-1.5338E-04	1.8370E-03	-4.789	
100	1.3825E+02	9.1530E-04	-7.6689E-05	9.1851E-04	-4.789	
50	3.4564E+01	4.5765E-04	-3.8344E-05	4.5925E-04	-4.789	
B. RCV Antenna with 71.941+j0.515-Ohm Load						
XMT Ant		RCV Ant				
Epeak	Power	Ireal	Imag	Imag	Iphase	
200	5.5302E+02	9.1530E-04	-7.6694E-05	9.1851E-04	-4.790	
100	1.3825E+02	4.5765E-04	-3.8347E-05	4.5925E-04	-4.790	
50	3.4564E+01	2.2883E-04	-1.9174E-05	2.2963E-04	-4.790	
Notes:	Epeak = peak excitation voltage at source					
	Receive antenna currents lists as peak values in both real/imaginary terms and in magnitude/phase angle terms					

Based upon our dipole tests, the monopole data meets our emerging expectations. Halving the transmit antenna source voltage halves the receive antenna's feedpoint current. Because we are using only a finite number of decimal places in the calculation steps, we notice a very tiny numerical difference between corresponding steps in the I-imaginary column, just enough to change the phase angle by 0.001 degree.

### *Dipole vs. Monopole Gain*

If we refer to the standard radiation patterns, we note that the monopole maximum gain is 3 dB greater than the maximum gain of the dipole in free space due to the addition of ground reflections as

simulated by image calculation techniques. We may fairly ask if we can find the same gain in the receiving current data.

The answer is affirmative if we do not leap directly into comparing the two receiving antennas in terms of the reported currents converted into dB values. Each current report occurs with reference to a particular feedpoint impedance. Therefore, we should first convert corresponding dipole and monopole current readings into power levels and then use the power version of the gain equation. Let's use the current magnitude values for a 200-volt source and a matched load in each case. The quick hand-calculator steps would have the following appearance.

$$P1 = I^2 R = (9.1530e-4)^2 * 36.146 = 3.0282e-5$$

$$P2 = I^2 R = (4.6095e-4)^2 * 71.941 = 1.5286e-5$$

$$\text{Gain} = 10 \log(P1/P2) = 10 \log(1.9811) = 2.969 \text{ dB}$$

The monopole over perfect ground (ignoring the slight difference in the current phase angles) has a 3-dB gain over the free-space dipole.

## More Complex Patterns

In the preceding episode of this series, we compared the transmit and receive patterns of a 6-element Yagi using a standard transmit format (EX 0 and RP 0 commands) followed by a normalized receive pattern created by using an EX 1 and a PT 3 command. The final step in our range-test exercise will be to see whether we

can replicate the results using transmit and receive patterns that substitute for the plane-wave excitation.

The first step is to re-create the 6-element Yagi used in the preceding episode.

```
CM 6-el 2M Yagi
CE
GW 1,21,-.6885686,.514604,0.,-.6885686,-.514604,0.,.0023813
GW 2,21,-.4312666,.5075174,0.,-.4312666,-.5075174,0.,.0023813
GW 3,21,-.3247898,.4746752,0.,-.3247898,-.4746752,0.,.0023813
GW 4,21,-.0300482,.461137,0.,-.0300482,-.461137,0.,.0023813
GW 5,21,.2583942,.461137,0.,.2583942,-.461137,0.,.0023813
GW 6,21,.6885684,.443992,0.,.6885684,-.443992,0.,.0023813
GE 0
FR 0,1,0,0,146.
GN -1
EX 0,2,11,0,1,0.
RP 0,1,361,1000,90.,0.,0.,1.,0.
EN
```

**Fig. 7** shows the Yagi pattern using the normal EX 0 and RP 0 combination of commands. The gain is 10.29 dBi. The Yagi provides us with more than one check point for verifying that the receive pattern is the same as the transmit pattern without resorting to developing an external polar plot. The 180-degree front-to-back ratio is 35.98 dB. Not shown in the analysis is the worst-case front-to-back ratio (which may also be called the front-to-sidelobe ratio). The reported value is 24.28 dB. Finally, we have the half-power or 3-dB point at 27 degrees from the main forward lobe heading. For reference, the feedpoint or source impedance is  $50.00 + j9.53$  Ohms.

Reference Free-Space  
E-Plane Pattern  
6-Element Yagi

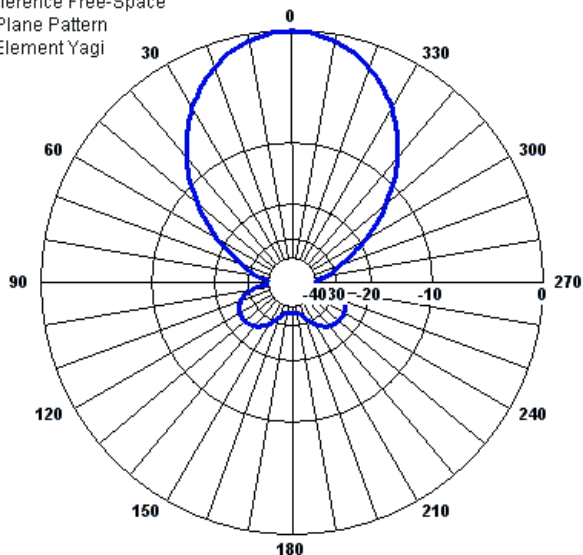


Fig. 7

#### Pattern Analysis

##### Max Gain (Front)

Gain = 10.29 dB (0.0 dB)

Phi = 0 Deg

##### Gain (Back)

Gain = -25.69 dB (-35.986 dB)

Phi = 180 Deg

##### - 3dB (Left of Max)

Gain = 7.14 dB (-3.150001)

Phi = 27 Deg

##### - 3dB (Right of Max)

Gain = 7.14 dB (-3.150001)

Phi = 333 Deg

##### 3 dB BeamWidth

54 Deg

##### Front/Back Ratio

35.986 dB

### Assessing the Receiving Pattern Shape

To evaluate the receiving pattern shape, we shall create a free-space range set-up identical to the one that we used for the dipole. The Yagi and the other range antenna (a dipole) will be 1 mile apart. We shall rotate the Yagi by adding a convenient GM command to the .NEC-format input or model file. However, entry-level software provides external convenient rotating means. The following model is one of two that we shall use.

```

CM 6-el 2M Yagi and dipole
CE
GW 1,21,-.6885686,.514604,0,-.6885686,-.514604,0,,.0023813
GW 2,21,-.4312666,.5075174,0,-.4312666,-.5075174,0,,.0023813
GW 3,21,-.3247898,.4746752,0,-.3247898,-.4746752,0,,.0023813
GW 4,21,-.0300482,.461137,0,-.0300482,-.461137,0,,.0023813
GW 5,21,.2583942,-.461137,0,.2583942,-.461137,0,,.0023813
GW 6,21,.6885684,.443992,0,.6885684,-.443992,0,,.0023813
GM 0 0 0 0 0 0 0 0 1 1 6 21
GW 7,21,1609.344,-.48641,0,1609.344,.48641,0,,.0023813
GE 0
FR 0,1,0,0,146.
LD 4 7 11 11 71.941 0.515
GN -1
EX 0 2 11 0 200.00000 0.00000
RP 0,1,361,1000,90.,0.,0.,1.,0.
EN

```

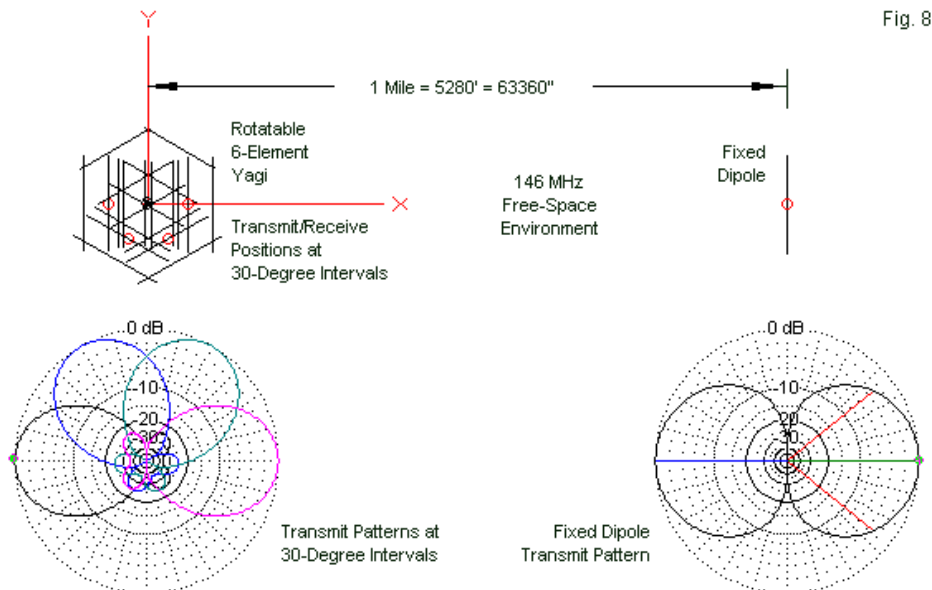
The dipole is GW 7. The GM line above it rotates the Yagi by changing the 00 entry to a number of degrees. We shall use 10-degree increments. However, since the Yagi pattern is symmetrical along only 1 axis, we shall work from 0 to 180 degrees. As we did in the case of the dipole, we shall use a 200 volt (peak) source voltage.

The EX 0 command shows that the source is on wire 2 of the Yagi. Note that the LD 4 command places a matched load on the dipole, where we derive the load value from the source impedance of the dipole in a transmit set-up ( $71.94 + j0.52$  Ohms). We read the current from the segment specified by the load. The alternative situation is to place the source on the dipole (wire 7, segment 11), and move the load to the Yagi (wire 2, segment 11). When we move the load, we also change its value to the Yagi matched value of  $50.00 + j9.53$  Ohms.

Rotating Antennas			146 MHz	Table 4
Rotating 6-Element Yagi			Free Space	
Fixed Dipole			XMT voltage: 200 pk	
	Yagi XMT		Dpl XMT	
	Dpl RCV: Ld=71.94+j0.52		Yagi RCV: Ld=50.00+j9.53	
Phi	Current		Current	
Heading	Mag.	Phase	Mag.	Phase
0	1.3916E-03	-6.54	1.3928E-03	-6.54
10	1.3265E-03	-6.93	1.3276E-03	-6.93
20	1.1450E-03	-8.20	1.1458E-03	-8.20
30	8.8510E-04	-10.71	8.8566E-04	-10.71
40	6.0009E-04	-15.27	6.0040E-04	-15.27
50	3.4455E-04	-23.74	3.4469E-04	-23.74
60	1.6003E-04	-41.18	1.6009E-04	-41.17
70	6.4659E-05	-79.69	6.4665E-05	-79.67
80	3.1354E-05	-128.53	3.1345E-05	-128.52
90	9.2492E-08	38.01	9.2523E-08	38.00
100	3.7560E-05	5.50	3.7556E-05	5.48
110	6.7247E-05	-9.83	6.7256E-05	-9.85
120	8.2529E-05	-24.91	8.2561E-05	-24.92
130	8.4217E-05	-38.99	8.4272E-05	-39.00
140	7.4359E-05	-49.58	7.4426E-05	-49.59
150	5.5181E-05	-53.17	5.5247E-05	-53.18
160	3.3355E-05	-42.32	3.3411E-05	-42.34
170	2.2095E-05	-6.98	2.2135E-05	-7.05
180	2.2169E-05	13.58	2.2226E-05	13.45
Note:	Yagi always rotates; dipole is fixed broadside to the Yagi position.			

**Table 4** records the data from the two runs. In both cases, we rotate the Yagi. However, the left data columns record the current

on the dipole feedpoint when the Yagi transmits. The right data columns record the current at the Yagi feedpoint when the dipole transmits. **Fig. 8** shows the general scheme of what the pattern assessment demonstrates.



NEC Modeling of a Test-Range in Free Space with Reversible Transmit-Receive Functions

The first notable fact about the demonstration data is the virtual identity of the received current values using the same source excitation voltage, regardless of which antenna transmits and which receives. We may also note that the current at 180 degrees is slightly higher than the current at 170 degrees, which corresponds

to a slight rearward increase in transmit gain at 180 degrees for the Yagi when modeled alone.

However, to confirm that the pattern in the receive mode on the range test coincides with the standard transmit pattern of **Fig. 7**, we need further check points. We may apply the same sort of gain calculations that we used with the dipole, but more points of reference on the pattern. For example, we may compare the maximum current at zero degrees with the current at 180 degrees to see if the value coincides with the front-to-back ratio. As well, we may perform the same calculation with respect to the front-to-sidelobe (or worst-case front-to-back ratio). In this case, the heading of the standard value is 126 degrees, so we may use the closest recorded heading, 130 degrees. Finally, as we did for the dipole, we may bracket the half-power points using the values at 20 and 30 degrees for the 27-degree heading of the half-power point. Moreover, we may use either set of currents--or both for the sake of demonstration. **Table 5** shows the results of the calculations.

Antenna Tests vs. Radiation Pattern Data			
Test	180-Degree Front-to-Back Ratio		
Rad Pat		35.98	dB
Yag XMT		35.96	
Dpl XMT		35.94	
Test	Front-to-Sidelobe Ratio		
Rad Pat	126 deg	24.28	dB
Yag XMT	130 deg	24.36	
Dpl XMT	130 deg	24.36	
Test	Half-Power Point		
Rad Pat	27 deg	3.15	dB
Yag XMT	20 deg	1.69	
	30deg	3.93	
Dpl XMT	20 deg	1.70	
	30 deg	3.93	
Rad Pat = NEC radiation pattern data			
Yag XMT = Yagi transmits, dipole receives			
Dpl XMT = Dipole transmits, Yagi receives			
See Fig. 7 for radiation pattern and data.			
			Table 5

The result show that the range set-up not only confirms that NEC honors reciprocity, but as well, that range testing is in principle a reliable way to determine that shape and relative strength of an antenna pattern. Of course, range testing was in use long before NEC was born, but we have nearly a generation of antenna modelers who may never have seen an antenna test range in operation. Hence, the NEC demonstration provides a means for a

modeler to teach himself or herself what range testing involves--minus certain intervening variables, of course.

### Yagi Forward Gain

All that we lack to complete the data--at least as far as this simplified demonstration goes--is the forward gain of the Yagi. We have already compared the gain of a dipole in free space to a monopole over ground. We may apply the same procedures to comparing a free-space dipole to a Yagi when both are in free space. **Fig. 9** shows the model set-ups.

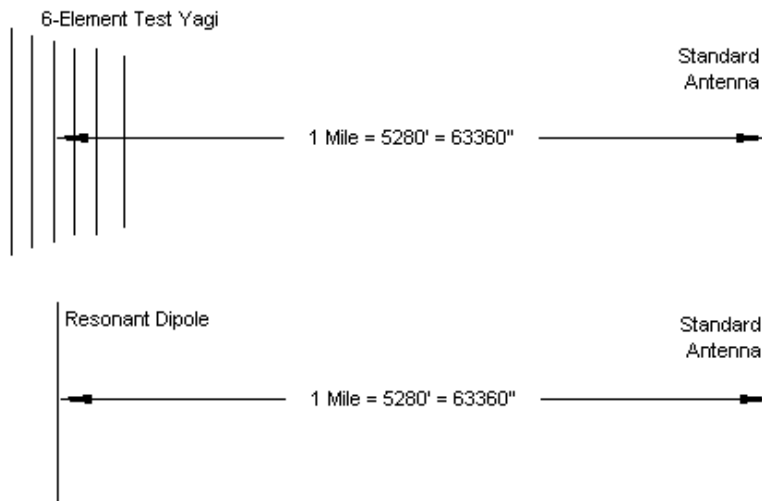


Fig. 9

Using a Reference Antenna to Obtain a Forward-Gain Value

We already have the necessary data for both the dipole and the Yagi when both test set-ups use the same excitation voltage. Since the antennas have different impedances, we cannot simply compare current data. However, by using the current and impedance information together, we can obtain appropriate power values and then use the dB-conversion equation to obtain the gain of the Yagi over the dipole. The following calculation uses data for a 200-volt source.

$$\begin{aligned}P_1 &= I^2 R = (1.3928e-3)^2 * 50.003 = 9.7000e-5 \\P_2 &= I^2 R = (4.6163e-4)^2 * 71.941 = 1.5331e-5 \\Gain &= 10 \log(P_1/P_2) = 10 \log(6.3272) = 8.012 \text{ dB}\end{aligned}$$

These calculations are slightly simplified in view of the relatively small phase angles involved. However, the Yagi shows a gain of about 8.0 dBd(r), that is, 8.0 dB over a dipole under identical range conditions.

## Conclusion

These small and simple demonstrations illustrate several facets of modeling of which the beginning modeler may not be aware. First, they show that one may model reciprocity without requiring plane-wave excitation and receive patterns. The methods used here make use only of the facilities available on the most basic entry-level software.

Second, if we approach antennas--as so many amateur radio operators do--without a thorough grounding in antenna basics, we

may use NEC software to teach ourselves various fundamental principles. In this instance, we have explored the terms of the reciprocity theorem at a practical level. (College texts can provide additional grounding at a level that is even more fundamental.)

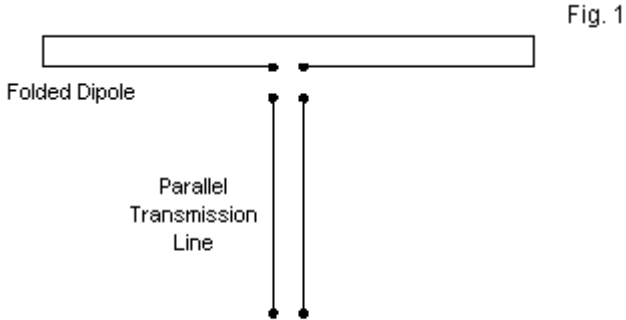
Third, we may also look at modeling as an analog to range testing when we correctly set up a model. Moreover, we may expand the range-testing set-up to examine the effects of structures on antenna patterns, correlating the currents in such an intervening structure to the modifications it may make in a radiation pattern without the structure.

Our little exercise that began in seeming pursuit of reciprocity has had much to teach us about antennas and antenna modeling that extends far beyond reciprocity itself.

## Chapter 123: Radiating and Transmission-Line Currents

In episode 100 of this series, we examined the modeling work-around often used to test a coaxial-cable-fed antenna for common mode currents. However, we seem to have no comparable work-around for detecting common-mode currents when we use parallel transmission lines. In fact, the help screens that accompany EZNEC record the following statement: "I don't know of any way to accurately model common-mode effects on a two-wire transmission line (that is, how to model a radiating two-wire line). If it's necessary to do this, the line will have to be modeled as two parallel wires."

Interestingly, if we model a resonant dipole and a resonant folded dipole at the same frequency, we may examine the current tables and discover that the current magnitudes and phase angles that we encounter seem to have very little in common. We can perform the same test with a folded monopole and a single-wire monopole. The results will be the same. Both of the single-wire antennas will show a near-cosine-wave decrease in current magnitude as we move from the feedpoint to the wire end, and the phase angle will change by only a few degrees. The folded versions show current values very different from the single-wire models.



What Do These Items Have in Common?

**Fig. 1** shows the physical arrangement of both the parallel transmission line and the folded dipole. It also raises the question of what these two structures have in common, besides the parallel wires, of course. The answer is quite straightforward. The currents that we record in models are actually composites of two types of currents. Because we have closely spaced wires that form transmission lines in both cases, we should expect to find transmission-line currents ( $I_T$ ). At any selected pair of point directly opposite each other along the line-pair, we should find current magnitudes that are equal, but with phase components that are 180 degrees opposite.

If the current values that we record in our model (assuming a reasonably well constructed model) do not meet this condition, then we also have radiation currents ( $I_R$ ). Radiation currents have the same phase angle on both wires. When we encounter them on the antenna structure proper, such as along a folded dipole, we find the

currents that are effective in making the wire structure an antenna. When we encounter them on a parallel transmission line, we usually (but not always) groan, since we generally do not wish our feedlines to radiate. As well, such currents, unless remediated, can create a number of problems at the equipment end of the feedline. Under these conditions, we tend to call radiation currents by a different name: common-mode currents. However, we are still talking about radiation currents.

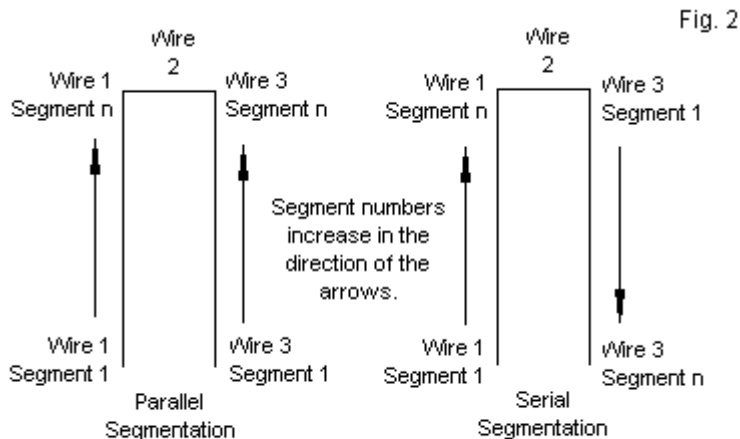
The radiation currents that we find on parallel transmission lines are the same as the currents that we sometimes find on the outer surface of the outer conductor in a coaxial cable. However, skin effect gives transmission-line and radiation currents separate paths in a coaxial cable. This condition also changes the methods of remediation or control of those currents, since we may introduce methods of attenuating the common-mode currents without affecting the transmission-line currents. When we have a parallel transmission line, we have difficulty sorting out the two types of currents, let alone attenuating one type without affecting the other type. Antenna models that create parallel transmission lines using wires will record only the composite current values.

## **Externally Calculating Radiation and Transmission-Line Currents**

As much as we might wish our NEC and MININEC software to perform all antenna and feedline calculations for us, there are many useful calculations that we must perform externally to the core computations. Some are so widely used that those who implement

NEC and MININEC often include them in their packages. Typical examples are the SWR calculations on which we rely. Some packages also include the calculation of the left-hand and right-hand components of circular polarization. Both of these calculations are further derivations from the output results of the core and not performed by the core itself.

No package (to my knowledge) includes the calculation of transmission-line and radiation (common-mode) currents as a post-core facility. Therefore, if we wish to separate the two current components of parallel wires--whether as part of the antenna or as part of a modeled transmission line--we shall have to set up a spreadsheet or similar calculating convenience. The technique that we shall use derives from the account of "The Hairpin Monopole" in Kuecken's classic *Antennas and Transmission Lines*, pp. 224 ff. We shall have to modify the procedure to coincide with the way in which we set up the parallel wires in a model.



Wire Segment Organization Makes a Difference  
to Radiation and Transmission-Line Current Calculations

**Fig. 2** shows the two possibilities. On the left we have the procedure that I have arbitrarily called parallel segmentation. In this case, we start each of the parallel wires at some coordinate and move both wires in steps either down-up or left-right. The alternative modeling convention, on the right in the figure, we can call serial segmentation. In this case, we tend to create wires "around the horn," so that end 2 of each wire in the model coincides with end 1 of the succeeding wire.

If we model a simple structure, say a folded monopole over perfect ground, we may view the relative current magnitudes, as shown in **Fig. 3**. Viewing current magnitude alone will yield no differences in the portrait under each of the modeling alternatives. The only

significant difference between the current tables for the alternative modeling conventions would appear in column that lists the current phase angle.

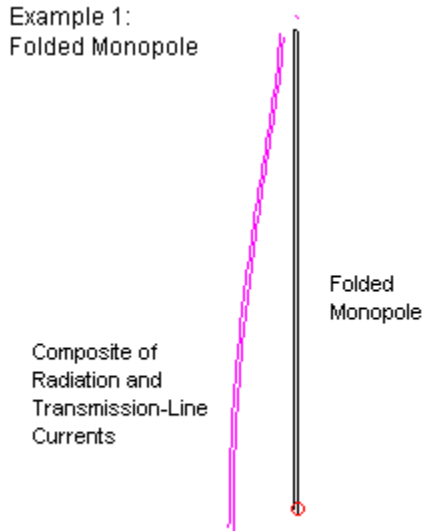
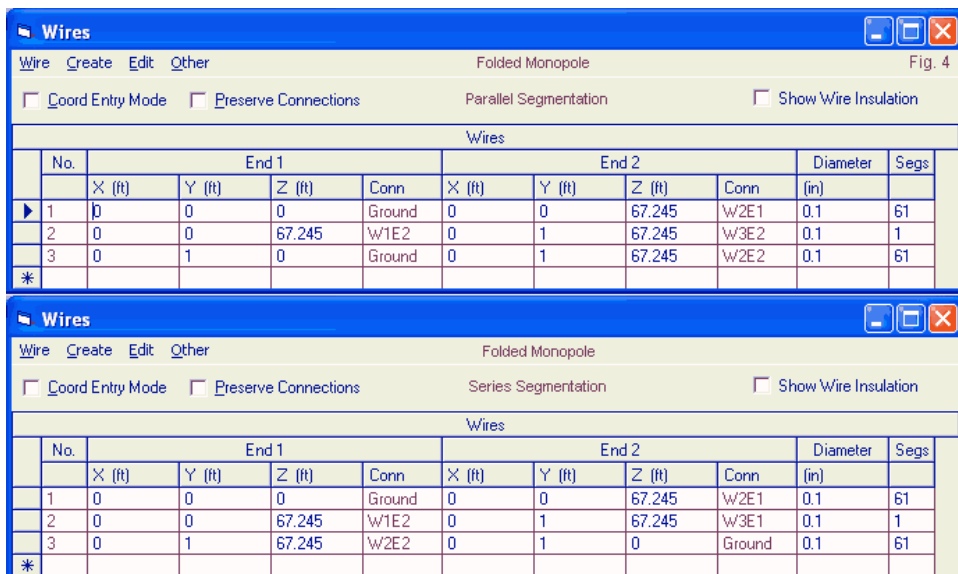


Fig. 3

To determine which of the following procedures that we should use, we must rely on the list of wires in the model. **Fig. 4** shows the alternative wire tables that we obtain by each method, using our simple folded monopole over perfect ground. The tables come from EZNEC software.



In the following notes, I shall present the requirements for setting up a calculation aid in rather more detail than required by engineers. However, many newer models, including radio amateurs, are keenly interested in radiation and common-mode currents. Hence, a little extra guidance is in order.

### *The Calculations for Parallel Segmentation*

When we use a parallel-segmentation structure for parallel wires within an antenna element or a modeled transmission line, we begin with the basic relationship of the currents on the two wires (A and B) at any facing point along the parallel line.

$$I_A = I_R + I_T \quad I_B = I_R - I_T$$

With the lines segmented in parallel, the current on line A is the sum of the radiation and the transmission-line currents. The current on line B is the difference of the two currents, with the transmission-line current subtracted from the radiation current. (When we use series segmentation, these basic conditions will change, as will everything past this starting point.) Using this starting point, we can derive simple equations for  $I_R$  and  $I_T$ .

$$I_R = \frac{I_A + I_B}{2} \quad I_T = \frac{I_A - I_B}{2}$$

These equations are deceptively simple, since they do not take into account that the currents we encounter on each wire at facing points have a magnitude and a phase angle. Many current tables made available to the software user will provide only the current magnitude and phase. The NEC and MININEC output tables provide the current information in this form and as a pair of real and imaginary components. We shall need the components in further steps. If the available current table does not provide them, we can easily derive the values.

$$I_{REAL} = \cos I_P \cdot I_M \quad I_{MAG} = \sin I_P \cdot I_M$$

Suppose that we have a current magnitude of 1.0 at 30 degrees. Then the real component will be 0.866 and the imaginary

component will be 0.5. (We shall assume that the units of measure derive from whatever source your software provides.)

We are looking for the magnitude and phase angle of the radiation current and of the transmission current. Once we have found the components of the original values on wires A and B, we can combine them and derive a current magnitude.

$$I_R = \frac{\sqrt{(I_{A-REAL} + I_{B-REAL})^2 + (I_{A-IMAG} + I_{B-IMAG})^2}}{2}$$

Since  $I_R$  involves the addition of components, we add the real and then the imaginary component values and then obtain the magnitude by taking the square root of the sum of the squares, finally dividing by 2 to obtain the final value. Obtaining  $I_T$  involves taking differences, so the equation appears in the following form.

$$I_T = \frac{\sqrt{(I_{A-REAL} - I_{B-REAL})^2 + (I_{A-IMAG} - I_{B-IMAG})^2}}{2}$$

If we wish to know the phase angle of the currents that we just calculated, we use the following equations:

$$I_{R-PHASE} = \tan^{-1} \frac{I_{A-IMAG} + I_{B-IMAG}}{I_{A-REAL} + I_{B-REAL}}$$

$$I_{T-PHASE} = \tan^{-1} \frac{I_{A-IMAG} - I_{B-IMAG}}{I_{R-REAL} - I_{B-REAL}}$$

Many spreadsheets only perform trig calculations using radians. Therefore, when obtaining the real and imaginary components of the initial current magnitude and phase, you may have to convert the phase into radians before taking a sine or cosine value. Likewise, the final two equations may return their results in radians, and you may have to convert into degrees (unless you habitually work with radians).

Before we examine what we obtain for our efforts in setting up a calculation aid, let's set out the calculations for the alternative modeling convention.

### *The Calculations for Series Segmentation*

When we model parallel wires serially, our first caution will be to count segments carefully so that we specify exactly facing segments for Wire A and Wire B at any calculation point. If the segments do not exactly align, the calculations will be worthless.

When we model parallel wires in a serial fashion, the basic terms of the current on the two wires change. The change results from the changes in the phase angle of the currents on one of the two wires.

$$I_A = I_T + I_R \quad I_B = I_T - I_R$$

Under these conditions, the derived values for  $I_T$  and  $I_R$  will also change. Note that which current sums the wire currents and which current takes their difference have reversed relative to parallel segmentation.

$$I_T = \frac{I_A + I_B}{2} \quad I_R = \frac{I_A - I_B}{2}$$

Once we have gone this far, the remainder of the calculation-aid set-up is similar to the procedures for parallel segmentation. Obtaining real and imaginary components for the current magnitudes and phase angles in Wires A and B is identical. In the calculation of  $I_R$  and  $I_T$ , we simply reverse the equations shown. The same cautions about spreadsheet conventions apply to serial segmentation.

## A Few Worked Examples

We may look at a few examples of the analysis in action both to test one model set-up against the other and to see if the results make good sense.

### *The Folded Monopole*

In **Fig. 3** and **Fig. 4**, we saw the outlines of a folded monopole for 3.5 MHz. The model uses perfect ground for simplicity--a real ground would have required a radial system. Our interest in the model lies in the currents along the two wires. From the relative

current magnitude graph, we can see that the current level does not go to zero at the tip of the antenna, a phenomenon that we would expect of a single-wire monopole.

Folded Monopole: 3.5 MHz, perfect wire, perfect ground									Table 1
0.1" dia. perfect wire, 1" separation, 67.245', 61 segments									
Parallel Segmentation									
	Wire 1		Wire 2		Radiating Currents		Trans-Line Currents		
Segment	Imag	Phase	Imag	Phase	I-mag	I-phase	I-mag	I-phase	
1	1.0000	0.00	1.0004	1.82	1.0001	0.91	0.0159	-89.83	
11	0.9702	-4.71	0.9685	3.37	0.9669	-0.67	0.0683	-89.97	
21	0.8871	-9.30	0.8801	5.90	0.8759	-1.73	0.1169	-90.00	
31	0.7550	-14.68	0.7411	9.76	0.7311	-2.57	0.1585	89.99	
41	0.5821	-22.35	0.5617	16.50	0.5393	-3.29	0.1904	89.98	
51	0.3850	-37.06	0.3613	31.70	0.3080	-3.92	0.2109	89.97	
61	0.2236	-81.67	0.2186	81.42	0.0326	-4.49	0.2187	89.97	
Series Segmentation									
	Wire 1		Wire 2		Radiating Currents		Trans-Line Currents		
Segment	Imag	Phase	Imag	Phase	I-mag	I-phase	I-mag	I-phase	
1	1.0000	0.00	1.0004	-178.20	1.0001	0.90	0.0157	-89.85	
11	0.9702	-4.71	0.9686	-176.60	0.9670	-0.66	0.0686	-89.98	
21	0.8871	-9.30	0.8801	-174.10	0.8833	-1.73	0.1169	-90.00	
31	0.7550	-14.68	0.7412	-170.20	0.7311	-2.55	0.1587	89.99	
41	0.5821	-22.35	0.5617	-163.50	0.5394	-3.29	0.1904	89.97	
51	0.3850	-37.06	0.3614	-148.30	0.3081	-3.92	0.2110	89.96	
61	0.2236	-81.67	0.2186	-98.59	0.0326	-4.48	0.2187	89.97	

**Table 1** provides the results of a spreadsheet calculating aid. The two parts of the table show the results for both parallel and series segmentation conventions. In both cases, the reported current values at 10-segment intervals along Wire 1 of the pair (ignoring the short end wire) are the same. In the column labeled Wire 2, we find virtually identical reports of current magnitude. However, the phase angles of these currents are very different, in fact, 180

degrees different. The phase angle difference forces the change in the basic conditions and progression of calculations.

When we use the correct progression of calculations for the model set-up, we obtain virtually identical values for both the radiation and the transmission line currents. We may note in passing that the transmission-line current phase angles are about 90 degrees out of phase with the radiation currents. However, the phase values may change from + to - and back again depending upon the exact relationship between the currents on facing positions on the monopole. Folded dipole transmission-line currents will exhibit similar shifts.

The folded monopole was resonant at the length shown in the wire table. In the radiation current magnitude columns, we note a very low value that is consistent with the fact that the sampling point is not precisely at the tip of the antenna, but inboard by virtually 6". To see if the radiation currents coincided with those we might expect from a single-wire monopole, I constructed two single-wire monopoles. One used the same length as the folded monopole and increased the diameter (to 2.7") to achieve resonance. The second used the same wire diameter as each wire in the folded monopole and increased the length to achieve resonance. **Table 2** shows the radiating currents of all three models. Of course, for the single-wire monopoles, the radiating current level is the NEC report of the current on the prescribed segment.

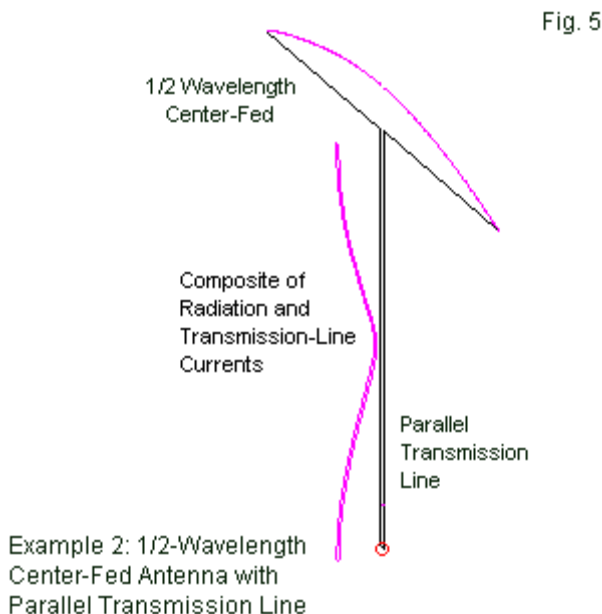
Monopoles vs. Folded Monopole Radiating Currents						Table 2		
Monopoles: 3.5 MHz, perfect wire, perfect ground			Folded Monopole Radiating Currents					
2.7" dia, 67.245', 61 segments			0.1" dia, 68.45', 61 segments			0.1" dia, perfect wire, 1" separation, 67.245', 61 segments		
Segment	I-mag	I-phase	Segment	I-mag	I-phase	Segment	I-mag	I-phase
1	1.0000	0	1	1.0000	0	1	1.0001	0.91
11	0.9675	-1.84	11	0.9658	-1.01	11	0.9669	-0.67
21	0.8770	-3.01	21	0.8712	-1.74	21	0.8759	-1.73
31	0.7327	-3.93	31	0.7214	-2.33	31	0.7311	-2.57
41	0.5411	-4.72	41	0.5244	-2.83	41	0.5393	-3.29
51	0.3090	-5.41	51	0.2895	-3.28	51	0.3080	-3.92
61	0.0264	-6.04	61	0.0176	-3.68	61	0.0326	-4.49
Zm = 35.95 - j0.072 Ohms			Zm = 36.07 - j-.076 Ohms			Zfm = 143.5 - j0.081 Ohms		

The current magnitudes show a very close correspondence among the three vertical antennas. From the mid-point toward the element end, the folded monopole current phase falls between the values for the two single-wire models. Below that level, the phase angle of the folded monopole is shifted slightly more positive by the fact that at the first segment, the currents on the two wires are not precisely equal. Nevertheless, the sorting of radiation from transmission-line currents produces a radiation-current pattern that would be virtually indistinguishable from the current pattern for a comparable single-wire monopole.

### *A Center-Fed 1/2-Wavelength Antenna with a 1/2-Wavelength Parallel Feedline*

The folded monopole example tends to confirm the adequacy of the analysis that sorts radiation from transmission-line currents for the case of a folded antenna element. However, it does not speak to the question of parallel feedline radiation. We may legitimately wonder if the same analysis is adequate to this task.

To test this question, we may begin with a center-fed half-wavelength antenna constructed from AWG #12 copper wire. Rather than place the feedpoint on the center segment, we may also construct from the same wire a parallel feedline. For this and following examples, the test frequency is 28.5 MHz to minimize the model size. The feedline for the first sample model in this series is just long enough (209.1") to achieve resonance (77.7 - J0.1 Ohms). The feedline proceeds away from this free-space antenna at right angles, as shown in **Fig. 5**.



The current magnitude curves show that the current peaks on the feedline are at least as high as the peak current on the antenna element. However, we learned early in our experience with practical antennas that the set-up for the model minimizes radiation currents. Hence, we would anticipate that the calculations will place virtually all of this current in the transmission-line current columns.

Center-Fed Half-Wavelength with 1/2-Wavelength Parallel Feedline								Table 3	
28.5 MHz Free-Space, AWG #12 Copper Wire									
Parallel Segmentation									
Segment	Wire 1		Wire 2		Radiating Currents		Trans-Line Currents		
	Imag	Phase	Imag	Phase	I-mag	I-phase	I-mag	I-phase	
1	1.0040	179.71	1.0040	-0.28	0.0001	89.72	1.0040	-0.28	
50	0.7453	-172.20	0.7454	7.84	0.0003	82.76	0.7453	7.82	
100	0.1551	-103.30	0.1556	76.63	0.0002	53.80	0.1553	76.66	
150	0.6961	-9.13	0.6961	170.87	0.0000	-9.13	0.6961	-9.13	
200	0.9998	-0.15	0.9998	179.85	0.0000	0.00	0.9998	-0.15	
Series Segmentation									
Segment	Wire 1		Wire 2		Radiating Currents		Trans-Line Currents		
	Imag	Phase	Imag	Phase	I-mag	I-phase	I-mag	I-phase	
1	1.0040	179.71	1.0040	179.71	0	0	1.0040	-0.29	
50	0.7453	-172.20	0.7348	-171.90	0.0056	-12.36	0.7400	7.95	
100	0.1551	-103.30	0.1527	-97.55	0.0078	-1.75	0.1537	79.55	
150	0.6961	-9.13	0.7071	-8.85	0.0057	8.38	0.7016	-8.99	
200	0.9998	-0.15	0.9998	-0.15	0	0	0.9998	-0.15	

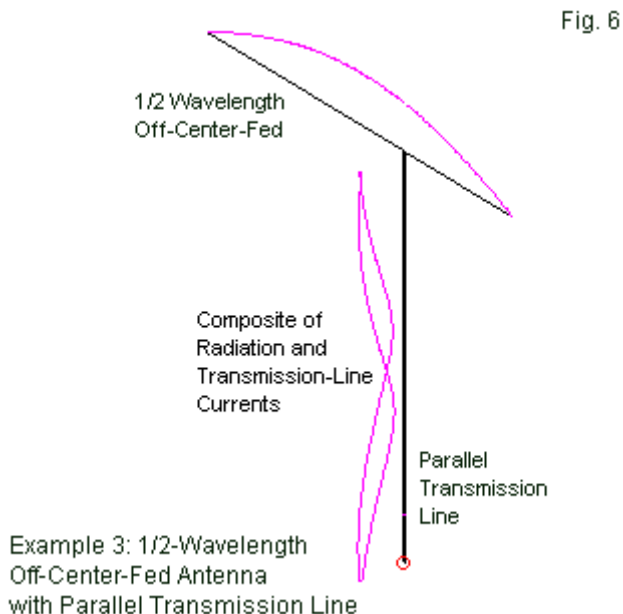
**Table 3** shows spot checks of the currents along each wire using both parallel and series model set-ups. The wire-2 values have the same magnitude for both set-ups, but the current phase values differ by 180 degrees. Because the radiation currents are so low, we find variability between the values produced by the two set-ups. However, the highest current value is less than 1% of the feedpoint current (1.0), rendering the calculated differences insignificant at a practical level. As we anticipated, we find much higher values in the

transmission-line current column, and the two set-ups show a close fit in phase angle values.

The bottom line of this initial exercise is that a center-fed wire antenna with a parallel transmission line at right angles to the antenna element wire exhibits virtually no radiation current. Were it not for the role this model plays as a comparator for succeeding examples, the exercise would be superfluous.

### *An Off-Center-Fed 1/2-Wavelength Antenna with a 1/2-Wavelength Parallel Feedline*

If we move the wire's feedpoint away from center, the two wires of the transmission line will show a differential in current magnitude not only at the junction with the antenna wire, but also long the entire length of the feedline. The sample model moves the feedpoint 30" toward one end of the wire and adjusts the segmentation of the antenna element wires accordingly. However, I left the length of the feedline at 209.1", a length of antenna and feedline that yields a somewhat non-resonant feedpoint impedance ( $113.7 - j20.0$  Ohms). **Fig. 6** shows the general layout of the antenna as well as the relative current magnitude values along both the antenna and the feedline.



From just the looks of this situation, we would expect that the radiation current levels on the transmission line will not be as insignificant as in the case of the center-fed antenna. **Table 4** shows the results obtained for the OCF antenna feedline using both model set-ups and the same checkpoints along the feedline that we used in the preceding example.

Off-Center-Fed Half-Wavelength with 1/2-Wavelength Parallel Feedline								Table 4	
28.5 MHz Free-Space, AWG #12 Copper Wire									
Parallel Segmentation									
Segment	Wire 1		Wire 2		Radiating Currents		Trans-Line Currents		
	I-mag	Phase	I-mag	Phase	I-mag	I-phase	I-mag	I-phase	
1	0.9974	-177.20	1.0071	-3.59	0.0561	-85.42	1.0007	-0.41	
50	0.9809	-167.50	0.5941	14.91	0.1941	8.81	0.7873	13.41	
100	0.4580	-143.80	0.3435	128.85	0.2926	0.29	0.2798	74.01	
150	0.4700	-22.49	0.9060	166.84	0.2244	-3.39	0.6859	-16.34	
200	0.9920	-0.16	1.0066	179.77	0.0073	-4.98	0.9993	-0.20	
Series Segmentation									
Segment	Wire 1		Wire 2		Radiating Currents		Trans-Line Currents		
	I-mag	Phase	I-mag	Phase	I-mag	I-phase	I-mag	I-phase	
1	0.9974	-177.20	1.0071	176.41	0.0561	-85.42	1.0007	-0.41	
50	0.9809	-167.50	0.5940	-165.10	0.1941	8.83	0.7873	13.41	
100	0.4580	-143.80	0.3434	-51.16	0.2925	0.30	0.2798	74.00	
150	0.4700	-22.49	0.9058	-13.16	0.2243	-3.38	0.6858	-16.34	
200	0.9920	-0.16	1.0066	-0.23	0.0073	-4.98	0.9993	-0.20	

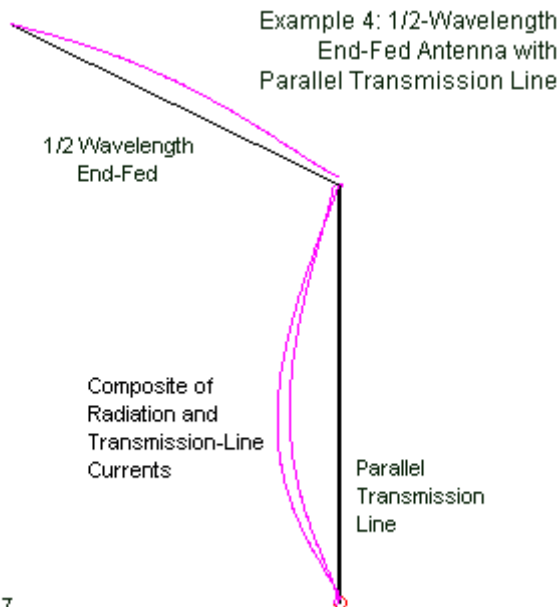
Wire 2 of the data from the NEC report shows the same close coincidence of magnitude values and the same 180-degree shift in phase angle for the two model set-ups that we have seen in all of the models so far explored. The transmission-line currents are not very distant in value from those we found on the centered feedline. The key change occurs in the radiation current column. Because the values are no longer trivially small, we find a very close coincidence of values between the two model set-ups. As we expected, the radiation current magnitudes values are much higher, amounting at their peak to about 27% of the peak current value at the center of the antenna element.

In practical terms, we might be hard-pressed to detect a difference in the radiation pattern between the center-fed and the OCF antennas at any moderate height (perhaps less than 1 wavelength

but greater than  $1/2$  wavelength) above ground. Peak radiation current occurs about halfway up the feedline toward the antenna element and is considerably weaker than the antenna current peak value. Nevertheless, the radiation currents do exist and would be measurable.

### *An End-Fed 1/2-Wavelength Antenna with a 1/2-Wavelength Parallel Feedline*

Let's move the transmission line to the end of the  $1/2$ -wavelength wire element. Our next model in fact leaves one segment on one side of the line to reflect the usual bits of wire that terminate the open side of an end-fed antenna. The remainder of the element connects to the other side of the transmission line. The line length is unchanged at 209.1". The outline and current magnitudes appear in **Fig. 7**.



One of the lines appears to have a higher current peak than the other, although the graphic does not show us the current phase. Hence, we cannot know from the sketch whether the peaks or their differential mean anything yet for radiation currents. The peak current in the transmission line does seem to exceed the peak current on the antenna wire. That phenomenon results from the very high source impedance of the model:  $2410 - j4020$  Ohms. To obtain a look at the radiation and transmission-line components of the currents shown in **Fig. 7**, we must subject the NEC current

reports to the sorting process. **Table 5** provides the data for both forms of model set-up.

End-Fed Half-Wavelength with 1/2-Wavelength Parallel Feedline									Table 5
28.5 MHz Free-Space, AWG #12 Copper Wire									
Parallel Segmentation									
	Wire 1		Wire 2		Radiating Currents		Trans-Line Currents		
Segment	I <sub>mag</sub>	Phase	I <sub>mag</sub>	Phase	I <sub>-mag</sub>	I <sub>-phase</sub>	I <sub>-mag</sub>	I <sub>-phase</sub>	
1	0.3418	-158.20	1.1666	-19.01	0.4675	-32.83	0.7214	-10.10	
50	9.2568	-155.50	7.2750	33.67	1.1884	-4.70	8.2398	28.53	
100	12.6920	-155.10	9.8656	38.69	1.9498	-12.19	11.1985	30.93	
150	8.5730	-154.00	6.5826	43.76	1.5281	-15.07	7.4885	33.70	
200	0.8321	-4.03	0.9302	174.58	0.0502	-17.01	0.8811	-4.76	
Series Segmentation									
	Wire 1		Wire 2		Radiating Currents		Trans-Line Currents		
Segment	I <sub>mag</sub>	Phase	I <sub>mag</sub>	Phase	I <sub>-mag</sub>	I <sub>-phase</sub>	I <sub>-mag</sub>	I <sub>-phase</sub>	
1	0.3418	-158.20	1.1663	161.00	0.4673	-32.83	0.7212	-10.09	
50	9.2568	-155.50	7.2730	-146.30	1.1903	-4.74	8.2387	28.55	
100	12.6920	-155.10	9.8617	-141.30	1.9517	-12.16	11.1965	30.93	
150	8.5730	-154.00	6.5795	-136.20	1.5309	-15.07	7.4866	33.72	
200	0.8321	-4.03	0.9303	-5.42	0.0502	-17.01	0.8811	-4.76	

The division of current between radiation and transmission-line components (with a 1/2-wavelength transmission line) may seem surprising. The transmission-line component rises to a very high level (given the source current of 1.0). In fact, the transmission line current peak (from the sample) is over 5 times the value of the peak radiation current level. In turn, the radiation current peak on the transmission line is only about half the value of the peak current that appears along the antenna element. The relative values of peak current between the transmission line and the antenna have steadily risen as we moved the transmission-line position from the antenna wire center toward the end. However, within the scope of the basic antenna parameters used to create the models, the

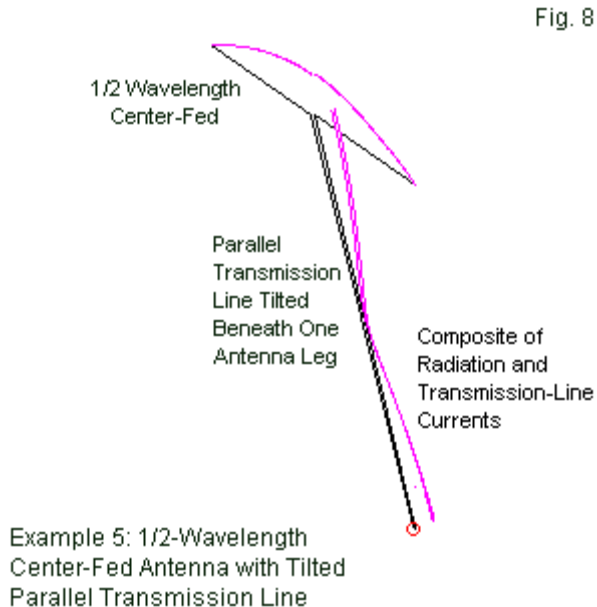
feedline radiation has not challenged the dominant role of the antenna wire in setting the radiation pattern for the system. Moreover, had we used only the unsorted or composite current reports for the end-fed antenna, we might well have reached an unwarranted conclusion about feedline radiation.

### *A Center-Fed 1/2-Wavelength Antenna with a Tilted 1/2-Wavelength Parallel Feedline*

All of the examples using the 209.1" feedline position the feedline at 90 degrees to the axis of the antenna wire. As a result, they show essentially the radiation current levels on the feedline as they result from the natural balance or imbalance of currents at the junction of the feedline with the antenna wire. Common practice is to extend the feedline at right angles to the antenna element for the greatest distance possible to avoid currents that might be induced in the feedline by coupling to the antenna fields.

The analysis that separates the radiation from the transmission-line currents is also applicable to examining the situation in which we bring the feedline away at an angle other than 90 degrees. For a sample, let's begin with a center-fed wire. Then we may bring the feedline from the junction to a point directly under one leg of the antenna element. In fact, I terminated the feedline at the point directly under one end of the center-fed wire. The vertical distance between the wire and the source end of the feedline is about 184.5", resulting in a total line length that is almost exactly the same as for the original center-fed model--a little over 209". The result was a feedpoint impedance not very different from the

original model:  $73.1 + j0.4$  Ohms for the tilted line model and  $77.7 - j0.1$  Ohms for the original model. **Fig., 8** shows the basic outline of the tilted-feedline model.



The sketch can mislead by virtue of the perspective, which I selected to show the current magnitude curves. The total antenna wire length is the same (within a few inches) of the transmission-line length. The feedline is about 28 degrees off vertical. The tilt is not radical, but clearly noticeable. Our next question is whether the tilt makes a difference in the radiation currents on the feedline.

**Table 6** compares the currents for the original center-fed wire and the new version with a tilted feedline. Both tables use the series segmentation set-up.

Center-Fed Half-Wavelength with 1/2-Wavelength Parallel Feedline @ 90 Degrees									Table 6
28.5 MHz Free-Space, AWG #12 Copper Wire									
Segment	Wire 1		Wire 2		Radiating Currents		Trans-Line Currents		
	I-mag	Phase	I-mag	Phase	I-mag	I-phase	I-mag	I-phase	
1	1.004	179.71	1.004	179.71	<b>0</b>	0	1.0040	-0.29	
50	0.7453	-172.2	0.7348	-171.9	<b>0.0056</b>	-12.36	0.7400	7.95	
100	0.1551	-103.3	0.1527	-97.55	<b>0.0078</b>	-1.75	0.1537	79.55	
150	0.6961	-9.13	0.7071	-8.85	<b>0.0057</b>	8.38	0.7016	-8.99	
200	0.9998	-0.15	0.9998	-0.15	<b>0</b>	0	0.9998	-0.15	
Center-Fed Half-Wavelength with 1/2-Wavelength Tilted Parallel Feedline									
28.5 MHz Free-Space, AWG #12 Copper Wire									
Segment	Wire 1		Wire 2		Radiating Currents		Trans-Line Currents		
	I-mag	Phase	I-mag	Phase	I-mag	I-phase	I-mag	I-phase	
1	1.0369	178.32	0.9726	-178.8	<b>0.0409</b>	-38.37	1.0044	-0.29	
50	0.7781	-174.7	0.7155	-169.9	<b>0.0442</b>	-37.30	0.7461	7.60	
100	0.1439	-115.8	0.1711	-94.66	<b>0.0318</b>	-40.03	0.1549	75.69	
150	0.6647	-7.92	0.7269	-9.7	<b>0.0329</b>	-27.99	0.6957	-8.85	
200	0.9984	-0.9	1.0012	-0.19	<b>0.0063</b>	76.90	0.9998	-0.54	
Note: Both models use series segmentation.									

We find very little difference between the two models in the transmission-line current columns. In the radiation current magnitude column, we find a significant difference. Radiation currents have increased by nearly a ten-fold average. The intrinsic current level is certainly not sufficient to alter that antenna radiation pattern. However, if we call the radiation current by their other name, common-mode currents, we may or may not have a cause for concern. At the equipment end of the feedline, the level of RF current necessary to create interference with sensitive solid-state circuitry is not very high at all. It is not at all clear from the sample

model that we have surpassed the required threshold, which will vary with the power actually applied to the antenna-and-feedline system. The sample does nevertheless confirm that feedline routing can play a role in the level of radiation current on the feedline.

## Conclusion

These brief notes have tried to show that an analysis of radiation or common-mode currents is possible for parallel two-wire transmission lines and that such an analysis is a potential utility. The analysis makes use of current data from NEC models, but processes the data externally to NEC. NEC and MININEC are not ends in themselves, but a source of data that has extended utility once we know how to use the data.

The sample models are simplified, since the goal was to show the technique of analysis, not to produce definitive results. To analyze an actual situation, the models would undergo many changes that only begin with replicating the actual antenna and feedline. The model would route the feedline exactly as it occurs, and would add a real ground to the model.

Not everything that we may learn from NEC and MININEC models appears in the NEC output report data. The data may be a resource for numerous rounds of further analysis. We have only examined one such effort here.

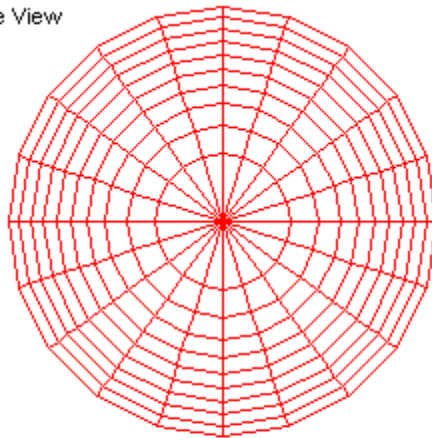
## Chapter 124: Modeling (with) Parabolic Reflectors

**M**odeling with non-uniformly shaped wire-grid structures carries a considerable collection of cautions and warnings. Newer modelers are likely to overlook many of them while focusing on the complexities of the structure itself. Therefore, it may be useful to review some of the potentials and the limitations of models that include them. We shall focus on the parabolic reflector as one of the most popular wire-grid structures, paralleling the popularity of physical implementations in many aspects of UHF communications. However, virtually all of the notes along the way will apply equally to other not-uniform shapes.

We employ uniform wire-grid structures when we create the rectangular shapes that form planar and corner reflectors. In these structures, the individual wires or wire segments are almost equal in length in both directions. Therefore, we may size the wire easily to form a good simulation of a solid surface. As we shall see, parabolic reflectors do not admit of such easy calculations.

Face View

Fig. 1



Edge View



A Typical Parabolic Reflector Outline

A parabola, of course, is a graphical solution to a certain type of quadratic equation. The antenna structures that we commonly call parabolas are paraboloids with uniform dimensions, as suggested by the 2 views in **Fig. 1**. The center of the dish is the vertex. The distance from the vertex to a point that is in line with the lip of the dish is the depth ( $d$ ). The distance across the widest pair of points on the lip of the dish is the diameter ( $D$ ). The parabolic reflector also has a focal point, and we can calculate the distance from this point to the vertex by a common equation.

$$f = \frac{D^2}{16d} \quad f = \text{focal length}; D = \text{diameter}; d = \text{depth}$$

The focal length will equal the depth of the parabolic reflector under the condition that the depth is 1/4 the diameter. Most antenna handbooks will provide further information on parabolic reflectors. Our main concern is modeling the device.

Most applications allow us to create the dish model by using a shape-synthesizing program of some sort. To create a parabola, we need only specify the depth, the radius, the wire diameter, and the desired segmentation. The program allows us to specify the coordinates for the 2 radii (that is, X-Y, Y-Z, etc.) and also allows us to use separate values for the pair. We shall use a circular outline for simplicity.

We shall save the file that we generated in .NEC format for direct importation to any NEC implementation. However, like other synthesis programs, we must use caution. The product is not a complete model file, but only the geometry of a model, along with the frequency specified.

CM Generated by NEC-type program

CE

GW 1 1 0.31623 0.00000 0.05000 0.30075 0.09772 0.05000 0.00500

GW 2 1 0.30075 0.09772 0.05000 0.25583 0.18587 0.05000 0.00500

GW 3 1 0.25583 0.18587 0.05000 0.18587 0.25583 0.05000 0.00500

GW 4 1 0.18587 0.25583 0.05000 0.09772 0.30075 0.05000 0.00500

GW 5 1 0.09772 0.30075 0.05000 0.00000 0.31623 0.05000 0.00500

-----

GW 396 1 0.00000 -0.94868 0.45000 0.00000 -1.00000 0.50000 0.00500

GW 397 1 0.29316 -0.90225 0.45000 0.30902 -0.95106 0.50000 0.00500

```

GW 398 1 0.55762 -0.76750 0.45000 0.58779 -0.80902 0.50000 0.00500
GW 399 1 0.76750 -0.55762 0.45000 0.80902 -0.58779 0.50000 0.00500
GW 400 1 0.90225 -0.29316 0.45000 0.95106 -0.30902 0.50000 0.00500
GS 0 0 1.000000
FR 0 1 0 0 299.800000 1

```

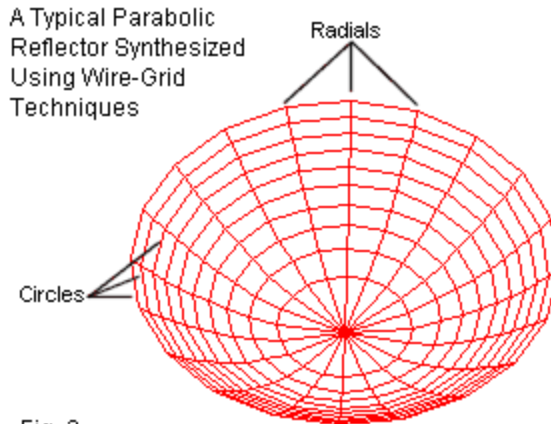
To complete the model, we must add a driver--if we are not exciting one of the wires in the assembly. We must also specify the excitation, add any material or other loading that we need, and request some of our output. Therefore, the lower portion of the incomplete sample shown requires some variation of the following set of lines. The request for far-field patterns is only one of numerous outputs that we might request.

```

GW 396 1 0.00000 -0.94868 0.45000 0.00000 -1.00000 0.50000 0.00500
GW 397 1 0.29316 -0.90225 0.45000 0.30902 -0.95106 0.50000 0.00500
GW 398 1 0.55762 -0.76750 0.45000 0.58779 -0.80902 0.50000 0.00500
GW 399 1 0.76750 -0.55762 0.45000 0.80902 -0.58779 0.50000 0.00500
GW 400 1 0.90225 -0.29316 0.45000 0.95106 -0.30902 0.50000 0.00500
GW 501 11 0 -.24 .5 0 .24 .5 .005 !driver
GS 0 0 1.000000
GE
FR 0 1 0 0 299.800000 1
EX 0 501 6 0 1 0
RP 0 361 1 1000 -90 90 1.00000 1.00000
RP 0 361 1 1000 -90 0 1.00000 1.00000
EN

```

If we were to run the incomplete model, all that we would obtain for our trouble is an output report that provides a set of segments and their connections. However, even this much information can be useful to us, since we may use the information to evaluate why the parabolic reflector is a non-uniform wire-grid structure. In lieu of the data lines, we may examine more closely the graphic portrait of the reflector, as shown in **Fig. 2**.



The wire-grid assembly uses straight wires to approximate curved surfaces. It consists of several radials connected at semi-regular points by circles of wires. Normally, in a synthetic structure, each wire has 1 segment. The dish shown is 2 wavelengths in diameter and 0.5 wavelengths deep. Note that virtually no junction of wires at a right angle involves wires of equal length. The wires forming the circle increase their length systematically as we move from the vertex to the lip of the dish. The wires forming radials use equal length segments except at the innermost section. An ideal radial would have one more circle to achieve equal length segments throughout. However, the wires for the missing innermost circle would become exceptionally short.

Missing from the line graphic is any indication of the wire diameter used in the parabolic structure. The selection of wire diameter

interacts with the selection of the number of radials at the vertex, where all radials join. The model shown uses 20 radials as a minimum value to form a close approximation of a circle. Adjacent wires at the vertex form a small angle. As we increase the number of radials or as we increase the diameter of the wire, press the NEC limits for the inter-penetration of wires at the vertex. However, if we make the wires too thin, we run the risk of creating a leaky reflector, that is, one that does not approximate a solid surface.

To examine the consequences, let's provide our 2-wavelength-diameter dish with a dipole placed at the focal point. Since the depth is  $1/4$  of the diameter, the focal point is 0.5-wavelength from the vertex, that is, even with the lip of the dish. We shall begin with a reflector-wire diameter of 0.01-wavelength and increase it up to 0.08-wavelength. **Table 1** shows the results of these trials.

Table 1. Reflector wire thickness vs. model performance

Wire dia. $\lambda$	Distance $\lambda$	Gain dBi	F-B Ratio dB	AGT	Cor. Gain dBi
0.01	0.45	10.82	13.20	1.00043	10.73
0.02	0.5	11.58	17.89	1.00867	11.54
0.03	0.5	11.82	23.40	1.01060	11.77
0.04	0.5	11.92	29.48	1.01434	11.86
0.05	0.5	11.99	33.39	1.01927	11.91
0.06	0.5	12.03	29.47	1.02494	11.92
0.07	0.5	12.07	25.93	1.03149	11.94
0.08	0.5	12.09	26.30	1.04457	11.90

## Notes:

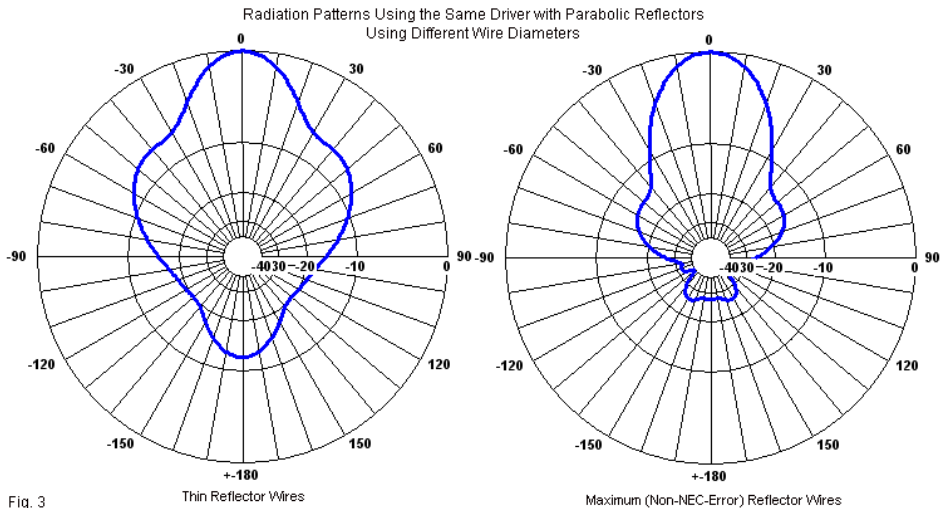
1. Driver is a single dipole with a constant length and diameter for all tests.
2. Wire diameter applies to all and only reflector wires. Reflector diameter is  $2\lambda$  for this example.
3. AGT is the average gain test value.
4. Cor. Gain is based on adjusting reported gain via the AGT value.
5. 0.08- $\lambda$  reflector wire produced NEC core warnings and is too large to use. Wire diameter limit will vary with the wire-grid particulars.

This simple experiment has several dimensions. First, as we examine the maximum gain column, we notice a steady rise in gain solely by virtue of the increase in wire diameter. The gain appears to peak at the last entry. However, we should also note the average gain test (AGT) column, which shows a value that departs slowly but surely away from the ideal value of 1.0 for the free-space lossless model. We may convert the AGT value to decibels and correct the reported gain. The corrected gain shows a maximum value with 0.07-wavelength diameter wire. In addition, the 0.08-

wavelength version of the model contains numerous warnings about wire inter-penetration.

Given the curve of peak gain values, wire diameters between 0.05-wavelength and 0.07-wavelength are likely equally usable in most applications as the closest approximations of a solid surface parabolic dish. The technique shown here or a reasonable variation is the only way to discover how close to a solid surface that we may approximate with the non-uniform structure of the assembly.

Second, we may also test the assembly by examining the far-field patterns produced by the parabola and its driver. **Fig. 3** shows patterns for our basic dipole driver and the dish using thin wires and thick wires. The thin-wire version of the dish yields results that are far from those of a solid-surface dish. The fat-wire version is closer to the mark.



Third, numerous modelers are surprised by the fact that even a solid surface--or our closest approximation of it--yields a set of rearward lobes, however, small that may be. Most texts focus on how rays intercept the dish surface and reflect in the forward direction. However, a parabolic dish shares some significant properties with rectangular reflectors. There are both semi-shadow and shadowed areas. As well, we encounter diffraction at the dish lip. Hence, every parabolic dish will have rearward far-field lobes. Advanced techniques of feeding the dish concentrate on minimizing these lobes while illuminating the dish to maximum advantage.

Finally, we should note the gain values for the dipole driver. A number of texts provide an equation to calculate the gain of a dish relative to its diameter at the frequency of use.

$$Gain_{dB_i} = 10 \log_{10} k \left( \frac{\pi D}{\lambda} \right)^2 \quad k = \text{efficiency factor, } D = \text{diameter; } \lambda = \text{wavelength}$$

The equation has a fudge factor,  $k$ , the efficiency factor, given as 0.00 through 1.00. Most sample calculation use values between 0.5 and 0.55. However, the highest gain value in our table only emerges if we reduce the value of  $k$  to about 0.4. Most initial gain calculations presume an isotropic source of excitation. If we exchange the single dipole for a pair of turnstiled dipoles, the gain values do not change, but the source comes closer to be isotropic in free space. So we are left with a quandary: is the efficiency presumption behind the gain calculations off the mark, or is the model deficient enough to account for the difference between reported gain and pre-calculated gain? One of the limitations of modeling parabolic dishes in the absence of appropriate range or chamber tests is that we lack any means of forming an answer to the question.

One interesting facet of modeling parabolic reflectors is the optimal placement of the driver assembly relative to the focal point of the parabola. Our initial test showed very little variation in position relative to reflector wire thickness. However, we did not survey the gain behavior of the total antenna as we changed the position of the driver. A small survey may be useful in terms of showing what

to expect from modeled parabolic assemblies. Therefore, let's use our 2-wavelength diameter dish with a depth of 0.5-wavelength and a focal length of 0.5-wavelength. For comparison, we may create a 3-wavelength diameter dish that also uses a depth of 0.5-wavelength. The equation with which we began or simplified view of parabolas tells us that the focal length is 1.125-wavelengths. In both cases, we shall use a turnstiled-dipole driver for simplicity. (Remember that these notes do not focus on parabolic reflector technology, but upon modeling the reflector. Therefore, we may justifiably use simplified driver assemblies.)

Table 2. 2- $\lambda$ -diameter reflector: reported performance vs. distance from reflector vertex to a turnstile-dipole driver

Distance $\lambda$	Gain dBi	F-B Ratio dB	Beamwidth degrees
0.3	11.69	23.24	46
0.4	11.91	24.89	44
0.5	12.08	26.05	36
0.6	11.81	27.54	30
0.7	10.87	28.07	28
0.8	10.83	25.73	36
0.9	11.02	23.38	38
1.0	11.09	20.42	38
1.1	10.65	16.05	34

The smaller dish uses 0.07-wavelength wire in the reflector assembly. **Table 2** provides us with some basic data on the modeled performance as we move the driver from 0.3-wavelengths to 1.1-wavelengths away from the vertex. The peak gain occurs at



**Fig. 5** overlays 3 patterns for the smaller dish and its turnstiled dipole driver at the driver position for maximum gain. The three traces are almost indistinguishable. The smaller dish appears to show a coincidence with basic calculations in every way, except perhaps for the gain deficit. (We may note in passing that we find a secondary gain peak with the driver at 1.0-wavelength away from the vertex, but this peak is considerably lower than the main peak.)

Let's turn to the larger dish that is 1.5 times the diameter of the smaller one. The diameter is 6 times the largest dimension of the driver. The depth remains at 0.5-wavelength. The focal point by calculation is 1.125-wavelengths from the vertex. For this dish, a wire of 0.06-wavelength diameter proved to be the largest usable value. If we move the turnstiled dipole driver from a closer point to a further point from the vertex, we obtain the data in **Table 3**.

Table 3.  $3\text{-}\lambda$ -diameter reflector: reported performance vs. distance from reflector vertex to a turnstile-dipole driver

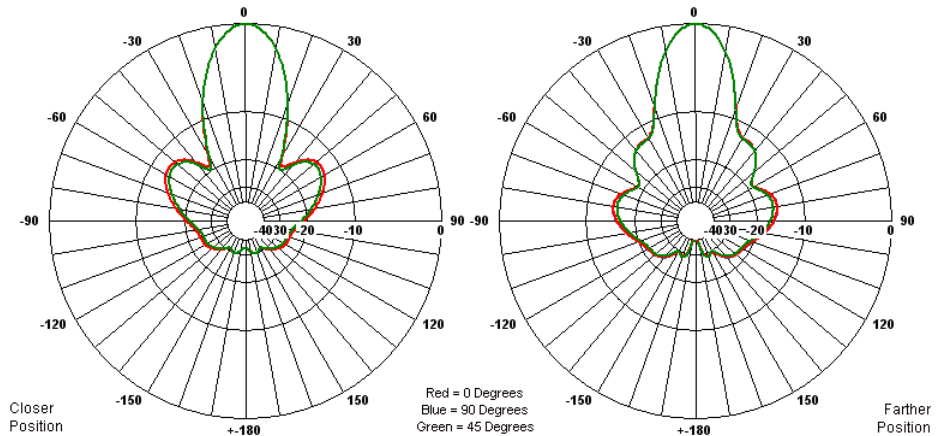
Distance $\lambda$	Gain dBi	F-B Ratio dB	Beamwidth degrees
0.75	15.18	38.43	26
0.875	14.81	33.60	26
1.0	13.74	31.87	24
1.125	13.11	34.29	18
1.25	14.37	49.14	22
1.375	14.90	39.09	24
1.5	14.48	31.88	24

The optimal distance for maximum gain is not the focal point, but a different point considerably closer to the vertex. At a distance of 0.75-wavelength, we obtain maximum gain with a beamwidth about 3 degrees wider than the calculated value. A secondary gain peak occurs at a distance of 1.375-wavelengths and is only about 0.3-dB lower than the near-position gain. The beamwidth at the farther position is closer to the calculated value.

The modeling result produces gain peaks that depart from standard rudimentary theory (but not perhaps from more advanced calculations). As well, the secondary peak is now a contender for use. **Fig. 6** compares the patterns for the two position--again using an overlay of 3 patterns for each driver position. The two driver positions yield very distinct low-angle lobe structures. What we cannot specify solely on the basis of the models is whether the pictures are accurate to the behavior of a solid-surface dish on a test range.

3-Wavelength Diameter Parabolic Reflector with a Turnstile-Dipole Driver at 2 Maximum-Gain Positions  
Free-Space Patterns

Fig. 6



The gain values produced by the larger dish are also deficient compared to standardized calculations. Once more, a value of about 0.4 for  $k$ , the efficiency factor, would align the model report with the standard calculation of peak gain. One limitation of the system is that fully half of the radiation of the driver is away from the reflector. Therefore, we might wish to explore, in perhaps the crudest manner, what happens if we focus more energy on the reflector.

3-Wavelength Diameter Parabolic Reflector  
with a Turnstile-Yagi (3-Element) Driver

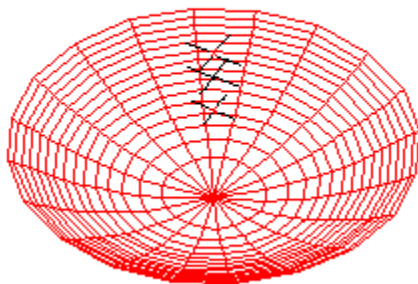


Fig. 7

**Fig. 6** shows our final experiment. It replaces the simply driver with crossed or turnstiled Yagi elements forming a circularly polarized 3-element beam. The performance is modest, with about 7.5-dBi free-space forward gain and 11-dB front-to-back ratio. The array reflector elements are just over 0.5-wavelength long, and the boom length is exactly 0.5-wavelength. We shall direct the Yagi toward the reflector and try to find a mounting position that maximizes the gain. **Table 4** summarizes the results for the 3-wavelength diameter dish. The listed distances are to the reflector, with the director 0.5-wavelength closer to the vertex.

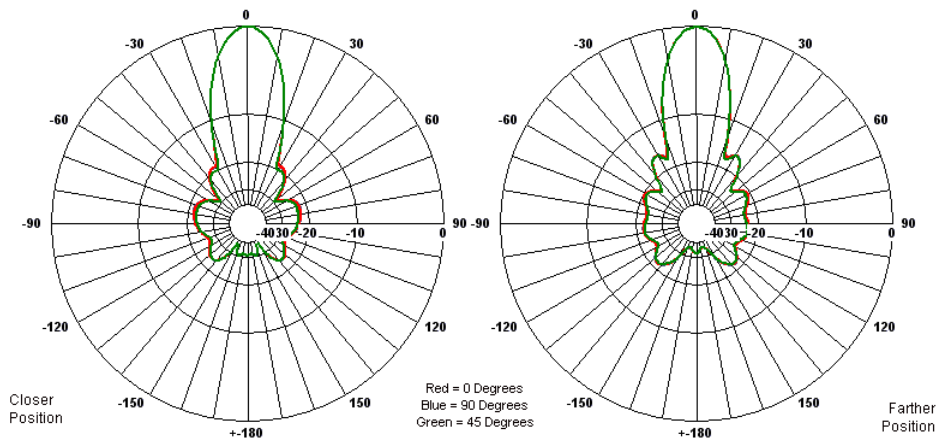
Table 4. 3- $\lambda$ -diameter reflector: reported performance vs. distance from reflector vertex to a turnstile-3-element Yagi driver

Distance $\lambda$	Gain dBi	F-B Ratio dB	Beamwidth degrees
0.9	17.18	27.12	22
1.0	17.80	31.16	22
1.1	17.43	34.45	22
1.2	16.98	35.24	22
1.3	16.97	33.91	22
1.4	17.85	32.18	22
1.5	17.84	31.12	22
1.6	17.11	30.83	22

Once more we find a pair of distances at which the array gain peaks: 1.0-wavelength and 1.4-wavelength. (Subtract 0.25-wavelength for the distance to the center of the Yagi and 0.5-wavelength for the distance to the director.) Unlike the dipole driver, the Yagi gain values are very comparable. (Corrected for the AGT values, they are almost identical.) As well, we find nothing to choose in the beamwidth and front-to-back values. The comparative patterns for the two positions appear in **Fig. 8** and show may major reasons in the sidelobe structure for selecting one position over the other.

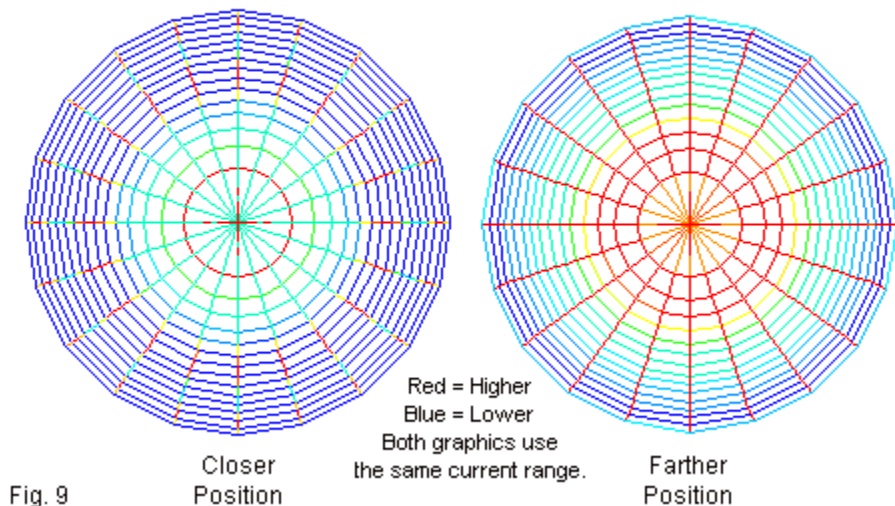
3-Wavelength Diameter Parabolic Reflector with a Turnstile-Yagi Driver at 2 Maximum-Gain Positions  
Free-Space Patterns

Fig. 8



The gain values recorded by the Yagi driver with the 3-wavelength dish are above the pre-calculated gain values for dishes, largely as a result of the improved focus of energy from the driver onto the parabolic surface. Indeed, for some purposes, a modeler may wish to examine the current distribution on the modeled dish wires under various circumstances. Solely as an example of how we might find differences, I set the range of currents from  $1.5e-3$  down to  $3.0e-4$  to provide a range of color variation on the dish wires. Using the 2 positions of maximum gain, I obtained the graphical representations in **Fig. 9**.

3-Wavelength Diameter Parabolic Reflector with Yagi Driver  
Relative Current Distribution vs. Driver Position



The two current magnitude plots show very different patterns of current distribution. (The closer position shows some red lines at the center; these are from the Yagi elements.) The farther driver position appears to illuminate the radials to a considerable degree, in contrast to the closer position situation. Whether this factor has a bearing on the reliability of the wire-grid reflector as a model for a solid-surface reflector remains unknown if we remain completely at the level of modeling.

## Conclusion

These notes have not attempted to answer any questions about parabolic reflectors as physical antenna structures. Instead, we have been focusing on the parabola as an example of a non-uniform wire-grid modeling structure. We initially concentrated on the ways in which such structures press the limits of NEC guidelines. We found limits beyond which we could not go, especially in terms of the number of radials that we might use vs. the wire diameter that we might assign to the reflector. However, since the reflector is wholly passive--or at most parasitic--pushing the limits does not yield unusable AGT values.

We also looked at some rudimentary models of parabolic arrays. Our goal was to develop some preliminary expectations of such models with a wire-grid parabolic reflector. We found ways in which the models fail to coincide with fundamental calculations associated with reflectors of this order. However, modeling alone does not provide corrections either to itself or to the basic equations. (I have for the most part resisted the temptation to suggest first-order possible explanations for some phenomena. For example, the driver assemblies are all within coupling range of the reflector, and it is uncertain whether the results deviate from a solid surface due to coupling to individual wires within the wire grid.)

The net result--applicable to any non-uniform wire-grid structure--is that we can only use such structures with caution and with attention to all of the tests that we might apply to the model. The models are eminently useful so long as our expectations are suitably modest.

## Chapter 125: When to Worry and When Not: a Case Study

Everyone who models conscientiously using either NEC or MININEC worries over the results. Essentially, we find two general categories of worry. First is the basic adequacy of a model. Within NEC--and assuming adherence to the guidelines--the chief measure of model adequacy is the average gain test (AGT), which we have discussed extensively in past columns. Ideally, a free-space lossless model should show an AGT of 1.000 (2.00 for models using a perfect ground). There are no absolute rules for when an AGT score other than 1.000 renders a model inadequate. However, the more comparative and systematic a modeling exercise is, the closer to 1.000 that we require the AGT values to validate comparisons among models.

The AGT rests upon performing a full spherical far-field scan for a model in free space (a hemisphere over perfect ground). Using sufficient and equally spaced (angularly, of course) increments for the sample, the average far-field gain should equal the reference gain so that the ratio is 1.000. As we examine more complex geometries, we should reduce the increment between each sampled point on the sphere to obtain the most accurate average value. (Automated AGT scans offered by some implementations of NEC often use 5-degree increments, which is normally adequate for linear elements in various arrays. However, changing the increment to a lower value is a good check to ascertain the best value to use in a given exercise.)

We may often obtain corrected values for raw NEC gain reports by converting the reported AGT value into dB. The conversion consists of taking the log of the reported AGT value and multiplying by 10. A reported AGT score of 1.010 converts to 0.04 dB. Since the AGT score is greater than 1, we subtract the converted value from the reported gain. Hence a raw gain report of 5.00 dBi becomes 4.96 dBi. Reported AGT values below 1.000 results in increases to the raw far-field gain report. An AGT report of 0.960 becomes -0.18 dB. Had the gain report been 5.00 dBi, the corrected gain value would be 5.18 dBi.

We may also correct the resistive component of the reported source impedance using the AGT directly. The correction works best when the impedance is close to resonant, that is, has a relatively low reactive component. (Results with high reactive components appear to be mixed, with some results appearing to coincide with range test results and some appearing to diverge considerably.) To correct the impedance value, simply multiply the AGT score times the resistive component. Assume a reported value of 150 Ohms. An AGT score of 1.01 would convert this value to 151.5 Ohms. An AGT value of 0.960 would correct the reported resistance to 144 Ohms. How significant these corrects are depends upon the terms of the modeling exercise. If I were building an antenna with a target feedpoint impedance of 150 Ohms, I might expect construction variables to outweigh the range of variation within the example. However, for a sequence of modeled antenna geometry variations, I might wish to use corrected source impedance values in order to obtain a reasonable sequence of

values associated with the variations, especially if each variation produces a different AGT value.

The notion of construction variables leads us to the second major category of worry. The basic concern is how well a model conforms to a reasonable physical implementation of a modeled antenna. As we move ever higher in frequency, the bumps and the short leads that we usually do not model take on increased importance, since they grow as a function of a wavelength at higher frequencies. We might usefully make a catalog of compensatory measures that we sometimes take to overcome anticipated construction variations. However, we shall save that level of concern for some future column. Assuming that we would use general care in constructing a physical implementation of a modeled antenna, we shall restrict our concerns to general expectations for relative gain among relevantly comparable antennas and for their feedpoint impedances.

Modeling yields numbers derived from calculations within the particular modeling core that we might use. Many implementations of NEC include graphical representations of those numbers, but the basic NEC output is a large collection of numbers. When we find differences between two sets of numbers, we tend to worry. However, only in some cases is the worry justified. To distinguish between justified worries and unjustified worries, let's look at a case study.

## Closed 1-Wavelength Loop Elements

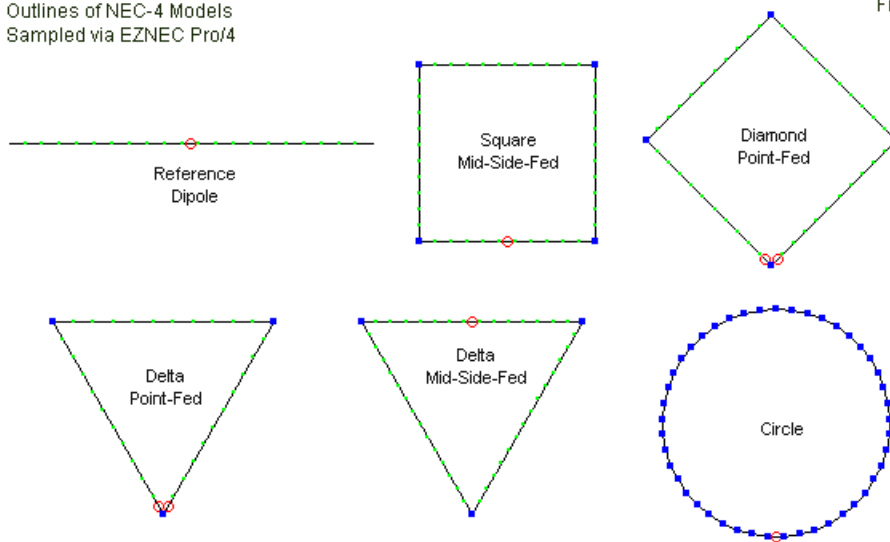
A closed 1-wavelength loop element with a single feedpoint provides major bi-directional far-field lobes broadside to the plane of the loop. There are two significant properties for us to note initially. First, the 1-wavelength loop provides directional gain over a simple half-wavelength resonant dipole. In fact, we may usefully analyze the 1-wavelength loop as constituting two dipoles fed in phase with an average distance apart of about 1/4-wavelength. Second, whereas a physical dipole will be shorter than 1/2-wavelength at resonance, a full-wavelength loop circumference will be greater than 1-wavelength at resonance. Part of the lengthening results from the mutual coupling between the two dipole elements presumed to be in the loop: resonance requires that we lengthen each of them by a small amount.

Amateur antenna builders continually look for so-called "cutting formulas," those seemingly magical simplifications that supposedly give the right answer for element length using only a single constant and the design frequency. Unfortunately, the world of antennas is more complex than cutting formulas imagine. Even in free space, the required length for a dipole or a closed loop--at resonance--will vary with the wire diameter and to a much lesser degree on the material loss of the antenna wire or tubing. For our exercise, all antennas will be in free space and use 0.002-m (2-mm) lossless or perfect wire. Horizontally polarized antennas are also prone to variations in the required length for a resonant impedance as a function of the antenna height above ground, especially below 1-wavelength.

The exercise that led to these notes emerged from a variety of claims that one hears about various closed loop configurations. One claim is that a perfectly circular loop has a significantly higher gain than a conventional square-sided loop (arranged to form either a square or a diamond). Presumably, the circle is a figure with an indefinitely high number of sides, compared to the 4 sides of the conventional HF quad loop. However, that account is at odds with claims made for a triangular or delta closed loop with equal side lengths, namely, that it is just as good as the 4-sided loop, again with equal side lengths. So I decided to example some models (free-space using 0.002-m diameter lossless wire) involving the configurations shown in **Fig. 1**. The test frequency is 300 MHz.

Outlines of NEC-4 Models  
Sampled via EZNEC Pro/4

Fig. 1



The dipole, of course, provides a reference against which to measure the increased gain offered by each closed-loop configuration. The sequence of models included both square and diamond-shaped 4-sided loops. To place the feedpoint at conventional positions required a mid-side position for the square loop and a position at the lower point for the diamond-shaped version. The two delta or triangular loops are both equilateral triangles and differ only in the feedpoint position. Since the model is in free space, moving the mid-side position to the top wire makes no difference in performance relative to inverting the entire structure. The loops have from 33 to 44 segments total, so the circular loop uses 45 wires to complete the simulation of a true circle. In some implementations of NEC, one may use the GA (arc) command to create the circle. The software used here--EZNEC-Pro/4--creates circles using separate wires. However, the results are identical to circles created with the GA command.

The sequence of seemingly comparable models yields the data shown in **Table 1**. With respect to the AGT values, we may note that the dipole and the circular loop achieve virtually perfect values, while the two angular loops fed at mid-side positions have identical very good values. Both require only a 0.02-dB decrease in the reported gain value.

Single (1- $\lambda$ ) Resonant Loop Elements

Table 1

NEC-4 Models (EZNEC Pro/4): Free-space environment, 0.002-m zero-loss wire

Antenna	Circumference	Gain	AGT	Cor. Gain	Feed Impedance
Reference dipole	0.4746 $\lambda$	2.13 dBi	1.000	2.13 dBi	71.9 + j 0.3 $\Omega$
Square, mid-side fed	1.0944	3.40	1.004	3.38	130.5 - j 0.0
Diamond, point fed	1.0963	3.23	0.962	3.40	136.8 + j 0.8
Triangle (delta), point fed	1.1160	2.76	0.936	3.05	134.6 + j 0.2
Triangle (delta), mid-side fed	1.1070	3.06	1.004	3.04	121.4 + j 0.6
Circle (45 segments)	1.0631	3.67	0.999	3.67	142.2 - j 0.1

Note: Dipole "circumference" = dipole length

The point-fed angular loops, however, tell a different story. The AGT values diverge more widely from the ideal value as the angle between the sides decrease. As indicated in **Fig. 1**, both point-fed models use a "split-source" feed, that is, a pair of sources on segments adjacent to the point. The reported source impedance value is the sum of these series sources. Removing one of the sources does not change the result (or the AGT value) significantly.

The table provides corrected maximum far-field gain values based on the raw report and the AGT score. We may note in more than a passing way that the corrected gain value for each point-fed model coincides very closely with the corresponding value for a mid-side source position. (In fact, the gain values form a progression from low to high as we move from the most angular structure--the delta or triangle--to the least angular--the circle.)

The table does not list corrected source resistance values. Only the values for the point-fed positions would change noticeably. The

corrected source resistance for the point-fed square-diamond becomes 131.6 Ohms, only 1 Ohm different from the mid-side fed square. Likewise, the adjusted point-fed delta source resistance becomes 126.0 Ohms, about 5 Ohms away from the mid-side source value.

## A MININEC Trial

We may note two facts about the NEC models. First, NEC models place a source within a segment. Hence, we cannot obtain a perfect point-fed source location. For many purposes, the split-source work-around to this small limitation proves to be very satisfactory. However, in this particular exercise, the split-source technique does not provide models that are sufficiently adequate to let us make the comparisons required by the exercise goals, at least, not without correcting the reported gain and source resistance values. Second, the AGT departs more widely from the ideal value as we sharpen the angle between wires at the point feedpoint. The wire angles themselves--in these NEC-4 models--do not create a problem, since the mid-side feedpoints yield very good AGT values. Only when we place the feedpoint at the angular junction of two wires do we encounter the difficulty.

MININEC (3.13) does not suffer one of the problems that we have just noted. We may place a source directly on a diamond or delta point, since MININEC places sources (as well as loads) on pulses, that is, on the junction between segments. However, uncorrected MININEC 3.13 suffers other difficulties, especially with angular junctions. Antenna Model is a highly corrected version of MININEC

that has to a very large measure overcome the limitations of raw MININEC. It has several other features as well, including the ability to provide an AGT value and the ability to import NEC models. The latter feature is useful in ensuring that the models used in MININEC trials are as precise to their NEC-4 originals as is feasible. The result is a set of models with the outlines shown in **Fig. 2**.

Outlines of MININEC Models  
Sampled via Antenna Model

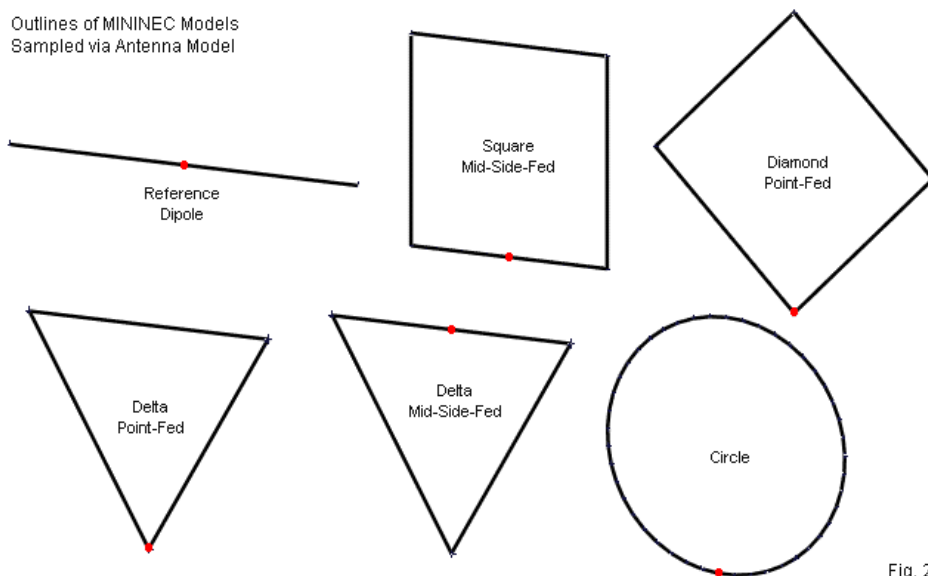


Fig. 2

Since MININEC requires a pulse or segment junction for the mid-side fed models, Antenna Model automatically increases the segment count on the affected wire by 1 to obtain an even number of segments. To assure equal segments on equal-length wires, I

increased the count on the other wires of the square and the mid-side fed delta to coincide with the count on the source wire. Otherwise, the models are identical to their NEC originals.

Single ( $1-\lambda$ ) Resonant Loop Elements

Table 2

MININEC Models (Antenna Model): Free-space environment, 0.002-m zero-loss wire

Antenna	Circumference	Gain	AGT	Cor. Gain	Feed Impedance
Reference dipole	0.4746 $\lambda$	2.12 dBi	0.999	2.12 dBi	71.7 – j 0.0 $\Omega$
Square, mid-side fed	1.0944	3.37	0.996	3.39	130.3 – j 10.6
Corrected	1.1016	3.39	0.996	3.41	133.2 – j 0.0
Diamond, point fed	1.0963	3.38	0.997	3.39	133.4 – j 15.8
Corrected	1.1065	3.41	0.997	3.42	138.5 – j 0.8
Triangle (delta), point fed	1.1160	3.04	0.999	3.04	131.8 – j 36.9
Corrected	1.1430	3.07	0.999	3.07	151.2 + j 0.5
Triangle (delta), mid-side fed	1.1070	3.01	0.997	3.02	120.6 – j 13.4
Corrected	1.1160	3.04	0.997	3.05	123.1 – j 0.4
Circle (45 segments)	1.0631	3.68	1.000	3.68	141.8 – j 0.4

Note: Corrected versions re-sized to achieve resonance within  $\pm j 1 \Omega$ .

**Table 2** lists the results of the trials. The reference dipole and the circular loop provided excellent AGT values and showed resonance within the project limit of  $\pm j 1.0$  Ohm reactance. However, all other models required some dimensional alteration to bring them to resonance within the same limits. The table shows the initial impedance reports as well as the circumference of the corrected models. (Of course, the side lengths are the circumference divided by 4 for the square models and divided by 3 for the deltas.) All of the models display excellent AGT values. The gain values for each type of loop coincide relative to mid-side and point feeding, and the progression is virtually the same as we found in the NEC models, with increasing gain as we move from the triangle toward the circle.

In a general way, our worries over the deviant AGT values provided by the NEC models were well founded.

However, one worry was not as significant as it might seem at first sight. The angular models showed a departure from resonance of at least  $j10$  Ohms, occasioning the work of revising the dimensions to bring the model back to resonance. If we bring a mere numerical sense of resonance to the project, the departure may seem large. However, we should also note that the feedpoint resistance ranges from about 120 to 150 Ohms. Therefore  $j10$  Ohms departure is far less troublesome in any respect than the same reactance with a feedpoint resistance of 50 Ohms.

To see how much of a worry the departure from resonance might be, I calculated the change of dimension between the imported NEC models and the corrected versions. The results appear in **Table 3**. The table lists the ratio of corrected to uncorrected circumference, the amount of change as a percentage, and the SWR of the original model relative to the reported feedpoint resistance.

Degree of Correction: MININEC to NEC-4

Table 3

Antenna	Circumference Change ( $\lambda$ )	(%)	SWR of Initial MININEC Model
Reference dipole	0.0	0.0	1.00:1
Square, mid-side fed	1.0066	0.7	1.08:1
Diamond, point fed	1.0093	0.9	1.13:1
Triangle (delta), point fed	1.0242	2.4	1.32:1
Triangle (delta), mid-side fed	1.0081	0.8	1.12:1
Circle (45 segments)	0.0	0.0	1.00:1

Note: SWR values are relative to resistive component.

All but one of the models show less than a 1% required dimensional change. For these models, it would be inappropriate to worry about the differences relative to an eventual physical implementation of the loop structures. Construction variables would likely wash out the difference between the original and the adjusted dimensions. In practice, we likely could not distinguish between construction and modeling variations. As the title of this column suggests, some modeling differences are worth the worry; others are not.

The one case in which we needed to change dimensions by more than 1% involves the point-fed delta loop. The 2.4% increase in the circumference to restore resonance in the MININEC model leaves us with a small worry that is more prominent in this program than in NEC. From **Table 2**, we find a corrected feedpoint impedance that is very much higher than expected. Indeed, the value is higher than the source impedance of the circular loop. The model from which

we derived the feedpoint impedance uses only 16 segments per side. To MININEC models we may apply the convergence test, raising the number of segments per wire until the values for gain and impedance stabilize. For the point-fed delta, gain is not a problem, but the source impedance may be. Therefore, I increased the segmentation to 44 segments per side in small increments. At this level, the Antenna Model AGT value became 0.999, with a gain that was still 3.05 dBi. However, the resonant source impedance dropped to  $132.6 - j 0.3$  Ohms. Arriving at resonance at the converged value required a reduction in the delta circumference to 1.122 wavelengths. This circumference is very close to the original NEC-model value. At the same level of segmentation, the delta using a mid-side feedpoint showed no change in either the far-field gain of the source impedance. However, the circumference at resonance decreased to 1.109 wavelengths, virtually the same as required by the original NEC model.

## A Final Test

The MININEC divergence between source impedance values using a point-fed source position and a mid-side source position remains somewhat worrisome when we compare those values to values derived from NEC models and corrected with reference to the AGT values. The worries may be minuscule in the context of developing a model that prepares us to construct a physical implementation of the antenna. However, from the perspective of systematic modeling for comparative purposes, the worries grow in both size and number.

Instead of a single concern, we now have two, one general to modeling, the other specific to the present exercise. First, the MININEC AGT scores are universally exceptionally good, despite shortcomings that we found in some of the models. Whereas NEC AGT values are valuable up to an indefinable limit in providing corrected values to the reported gain and impedance, they are less valuable in MININEC. Instead, the convergence test provides perhaps the most critical test for MININEC model adequacy.

Second, the point-fed model source impedance values do not show reasonable agreement between the NEC and the MININEC models, although all other models show good coincidence. Moreover, the MININEC models suggest that the impedance of a point-fed model (both diamond and delta) will be higher than the value exhibited by mid-side fed models. In contrast, NEC models suggest that the source impedance for mid-side and point feeding will be quite similar.

In order to provide some resolution to this question, I compared three NEC models of the delta using a point source location. The first is our original models using split source, but with the segmentation density increase to 33 segments per wire. The second model blunted the feedpoint by inserting a 1-segment "bridge" wire to replace the sharp point. The segment length is identical to the segment length used in the long wires. The third model increased the length of the bridge wire to accommodate 3 segments so that the segments adjacent to the source segment are in the same plane as the source segment and have the same

length. **Fig. 3** shows the point end of the deltas under all three conditions.

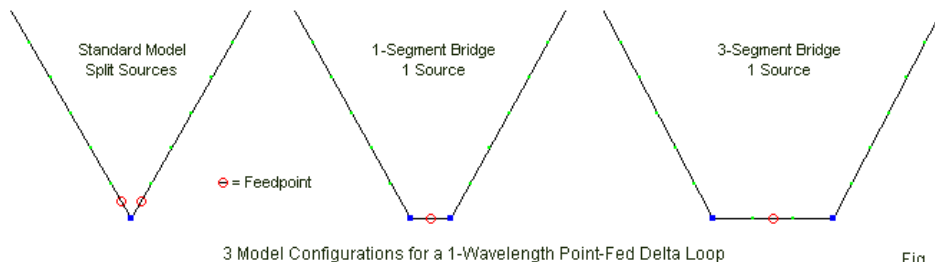


Fig. 3

The results from all three models appear in **Table 4**. The data show a progressive increase in the AGT value toward the ideal, with the final model only slightly imperfect. The nature of the AGT values strongly suggests that the angle of the wires that approach the source segment plays a strong role in yielding less than adequate models. Only when we isolate the source segment from the angled wires do we arrive at a model that passes NEC AGT muster.

NEC-4 Re-Modeling of Point-Fed Delta Loop

Table 4

Antenna	Circumference	Gain	AGT	Cor. Gain	Feed Impedance
Single Point, Split Sources	1.1202 $\lambda$	2.60 dBi	0.901	3.05 dBi	141.2 - j 0.5 (127.2)
1-Segment Bridge, 1 Source	1.1192	2.86	0.947	3.10	131.3 + j 0.8 (124.3)
3-Segment Bridge, 1 Source	1.1220	3.19	1.006	3.16	120.7 - j 0.1 (121.4)

Note: Models use 33 segments/side; segment length 0.011  $\lambda$  throughout.

The bridge wire technique has two interesting consequences relative to the reported and corrected output data. First, the gain

report is higher than for the original mid-side fed delta. It is likely that the length of the 3-segment bridge wire that is parallel to the far side of the delta may account for the small increase in reported gain--an amount that is numerically significant in this comparative exercise but not in operational terms. The second result is the corrected source impedance value, which is identical to the value yielded by the mid-side fed model of the delta. This result suggests that ideal models would show very comparable source values for resonant 1-wavelength closed loops of the same shape, regardless of whether the loop uses a mid-side or point source location.

## Conclusion

Systematic modeling exercises raise numerous concerns along the way. The present exercise sought to compare 1-wavelength closed loops to examine a number of conflicting claims about their performance. Our interest in the exercise has less to do with the conclusions that we might reach about such loop structures than about the worries raised by the modeling effort. Some worries proved to be relatively insignificant. Other gave us pause and required us to employ all relevant model adequacy tests and even work-arounds to resolve. In the process, we also considered different contexts, some of which made the worries important and other of which reduce them to mere footnotes on the modeling effort.

Knowing when to worry, how much to worry, and what to do about the worry are all parts of mastering the art and craft of antenna modeling.

## Chapter 126: "Ideal" Polar Plots

**NEC** outputs are strictly tabular. Most NEC users obtain a commercially available package that includes--as a matter of course--a polar plot facility for graphing the radiation pattern of an antenna model. Very often, we lose track of the fact that the software writer as a service to users adds these modules in order to make the results of a simulation more (visually) accessible to the modeler. Especially if we have used only one package, we face the temptation of thinking that the graphing facility is an integral part of the NEC calculation core.

As post-calculation facilities, polar plot facilities come in many flavors. Commercial packages tend to develop modules to serve the widest range of users equally. However, numerous firms have developed their own modules for special purposes, for example, satisfying FCC requirements for antenna patterns. Many polar plot facilities offer a wide range of plotting alternatives. Some offer a choice between linear or log scaling of the plot. Many also offer a selection of what data to graph, including the total gain, component gain (either major-minor axis or vertical-horizontal), and possibly the phi and theta voltage components of the far field. A few offer left-hand and right-hand circularly polarized patterns. One package even offers azimuth patterns for ground-wave calculations.

Polar plots are generally available for either azimuth/phi or elevation/theta patterns, as dictated by the selections available for calculation within NEC. These pattern choices use conventions

inherent to the NEC coordinate system. An azimuth or phi pattern within NEC software generally is a pattern in the X-Y plane, with a user-selected angle relative to that plane (elevation) or to the zenith (theta). An elevation or theta pattern calculates values with the Z-axis as the basis and on a plane that the user selects by specifying a phi or azimuth angle, where zero degrees coincides with the X-axis in the model geometry. Free-space elevation/theta patterns may use a full 360-degree plot, but models employing a ground are restricted to the hemisphere above ground.

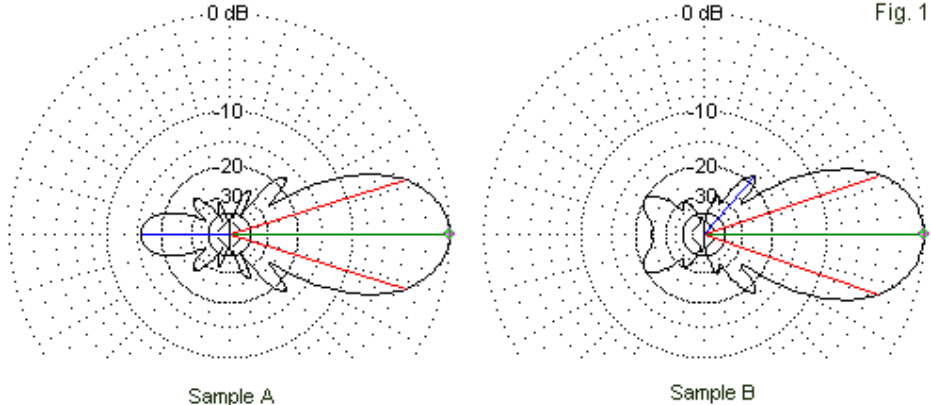
Within the polar plots, software writers try to provide a variety of critical information needed by most modelers. Therefore, patterns usually show a line from the pattern center along the heading of maximum gain. Where possible, the plot will also indicate with lines the limits of the half-power or 3-dB beamwidth. Some plotting facilities also show by a line the strongest lobe other than the maximum gain lobe. Finally, the plot may show one or another form of front-to-back ratio, usually in an inset to the plot and listed in tabular format. Indeed, in most cases, the key data registered by the bearing lines appears in the inset table.

As excellent as are the polar plot facilities offered by various implementations of NEC, they are not quite ideal from the perspective of a heavy user. These notes enumerate some of the shortcomings of polar plot facilities and some of the features that I would like to have available. These features would be part of what I would like to think of as an ideal polar plot facility. I shall list them without regard to their programming feasibility. Inevitably, we shall encounter situations that will tell us why I am unlikely ever to see a

polar plot facility that provides them. Even if I specify that they do not all need to appear at the same time, there are limitations arising from the nature of the antennas that we model that make many of the features impractical, if not impossible, to supply.

## Some "Back-and-Forth" Desires

Many patterns (phi or theta) display multiple lobes in a context in which we can easily identify a forward and a rearward direction. Modules that identify both the strongest lobe and the next strongest lobe suffer a limitation. In some patterns, the second strongest lobe may be a secondary forward lobe, while in others, the second strongest lobe may be the strongest rearward lobe. **Fig. 1** provides a sample of each type of pattern.



One Limitation of Conventional Polar Radiation Plots

Several difficulties arise from the fact that Sample A and Sample B identify different lobes as the second strongest, that is, as the major sidelobe. The accompanying data inset may identify the sidelobe, its bearing, and its strength (and relative strength to the main forward lobe). However, only Sample B gives us information on the main forward sidelobe; Sample A gives data for the main rearward lobe. Now suppose that we perform a frequency sweep for the subject antenna. In the course of the sweep, both patterns may appear, although at different frequencies. The sweep (for example, in EZNEC) will often record the data for the sidelobe strength. Unfortunately, such data is not usable as a record of the main forward sidelobe strength, since some of the values belong to a different lobe.

If we focus only upon directional antennas of the type whose patterns appear in **Fig. 1**, we may arrive at a nearly ideal request for additional information on the plot. **Fig. 2** summarizes in a series of color-coded lines a more satisfactory user situation. In viewing the figure, also imagine an enlarged inset with tabular data for all of the lines.

Some Useful Polar  
Plot Heading Lines

- Main Forward Lobe
- 3-dB Beamwidth Limit
- Secondary Forward Lobes
- 180-Degree Bearing
- Rearward Lobes

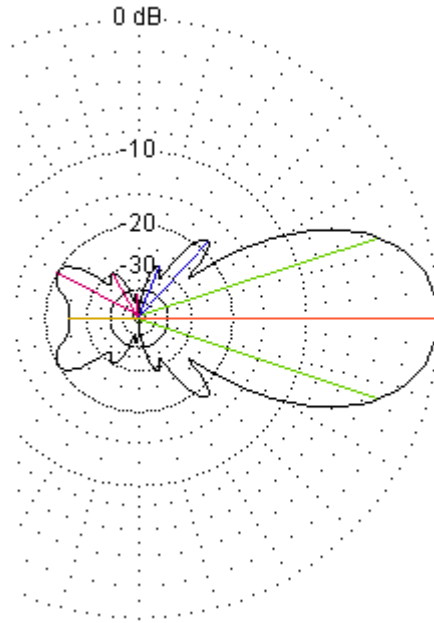


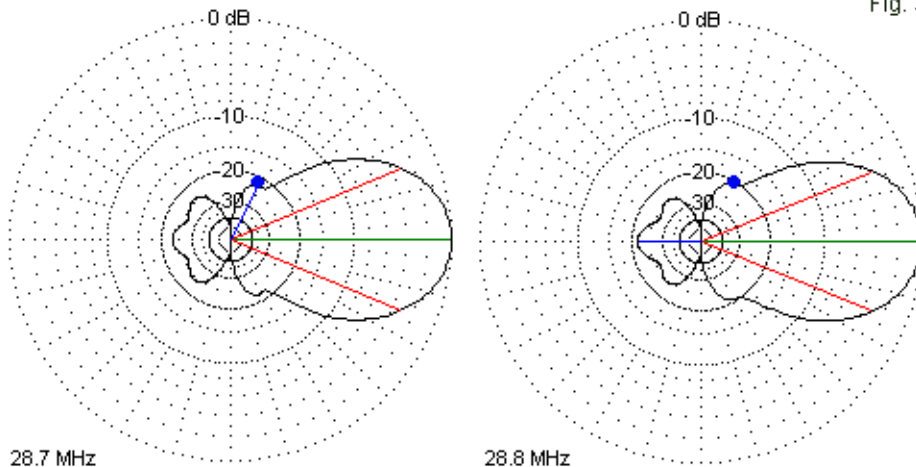
Fig. 2

First the plot should identify forward and rearward quadrants. This task is relatively easy for antennas with deep nulls that are 90 degrees off the main forward gain direction. As usual, the plot identified the main forward heading with a line, and also shows the 3-dB beamwidth limits. In addition to this information, the plot also identifies each of the remaining forward lobes. Immediately, we encounter a challenge, since there is no single standard for distinguishing a true lobe from a bulge in the pattern. We might apply a 3-dB rule, that is, to identify a lobe as such when there is a 3 dB difference between the lobe peak gain and both adjacent null

regions (regions with lower gain values). This rule would give each lobe its own half-power points. Anything less than 3-dB would be a bulge, a common feature of many long Yagis used above their design frequencies.

The more usual technique in identifying a lobe is simply to register when a pattern, following the progression of sampled plotting angles, shows an increase in gain relative to the values at both the preceding angle and the following angle. This method relieves the plotting facility of the need to determine if the lobe meets a 3-dB measure. The technique does not eliminate mere bulges, as illustrated in **Fig. 3**. The patterns are for the same Yagi, but with an operating frequency change of 100 kHz.

Fig. 3



The Difference Between a Lobe and a "Bulge"

Since the patterns are both symmetrical, the locating dot does not obscure the fact that each pattern shows an apparent projection at the dot location. In the left pattern, the dot at a phi angle of 63 degrees shows a higher gain than we obtain at 62 and 64 degrees. The progression, in dBi/degrees, is -9.68/62, -9.67/63, -9.70/64. A change of 0.01 dB suffices to mark a lobe, as the plot line indicates. 100 kHz higher, we find the following progression of values: -8.35/60, -8.40/61, -8.48/62, -8.58/63, -8.72/64. The progression shows a steady decrease in gain, but the rate of decrease changes through the sampled range. The changing rate of gain decrease is enough to yield a pattern bulge. (In some cases, but not this one, we may convert a bulge into a lobe by using a smaller increment

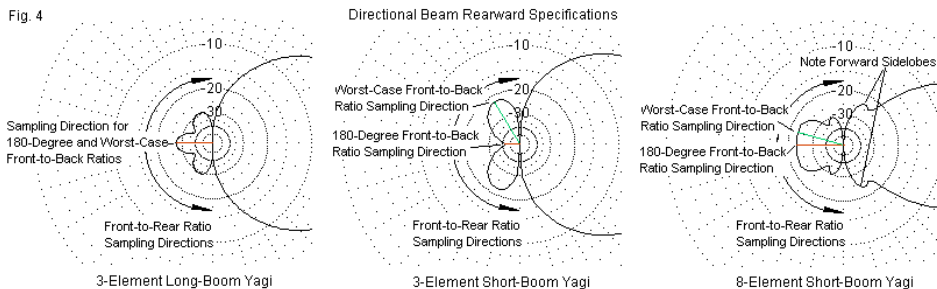
between samples, such as 0.1 degrees.) Although we may consider bulges to be incipient lobes, their location will likely always be a viewer task.

To the rear, we find in **Fig. 2** a 180-degree line that simply continues the line from the point of maximum gain. The line is marginally useful in distinguishing arrays with symmetrical patterns from those with non-symmetrical patterns (such as parasitic beams based on a corner-fed half square). More significant is the identification of each rearward lobe--with associated data shown on the tabular inset.

## Bringing Up the Rear

Once we move to the rear quadrants of a directional antenna, the data becomes more complex, since we are very often interested in some kind of front-to-back ratio. Since it is the easiest to calculate, most polar plot facilities provide the 180-degree front-to-back ratio value. The 180° front-to-back ratio is the main lobe forward gain (or the maximum antenna gain) minus the gain of the lobe (however big or small) that is 180° away from the heading of the maximum forward gain. If the main forward lobe is split or does not align with the graph heading, the 180° front-to-back ratio is 180° away from the direction of maximum pattern strength. Hence, the value may not be for a direction directly to the rear of the antenna structure. Since a Yagi is usually symmetrical, the maximum gain will normally be directly forward, and the 180° front-to-back ratio will indicate the relative strength to the direct rear. Note that if we use a normalized scale, we can read the front-to-back ratio directly from

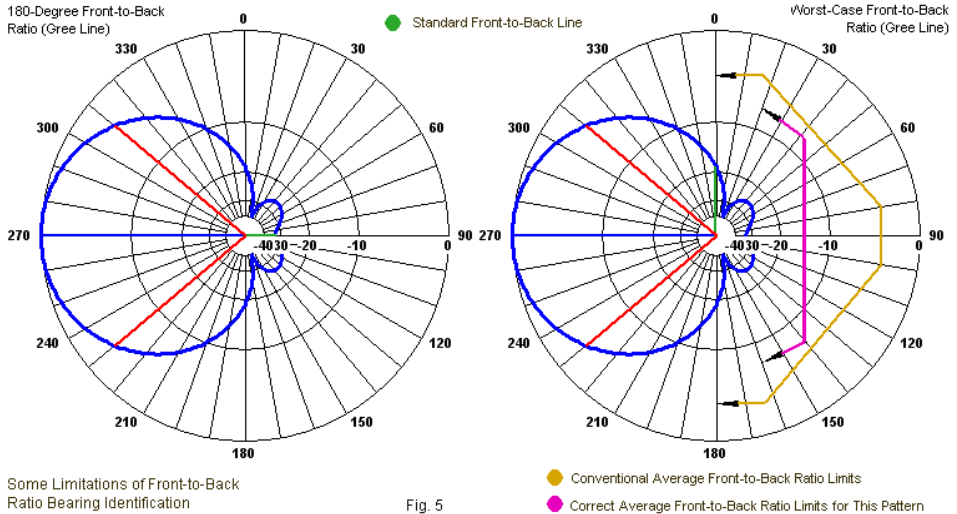
the plot--between 25 and 30 dB relative to the maximum gain of the antenna in the left-most pattern. The left portion of **Fig. 4** shows a part of a Yagi pattern in which the 180-degree lobe is the strongest rearward lobe.



In **Fig. 4**, the center pattern shows a 180-degree gain of very tiny proportions. Hence, the 180° front-to-back ratio is very large (over 40 dB compared to a "mere" 27 dB for the leftmost pattern). Yet, we find rearward lobes that have considerable strength. The line through one of those lobes indicates the direction of maximum strength. It is only about 22 dB weaker than the maximum gain. Some sources call this the worst-case front-to-back ratio, and its value is the maximum forward gain minus the highest value of gain in either rearward quadrant. For this antenna, the 180° front-to-back ratio does not give a true picture of the QRM levels from the rear, so some folks prefer to use this figure as a better indicator. The worst-case front-to-back ratio provides the most conservative value for rearward suppression of QRM. The rightmost graphic in **Fig. 4** shows that the 180° and the worst-case front-to-back values do not require separate lobes, even though the values differ.

We are not done with front-to-back ratios. Each sketch in **Fig. 4** contains an arc going from  $90^\circ$  on one side of the line of maximum gain around the rear to the other point that is  $90^\circ$  from the maximum gain line. Suppose that we add up all of the gain values at the headings that pass through the arc. Next take their average value. Subtract the average gain value to the rear from the maximum forward gain and you arrive at what some call the front-to-rear ratio. Others call this the averaged front-to-back ratio. A  $5^\circ$ -interval between rearward readings is often sufficient for this sampling. The rationale behind using the front-to-rear ratio is that it provides an averaged total picture of the rearward QRM suppression.

Although I am not aware of any software that provides an average front-to-rear ratio, at least one maker provides a user selection between the 180-degree and the worst-case values. The worst-case value is detected by using the main forward lobe bearing and creating sampling limits 90 degrees to the rear of that bearing. Within the rearward quadrants, the program then identifies the strongest lobe and uses its gain in the front-to-back calculation. The process sounds simple enough (at least arithmetically) until we encounter cases like the ones illustrated in **Fig. 5**.

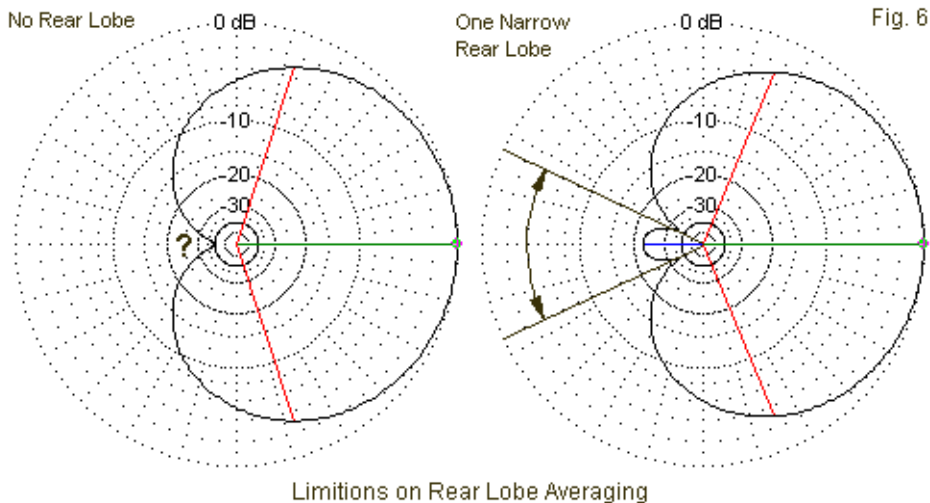


The azimuth pattern shown applies to a Moxon rectangle, which does not place its side nulls at the 90-degree mark relative to the heading of maximum gain. Rather, its nulls occur closer to 110 degrees off the main heading. Hence, the preset limit line for determining the worst-case front-to-back ratio uses a portion of the forward lobe as a legitimate direction for the worst-case front-to-back ratio calculation.

The same consideration--that is, the location of the deep side nulls--applies equally to the calculation of the average front-to-rear gain value. If one were to implement this additional front-to-back calculation, one might use the preset limits that gave the odd heading for the worst-case rearward lobe or one might use some

sort of comparative scheme to detect the deep side nulls and then to use the reduced scanning region to determine the average front-to-rear ratio.

Although the challenges of determining "proper" values of the worst-case and the average front-to-back ratios are significant, they are not insurmountable. However, not all azimuth patterns have detectable side nulls that occur--either at all or anywhere close to the side of the beam pattern. **Fig. 6** shows two cases--very typical for vertically oriented arrays--in which perhaps only the 180-degree front-to-back ratio makes good sense. On the left, we have a common cardioidal pattern with only one null directly opposite the main forward lobe direction. A worst-case direction would have to choose between the 180-degree direction or involve the main lobe. An averaged front-to-back ratio would have little, if any, meaning in this case.



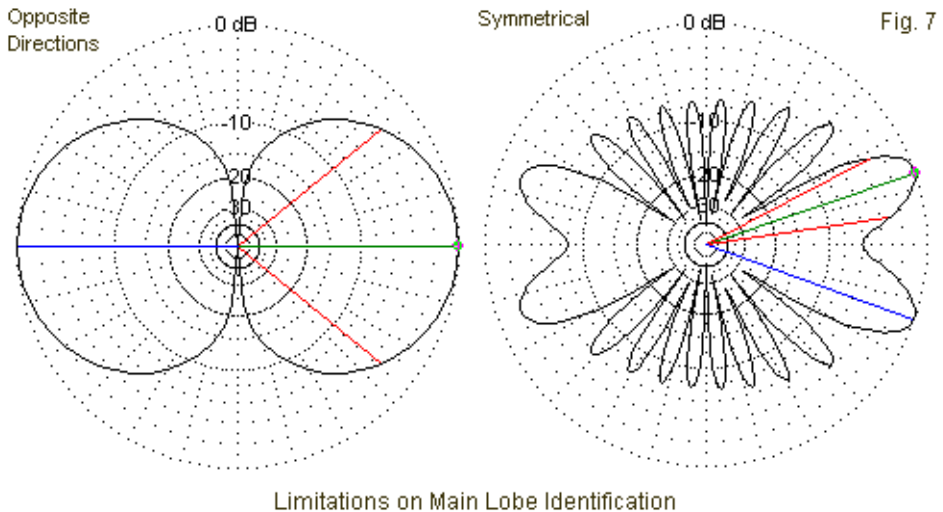
The right-side pattern has a rearward lobe, but it is problematic. Once more, the idea of a worst-case front-to-back ratio becomes co-terminal with the 180-degree front-to-back ratio. In theory, we can take an averaged front-to-rear reading using only the rearward lobe. However, the angles included in the calculation are so few as to make the calculation less than useful.

### Which Way Did He Go?

Our hope for an ideal polar plot facility that includes on screen all of the information that we might wish to see--whether all at once or serially--has significant limitations in the rearward mode for directional antennas. Very likely, programming various scans and

detection systems is less of a problem than having the system know when certain criteria are relevant and when they are not. Antenna models do not advertise themselves as having certain characteristics calling for the application of certain variations on standard measures. Rather, the patterns emerge from the data. At present, post-pattern interpretation remains a user operation.

Of course, many antenna patterns are not directional in the sense of having strict forward and rearward headings and a single forward lobe. A primary example is the simple dipole, which has an E-plane bi-directional pattern. The left pattern in **Fig. 7** shows the difficulty facing a polar plot facility.



The plot identifies one of the dipole lobes as the main lobe and relegates the other to the status of a rear, side, or secondary lobe. Ordinarily, the software decides on the main lobe by selecting the first lobe exhibiting maximum gain that it encounters in sampling the gain values starting at zero degrees. Zero degrees conventionally align with the X-axis in the coordinate system of the model geometry. Hence, for a dipole with the element ends aligned parallel to the -Y/+Y axis, the main lobe will be at zero degrees. Had the element been aligned parallel to the -X/+X axis, the main lobe would be at 90 degrees, counting in the phi or counterclockwise manner. (Special note: many polar plot systems also sample adjacent angles for a span that extends until the gain value changes; the system then centers the indicator line within the range of angles showing the maximum gain value. The NEC output report records gain values in dB using 2 decimal places. Hence, for broad lobes like those of the dipole or for small angular increments such as 0.1 degree, there may well be a considerable set of angles having the same gain value. Similar techniques may be applied to any of the headings identified in terms of gain, such as rear and side lobes.)

In fact, the identification of the first-encountered lobe as the main lobe and the other dipole lobe as non-main is arbitrary and a function of the polar plot system design. Electrically, both lobes are equal. However, it remains a user task to examine the plot and the data included with it to establish that the pattern is equally bi-directional. Certain cases, such as very closely spaced wires of which only one has a source, may exhibit bi-directional patterns broadside to the wire pair but show a very tiny (and normally

operationally insignificant) differential in gain in the plane of the wires. For cases of true bi-directionality, the availability of a clear graphic representation of the pattern and confirming data tends to make the arbitrary designation of one lobe as the main lobe harmless.

The right side of **Fig. 7** present the same situation in a different context. Although the pattern is directional when looking at the plot from left to right, we find a symmetry when viewing the pattern vertically. (The pattern is for a single end-fed unterminated long-wire antenna, with the source at a position corresponding to the left side of the pattern.) Since this particular facility counts counterclockwise, the main lobe is at the first maximum-gain angle greater than zero. The sampling technique does not encounter the second and equal lobe until it is approaching 360 degrees in its sequential scan. Therefore, the lobe with the lower angular value receives the main lobe designation, with its equal mirror lobe receiving secondary status. Once, more, the user must use a careful review of the plot and associated data to confirm that the two lobes are equal.

A Complex Lobe  
Identification  
Problem

Many Lobes,  
Several of  
Equal Strength

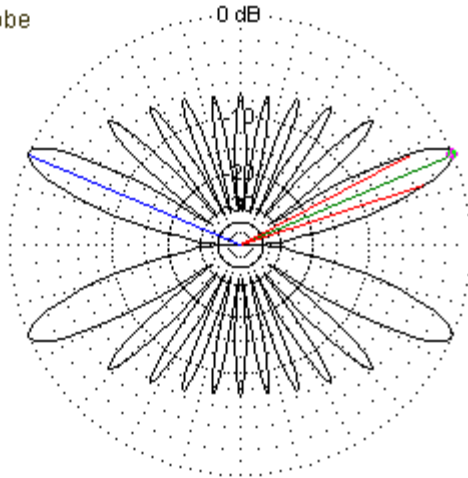


Fig. 8

We may complicate the task facing a polar plot facility even further by increasing the number of main-lobe equivalents. The pattern shown in **Fig. 8** is for a center-fed doublet that is many wavelengths long. The model extends the wire parallel to the  $-X/+X$  axis, so that the broadside direction is up and down relative to the page or screen. In this case, the program identifies the main lobe as the first lobe of maximum gain that it encounters counting counterclockwise from zero. The secondary lobe is the next lobe of maximum gain that it encounters as the angle of sampling increases. This lobe becomes the side lobe. However, two other lobes in the pattern have maximum gain values but receive no markers. In this case, the user who restricts himself to the graphics and data within the polar plot facility can only presume that the remaining main-lobe equivalents are in fact the symmetrical matches of the lobes

bearing designations. Confirming true symmetry in the model requires attention to the detailed radiation pattern data in the NEC output report or to any convenient truncated version provided by the software. For simple models, such as those used to illustrate these notes, a presumption of symmetry may be justified. However, for more complex geometries, the presumption may hide subtle differences.

By now, it should be clear that the desired identifications of all relevant lobes on a plot is likely impractical. This conclusion applies not only to the differentiation of all forward and rearward lobes for a directional antenna, but as well to antennas such as shown in **Fig. 7** and **Fig. 8**. Indeed, a plot with lines indicating each lobe would clutter the graphical presentation and obscure the pattern shape. At the same time, scanning the tabular data is often cumbersome, since a full azimuth/phi scan with 1-degree increments will have 360 entries. If we use an increment of 0.1-degree, the number of entries increases tenfold.

However, there is a technique that might be used to create a compact table that shows only the headings of lobes and nulls within the overall pattern. No system is likely to be perfect in the sense of recording where lobes should be but are mere bulges. For example, a vertical antenna placed well above ground will show a depression of both gain and null-depth values in elevation/theta patterns at the pseudo-Brewster angle. Nevertheless, a suitably programmed sampling and comparison routine could identify all of the lobes and nulls in a pattern using a simple comparison with values at adjacent sampled angles. When placed in tabular form,

the table might look something like **Table 1**, which records the lobes and nulls for the pattern in **Fig. 8**.

Lobe-Null Table: Fig. 7			Table 1
Angle	Total Gain	Lobe (l)/	Main:Lobe/
Degrees	dB	Null (n)	Null Ratio
0	-99.99	n	99.99
23	8.13	l	0
35	-24.29	n	32.42
43	3.99	l	4.14
50	-23.07	n	31.2
57	2.39	l	5.74
63	-24.93	n	33.06
69	1.46	l	6.67
74	-24.85	n	32.98
80	0.94	l	7.19
85	-24.64	n	32.77
90	0.98	l	7.15
95	-24.64	n	32.77
100	0.94	l	7.19
106	-24.85	n	32.98
111	1.46	l	6.67
117	-24.93	n	33.06
123	2.39	l	5.74
130	-23.07	n	31.2
137	3.99	l	4.14
145	-24.29	n	32.42
157	8.13	l	0
180	-99.99	n	99.99
203	8.13	l	0
215	-24.29	n	32.42
223	3.99	l	4.14
230	-23.07	n	31.2
237	2.39	l	5.74
243	-24.93	n	33.06
249	1.46	l	6.67
254	-24.85	n	32.98
260	0.94	l	7.19
265	-24.64	n	32.77
270	0.98	l	7.15
275	-24.64	n	32.77
280	0.94	l	7.19
286	-24.85	n	32.98
291	1.46	l	6.67
297	-24.93	n	33.06
303	2.39	l	5.74
310	-23.07	n	31.2
317	3.99	l	4.14
325	-24.29	n	32.42
337	8.13	l	0
360	-99.99	n	99.99
Note: Main to Lobe/Null Ratio is in dB; -99.99			
and 99.99 are place holder values.			

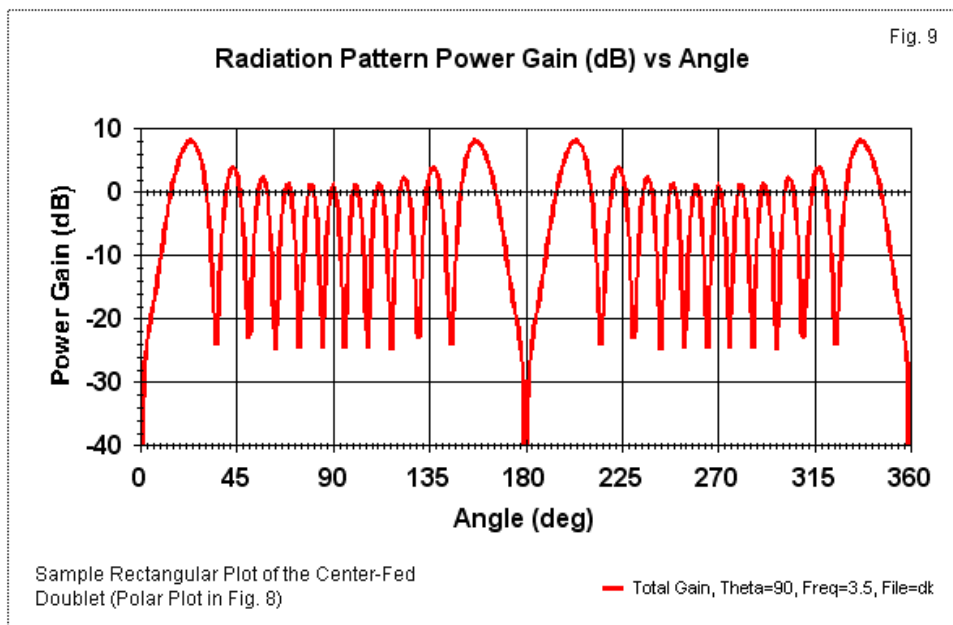
One might embellish the table with whatever other data one might wish to have. Pattern component information is readily available from the NEC output report. The table itself calculates the ratio between the pattern's maximum gain and the lobe or null value. Note that NEC uses a limiting value of -99.99 dB for values lower than that number. Hence, the calculations for the ratio also use 99.99 as a placeholder. One version of MININEC provides lobe data within its polar plot screen, so the technique is not beyond possibility. However, for extremely complex plots, like those we might obtain from an unterminated rhombic with extremely long legs, the table may require considerable size. Hence, an independent table might be a better program facility.

The existence of such a table can be quite useful. By examining the table and the polar plot together, the user may decide which lobes count as forward and rearward lobes for a non-standard directional antenna plot. As well, the short table allows quick identification of all equivalent main lobes and their headings. Moreover, the comparative null depth values in a many-lobed pattern can be very instructive. (Unfortunately, the information in **Table 1** does not result from software, but only from an eyeball scan of the full radiation pattern data in the NEC output file. However, the exercise may have converted my eyes into a different kind of software.)

## Conclusion

In my exploration of the "perfect" polar radiation pattern plot, I have purposely exceeded the boundaries of what we should expect such plots to show us, especially in the face of the great variety of

possible antenna patterns that might emerge from models. The pretext has provided an opportunity for us to refine that ways in which we look at such plots to derive from them--and the accompanying tabular data--the most data. At the same time, the exercise has alerted us to limitations inherent in converting tabular data into a graphic form.



We may overcome some of the limitations by creating external tables. For example, we might export the radiation pattern portion of the NEC output data to a spreadsheet which then automatically calculates the lobe and null information contained in **Table 1**. As

well, we might use that data to create a rectangular graph of the lobes and nulls for easier identification. Nevertheless, tabular data remains the most precise method for identifying and quantifying the many lobes and nulls in a radiation pattern, as well as obtaining an accurate measure of their relative values and the rates of change.

## Chapter 127: A Potpourri of Modeler Miscellanea

In the course of modeling, analyzing models, looking at modeling software, and sundry activities, I run across bits of information that might be useful to other modelers. Normally, I wait until I have a sufficient collection of information of a particular theme and then incorporate my scraps of information into the broader column. However, some useful items seem never to have a thematic home. So they sit forlornly on note-pad sheets, pieced by the old-fashioned spindle file that I use. Some scraps of paper have multiple holes, because I use the notes myself. Eventually, the paper begins to yellow and grow crisp around the edges. That is my warning to either use the data or lose it in a fit of housekeeping.

The notes in this chapter are my attempt to pass along some items that I have found useful. Perhaps the one common thread is that all of the small entries share is an involvement with numbers. None of these matters is particularly new. Instead, each matter represents something useful that we do not happen to find in common handbooks, especially those directed toward radio amateurs. A few are matters that we forget with age and distance from school. And some are items that we all too easily overlook on the first go-around and never return for a second look.

### 1. Pseudo-Brewster Angles

Chapter 3 of *The ARRL Antenna Book* contains an excellent introduction to the effects of ground upon antennas of various sorts. An interesting section of the treatment concerns the pseudo-

Brewster angle (PBA) as applied to the radiation patterns of vertically polarized antennas (pp. 3-15 through 3-15 of the 20th edition). The PBA rests upon adapting optical concepts to the reflection of radio waves by the ground as a lossy medium. Let's assume that the radio source is a point that shines equally in all directions. It shines both downward and upward. Therefore, radio waves (or rays) at various angles above ground will sometimes add and sometimes subtract from each other, creating the lobes and nulls that become familiar in elevation patterns we draw from antenna modeling software. Unfortunately, the current chapter does not illustrate the PBA with any such patterns, so many folks just pass over the material without realizing its implications. Therefore, let's approach the PBA from the other direction.

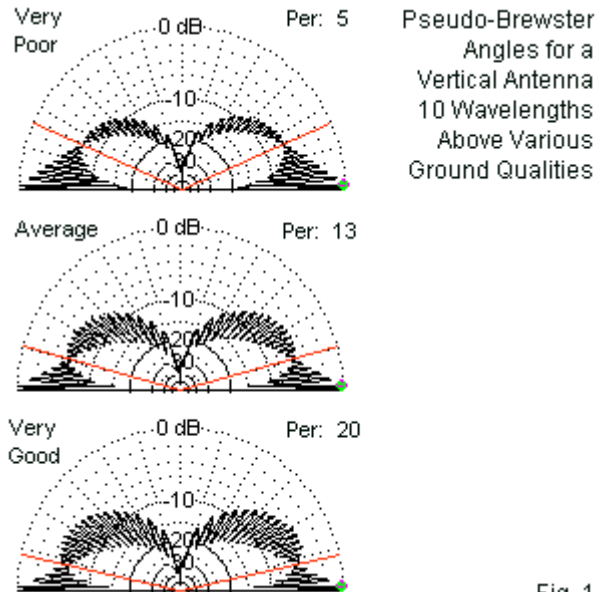


Fig. 1

**Fig. 1** shows the elevation patterns of a single vertical antenna (a J-pole), but over 3 different levels of ground quality. Very good ground has a standard definition of a conductivity of 0.0303 S/m and a relative permittivity (dielectric constant) of 20. The values for average ground are 0.005 S/m and 13; while for very poor ground, the values are 0.001 S/m and 5. The red lines in the figure indicate an elevation region in which the lobes diminish in strength and the nulls diminish in depth. The result is a gain level that is close to the free-space gain of the antenna. This is the PBA, the angle at which the incident and reflected rays neither add nor subtract from each other.

The next notable feature of **Fig. 1** is that the angle changes as we change the ground quality. The better the ground quality, the lower the elevation of the PBA. The effect occurs at all frequencies, although it has a major impact on lower HF antenna installations. As well, the effect results largely from waves already in the far field, so adding radials to a monopole to improve ground quality has minimal consequence for the PBA. The figure uses antennas a many wavelengths above ground so that the effect shows clearly in the elevation pattern that consists of many lobes and nulls.

The *Antenna Book* account provides a very precise and equally forbidding set of equations for calculating the PBA. They involve calculating the complex relative permittivity of the soil with the required frequency adjustments and then using this calculation in a long equation. In many instances, we only need to know the general vicinity of the PBA for the soil quality that we estimate beneath our feet. Over dry land, the soil conductivity plays only a small role in determining the PBA. Therefore, we may use the relative permittivity alone to calculate an estimated PBA that is good within perhaps +/-2 degrees of elevation over poorer soils and within perhaps +/-1 degree for better soils, all from the mid-HF region upward. One shortcut equation follows:

$$PBA = \sin^{-1} \left( \frac{1}{\sqrt{\epsilon}} \right)$$

Since we are only estimating the PBA, you might use either the arcsin or the arctan of the expression in parentheses, where

epsilon is the symbol for relative permittivity. For very good soil, we obtain an angle of about 12.5-13 degrees. Average soil gives a value between 15.5 and 16 degrees. Very poor soil yields 24 to 26 degrees. You may compare these values to the angles of the lines in **Fig. 1**.

The precise value of the PBA rests on several factors, such as the source being a true point, knowing with quite good accuracy the soil conductivity and permittivity at depths to which radio waves penetrate, and the frequency of operation. The crude estimate, which does not depart too far from the calculated values in the *Antenna Book* (Chapter 3, Table 3), bypasses most of these factors. Hence, its use is limited, mostly to partially explaining the depression region we find in elevation angles of all vertically polarized antennas and to setting an expectation that finds the depression region in these radiation patterns normal rather than odd. If your operating frequency is quite low or you are over salt water, use the entire equation in the *Antenna Book*.

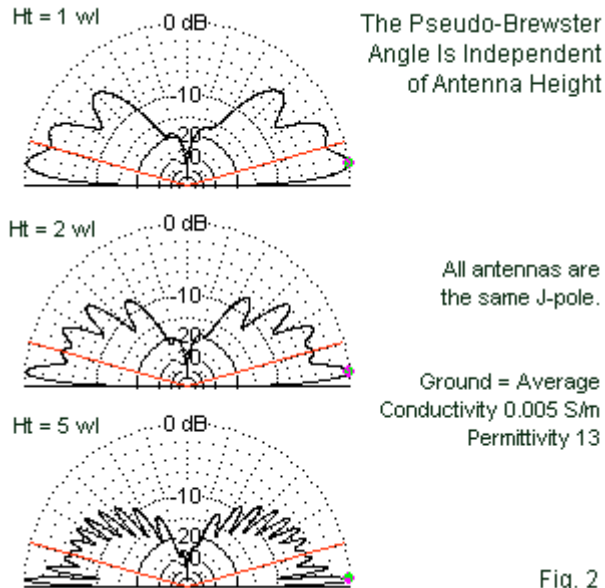


Fig. 2

One final note: the PBA is not dependent upon antenna height. As shown in **Fig. 2**, antennas at different heights show just about the same PBA or depression region of the elevation pattern. However, the patterns that we encounter for lower vertical antenna heights become ambiguous. Very often, we cannot tell if the depression is a PBA effect or a simple shallow null between lower-angle lobes. As we raise the antenna--in this case to a height of 5 wavelengths--the picture grows clearer. Without PBA, the null between the lower two lobes in the upper portion of the figure would be deeper. Still, since we are never without PBA when using a vertical antenna, we

cannot achieve the deeper null between lobes, at least not over dry land.

For modelers, the introduction of the crude PBA calculation should take the mystery out of elevation patterns for vertical antennas, especially those well above ground. Those who have only modeled a few such antennas may wonder whether the depression region is a software problem or a problem with their particular model. Actually, it is neither. Rather it is part of the normal propagation of far-field radiation. (Horizontal antennas do not share this effect, at least not in the same way or to the degree shown by vertical antennas.)

## 2. The Velocity Factor of Coaxial Cables

Most introductory texts for amateur radio operators present the concept of a coaxial transmission line or coaxial cable in an abbreviated and incomplete manner. **Fig. 3** outlines the essential dimensions of the cable necessary for calculating the characteristic impedance ( $Z_0$ ) of the line. The dimension  $D$  is the diameter of the inner surface of the shell or braid, also generally called the outer conductor. Dimension  $d$  is the outer diameter of the center or inner conductor. Due to skin effect at HF and above, current do not penetrate deeply into either conductor. Therefore, the outer surface of the braid or shell does not play a role in the transmission-line function of the cable. However, it may play a role in radiation or common-mode currents.

## Basic Terms of a Coaxial Transmission Line

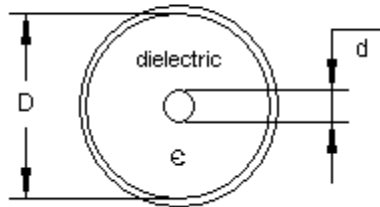


Fig. 3

Between the inner and outer conductors of a coaxial transmission line, there is a space that cable makers fill with an insulating or dielectric material. The material may range from dry air to an inert gas to a foam material to a solid plastic material. The dielectric plays a role in the determination of the cable's  $Z_0$  according to the relative dielectric constant or permittivity (epsilon) of the material. Therefore, the complete equation for calculating the  $Z_0$  of a coaxial cable requires that we include the factor:

$$Z_0 = \left( \frac{138}{\sqrt{\epsilon}} \right) \log_{10} \left( \frac{D}{d} \right)$$

In most lower-level treatments, we do not find epsilon. Rather, the treatments assume the improbable case of using dry air as the dielectric. Dry air has a relative permittivity of about 1.0, and so the term drops out. In fact, most of the cables used by radio amateurs (and professionals) use a dielectric other than air.

The missing term then creates a mystery. Independently, we are told that all transmission lines have a velocity factor (VF) such that the cables electrical length is always longer than its physical length. The ratio of physical length to electrical length defines the VF value. Hence, a cable with a VF of 0.67 is electrically 1 wavelength long when the cable is physically about 2/3-wavelength long. We may acquire a sense of the source of the velocity factor's source by noting differences in the dielectric material used on cables with the same designation but using different dielectric materials.

The unknown might go away if we began with the more complete equation for calculation of a cable  $Z_0$ . Then we could set up the relationship between epsilon and VF:

$$VF = \frac{1}{\sqrt{\epsilon}}$$

This version of the relationship requires that we know the dielectric constant for the material used between cable conductors. In fact, cable specification tables are more likely simply to name the dielectric material and to list a velocity factor value. Therefore, we may turn the simple equation around.

$$\epsilon = \frac{1}{VF^2}$$

Using this equation, we may easily derive the dielectric constant for the cable material. For example, one common dielectric material

used in cables is called FPE or foamed polyethylene. A typical cable VF using this dielectric is 0.78. Our handy equation yields a permittivity of about 1.6. Foamed polyethylene is a mixture of solid polyethylene and trapped dry air. Therefore, our exploration of the dielectric material must end here.

Cables with solid dielectrics are historically older and use a solid polyethylene material. A typical VF value is 0.66. By our equation, the resulting permittivity value is about 2.3. A table in Kraus' *Antennas* shows the value as 2.2, very close to our calculation. (In fact, a value of 2.2 yields a VF of 0.67, another value found in some tables for older coaxial cables.)

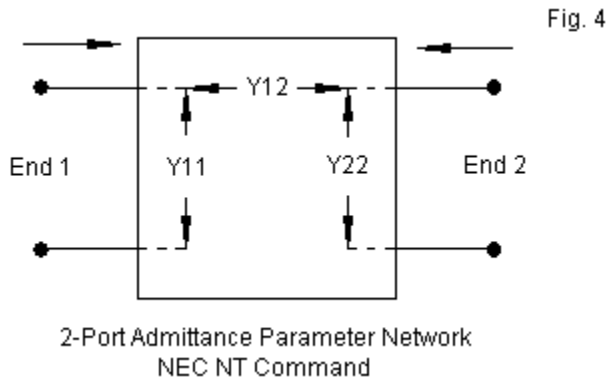
What we learn from this primitive little exercise is that the  $Z_0$  and the VF of a cable are intimately related and not simply independent facts about cables. Of course, we also need to learn that cable specification tables list nominal or typical values for a line's VF. If the length of a line is critical to a given application, such as the construction of a matching section, then the builder must determine the VF of the line to be used. The precise VF of a line varies from one manufactured batch to the next. For example, some foam lines listed as having a VF of 0.78 actually turned out to have a VF in the 0.70 to 0.72 range under tests in the high HF range.

### 3. Modeling a Transformer Using NT

In episodes 95 and 96 of this series, I examined the NEC NT or network command and introduced some rudimentary applications. Since writing those notes, I have acquired another application, but

not a sufficient number of others to form an entire episode. So I shall note it in this collection.

The NT or network command is less familiar to entry-level modelers, although its special application, the TL or transmission-line facility is very familiar. In NEC, a network is a 2-port y-parameter admittance network, as suggested by **Fig. 4**. The network has two ports, designated externally as end 1 and end 2. These ends simply attach to two different segments within the same model. For most applications, these segments require different wires, although the command allows the ends to be different segments on the same wire.



Internally, we must enter values for three shunt or parallel admittance values:  $y_{11}$ ,  $y_{12}$ , and  $y_{22}$ . See the earlier episodes for more details on the meaning of these entries. Here we wish to focus on a special application: the creation of a rudimentary

impedance transformer. To create the transformer, we must know the end-1 impedance ( $Z_1$ ) and the end-2 impedance ( $Z_2$ ). As well, we must decide upon a value for the  $Q$  of the end-1 side of the transformer. In our simplification, we may ignore the imaginary components (susceptances) of each entry and simply calculate values for the real components or conductances. We must also take two simple calculation steps before creating input values for the NT command. First, we calculate the ratio of the end-1 impedance to the end-2 impedance ( $Z_r$ ), an easy task. Second, we calculate the transformer turns ratio ( $T_r$ ), which is simply the square root of the impedance ratio. Under these conditions, we can easily calculate the required real values for the NT command.

$$y_{11} = \frac{Q}{Z_1} \quad y_{12} = -T_r \cdot y_{11} \quad y_{22} = Z_r \cdot y_{11}$$

To see how this works, let's examine a real model before and after installation of the transformer. Suppose that we have a resonant folded dipole, such as shown in the upper part of **Fig. 5.** A .NEC-format model might look like the following lines.

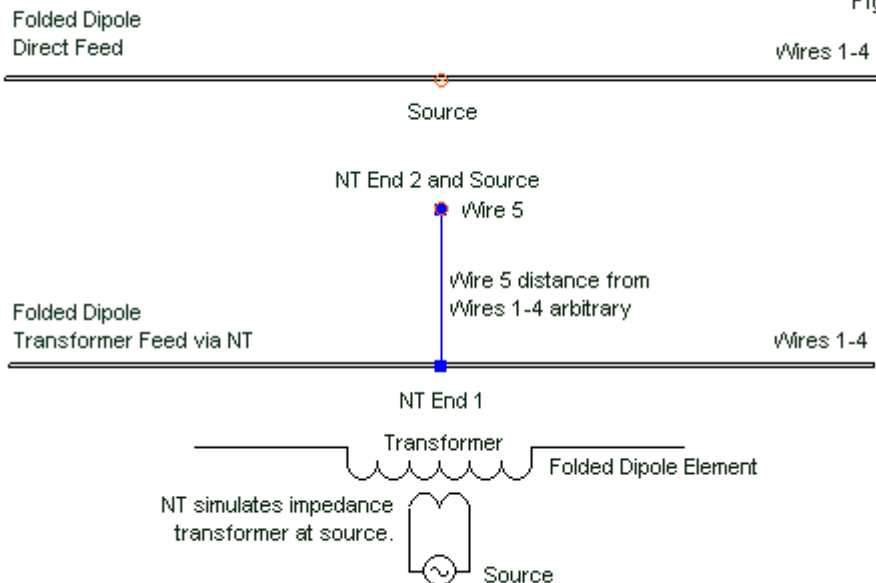
```
CM fd #18 cu 1" 28.5
CE
GW 1,199,-2.513,0.,0.,2.513,0.,0.,5.119E-4
GW 2,1,2.513,0.,0.,2.513,0.,.0254,5.119E-4
GW 3,199,-2.513,0.,.0254,2.513,0.,.0254,5.119E-4
GW 4,1,-2.513,0.,0.,-2.513,0.,.0254,5.119E-4
GE 0
LD 5,1,0,0,5.7471E+7,1.
LD 5,2,0,0,5.7471E+7,1.
LD 5,3,0,0,5.7471E+7,1.
LD 5,4,0,0,5.7471E+7,1.
```

```

FR 0,1,0,0,28.5
GN -1
EX 0,1,100,0,1,0.
RP 0,1,361,1000,90.,0.,0.,1.,0.
EN

```

Fig. 5



Sample Use of an NT Impedance Transformer with a Folded Dipole

If we run this model, we obtain a source impedance of  $288.7 + j0.7$  Ohms. Now let's suppose that we wish to install a transformer that yields a perfect match to 50 Ohms. The impedance ratio ( $Z_r$ ) is 5.774, while the turn ratio ( $T_r$ ) is 2.403. Selection of  $Q$  is arbitrary with the user, but should reflect a reasonable component value. Let's use 500 as the value. Under these conditions, the value of

Y11-real is 1.7319; the value of Y12-real is -4.1616; and the value of Y22-real is 10.0.

Now we may rebuild the model to incorporate the NT-transformer. We begin by adding a new wire at some arbitrary distance from the antenna wires. The new wire is short and thin and serves as the segment for end 2 of the NT. As well, we move the antenna source (EX) to this wire to show the transformed source impedance. The NT command places end-1 on the former source segment at the center of wire (or tag) 1 in the model at segment 100. The revised model has the following appearance.

```

CM fd #18 cu 1" 28.5
CM NT transformer
CE
GW 1,199,-2.513,0.,0.,2.513,0.,0.,5.119E-4
GW 2,1,2.513,0.,0.,2.513,0.,.0254,5.119E-4
GW 3,199,-2.513,0.,.0254,2.513,0.,.0254,5.119E-4
GW 4,1,-2.513,0.,0.,-2.513,0.,.0254,5.119E-4
GW 5,1,-.03048,0.,.9144,.03048,0.,.9144,5.119E-4
GE 0
LD 5,1,0,0,5.7471E+7,1.
LD 5,2,0,0,5.7471E+7,1.
LD 5,3,0,0,5.7471E+7,1.
LD 5,4,0,0,5.7471E+7,1.
LD 5,5,0,0,5.7471E+7,1.
FR 0,1,0,0,28.5
GN -1
EX 0,5,1,0,1,0.
NT 1,100,5,1,1.731902,0.,-4.161612,0.,10.,0.
RP 0,1,361,1000,90.,0.,0.,1.,0.
EN

```

In the model, note GW5, the new wire and the placement for the EX command. The NT command shows its connections and the parallel admittance values in order. The zeroes following each

numerical value entry represent the imaginary values that we skipped for this simplified transformer. If we run this model, we obtain a source impedance of  $50.1 + j0.1$  Ohms, just what we wanted.

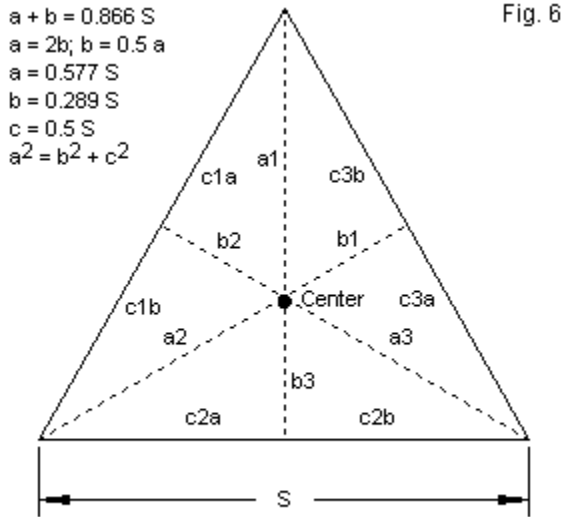
In using the NT command as a transformer, newer modelers should be cautious. First, be certain that you do not invert either the value of  $Z_r$  or of  $T_r$ . Suppose that we had a case of up-transformation, say, from 50 to 200 Ohms.  $Z_r$  is 0.25 and  $T_r$  is 0.5, working from end-1 to end-1 of the network. The temptation will be to think of the transformer as having a 4:1  $Z_r$  and a 2:1  $T_r$ , when the situation requires just the obverse. Second, the use only of conductance components in the network provides an illusion of frequency-independence for the transformer. Hence, we might press it into service as a modeled substitute for a 4:1 balun, many of which are rated for 3.5-30-MHz use. However, over a wide frequency range, we may encounter at least two major variations from our simplified model. The first variation involves the Q of the device components, which may change over a wide frequency range. Remember that we only selected a plausible value, not an actual value. The second variation lies in the device we are modeling. Not all real transmission-line transformers handle highly reactive loads (or antenna element impedances) in the same way as our basic model of a transformer. I have directed these cautions to the newer modeler on the assumption that experienced modelers will automatically be duly cautious.

## 4. The Center of a Triangle

Our next bit of information arises out of numerous models that I have examined and e-mail questions. Suppose that we wish to model a geometric shape with the coordinate origin ( $X=Y=Z=0$ ) at the center. The process is simple for squares and larger polygons. For example, if we have a horizontal square loop, we may take 1/2 the length of a side and use the number as the X and Y values (with suitable + and - designations) as the four corners of the loop. It is now centered on the coordinate system origin.

However, if we wish to set up an equilateral triangle with the same result, troubles begin. Most of the difficulties stem either from sleeping in trig class or from too many passing years since that lesson. Most of the models that come my way use eyeball measures for the corner positions. If it sort of looks equilateral, then it is close enough for the model.

The equilateral triangle is actually a model of simplicity if we remember that the sine of 30 degrees is 0.5 and the cosine of 30 degrees is 0.866. Each corner angle of the triangle will be 60 degrees, and we shall be interested in bisecting each angle into 30-degree angles to obtain a center triangle. **Fig. 6** shows the general layout and the essential relationships among the parts.



Some Handy Equilateral Triangle Relationships

Bisecting each corner angle produces three lines. Where they cross is the center of the triangle. The process creates 6 right triangles, with each composed of an a-, a b-, and a c-line. Because any long line ( $a + b$ ) is the side adjacent to the hypotenuse ( $S$ ) of the figure, its length of 0.866 times  $S$ . Every b-line is  $1/2$  a, or every a-line is twice b. Since the junction of every a-line with the extending b-line is the center of the triangle, the distance from the center to a corner (that is, a) must be  $2/3$  of  $a + b$ .  $2/3$  of  $0.866 S$  is  $.577 S$ . If we set up the triangle so that one corner is parallel to a coordinate axis (arbitrarily X), and if the center is at the system origin, then one corner of the triangle will be at  $0.577 S$  in that direction. The

remaining corners will be at  $-0.289 S$  along the X-axis. The Y coordinates will be + and - half the value of S. You may check your work by using Pythagoras' theorem in which the square of the hypotenuse (c) of a right triangle is the sum of the squares of the other two sides (a and b).

Suppose that I needed an equilateral triangle that is 45' per side. The point along the +X-axis will be +25.97 (with a Y coordinate of zero, of course). The remaining corners will have coordinates of -13.01, -22.50 and -13.01, +22.50. If I apply the theorem to these "back" corner coordinates, I should come out with the value of the X-axis coordinate. Allowing for rounding, a result of 25.98 is close enough to ensure excellent symmetry and a circumference that is on target with the project. (Your hand calculator may give you further precision by adding decimal places to the process, but you will have to decide how many places you enter into your model.)

There is, of course, nothing startling or new in all of this. The entire function of this note is to remind the forgetful (like me) that we can set an equilateral triangle with good precision. We can then use program rotation facilities to align the triangle however we need it. If the triangle is vertical, we can construct it in free space around the origin and raise it to height before adding a ground command.

## 5. Rho's Phase Angle

Thirty years ago, radio amateurs knew only one member of a famous trio: SWR (aka VSWR). Like the Ames Brothers other than Ed, the remaining members languished in obscurity. Today, we

know all of the names: SWR, reflection coefficient, and return loss. We also know that the three facets of transmission-line behavior are intimately interrelated. That interrelationship has come at a cost.

We ordinarily (in handbooks at least) begin with the reflection coefficient. The standard, slightly simplified equation has the following appearance, where  $R_0$  is the characteristic impedance of the feedline, and  $R_{in}$  and  $X_{in}$  are the resistive and reactive components of the antenna at the transmission line connecting point.  $|\rho|$  is the magnitude of the reflection coefficient.

$$|\rho| = \sqrt{\frac{(R_{in} - R_0)^2 + X_{in}^2}{(R_{in} + R_0)^2 + X_{in}^2}}$$

The simplification in the equation consists of omitting the reactive component of the transmission-line  $Z_0$ . The reactance for virtually all transmission lines is very small, and users often do not have access to the value without using manufacturer data sheets. Since the reactance is so small, we may omit it without incurring any significant error in the results.

Next, we often define VSWR based on the value of  $|\rho|$ .

$$VSWR = \frac{1 + |\rho|}{1 - |\rho|}$$

Of course, we may calculate the VSWR directly from the  $Z_o$  of the transmission line and the resistive and reactive components of the antenna feedpoint impedance. We simply substitute the  $|\rho|$  equation right side for each occurrence of  $|\rho|$  in the VSWR equation. Because the reflection coefficient fits more readily into other post-measurement calculations a bit more readily than the VSWR, more and more laboratory instruments using software-based calculations provide their results in terms of  $|\rho|$  rather than SWR. However, if we use the correct Y-axis scale for each, the curves will be identical.

The final member of the trio is return loss, RL.

$$RL = -20 \log_{10} |\rho|$$

We normally measure RL in dB. Since the reflection coefficient will be less than 1, its log will return a negative number. Older texts handle RL as a negative number, but modern instrumentation has multiplied the result by -1 (hence the - sign in the equation) to yield positive results. We multiply by 20 because the terms are for voltage and we wish a result in dB.

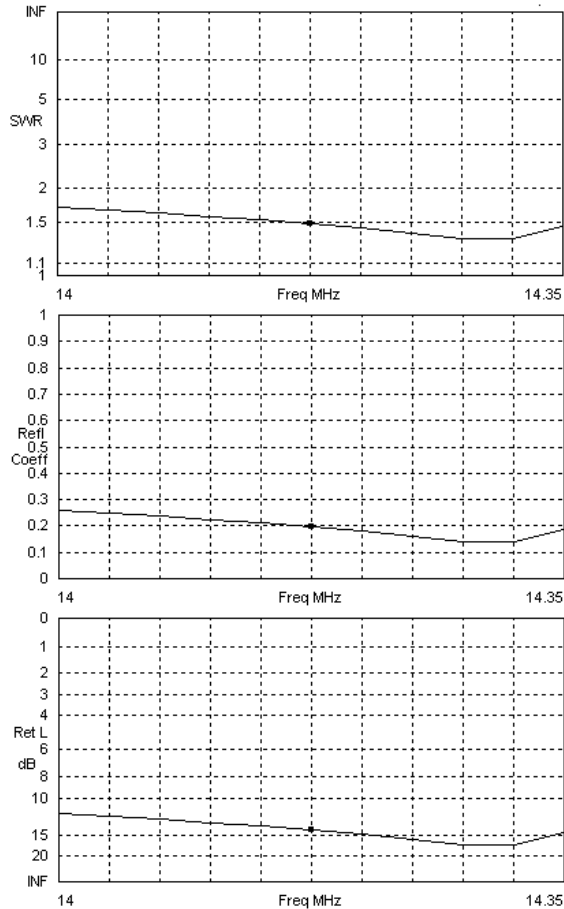
Since we can derive any member of the trio from the basic terms ( $Z_o$ ,  $R_{in}$ ,  $X_{in}$ ), the three members of the group are mathematical manipulations, each developed to serve a useful purpose, but nevertheless indicating a set of relationships among the basic terms. If we go only this far, we lose sight of why many texts

consider reflection coefficient to be the most fundamental of the three.

Reflection coefficient  $|\rho|$  not only has a magnitude, but a phase angle as well. Many texts aimed at radio amateurs omit the derivation of the reflection coefficient phase angle. (If the coefficient did not have a phase angle, we would not need to designate clearly that the calculated value is a magnitude by the use of  $|\rho|$ .) To fill the blank, you may calculate the phase angle of  $|\rho|$  by the following equation:

$$\angle\rho = \arctan \left[ \frac{R_{in} + R_0}{X_{in}} \right] - \arctan \left[ \frac{R_{in} - R_0}{X_{in}} \right]$$

From the magnitude and phase angle of  $|\rho|$  you may derive the real and imaginary components just as you would for any other phasor quantity.



Freq	14.175 MHz	Source #	1
SWR	1.49	Z0	50 ohms
Z	33.78 at -3.87 deg. = 33.7 - j 2.278 ohms		
Refl Coeff	0.1965 at -170.48 deg. = -0.1938 - j 0.03249		
<b>Ret Loss</b>	<b>14.1 dB</b>	1 Graph, 3 Scales	Fig. 7

I note this equation to complete the picture, not because you will have any major use for it. However, you may see the reflection coefficient used instead or or in addition to a value for VSWR, and the value of rho may include both a magnitude and a phase angle. For example, the latest implementation of EZNEC has a frequency sweep facility that lists all three members of the trio. **Fig. 7** samples the sweep graph for a 5-element Yagi design in all three modes. Note that the graph does not change, but the scale of the Y-axis does. (Some instruments may reverse the vertical order of return-loss scale markings.) The graphing line will only change with changes in the value of  $R_{in}$ ,  $X_{in}$ , or  $Z_o$ .

## Conclusion

Perhaps the only unifying theme within these notes is that all of them have generated questions from folks at various levels along the road to mastering the art and craft of modeling. Almost all of the answers that I have tried to give have also generated a similar response: "Of course! I should have thought of that!" In addition, I can now remove the papers from my spindle file and clear it for another batch of miscellaneous items that may be useful to one or another modeler.

## Chapter 128: When Not to Use NEC for Antenna Modeling

The following notes compile a number of replies that I have given to various theme-related e-mail inquiries on using NEC at or beyond the limits of its capabilities. In a number of cases, I have suggested that NEC (either -2 or -4) may not be the software of choice for various modeling enterprises. In other cases, I have suggested that the user must employ experimental calibration techniques prior to using NEC models, especially when the goal is to design a working antenna, even of ordinary types. Understanding what NEC can and cannot do is critical to making best use of the software. Let's examine a few interesting cases at or beyond the limits of NEC.

### Non-Round Elements

One of the most common inquiries in home antenna construction is whether one might substitute non-round wires for round wires that most handbooks suggest for antenna elements. Of course, there are practical reasons for using round antenna elements. For the most part, round elements slip the wind better than most of the alternatives, especially when the elements have a significant radius. As well, many materials accumulate snow and ice faster and thicker than round elements. However, elements with flat surface appeal to home antenna builders for numerous reasons. First, the materials are readily available from various local sources. Second, they have flat surfaces that many less-experienced builders find easier to handle and drill than round elements.

Rather than trying to adjudicate the pros and cons of element materials with flat surfaces, let's confine ourselves to the question of trying to use NEC to design or to refine the design of a typical antenna, perhaps a modest Yagi. Fundamentally, NEC begins with a thin-kernel model of all wires in the antenna geometry. The thin-kernel model presumes a bare round wire in free-space or its equivalent, that is, a vacuum or dry air. As the NEC-2 manual explains, "In the thin-wire kernel, the current on the surface of a segment is reduced to a filament of current on the segment axis. In the extended thin-wire kernel, a current uniformly distributed around the segment is assumed. The field of this current is approximated by the first two terms in a series expansion of the exact field in power of  $a^a$  [where  $a$  is the wire radius]. The first term in the series, which is independent of  $a$ , is identical to the thin-wire kernel, while the second term extends the accuracy for larger values of  $a$ . Higher order approximations are not used because they would require excessive computation time."

"In either of these approximations, only currents in the axial direction on a segment are considered, and there is no allowance for variation of the currents around the wire circumference. The acceptability of these approximations depends on both the value of  $a/\text{wavelength}$  and the tendency of the excitation to produce circumferential current or current variation. Unless  $(2 \cdot \pi \cdot a)/\text{wavelength}$  is much less than 1, the validity of these approximations should be considered." One potential arena in which the validity of these approximations may be tested is the modeling of a boom connected directly to the parasitic elements of a Yagi antenna. In practice, the connection or the very close

proximity of a boom to the parasitic elements alters the required length of the elements to preserve array performance. However, in NEC-2 and NEC-4--when modeled within the other limitations of the software--the boom has no effect upon the parasitic elements.

The NEC-2 manual goes on. "The accuracy of the numerical solution for the dominant axial current is also dependent on [the ratio of segment length to radius or  $L_s/R$ ]. Small values of [ $L_s/R$ ] may result in extraneous oscillation in the computed current near free wire ends, voltage sources, or lumped loads. Use of the extended thin-wire kernel will extend the limit on [ $L_s/R$ ] to smaller values than are permissible with the normal thin-wire kernel." In general,  $L_s/R$  must be greater than 8 for errors under 1% for the normal thin-wire kernel. This amounts to a segment length-to-wire-diameter ratio of 4:1, for programs that input wire thickness as a diameter. The manual notes that "reasonable solutions" have been obtained for the normal thin-wire kernel for  $L_s/R$  values down to about 2, with equally "reasonable solutions" for the extended thin-wire kernel for  $L_s/R$  values down to about 0.5.

In NEC-4, according to its manual, "the thin-wire approximation is now implemented with the current treated as a filament on the wire surface and the boundary condition enforced on the wire axis. With the boundary condition enforced on the wire axes, the openings at wire ends should be closed with end caps. This is particularly important when the ratio of segment length to radius is on the order of 2 or less. Wire ends are closed with flat caps in NEC-4, with the current and charge density assumed continuous from the wire onto the cap." NEC-4 also includes optional caps for use with voltage

sources with equally low values of  $L_s/R$ . "This approximate treatment was found to be about as effective as the extended thin-wire kernel included as an option in [NEC-2 and] NEC-3. The extended thin-wire kernel option (EK card) has been dropped from NEC-4."

I have repeated these extracts from earlier episodes in the series because every user needs periodically to review the fundamental premises underlying the software. These premises reveal to a large extent the limitations of the software. The thin-wire kernel model of the currents along an antenna element wire provides us with one of those limitations. We cannot automatically transfer the results of a model to a physical implementation that uses non-round elements.

For many substitute elements, we may use NEC models effectively if we carry out for the frequency and material that we propose to use a series of simple experiments. I had occasion to perform such a calibration exercise in connection with the design and implementation of several alternative versions of a 3-element Yagi for 146 MHz. The procedure that I used may be instructive. However, for a specific project, the required effort will be considerably shorter than I needed for a survey that involved numerous materials.

The first step involved constructing a series of round element dipoles for the test frequency. In this step, I was interested in learning to what degree physical antennas using the proposed construction methods might vary from models that included none of the hardware and other appurtenances that are required parts of

the proposed antenna. **Table 1** summarizes the results for a range of round 6063-T832 aluminum elements from 1/8" to 3/4" in diameter.

Table 1. Modeled and tested resonant lengths of round-element 146 MHz dipoles.

El. Diameter (inches)	Modeled Length (inches)	Tested Length (inches)
0.125	38.42	38.31
0.1875	38.28	38.25
0.25	38.10	38.06
0.375	37.80	37.81
0.5	37.60	37.44
0.75	37.30	36.94

The table itself does not comment on the accuracy of NEC software because it does not show the details of the models, such as the segment density. As well, it does not show the instrument calibration and accuracy. What the table does do is to provide me with a set of expectations relative to correlating other materials to round elements and from there to models.

The nature of the project involved a number of potential element materials with alternative cross-sections. **Fig. 1** shows the varieties that I subjected to tests. One might easily expand the shapes to include square tubing and U-channel aluminum stock. This particular collection happened to coincide with the project's overall goals.

## Conductor Shapes Correlated to Round Wires in 2-Meter Dipole Test

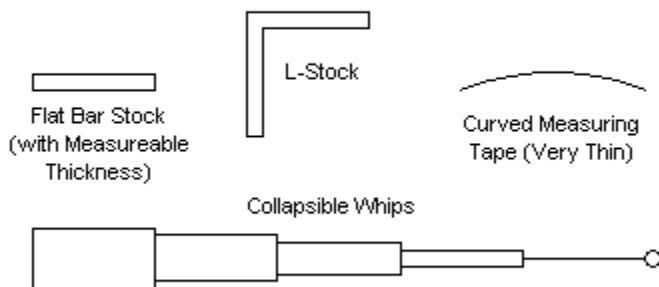


Fig. 1

For each material, I created a dipole and brought it to resonance at 146 MHz by the simple expedient of successively shaving the dipole out ends in small increments, using a disk sander for the final fine tuning. (Sanding, of course, does not apply to the collapsible whips.) **Table 2** summarizes the results and shows the conclusions that I reached regarding the correlation of the material at the test frequency to the nearest commonly available U.S. round element size.

Table 2. Tested 146-MHz resonant lengths of alternative element materials.

Material	Tested Length (inches)	Nearest Round Element
<b>Aluminum Flat Stock</b>		
1/2" by 1/16"	37.31	0.5
1/2" by 1/8"	37.19	0.5
3/4" by 1/16"	37.06	0.75
<b>Aluminum L-Stock</b>		
1/2" by 1/2" by 1/16"	37.44	0.5
3/4" by 3/4" by 1/16"	37.00	0.75
<b>Collapsible Whips</b>		
1. 5-section TV "rabbit ear," maximum extension 48.5" with "button" tip. Approximate diameters: 0.25", 0.219", 0.1875", 0.125", 0.0625"		
a. With largest sections fully extended	37.88	0.375
b. With smallest section fully extended	40.00	<0.125
2. Radio Shack 5-section cordless telephone replacement (#270-1405A); maximum extension 23" with button tip. Approximate diameters: 5-mm, 4.125-mm, 3.25-mm, 2.375-mm, 1.5-mm		
Roughly equal section extension	38.88	<0.125
<b>Metal Measuring Tapes</b>		
1" (15/16" with curve)	37.38	0.5
3/4" (11/16" with curve)	37.63	0.375-0.5
5/8" (9/16" with curve)	37.88	0.375
1/2" (15/32" with curve)	38.25	0.1875

One result that I found somewhat surprising was the close correlation between any of the flat or L shaped materials and round elements when I compared the element width measurement to the tubing diameter. So long as the stock has a significant thickness--1/16" at the test frequency--the width of the stock correlated to the round element with the same value for its diameter. However, for very thin materials, such as the measuring tapes, the simple correlations did not apply. However, the tests did not use

techniques that allowed me to separate any effects due to using a very thin element and effects from the ferrous materials used in measuring tapes.

The correlations allowed me to design and build working 3-element Yagis using any of the materials. In fact, I built one version that used a combination of materials as a demonstration. I can find no performance difference between it and its round-element counterpart. The use of calibration methods does allow the antenna builder to employ NEC in developing an antenna design, so long as one uses due caution. The calibration procedure used here applies to materials at the test frequency plus or minus about 20%. Beyond those limits, I would strongly urge a new set of calibration experiments. For example, if one wished to design a beam for the U.S. 223-MHz band or for the FM band, then one should use calibration experiments designed expressly for those frequencies.

## **The Medium Surrounding a Wire**

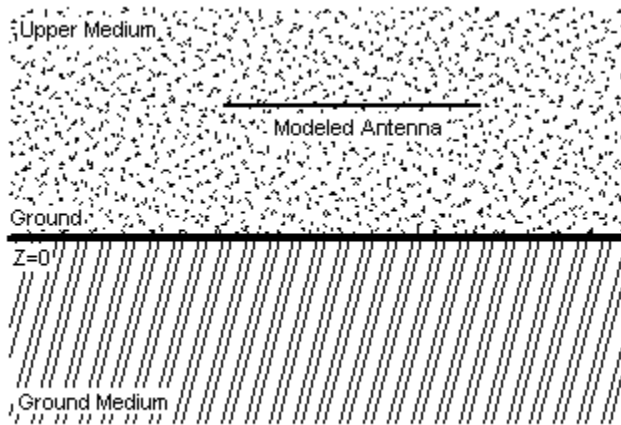
NEC-4 added the IS or insulated sheath command to the collection of control commands available to the user. A number of implementations of NEC-2 have added codes that either replicate or simulate this command. The command allows the user to specify a wire in the geometry and to encase specified segments in a material having a user-selected set of values that include the material's relative permittivity, conductivity, and outer radius. Thickness is simply the sheath radius minus the wire radius. Numerous inquiries over the years have wondered how far one might extend the sheath to form essentially a special medium for

the wire inside. Since the calculations that modify the fields calculated for the wire occur late in the sequence of NEC processes, it is likely that there is a practical limit about how thick one may make an insulated sheath, although I have seen no data on the precise limits.

Of course, modelers can use the command creatively. One such example is the development of a hollow thermoplastic tube near a radiating wire. To create the tube, the modeler added a wire to the geometry and assigned to it the conductivity of air. The wire diameter corresponded to the inner diameter of the tube. The modeler then added an IS command using the values appropriate to the plastic involved. He gave the sheath a radius corresponding to the tube's outer diameter.

The limitation of this technique is that one must need a round surface for the structure. However, most modelers are interested in flat non-conductive materials to which we may bond antenna wires. These substrates come in many forms. The next inquiry wondered if one might use the NEC-4 UM command to replicate the substrate. Unfortunately, the UM command has some limitations that largely preclude its use in this manner. **Fig. 2** shows the situation modeled by employing the UM command.

Fig. 2



Modeling Situation When Using the UM Command

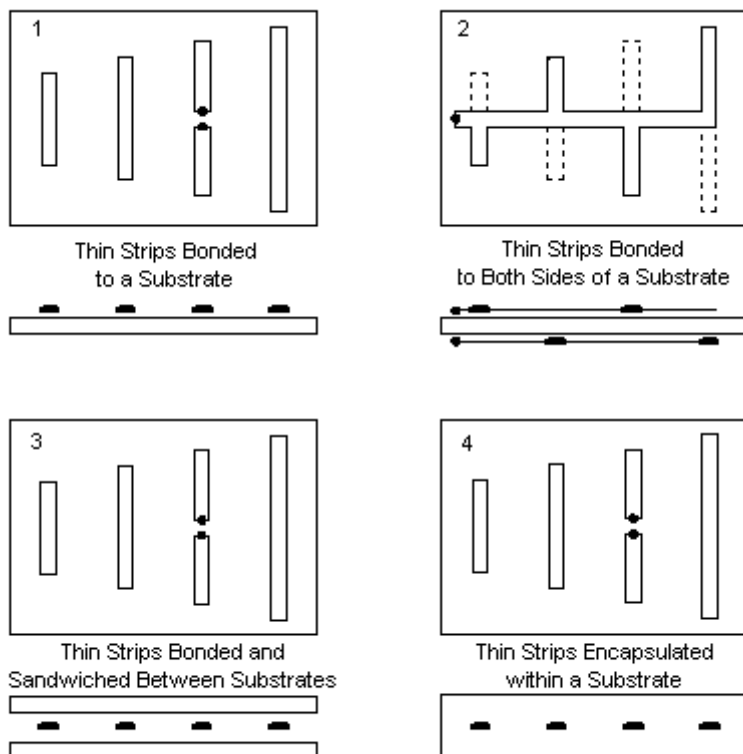
Most substrates have a finite dimension and thickness. The UM command uses a set of constants for the ground and another set for the upper medium. Except for the ground surface at  $Z=0$ , each medium is without limit. One may, of course, specify a second medium for the ground, but the depth of each medium will be without limit. Hence, we cannot limit a substrate to its actual thickness using the ground. The antenna environment is the upper medium, which also extends without limit in all directions in the hemisphere above ground. In addition, the UM command is usable only with the reflection coefficient approximation (RCA) ground calculation system, which has limitations of accuracy as the antenna is brought toward the ground surface.

In general, neither the IS nor the UM command provides a means of approximating the situation of antenna elements bonded to a substrate.

## Substrates and Strip Elements

A very wide range of antenna applications make use of modified printed circuit board techniques. The essential features of such antennas include the use of relatively wide strip elements having negligible thickness and the use of a substrate to which we bond the elements. The substrate has a certain set of dimensions, along with relevant values of conductivity and relative permittivity. **Fig. 3** shows some of the techniques commonly used to form such antennas. The edge views show element ends as an artificially thick line, although the actual strips are very thin.

Fig. 3



Some Structures for Which NEC Modeling  
is Difficult to Impossible

The most common type of antenna-substrate combination etches elements on one side of the substrate, as shown at the upper left. However, we may use both sides of the board, as shown at the

upper right, to create such antenna types as an LPDA. At the bottom are two variants of the theme, sandwiching the elements between two boards or fully encapsulating the antenna within a molded substrate. These latter forms provide the antenna with maximum protection from environmental or user damage.

Trying to model these antennas in NEC presents the analyst with numerous problems. First, the strips are very wide compared to the thickness. As our initial experiments using measuring tape showed, when the thickness becomes almost negligible, the material does not perform like a round wire of any predictable diameter. The only way to form any kind of usable correlation is to perform a series of calibration experiments in advance of any modeling.

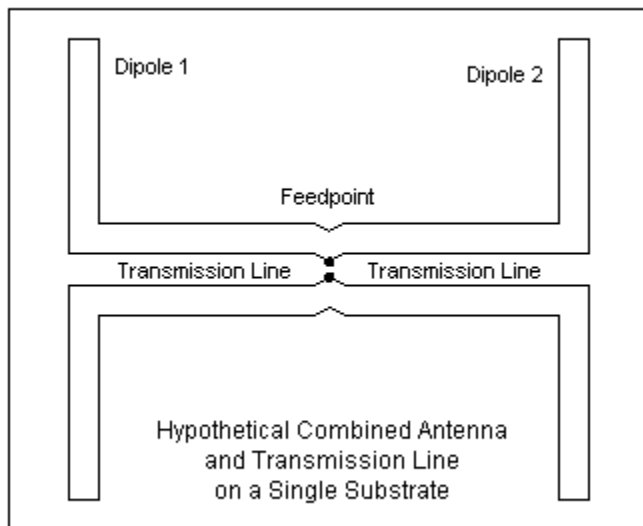
The existence of the substrate in contact with the strips on one or both sides and the limited size of the substrate in all dimensions present additional problems. Although one might reach a workable round-wire free-space approximation of the antenna plus substrate, the effort might require the pre-existence of the finished physical antenna before one could claim any utility to the modeled approximation. For simple antennas, such as dipoles, the problem may not seem difficult. However, for parasitic arrays, the substrate may modify the mutual coupling between elements as well as the performance of each element. Hence, the simple calibration procedure that we successfully used for element materials in free space may not be as successful in the presence of a substrate.

Many of the techniques that we have just described also involve UHF and higher portions of the spectrum. At these frequencies, the

width of the strip elements and even their round-wire correlates may press the limits of the segment-length to radius ( $L_s/R$ ) recommendations for accuracy in NEC.

Under these conditions, NEC may not be the software of choice for trying to model the antennas--at least not in detail. There are available hybrid programs, virtually all proprietary, that can handle the modeling situation more directly. In fact, many allow the direct input of CAD drawings, with appropriate translations for antenna calculations. These input potentials allow the user to handle the strip elements directly. In addition, they allow the inclusion of substrates having specific dimensions and properties. Some are also capable of handling an interesting circuit board possibility: the physical inclusion of both antenna and transmission-line strips, as suggested by **Fig. 4**.

Fig. 4



The sketch shows side-by-side phase line strips feeding the two dipoles from a centered location. (In some software, one may include circuitry beyond the limits of the antenna system.) The reality of the physical structure might use transmission-line strips on opposite sides of the board, where strip width and displacement, combined with the dielectric constant of the substrate, together permit a designer-selected characteristic impedance.

Many packages employ FDTD techniques in calculating antenna properties within the complex structural situation described here.

Although data is the critical calculation output, many such packages have labored long to present the outputs in very attractive graphical forms.

For modeling enterprises of the sort described here--and others even more complex--hybrid packages are likely the software of choice. In general, these enterprises are not suited to individual efforts, because the investment required is very considerable. NEC users are accustomed to using relatively low-cost software. There are entry-level packages ranging from freeware to commercial implementations with full support at under \$100 for NEC-2. NEC-4 requires a license, which is inexpensive for the individual serious user, and commercial NEC-4 packages run well under \$1000. Hence, the practicing consulting engineer can easily afford the best of NEC.

Full-featured hybrid packages may require \$50,000 or more, in addition to the cost of sales commissions and seminars to ease the very steep learning curve required to use the packages effectively. The hybrid packages tend to be corporate investments, with costs recovered from the mass sale of systems that emerge from their use. Because these packages do much more than just allow one to design and analyze antennas, it is impossible to apportion costs to a single function. Nevertheless, the packages tend to fall well outside the range that most individuals can invest.

I have not been more definite about the specific capabilities of hybrid packages because they also and easily fall outside my ability to afford. A web search or a recent issue of a journal for

professional RF engineers will provide contact with the vendors of such packages. Over the last decade, the number of vendors has shrunk due to purchases and mergers. In the process, the capabilities of individual packages have increased for the same reason.

## Conclusion

In these notes, we have examined three situations. The first involved the use of non-round shapes for which we can find for a given frequency range equivalent NEC wire sizes to provide accurate models of the physical antennas that use the odd materials. However, as we contemplate the combination of conductive and non-conductive materials in proximity, we may try to use some of the special commands available, especially in NEC-4. This second situation brought us to an understanding of some of the limitations of commands such as IS and UM. In general, these commands are unsatisfactory for use with strip elements bonded to substrates, a common construction technique for a wide variety of antennas used in the UHF and higher portions of the spectrum. This third situation brought us to the general conclusion that the round-wire, axial-current, free-space environment at the heart of NEC may not be the most apt vehicle for the design or analysis of the subject antennas. As versatile and flexible as NEC may be, it is not a universal software modeling system for all possible antennas.

For round-wire antennas, NEC remains the software modeling system in widest use. It is generally very cost effective, especially for amateurs, consulting engineers, and others dealing with the

design or analysis of one-of-a-kind antennas or antennas that fit its special capabilities. Indeed, the relatively low cost, even of NEC-4 plus a license, has led to the development of numerous workarounds for some of its limits. For example, many Yagi designers who use a direct connection or extremely close proximity between antenna elements and a supporting conductive boom introduce short, fat center element sections to account for the boom effects that NEC cannot directly calculate. In these notes, we have seen the relative ease of calibrating materials with an odd cross-section to NEC's round wires. Other episodes in this series have shown additional workarounds for situations that press NEC's limitations.

Nevertheless, in the field of antenna modeling, NEC cannot do everything.

## Chapter 129: Some Rudiments of Receiving Pattern Modeling

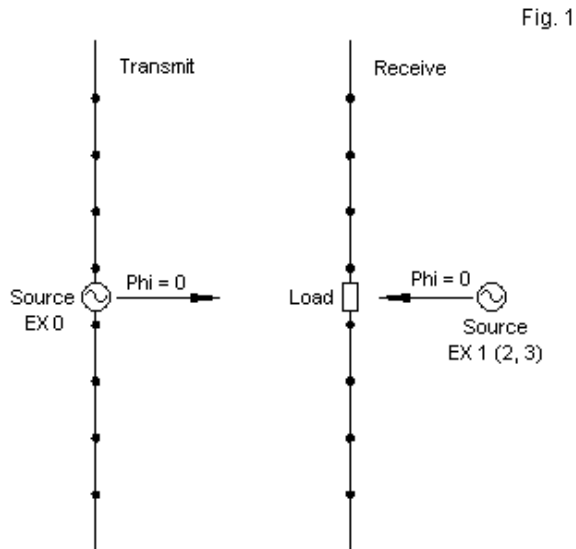
In Chapter 88 of this series, we examined the use of two commands that are essential to developing antenna receiving data: EX (1 through 3) and PT (1 through 3). Nevertheless, I continue to receive inquiries on the basic methods of developing receiving data from both new modelers and radio amateurs. The requests contain various questions, of which the following three may be a summary.

1. How do I obtain receiving data?
2. What does the data tell me?
3. Of what use is the data?

Therefore, we might wish to begin again. We shall re-examine the commands, but reduce the scope of their possibilities to a limited subset. Then we can apply the commands to a few examples that will illustrate the process of developing useful information. The samples will be very rudimentary and hence have little new to show us. However, we are more interested in the basic methods of generating the information. We shall discover that we may often have to resort to supplementary external calculations (easily done with a spreadsheet) to make full and meaningful use of the information that we collect.

## Getting Started: EX 1 and PT 1

To develop receiving patterns and data, we must have access to some control commands that many entry level implementations of NEC omit. (Even if our package has the commands, the odds are that we have not used them.) Most modelers use only the EX 0 excitation command to set the source voltage (or, indirectly, the current) on a selected segment of a modeled antenna geometry. The left side of **Fig. 1** shows the situation with which we are most familiar.



Key Differences between Transmit and Receive Models

To obtain receiving data, we must use different options available for the EX command, namely, EX 1, EX 2, or EX 3:

EX 1: incident plane wave, linear polarization

EX 2: incident plane wave, right hand (thumb along the incident vector) elliptic polarization

EX 3: incident plane wave, left hand (thumb along the incident vector) elliptic polarization

In these notes, we shall bypass the elliptical polarization options and work solely with linear polarization, EX 1. Regardless of which of these incident plane wave excitation modes that we select, note from the figure that the excitation is external to the antenna geometry. However, the figure has an inevitable flaw. By giving the excitation a position external to the antenna, the sketch invites the temptation to think of the excitation as a point having different angular directions to various parts of the antenna wire. A more accurate picture, but one that I do not know how to draw, is to place the source at an indefinitely large distance from the antenna wire so that the illumination is uniform over the entire antenna geometry.

We must set up the EX command to position the source relative to the antenna. The entry-line structure for them has a number of interesting properties that differ from the line structure of a simple voltage source. (Reminder: although you may use both an EX 0 voltage source and a plane wave source in the same model, the

last source type will determine the format of the output report and the function of any RP command.)

Com	I1	I2	I3	I4	F1	F2	F3	F4	F5	F6	F7	
ID	Type	#	Thta #	Phi	Not	Th angle	Ph angle	Eta	Theta	Phi	Axis	El. field
			angles	angles	used	to	to	pol.	angle	step	step	ratio
						vector	vector					V/m
EX	1	1	8	0	90	0	90	0	45	0	0	

The sample entry is for a linear plane wave. Hence, F6 is 0 by non-relevance. F7 also has a 0, but that value indicates a default value of 1 V/m. In some problems designed to ferret out coupling potentials among wires, you may use a specific value that closely approximates the value from the source signal at the structure being examined in model form. NEC-2 lacks the F7 field and hence always uses 1 V/m. As we shall see, this limitation is not a significant problem.

Most of the remaining entries define incident plane waves as a calculation loop within NEC (with some properties resembling the loop operation of frequency sweeps using the FR command). In the sample, for the sake of clarity, there is only one theta angle: 90 degrees. This angle is parallel to the plane of antenna elements that extend parallel to the X-Y plane and is equal to an elevation of 0 degrees. The sample specifies 8 phi-angle (azimuth-angle) steps at 45-degree increments, thus providing samples evenly spaced in the element plane.

The F3 entry, called Eta, under linear polarization is easy to memorize. With a value of 0, the polarization is in the +/-Z direction-vertically polarized for antennas over ground. If F3 is 90, the

polarization is in the X-Y plane--horizontally polarized for antennas over ground. We shall place our antenna in free space with the wire extended in the X-Y plane and then use horizontal polarization for simplicity, but there is no restriction against checking results when cross-polarized or with the polarization set to intermediate angles. When using EX 2 or EX 3, elliptical polarization, the entry changes its meaning and defines the major ellipse axis. (Remember that true circular polarization is simply a special case of elliptical polarization having equal axes.)

Having set up the excitation, we must then enter commands that will give us useful data. We might use an RP 0 command to request a pattern, but this information will be of use only to those interested in radar and similar work. The pattern that we obtain will be for scattering data, the reflection of radio wave off of the object. However, we shall set up an antenna and will be more interested in the energy that we receive from the uniform 1 V/m illumination. NEC calculates for each segment in the geometry the peak current. This is highly useful information. To obtain it we must use the PT control command. Like the EX command, it has several options.

PT -2: All current printed. This also occurs if PT is omitted altogether.

PT -1: Suppress printing of all wire-segment currents.

PT 0: Current printed for specified segments only.

PT 1: Currents printed in a format designed for a receiving pattern.

PT 2: Currents printed in a format designed for a receiving pattern, plus a normalized value for the last segment's current.

PT 3: Only the normalized current is printed.

The current tables that we obtain when using a modeled antenna with a voltage source result from not entering a PT command at all, which results in the PT -2 option by default. For receiving data, we need to look at the PT options from plus 1 through plus 3. In fact, we shall only use PT 1 in this episode, leaving the other options as (pardon the expression) an exercise for the reader. The PT entry is very simple.

Com	I1	I2	I3	I4
ID	Type	Tag #	1st Seg	Last Seg
PT	1	1	8	8

The command only requires that we specify the tag (wire) number in which we are interested, along with the range of segments on that tag. Although we might in many instances be interested in the current magnitude and phase on many segments in a model, the sample reduces the range to a single segment.

Let's combine these lines into a different set of concluding lines for our initial model.

```
PT 1 1 8 8
EX 1 1 37 0 90 0 90 1 10 0 1
XQ
EN
```

The EX 1 command specified 37 different readings separated by 10 degrees each on the phi circle, with all of them having a theta angle of 90 degrees. Eta is also 90 degrees, indication that if the antenna element is parallel to the X-Y plane, the excitation source will be polarized in plane with the element. Note that the PT command is not like RP, that is, it is not self-executing. Therefore, we must add the XQ command in order to force the program to calculate the currents.

### Orientation to a Specific Model

**Fig, 1** showed a model of a dipole. Let's confine ourselves to this familiar antenna and create a pair of models in a single model file (using the handy NX command) to illustrate the differences between a transmitting and a receiving situation.

```
CM dipole 300 MHz EX0/RP0
CE
GW 1 15 0 -.2373 0 0 .2373 0 .001
GE
FR 0 1 0 0 299.7925 1
EX 0 1 8 0 1 0
RP 0 1 361 1000 90 0 1.00000 1.00000
NX
CM dipole 300 MHz EX1/PT1 no load
CE
GW 1 15 0 -.2373 0 0 .2373 0 .001
GE
FR 0 1 0 0 299.7925 1
EX 1 1 37 0 90 0 90 1 10 0 1
PT 1 1 8 8
XQ
EN
```

The geometry section of both models is identical, as is the FR command. The upper model uses an EX 0 source command to provide transmitting data that we can obtain from the tabular outputs or from a handy graphical representation of the radiation pattern. As we might expect, NEC calculates free-space gain as 2.13 dBi, with a source impedance of  $71.72 - j0.16$  Ohms. (The source impedance is often more important for receiving data gathering than the transmitting gain, which equally applies to reception by virtue of reciprocity.)

At most, we might find a rectangular graph for the data gathered by the PT 1 command in the lower model. We can recognize that the specified tag and segment for the data is the very same segment that we used in the upper model as the source segment. Let's look at a few lines from the tabular data produced by the lower receiving model.

```
- - - RECEIVING PATTERN PARAMETERS - - -
ETA= 90.00 DEGREES
TYPE -LINEAR
AXIAL RATIO= 0.000
```

THETA (DEG)	PHI (DEG)	- CURRENT MAGNITUDE	- PHASE	SEG NO.
90.00	0.00	4.3935E-03	-3.08	8
90.00	10.00	4.2975E-03	-3.07	8
90.00	20.00	4.0208E-03	-3.03	8
90.00	30.00	3.5949E-03	-2.98	8
90.00	40.00	3.0627E-03	-2.91	8
90.00	50.00	2.4681E-03	-2.83	8

90.00	60.00	1.8475E-03	-2.75	8
90.00	70.00	1.2244E-03	-2.69	8
90.00	80.00	6.0886E-04	-2.65	8

As we move the plane-wave excitation source position, we can see that the current magnitude (in peak Amps) changes, as does the phase angle, on the segment of the antenna that formerly held the EX 0 voltage source. The question that arises next is how this data is meaningful to us. It is meaningful, but perhaps not just yet.

## Loading the Former Source Segment

The source segment on a transmitting antenna becomes the load segment on the same antenna when receiving. However, if we think of the load as the receiver terminals, we normally are less interested in the current at the terminals than we are in the voltage. As well, a receiver presents the antenna feed segment with a load. We shall ignore for this simple exercise the role of the transmission line in setting the load at the feedpoint segment and assume a direct connection. Hence, to acquire meaning full data in an extended sense from the model, we normally would place a load on the feedpoint segment, as suggested in **Fig. 2**.

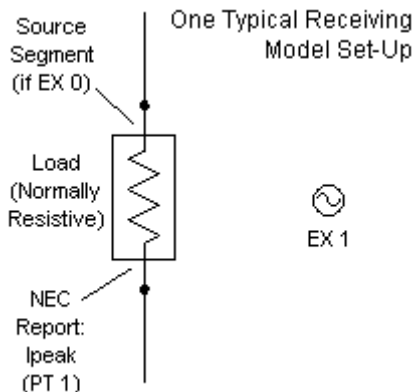


Fig. 2

The question that emerges is what load we should use. Let's explore a bit by placing resistive loads from 10 through 150 Ohms on the feedpoint segment (Tag 1, Segment 8). A simple LD 4 command will do the job. Then we can set up a model to progressively record the current that appears on the segment with each load value.

```

CM dipole 300 MHz EX1/PT1 loads
CE
GW 1 15 0 -.2373 0 0 .2373 0 .001
GE
FR 0 1 0 0 299.7925 1
EX 1 1 1 0 90 0 90 1 1 0 1
PT 1 1 8 8
XQ
LD 4 1 8 8 10 0
FR 0 1 0 0 299.7925 1
EX 1 1 1 0 90 0 90 1 1 0 1

```

```

PT 1 1 8 8
XQ
LD 4 1 8 8 20 0
FR 0 1 0 0 299.7925 1
EX 1 1 1 0 90 0 90 1 1 0 1
PT 1 1 8 8
XQ
LD 4 1 8 8 30 0
FR 0 1 0 0 299.7925 1
EX 1 1 1 0 90 0 90 1 1 0 1
PT 1 1 8 8
XQ

```

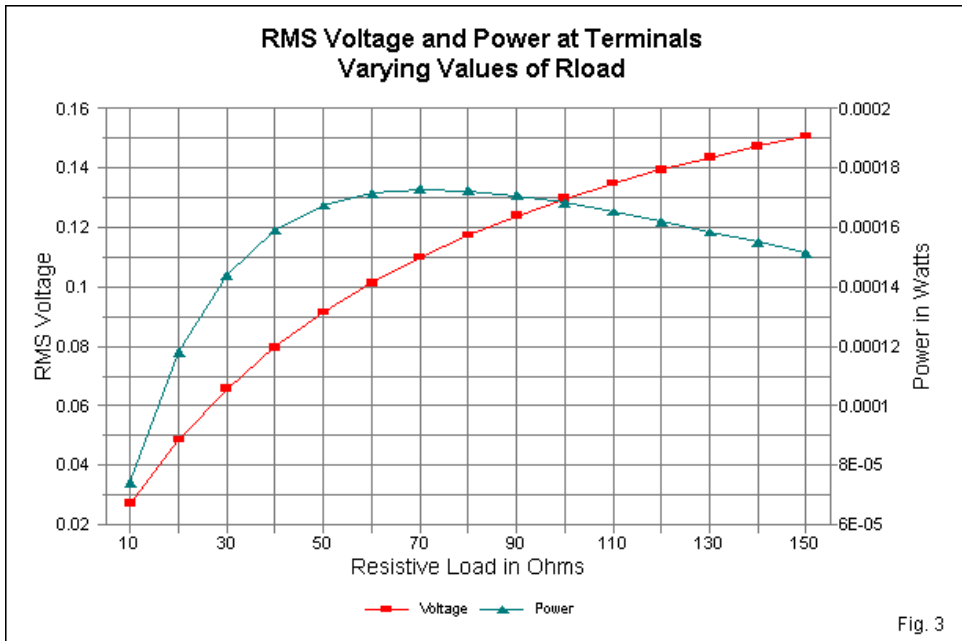
The partial model file shows the simple technique used to accumulate data on the performance of the antenna relative to feedpoint current using various resistive loads. (The file contains for reference a model version that uses no loading as a check on the model's formation.) We can place the results into a table on a spreadsheet, which will allow us to perform some supplementary calculations. See **Table 1**.

Dipole with linear excitation in plane: varying loads					EX1=1 w/m pk				Table 1
Load R	10	30	50	70	90	110	130	150	Ohms
Ipeak	0.003856	0.003098	0.002589	0.002224	0.001949	0.001734	0.001562	0.001421	A pk
Irms	0.002726	0.002190	0.001830	0.001572	0.001378	0.001226	0.001104	0.001005	A rms
P	0.000074	0.000144	0.000167	0.000173	0.000171	0.000165	0.000159	0.000151	W
Erms	0.027261	0.065704	0.091514	0.110041	0.123983	0.134853	0.143573	0.150718	V rms
Note: Load R is user specified; Ipeak is NEC report; other values calculated.									

The first data line below the resistive load values provides us with the data reported by NEC. Since we normally use RMS values of voltage and current for various purposes, the next line performs the

required conversion. The following lines provide the power and the voltage for each load.

The importance of placing a load on the feedpoint segment lies in the fact that it allows us to perform the last two calculations.  $P = I^2R$ , and  $E = IR = \text{SQRT}(PR)$ . Without the load value, we have no way to determine these values. The pattern of values simply confirms what basic texts teach about energy. As we raise the value of the load resistor, the voltage at the receiver/feedpoint terminals increases. **Fig. 3** graphs the rise in voltage with the increase in the selected load resistor.



The graph also includes the calculated power at the feedpoint terminals. Note the peak in the power level at approximately 70 Ohms load resistance. We obtain maximum power transfer when the load matches the source impedance. The transmit version of the antenna yielded a source impedance of about 72 Ohms, and the 70-Ohm load resistor comes closest to matching that value. (Numerous modelers arbitrarily place 50-Ohm loads across the antenna terminals without first checking the antenna's source impedance. In some cases, there are good reasons for doing so, although in other cases, the load is a matter of habit. If the

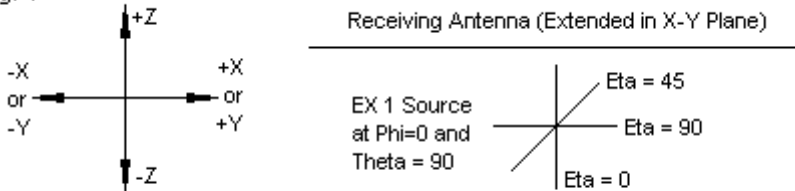
impedance of the antenna and the load are distant from each other and a transmission-line intervenes, then the load resistor may not accurately reflect the conditions at the receiver terminals.)

## The Effects of Eta

So far, we have only sampled the sorts of information that we likely knew about antennas under receiving conditions. Plane-wave excitation also permits us to sample some facets of performance that we have largely taken on faith. For example, we learn that cross polarization of linearly polarized antennas seriously degrades received signal strength. Our rudimentary experiments let us sample the effect in greater detail. The models that we are using are somewhat idealistic, since they use lossless wire in free space. However, as a start, they will give us a baseline against which to compare the results of antennas that we may place over ground.

The only variable in this new exercise is the value of Eta as we hold other values constant. **Fig. 4** shows the general situation. Let's retain the dipole set up parallel to the X-Y plane. Although the sketch shows a bit of displacement so as not to muddy the figure, the plane wave source is at 0 degree phi. If Eta = 90 degrees, it will be in-plane with the dipole. If Eta = 0 degrees, it will be cross polarized relative to the receiving dipole. As indicated by the sketch, we may select any angle in between.

Fig. 4



## Exploring the Effects of Cross Polarization

In order to give sense to the data, we must use a single value for the load resistor. For the runs that we shall make, 70 Ohms seems appropriate. We may set up a model following the same procedures used in the initial exercise.

```

CM dipole 300 MHz EX1/PT1 70-Ohm load, variable Eta
CE
GW 1 15 0 -.2373 0 0 .2373 0 .001
GE
FR 0 1 0 0 299.7925 1
EX 1 1 1 0 90 0 90 1 1 0 1
PT 1 1 8 8
XQ
LD 4 1 8 8 70 0
FR 0 1 0 0 299.7925 1
EX 1 1 1 0 90 0 90 1 1 0 1
PT 1 1 8 8
XQ
LD 4 1 8 8 70 0
FR 0 1 0 0 299.7925 1
EX 1 1 1 0 90 0 80 1 1 0 1
PT 1 1 8 8
XQ

```

```

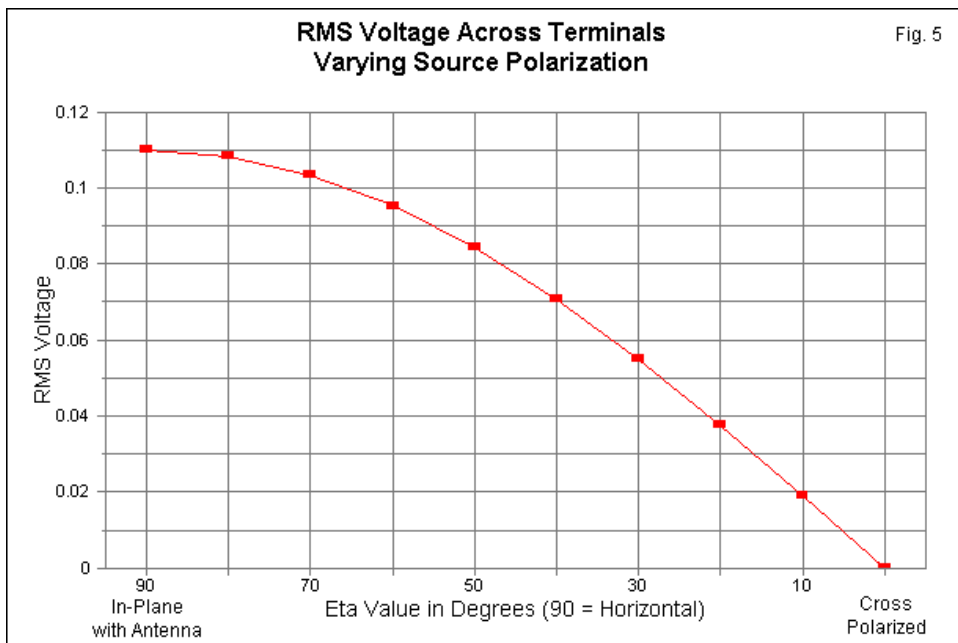
LD 4 1 8 8 70 0
FR 0 1 0 0 299.7925 1
EX 1 1 1 0 90 0 70 1 1 0 1
PT 1 1 8 8
XQ

```

In the new model shown partially above, the LD4 command is the same in each case. However, the F3 position of the EX 1 line changes in 10-degree steps from an in-plane condition toward a cross-polarized condition. Once more, we may tabulate the results and calculate the effects on the receiver terminal voltage, as shown in **Table 2**.

Dipole with linear excitation with 70-Ohm load, varying polarization						EX1=1 w/m pk				Table 2	
Angle	In-Plane					Cross					Degrees
Eta	90	80	70	60	50	40	30	20	10	0	
Ipeak	0.002224	0.002190	0.002089	0.001926	0.001703	0.001429	0.001112	0.000760	0.000386	0.000000	A pk
Irms	0.001572	0.001548	0.001477	0.001361	0.001204	0.001010	0.000786	0.000538	0.000273	0.000000	A rms
P	0.000173	0.000168	0.000153	0.000130	0.000102	0.000071	0.000043	0.000020	0.000005	0.000000	W
Erms	0.110041	0.108368	0.103404	0.095298	0.084296	0.070731	0.055018	0.037636	0.019108	0.000000	V rms
Note: Eta value is parallel to X-Y if Eta = 90 and parallel to Z if Eta = 0.											

The gradual decrease in the terminal voltage comes as no surprise in the progression of Eta values. The rate of decrease becomes apparent if we graph the voltage, as shown in **Fig. 5**.



The graphs show the increasing rate of voltage decrease at the receiver terminals as we get farther away from an in-plane condition. In free space, the full cross-polarized condition results in zero volts. Over ground, we would not likely see the absolute zero shown by the free-space model. Ground reflections alone are sufficient to leave a remnant voltage (and segment current), although in models, the level is usually below the level of anything usable. In the real world, with many objects to reflect, refract, and diffract radio waves, we may find usable, if difficult signal levels.

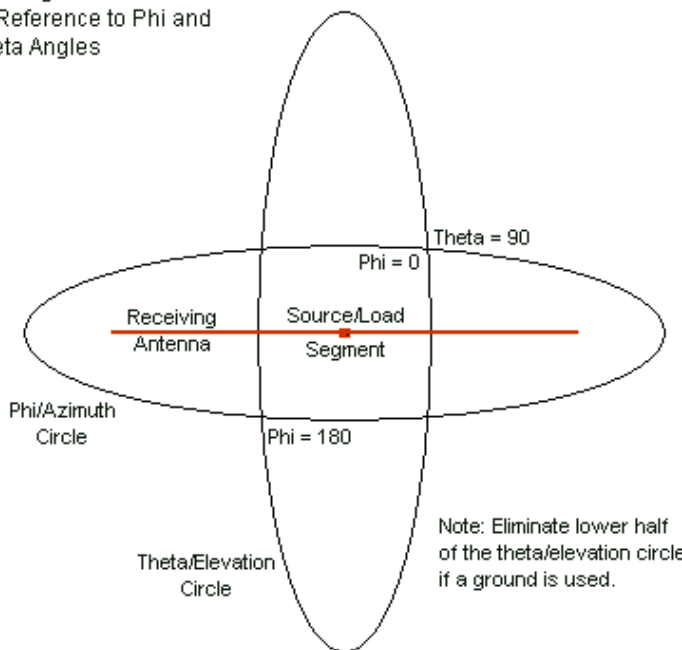
## Varying the Excitation Position

One of the most useful features of plane-wave excitation is the ease with which we may change the angle of the incident wave. By the proper selection of a range of theta and phi angles, we may not only change the angle of the incident wave, but we may survey a large collection of angles. **Fig. 6** suggests the scope of the possibilities.

Locating the EX 1 Source  
by Reference to Phi and  
Theta Angles

Theta = 0

Fig. 6



I have drawn the circles as ovals for clarity. We may choose a starting value for theta and then select an increment and the number of theta steps. We may do the same for phi. How large we make the resulting table depends on both good sense and how large a table we are prepared to read. For the dipole, it would make no sense to sample more than a single theta angle, since we would obtain the same free-space results with every sequence of phi angles. Since we only need samples, we may use phi angles in 10-degree increments between 0 and 90 degrees. Beyond that point, we would replicate values. The model that we need--using a 70-Ohm feedpoint segment resistor--is very simple.

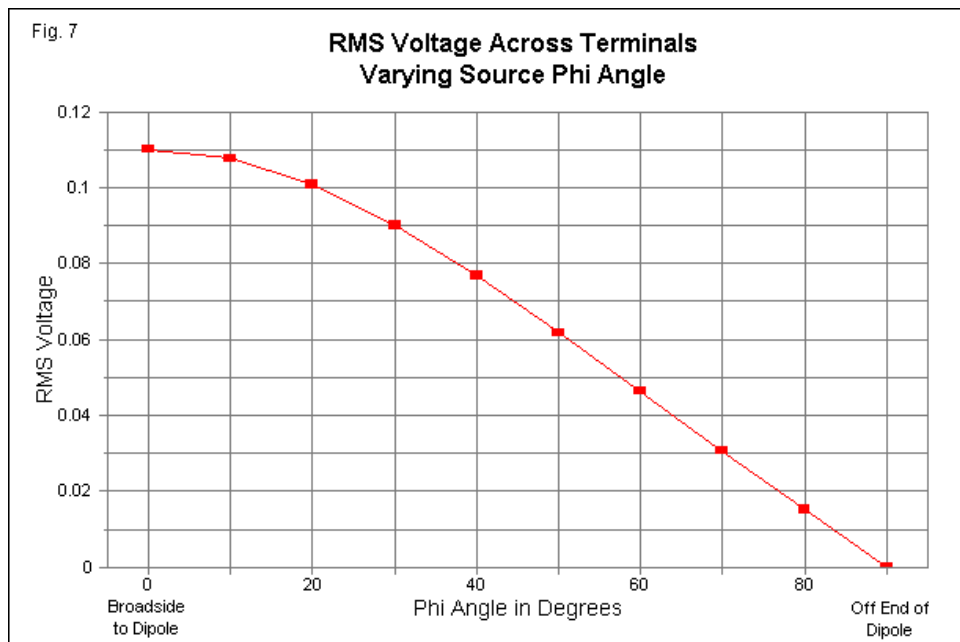
```
CM dipole 300 MHz EX1/PT1 70-Ohm load, variable phi
CE
GW 1 15 0 -.2373 0 0 .2373 0 .001
GE
FR 0 1 0 0 299.7925 1
EX 1 1 10 0 90 0 90 1 10 0 1
LD 4 1 8 8 70 0
PT 1 1 8 8
XQ
EN
```

The results are once more amenable to tabulation, as shown in **Table 3**. The final data entry is technically incorrect. The actual reported value is 8E-15, but it would have shown up as zero if entered in that form.

Dipole with linear excitation, 70-Ohm load, varying phi angle										Table 3	
Position	Broadside									End	Degrees
Phi	0	10	20	30	40	50	60	70	80	90	
Ipeak	0.002224	0.002175	0.002035	0.001819	0.001550	0.001249	0.000935	0.000619	0.000308	0.000000	A pk
Irms	0.001572	0.001538	0.001439	0.001286	0.001096	0.000883	0.000661	0.000438	0.000218	0.000000	A rms
P	0.000173	0.000165	0.000145	0.000116	0.000084	0.000055	0.000031	0.000013	0.000003	0.000000	W
Erms	0.110041	0.107631	0.100702	0.090037	0.076705	0.061818	0.046272	0.030642	0.015249	0.000000	V rms

Note: Phi (azimuth) angles from 0 to 90 repeat themselves for the dipole in question.

We may also graph the calculated voltage values, along the way noticing differences between these voltages and those appearing in the data and graph for the Eta experiment. **Fig. 7** gives us the visual reference.



Although we shall not work these values in this exercise, you may wish to compare them with other data that you collect from models. For example, compare the voltage values as we move the incident-wave angle and compare the results with the gain values in the original transmitting antenna, especially as the transmitting antenna gain passes the -3-dB marks that define the bandwidth. The transmitting plot reports a beamwidth of 80 degrees or 40 degrees each side of  $\phi = 0$ . At the 40-degree marks in Table 3, we find that the calculated power is just about half the value shown for 0-degrees  $\phi$ . Of course, the current and voltage each show values that are about 0.7 of the values for 0-degrees  $\phi$ .

## Conclusion

Our goal has not been to uncover anything new about dipoles. Instead, these notes have aimed at familiarizing you with the modeling moves necessary to let receiving data perform useful, even if mundane work. Varying the load resistor, the value of  $\eta$ , and the angle of the incident wave relative to the antenna are three variations that we may use individually or in concert to analyze the receiving behavior of simple or complex antenna geometries.

Although we have used the NEC-2 given excitation value of 1 V/m, in NEC-4, we may select virtually any field strength value we might need for a given project. However, since we supplemented the reported data with rudimentary calculations of other values that we might need or want, we may as easily add a line adjusting the reported current values for adjusted excitation field strength values.

The reported current will be directly proportional to the excitation voltage, from which other values will calculate as easily.

Since our goal has been to display the main manipulations that we may require, we have also bypassed results that we might obtain using elliptically polarized plane-waves. For NEC, an axial ratio of 1.0 indicates a circularly polarized wave, while 0.0 yields linear polarization. By a judicious selection of the ratio of minor to major axis ratio and of the value of Eta, we can obtain virtually any desired degree of ellipticalness.

Receive data can provide even newer modelers with important data on antenna performance, so long as the implementing software allows access to the EX 1 through EX 3 and the PT 1 through PT 3 commands. Supplementing NEC reports with additional calculations can extend the utility of the information.

## Chapter 130: Models vs. Prototypes: Why Field Adjustment Will Always be Necessary

**W**ithin the limits of their guidelines, NEC and MININEC produce highly accurate models of round-wire antennas when the environment is a vacuum or dry air. Over the years, I have designed some antennas such that the models when translated into a physical reality required no post-assembly adjustment to operate in accord with the specifications predicted by the model. Although most of the antennas were for the HF range, some had design frequencies well into the VHF and UHF region. Not all of them used simple geometries, such as uniform-diameter linear elements. For example, many used stepped-diameter elements and a few (Moxon rectangles and quads, especially) used non-linear elements. Even some designs using phase lines, such as LPDAs or dual-driver Yagis, have tightly fit predicted operating curves immediately upon assembly. My experiences are not unique.

However, lest we begin to believe that there may be a "green-thumb" equivalent in antenna design work, my accumulated experience yields the conclusion that field adjustment of antenna prototypes is needed more often than not. Rarely are the adjustments gross. Rather, they fall into the range of fine-tuning. How finely we demand the tuning to be is always a matter of judgment. My first 10-meter stepped-diameter Moxon rectangle showed its SWR minimum 25 kHz below the model's prediction, well under 0.1% of the design frequency. Nevertheless, I dutifully

shortened the elements enough to bring the array into alignment with the design model.

There are a number of reasons why field adjustment is always a necessary step in the transition from a design model to a working antenna. Some of the reasons relate to modeling, and other to antenna construction. It may be useful to catalog a few of the situations that are almost guaranteed to require adjustment. The exercise will alert us to the relationship between cautions that we accumulate in the design process and the need always to be prepared to make field adjustments.

### *1. Pressing NEC Limits and the AGT*

One of the most common reasons for a model requiring from moderate to extreme levels of field adjustment in the prototype stage is using a model that presses one or more of the limitations of NEC. Many of the limitations have received treatment in past episodes, although others remain less formally listed. In many cases, the limits are not absolute. Instead, as the modeler approaches the limit, the numbers gradually become less accurate.

One of the most reliable general tests that a model is pressing limits, especially those for which NEC and its implementations issue no warnings, is the Average Gain Test (AGT). Too many modelers--both amateur and professional--fail to give the test due heed. Even though the AGT test is a necessary condition of model adequacy, it is not a sufficient condition, and there are configurations that achieve nearly ideal scores but still show

aberrations. Despite this limitation, the AGT score is a relatively good guide that there is a potential need for prototype field adjustment.

Fig. 1



Highly Segmented (51) Stepped-Diameter Element

As a sample, we may resort to a very common case: the stepped diameter HF element. **Fig. 1** shows a highly sectioned center-fed dipole element for 14.175 MHz. The element contains 51 segments total so that all segments are approximately the same length. **Fig. 2** shows the element structure in an EZNEC Wires table, along with the usual method of handling such elements, the Leeson substitute element formulation.

Wires Fig. 2

Wire Create Edit Other

Coord Entry Mode  Preserve Connections  Actual Element Structure  Show Wire Insulation

No.	End 1				Conn	End 2				Diameter (in)	Segs
	X (in)	Y (in)	Z (in)			X (in)	Y (in)	Z (in)	Conn		
1	-205.75	0	0		-138	0	0	W2E1	0.5	8	
2	-138	0	0	W1E2	-96	0	0	W3E1	0.625	6	
3	-96	0	0	W2E2	-48	0	0	W4E1	0.75	6	
4	-48	0	0	W3E2	-4	0	0	W5E1	0.875	5	
5	-4	0	0	W4E2	4	0	0	W6E1	3.419	1	
6	4	0	0	W5E2	48	0	0	W7E1	0.875	5	
7	48	0	0	W6E2	96	0	0	W8E1	0.75	6	
8	96	0	0	W7E2	138	0	0	W9E1	0.625	6	
9	138	0	0	W8E2	205.75	0	0		0.5	8	

\*

---

Stepped Diameter Correction Fig. 2

Edit Other

Leeson Substitute Element

No.	End 1				Conn	End 2				Diameter (in)	Segs
	X (in)	Y (in)	Z (in)			X (in)	Y (in)	Z (in)	Conn		
1	-199.338	0	0		-133.7	0	0	W2E1	0.674389	8	
2	-133.7	0	0	W1E2	-93.0085	0	0	W3E1	0.674389	6	
3	-93.0085	0	0	W2E2	-46.5042	0	0	W4E1	0.674389	6	
4	-46.5042	0	0	W3E2	-3.87535	0	0	W5E1	0.674389	5	
5	-3.87535	0	0	W4E2	3.87535	0	0	W6E1	0.674389	1	
6	3.87535	0	0	W5E2	46.5042	0	0	W7E1	0.674389	5	
7	46.5042	0	0	W6E2	93.0085	0	0	W8E1	0.674389	6	
8	93.0085	0	0	W7E2	133.7	0	0	W9E1	0.674389	6	
9	133.7	0	0	W8E2	199.338	0	0		0.674389	8	

The total element length is set to provide a resonant feedpoint impedance when modeled in the substitute-element mode. The following table shows the results of modeling the element in that mode, plus modeling it with both NEC-2 and NEC-4 in uncorrected modes.

## Modeled Results for a Stepped-Diameter Element at 14.175 MHz

Total Length	Version	Feedpoint Z (Ohms)	FS Gain	AGT	AGT-dB
411.5"	Leeson	71.16 + j 0.11	2.18 dBi	1.010	0.04
	NEC-4	61.25 + j 3.05	3.07	1.235	0.92
	NEC-2	43.54 + j11.51	4.68	1.786	2.52
410"	NEC-4	60.50 - j 0.05	3.07	1.235	0.92
408"	NEC-2	41.04 + j 0.74	4.66	1.784	2.51
398.68 x 0.6743"		71.89 - j 0.07	2.14	1.000	0.00

The NEC-2 results are the least accurate and also show the least ideal AGT score. Had we tried to model the element without the Leeson corrections, we would have ended up with a 408" element length and expectations of a 40-Ohm resonant feedpoint impedance, as shown lower down in the table. NEC-4 produces better results as a consequence of the current-calculation algorithm revision. However, it shows a significantly non-ideal AGT score, excessive gain, and an impedance about 10 Ohms lower than shown by the Leeson model. Had we used NEC-4 without correction and aimed the model for a resonant impedance, we would have ended up with a 410" element, but our impedance expectations would still be 10 Ohms low.

Perhaps surprising to some folks is that fact that the Leeson-corrected substitute element is not perfect as shown in the lower portion of **Fig. 2**. The element has a special feature used by many modelers to simulate elements that connect directly to a conductive boom. The center section is short and very fat. The step from the center section diameter to the actual element diameter is large. In addition, the center section length allows only a single segment. Therefore, the segments adjacent to the source segment have lengths that differ from the center section. The combination of

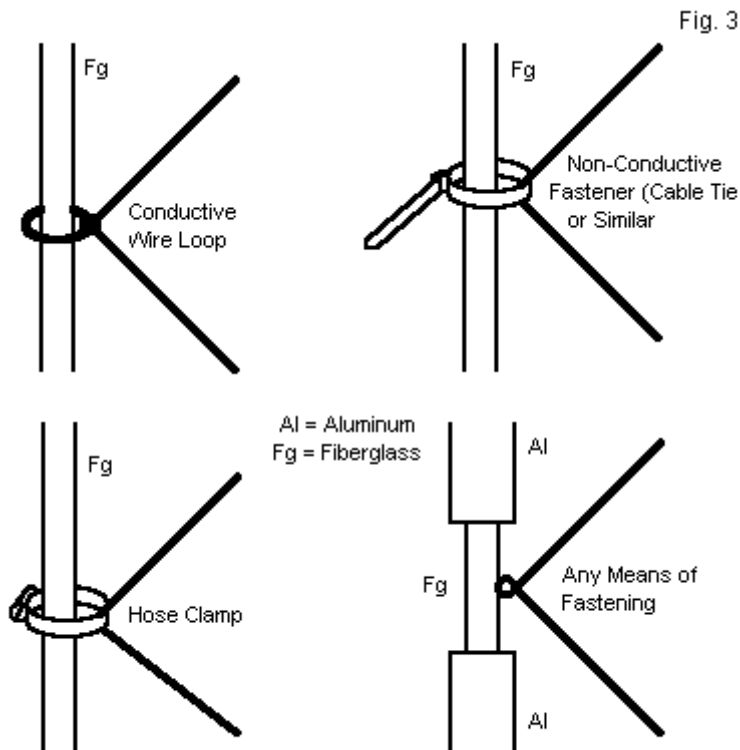
ingredients is enough to yield a slightly non-ideal AGT value and a slightly high gain report. If we replace the sectioned Leeson element with a single wire having the same overall length and the Leeson-specified diameter with the same total number of segments, we obtain the results in the bottom line. The AGT score is ideal and the gain report is correct for the free-space environment. Fortunately, the impedance does not change enough to suggest that we might have a problem using a Leeson-corrected model.

The results of the test suggest several conclusions regarding the need for prototype field adjustment. Had we modeled the element using uncorrected NEC-2, the resulting dimension would need serious field revision to reach resonance at the design frequency. Had we used uncorrected NEC-4, we still would need significant field adjustment. Modeling the complexly structured elements using the Leeson substitute element (which yields identical results in both NEC-2 and NEC-4) would likely require the least adjustment, or perhaps none at all, depending on the designer's level of fussiness.

There are innumerable other ways to press NEC limitations. The AGT test will catch most of them. The greater the degree to which the AGT score is not ideal (above and below 1.000 in free space), the greater will be the degree of likely field adjustment involved in the prototype.

### *Unmodeled Wire Structures*

To the degree that a model fails to include all geometric features within its structure, the model's reported performance will be off the mark and require field adjustment in any physical prototype. This generalization has greater or lesser application, depending upon what we omit from a model. For example, with a Yagi, if the elements are well insulated and isolated from any conductive boom, omitting the boom from the model will do no harm. If the elements physically connect to the boom, modeling it will not produce more accurate results, since NEC does not calculate transverse currents. This case falls within the preceding category of modeling within NEC limitations and guidelines. However, there are a myriad of different kinds of cases in which we habitually model elements and then construct them in a different manner, where that manner results in a structure that differs by at least a small amount from the model.



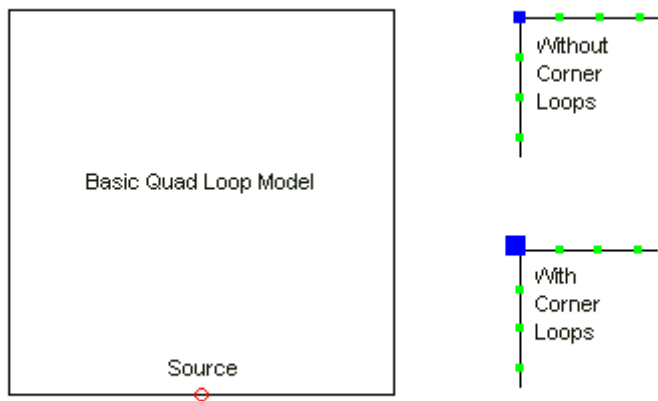
Some Methods of Attaching Quad Loops to Support Arm

Perhaps one of the classic cases revolves around modeling quad loops. **Fig. 3** shows four general ways in which builders physically connect the loop elements to the support arms of HF wire-loop quad antennas and arrays. In three of the four cases, we have conductive materials in proximity to each of 4 presumed corners for

a square or diamond-shaped quad. Only the version with an RF-transparent support arm and an equally RF-transparent connector will reflect the structure that we normally model. Two of the remaining modes of construction employ conductive rings either in contact with or very closely coupled to the main loop. Each of these rings represents a closed 1-turn inductor that to one or another degree will detune the main loop relative to its modeled performance without the rings.

To demonstrate the degree of detuning that is possible, consider a model of a square quad loop that is resonant when modeled without accounting for the ring connectors. The subject model is for 28.5 MHz and uses AWG #14 wire for the element. **Fig. 4** shows the general outline of the quad loop, along with two variations.

Fig. 4



Test Modeling What We Normally Do Not Model

The top-right partial outline shows one corner of the basic loop as normally modeled. The lower sketch shows the same corner with a 1" square loop attached, simulating the ring connector often used in physical quads. Since the quad loop is about 109.5" per side exclusive of the loops, the small additions seem insignificant, even when we multiply the one shown by four. The following table tells another story.

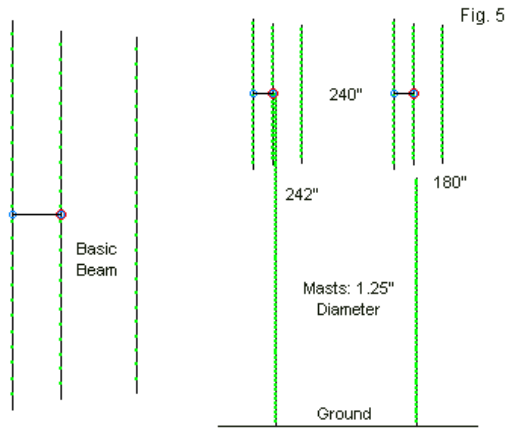
**A Quad Loop With and Without Corner Attachment Loops**

Version	Impedance (Ohms)	Max. Gain (dBi)	AGT	AGT-dB
Without	125.4 - j 0.5	3.30	1.002	0.01
With	128.1 + j24.5	3.29	1.001	0.01

The sample will not exactly correspond to the loops and construction methods in any particular case, but it does show the degree to which the model may depart from reality in that reality contains loops the size of the ones included in the revised model. For every case of omitting details from models, the prototype will require adjustment to center the performance curves where the design model intended them to be. The problem becomes more acute with parasitic elements. One may use either a detailed or a shortcut procedure. The shortcut simply applies the percentage of change to the driver loop length to each of the parasitic elements. For greater precision, one would need to determine the resonant frequency of each parasitic element in the model and then adjust each corresponding physical element to self-resonance at the same frequency.

As we increase the operating frequency, "lumps" and "gobs" that make no difference in the HF range may begin to make considerable difference in the UHF range. An element wire made from common materials becomes a significant percentage of a wavelength at UHF. Hence, some common practices related to fastening loops to cable connectors may take on some detuning significance. We often create closed wire loops by overlapping, twisting, and then soldering wire ends, a generally invisible practice at HF. However, doubling the wire diameter, even for a small part of a UHF loop can detune it from its uniform diameter in the model. As well, closing a loop at a current maximum or a current minimum point can also make a difference.

Because we are wedded mentally to the arrangement of antenna features in horizontal beams, we often forget to make appropriate adjustments when rotating such beams for use with vertically polarized signals. A horizontal beam requires no attention to the mast, since the support is at right angles to the elements and the plane of the radiation pattern. Hence, we typically model horizontal beams without modeling the mast. When we turn the beam to orient it vertically, we cannot be so careless. **Fig. 5** shows a vertically oriented beam with no boom modeled, along with two types of cases in which we model the support mast. One of the cases extended the conductive boom to a point 2" above the Yagi's boom at 240" (20') above average ground. The other case limits the conductive portion of the support mast to 180" (15') above ground, with a presumably RF-transparent mast section above that point.



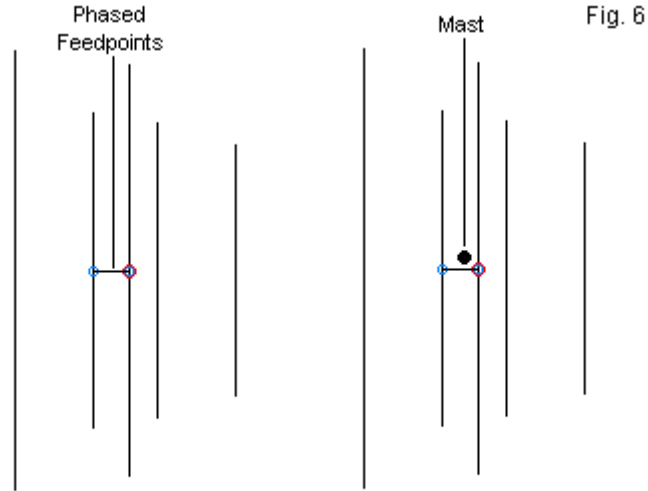
Modeling Masts for Vertically Oriented Antennas

The test frequency for the antenna is 52 MHz, which makes the two mast lengths close to even multiples of a half wavelength. The following table catalogs the modeled results for the three cases.

A Vertical 6-Meter Phase-Fed Yagi with Different Mast Situations				
Version	Impedance (Ohms)	50-Ohm SWR	Max. Gain (dBi)	To Angle (Deg.)
No Boom	43.6 + j 7.9	1.24	7.42	9
242" Boom	26.2 + j17.9	2.23	6.31	27
180" Boom	41.3 + j 5.8	1.26	7.24	9

Carelessly using a full-length conductive mast results not only in a detuning of the closely spaced driver, but also distorts the pattern to raise the elevation angle of greatest field strength to an unusable high level. Shortening the conductive portion of the mast returns to the beam to nearly full "no-mast" performance. Still, a builder might wish to do further modeling to ascertain just how long the conductive portion of the support mast can be and not affect performance at all.

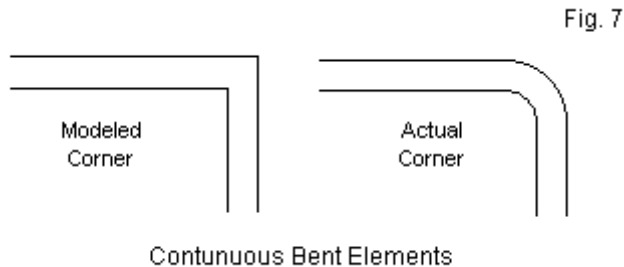
Under certain circumstances, the close proximity of a mast can affect even a horizontal beam. **Fig. 6** shows a 2-band Yagis with a common feedpoint. On the left is the typical mast-less model. The outline suggests that we are using a direct connection between the drivers for the two bands, a short section of exposed parallel transmission line.



Mast Consequences for a Horizontally Oriented Beam

On the right is an added dot representing the likely placement of the support mast in order to support the beam near its center of mass. The position is beside the transmission line connecting the two drivers. The combination of the mast and the plate-hardware combination used to join the mast and the boom may have a significant effect on the driver connection line, even if the metal mass leaves the elements themselves unaffected. For example, it may alter the effective characteristic impedance of the line, resulting in altered driver impedances on one or both bands. To forecast the potential effects of a closely spaced mast assembly, we may wish to model a short thick wire in the vicinity (but

unconnected to the antenna elements) to see what may happen with a prototype. The exercise may also allow us to pre-plan for the adjustments that we may make to the prototype by indicating trends in effects and which modifications restore performance. It is easier to go through the head-scratching process in front of a computer than at the top of the prototype's support structure.



There are innumerable instances in which a model will be at variance with the prototype without any way of compensating within the model. The sketches in **Fig. 7** show the modeled and the actual situation that we often encounter with elements that necessarily change direction and yet have a significant element diameter. For example, we might encounter this situation in a Moxon rectangle in which the elements are relatively fat for the operating frequency and yet are metallically continuous. The physical antenna will require a bend on a radius that accommodates the element's diameter without weakening the structure. The bend radius "cuts" the corner, requiring an adjustment to both the left-right and the front-back dimensions to maintain the total element length. By

using enough segments in the model's elements, we can often model an angular corner. However, we must ensure that we do not adversely affect the AGT score in the process so that we may correctly correlate the results of the corner simulation to the original model and to the physical prototype.

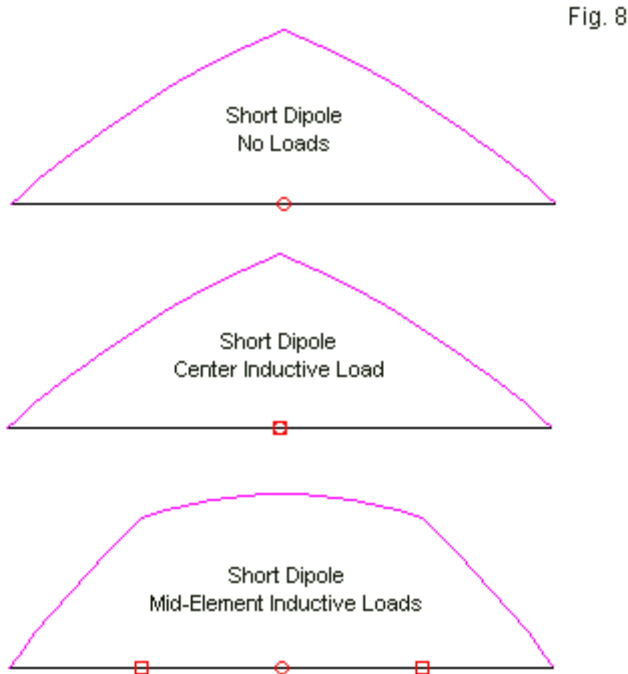
Although we have looked at a number of cases in which our models omit certain details of the physical prototype, we have not exhausted the list of possibilities. Nevertheless, perhaps this abbreviated catalog will suffice to alert modelers to the potentials for variation between the model and the physical.

## **Inductive Loading**

All forms of R-L-C loading in NEC models present limitations, some of which can affect the model-to-prototype correlation. These types of loads, whether set up as series or parallel circuits, have no geometric dimension and therefore play no role in the initial matrix calculations. Instead, the program applies the load's equivalent resistance and reactance (real and imaginary components of the load impedance) to the assigned segment after initial calculations. The result is a modification of the current on the loaded and other segments, with further consequences for the calculation of overall antenna fields.

Inductive loads are susceptible to a growing inherent error as we move the inductance further from the high-current region of the antenna. In this connection, we might study the behavior of the

current magnitude as we move loading inductances away from the center of a dipole, as shown in **Fig. 8**.



Current Distribution with Different Types of Inductive Loads

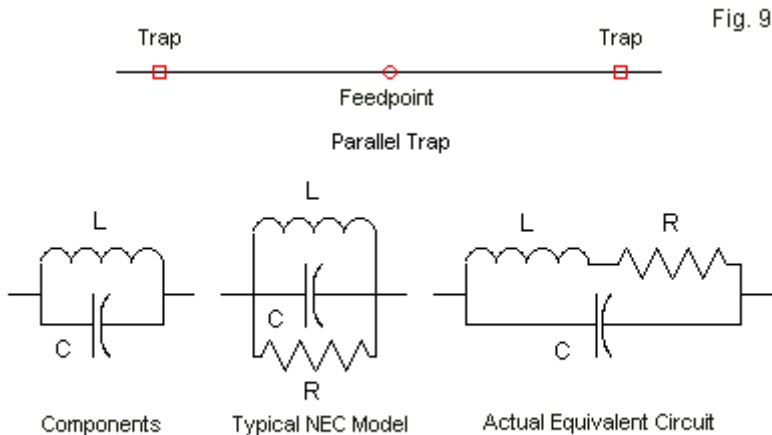
The top current distribution curve applies to an unloaded short dipole that shows a source impedance of  $29.45 - j402.6$  Ohms. To bring the dipole to resonance, we may add an inductive load on the center segment, which is also the source segment. The reactance

of the load is  $j402$  Ohms. The equivalent inductance at 28.4 MHz is 2.25  $\mu\text{H}$ . If we omit a series resistance and assume an indefinitely large value for the inductor's  $Q$ , we obtain a gain of 1.88 dBi in free space (for either the loaded or the unloaded dipole). The center-loaded dipole reports a source impedance of  $29.45 - j0.56$  Ohms. Assuming a  $Q$  of 300 requires that we add a resistance of 1.34 Ohms, and the gain drops to 1.69 dBi. The resistive center load component adds to the unloaded resistive component, so the source impedance becomes  $30.79 - j0.56$  Ohms.

Center inductive loads are most accurate in NEC (equivalent to base-loading in a ground-mounted monopole) because the current at each end of the loaded segment is equal. This condition assures that the inductance reflects most closely a physical, that is, a virtually pure inductor. As we move the load outward from center, the situation changes as shown in the lowest outline in **Fig. 8**. Assigning the two loading inductors positions that are midway from the source segment to the element tip, each inductive load requires a reactance of  $j402$  Ohms to affect resonance. This value is equivalent to installing two 2.25- $\mu\text{H}$  coils, one on each side of the center segment. With these inductors installed (without regard to inductor  $Q$ ), the model reports a source impedance of  $46.68 - j0.13$  Ohms. If we add a series resistance to each inductance to equate with a  $Q$  of 300, we obtain a source impedance report of  $48.69 - j0.23$  Ohms. The gain with an infinite  $Q$  is 1.91 dBi and with a  $Q$  of 300 it is 1.73 dBi. (Note that there is no significant gain advantage to mid-element loading over center loading in dipoles.)

The current distribution curve for the mid-element loading example points to a significant facet of load behavior if we assume the use of solenoid inductors. The current at each end of the inductor is different. To the degree that the current levels differ, the wire within the inductor serves a second purpose in addition to creating an inductive reactance. The wire also serves as part of the length of the antenna, even if so oriented that it cannot contribute significantly to the antenna's radiation. The wire in the uncentered inductor(s) will have an effect on the length of dipole necessary to achieve resonance. However, since the inductors in the model have no wire (in the sense that the segmented wires of the element do have wire), the model cannot show the contribution of the physical inductor wire to the antenna's length. As a result, a physical element that is highly loaded away from the high-current region of the antenna will not have the same length as modeled. The net consequence is a requirement for field adjusting the physical prototype.

Allied to the inherent inaccuracy (not severe but noticeable) of inductive loads away from the elements high-current region is a modeler oversight often encountered in models of trap elements. Consider an element designed for the amateur 12- and 17-meter bands, specifically 24.94 MHz and 18.118 MHz. A correctly modeled trap dipole would show source impedance values in the 71- to 73-Ohm range for each band using traps with a coil Q of 300. However, many modelers fail to achieve such results. We may understand why if we examine the trap situation shown in **Fig. 9**.



Some Elements of Trap Modeling

With respect to components, a trap consists of a parallel combination of an inductance and a capacitance. NEC offers only series and parallel load configurations, as shown at the center of the figure. The parallel combination is the most apt, but does not capture the equivalent circuit of a trap, such as shown at the right. Therefore, we must convert the series R-L leg of equivalent circuit into a parallel combination of resistance and inductance to obtain the required components for a parallel circuit.

Now we may add a further complication. We normally design traps for frequencies either at or just below the lower end of the band for which they operate as traps. The design frequency for the trap in the same antenna is 24.5 MHz. At the antenna's design frequency of 24.94 MHz, the trap serves as a slightly off-resonance parallel

tuned circuit that presents a high impedance, thus terminating the antenna at the trap. At the lower frequency, many modelers simply presume that the capacitor disappears and that the remaining element loading is solely a function of the inductor value. Unfortunately, this assumption is incorrect. The loading reactance in each off-frequency trap (at 18.118 MHz) is a function of both components in a non-resonant parallel circuit. We cannot even preserve the parallel resistance that we used to set up the trap at the original frequency, since its value will also change. A model that uses only the value of the inductor (and its series resistance) to load the element for the lower band will be nearly 2' longer at resonance than one that re-calculates the net impedance of the entire trap.

Now we may add in the previously noted difficulty with inductive loads inserted well away from the antenna's high-current region. Although we may not need to make a significant adjustment to the inner length of the element on 12 meters, we can expect to require a fairly sizable adjustment to the overall length of the element when operating on 17 meters, even if we correctly calculate the loading of the trap on the lower band.

## Conclusion

Catalogs must end somewhere, and this point is probably as good as any. Our fundamental theme has been the fact that there are many circumstances that will dictate a need for field adjustment to a physical prototype of any antenna designed via NEC software. Some of those circumstances involve pressing NEC limitations,

whether those limitations relate to guidelines for adequate model geometry or to software techniques for loading and other non-geometric program functions. Other circumstances involve limitations on how precisely we may reflect reality within a model, with some limitations relating to the software and others to the habits and conventions we bring to the modeling process.

There are a large number of antennas that we can accurately model so that the model's specifications translate virtually exactly into a physical antenna that performs in accordance with model predictions. However, the number of cases that inherently call for field adjustment of the physical prototype is even larger. When converting a design model into a physical antenna, we should always be prepared to make such adjustments. If we use the software wisely, we can often know in advance the kinds of adjustment maneuvers that are most likely to bring the antenna into alignment with our design specifications.

## Chapter 131: AM BC Modeling with NEC

### 1. Basic Considerations

Over the past few years, the National Association of Broadcasters (NAB) has been studying the possibility of using antenna modeling software for some of its submission to the Federal Communication Commission (FCC). The details of these discussions properly belong to the broadcasters, the consulting engineers, and the representatives of the Commission. These notes do not in any way constitute a commentary on the overall merits of the proposals.

Instead, these notes have a much smaller mission. The program used by many consulting broadcast engineers is a proprietary version of MININEC. To the date of writing--likely long ago in terms of the time of publication--the use of NEC cores (either -2 or -4) has not received full attention. One seeming drawback to the use of NEC has been the absence of a ground calculating system equivalent to the MININEC ground calculating system. The latter system allows effective modeling--within limits--for ground-mounted monopoles without the need for modeling a full set of buried radials. A second limitation perceived to surround NEC is the absence of RMS inputs and outputs. A third note often made is that NEC typically calculates azimuth angles in terms of phi- or counter-clockwise-conventions rather than in terms of the compass rose azimuth headings that correspond to typical maps used in FCC submissions. The list goes on, but is perhaps not very convincing, since most of the items require relatively simple pre-core and post-core calculations.

These notes will address some of the fundamental modeling steps needed to obtain from NEC (either -2 or -4) essentially the same outputs that might be obtained with any other modeling program. My object lies only in the steps required to obtain the outputs and their correlation with appropriate MININEC outputs. Where correlations are required, I shall use Antenna Model, a highly corrected version of MININEC 3.13--indeed so much corrected that its results are comparable to NEC-4 results well into the UHF region. However, like all forms of MININEC, Antenna Model has no limitations with respect to junctions of wires have different diameters. For such instances, NEC has well-proven work-arounds.

These notes will use standard ASCII input files for NEC. GNEC by NSI is handy in this regard, since it makes both the NEC-2 and NEC-4 cores available to explore differences (things have changed since writing this. Be aware that NSI software is incompatible with Windows OSes beyond Win2K and *may* run/have issues with XP and not known to run on Vista at all — no upgrades in sight at this time). As well, the program makes use of peak values of voltage and current and so will alert us to when we need to make certain external calculations. Some implementations of NEC, such as EZNEC, already employ RMS values of voltage and current as user inputs and as tabular outputs. Such implementations save the routine calculation steps. However, by using the more rudimentary I/O facilities, we may better understand what the core does and what we must do in conjunction with the NEC cores.

## Setting Up the Most Basic Model

The models used in preparing these notes all use 1 MHz as the working frequency. As well, the material used will be lossless or perfect wire. Initially, we shall use perfect ground, although we shall examine other options along the way to master their use. The models will also use only single monopoles to make clear the NEC-modeling steps that we must take.

The first step is to model a monopole with a uniform diameter or radius over perfect ground. Consulting engineers have recommended that we may substitute for the typical triangular and square towers found in the industry a single wire with certain dimensions. We shall begin with a triangular tower having a face width of 2' (24").

### Recommended Substitute Single-Wire Dimensions for Multi-Face Towers

Tower Type	Diameter	Radius
Triangular	$D = 0.74 * \text{Face Width}$	$R = 0.37 * \text{Face Width}$
Square	$D = 1.12 * \text{Face Width}$	$R = 0.56 * \text{Face Width}$

Note: D and R are in the same units as the Face Width

Perhaps the simplest model that we might construct in NEC has the following input file.

```
CM resonant monopole, perfect ground
CE
GW 1 41 0 0 234 0 0 0 0.74
GW 30901 1 9901.0000 9901.0000 9901.0000 9901.0001
9901.0001 9901.0001 .00001
GS 0 0 .3048
```

```
GE 1
GN 1
EX 0 30901 1 0 0.0 1.0
NT 30901 1 1 41 0 0 0 1 0 0
FR 0 1 0 0 1 1
RP 0 1 361 1000 90 0 1 1
EN
```

The model requests a simple far-field radiation pattern (RP0) that is an azimuth pattern at zero-degrees elevation (90 degrees theta), which is allowable with a perfect ground. The first wire entry (GW1) lists the wire, specified in terms of feet. The last entry in the GW line is the radius, which meets the recommended calculation. The 234' vertical dimension is just long enough to achieve resonance with perfect ground at the design frequency.

The model has an additional feature. It employs the standard NEC method of implementing a current source at the lowest of the 41 segments in the monopole, the one that makes contact with ground. The technique requires a remote substitute source wire, specified in GNEC as tag 30901 to keep it invisible in the antenna viewing system. In fact, if the user constructs the current source within NEC-Win Plus, the wire will remain invisible to the user, as it does in the EZNEC implementation of current sources. The wire's remoteness and small size prevent the substitute source wire from having any impact whatsoever on the current and radiation calculations for the monopole itself. The method also requires the setting of a network (NT command) between the remote wire and the monopole base segment. Since the NT "connection" has no physical or geometric dimension in the model, the remote wire is

wholly acceptable. The NT command creates a 90-degree phase shift in the applied voltage and results in a current of the same magnitude appearing at the monopole base segment. For the first model, the source command (EX) specifies the remote wire as the source location and advances the phase of the applied voltage by 90 degrees. Hence, the last 2 entries in the EX line are the reverse of what we would find in a standard voltage-source situation. The real voltage is 0.0 and the imaginary voltage is 1.0. In standard versions of NEC, these are peak values.

Our first concern is the reported source impedance of the monopole. The following GNEC tabular output gives us the NEC-4 report.

Input Impedance and VSWR

Frequency	Tag	Seg.	Real(Z)	Imag(Z)	Mag(Z)	Phase(Z)
1.000000	1	41	36.020	0.307	36.021	0.488

If we construct the identical 234', 1.48' diameter, 41-segment perfect-ground model in MININEC, we shall find one major difference. The source location will be exactly at the junction of the lowest segment and ground. MININEC places sources and loads at pulses, which occur at segment junctions or on the last segment of a modeled wire. In contrast, NEC places sources, loads, transmission lines, and networks on a segment, conveniently but somewhat misleadingly said to be at the center of the segment. The MININEC current pulse extends from the center of a segment to the center of the adjacent segment. The NEC current extends from one

segment junction to the next. (However, for the purpose of wire intersection, we may usually take the current to be most sensitive to impinging influences within the center third of a segment. Hence, intersecting wires should have radii that avoid penetration into this region.)

Despite the differences in the source position, the MININEC model yields a source impedance of 35.96 - 0.10 Ohms. The difference between this value and the NEC-4 value is less than the differences we are likely to see within one program moved between computers with different CPU architectures. One reason for the close correlation between source impedance values is the use of adequate segmentation in the NEC model. For a NEC model to most closely approximate the impedance at the junction with ground, the segments should be as numerous as the wire radius allows. The segments in the NEC model are about 5.7' long, which yields a segment-length-to-radius ratio of about 7.7:1.

The second concern is the current magnitude and phase on the monopole's lowest segment--its feedpoint. In the listed model, this

FREQUENCY (MHz)	SEG. NO.	TAG NO.	COORD. OF SEG. CENTER			SEG. LENGTH	CURRENT (AMPS)			PHASE
			X	Y	Z		REAL	IMAG.	MAG.	
1.000000	41	1	0.0000	0.0000	0.0029	0.00580	1.0000E+00	-7.5894E-19	1.0000E+00	0.000

In conjunction with the current value, we also need to examine the power budget.

```

- - - POWER BUDGET - - -
INPUT POWER   = 1.8010E+01 WATTS
RADIATED POWER= 1.8010E+01 WATTS
WIRE LOSS     = 0.0000E+00 WATTS
EFFICIENCY    = 100.00 PERCENT

```

With a current magnitude of 1.0 (phase angle 0.0 degrees), the power supplied to the antenna (with 100% efficiency in this simplified case) is 18.01 Watts. However, most modelers would be interested in the current with some prescribed power level at the antenna source. Let's suppose that the power level is 1000 Watts. The ratio between the desired power level and the reported power level is 55.52. To adjust the source current, we need to take the square root of this ratio, or 7.45. The new value for the source current is simply the initial value times this value, an easy calculation, since the initial value was 1.0. Therefore, we may modify the starting model to arrive at the next one.

```
CM resonant monopole, perfect ground
CM adjusted source current for 1000 watts power
CE
GW 1 41 0 0 234 0 0 0 0.74
GW 30901 1 9901.0000 9901.0000 9901.0000 9901.0001
9901.0001 9901.0001 .00001
GS 0 0 .3048
GE 1
GN 1
EX 0 30901 1 0 0.0 7.4515
NT 30901 1 1 41 0 0 0 1 0 0
FR 0 1 0 0 1 1
RP 0 1 361 1000 90 0 1 1
EN
```

The only change occurs in the EX line, where we replace the imaginary current value for this current-source model. The power budget reflects the change.

- - - POWER BUDGET - - -

```

INPUT POWER      = 1.0000E+03 WATTS
RADIATED POWER= 1.0000E+03 WATTS
WIRE LOSS        = 0.0000E+00 WATTS
EFFICIENCY       = 100.00 PERCENT
  
```

The power level is now 1000 watts, and the corresponding current on segment 41 appears in the current table.

FREQUENCY (MHz)	SEG. NO.	TAG NO.	COORD. OF SEG. CENTER			SEG. LENGTH	- - - CURRENT (AMPS) - - -			PHASE
			X	Y	Z		REAL	IMAG.	MAG.	
1.000000	41	1	0.0000	0.0000	0.0029	0.00580	7.4515E+00	-3.4694E-18	7.4515E+00	0.000

The reported current is 7.4515 Amps, as we would expect, except that this is a peak value for the current. To arrive at an RMS value, we must divide the reported value by the square root of 2 (or multiply by 0.7071). We thus obtain an RMS feedpoint-segment current of 5.269 Amps. From the current and the source impedance, we can easily calculate the source voltage at 189.8 Volts (RMS) at 0.48 degrees phase angle. (EZNEC allows a user-selected power level among its options and provides both input and output values in RMS, thus saving the need for these hand calculations, even though the arithmetic is very simple.)

## Field Strength

Using NEC for single-monopole analysis normally does not require much attention to the circular azimuth pattern or even the double-hump elevation pattern. Interest in those patterns becomes more intense with the use of multiple towers with phased feed systems.

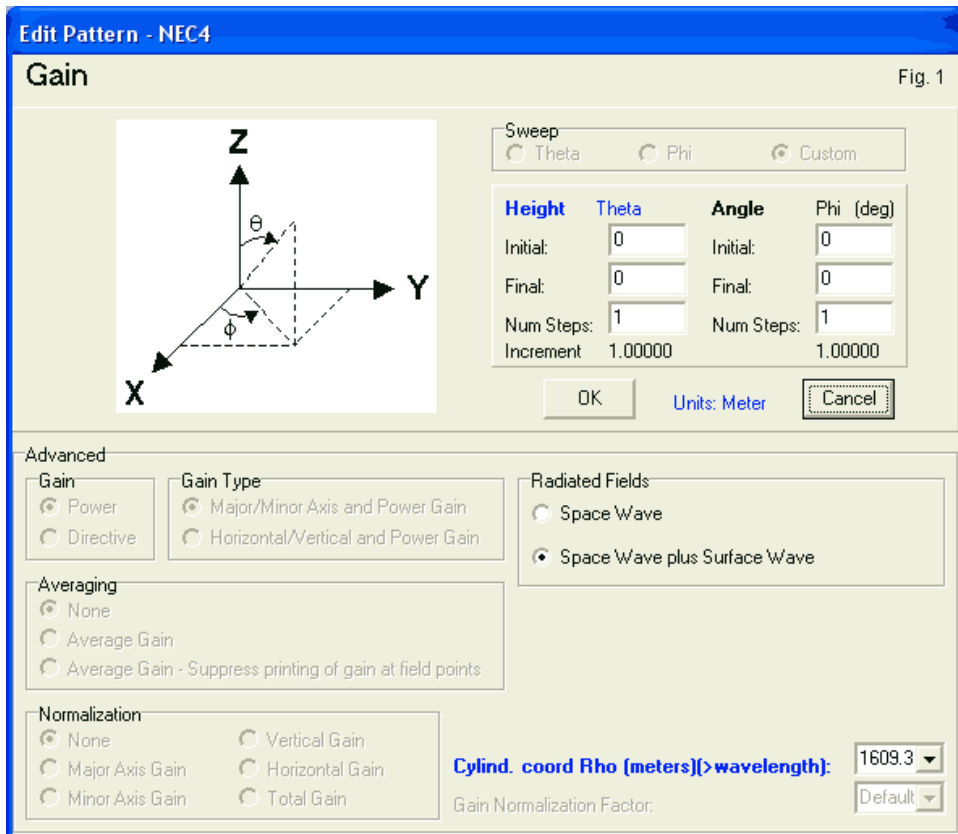
That exercise lies in our future, but at the moment, we shall remain with our single tower at 234' and a design frequency of 1 MHz.

The central interest becomes the electrical field-strength initially over perfect ground. To obtain the field strength output, we need add only 1 line to our model (retaining the adjustment to the EX line that set the power level). The revised model below has a familiar look.

```
CM resonant monopole, perfect ground
CM field-strength
CE
GW 1 41 0 0 234 0 0 0 0.74
GW 30901 1 9901.0000 9901.0000 9901.0000 9901.0001
9901.0001 9901.0001 .00001
GS 0 0 .3048
GE 1
GN 1
EX 0 30901 1 0 0.0 7.4515
NT 30901 1 1 41 0 0 0 1 0 0
FR 0 1 0 0 1 1
RP 0 1 361 1000 90 0 1 1
RP 1 1 1 0000 0 0 1.00000 1.00000 1609.344
EN
```

I have left the RP0 line in the model to allow comparison with the less-used RP1 output line. For a single frequency, both lines will yield outputs with only one FR line. However, if using a frequency sweep, repeat the FR line before the second radiation pattern request or the second RP line will show an output only for the highest frequency in the sweep loop.

The RP1 request changes some of the meanings of entries relative to the more regularly used RP0 command. The last entry specifies a distance in meters from the coordinate system in the X-Y plane and presumably from the antenna. The number in the last entry is 1 mile, expressed, as all control command distances and dimensions must be specified, in meters. The theta (or elevation) angle changes meaning and becomes the height of the observation, again in meters. We may get a better sense of the entries by viewing the GNEC help screen for RP1 commands in **Fig. 1**.



The command entries allow us to specify a start and a stop height, along with the number of steps. The program will perform the division to arrive at the value for the increment between steps. For the basic sample, I have set the height at 0 meters above Z=0, which is the value used automatically by MININEC post-core

calculations of field-strength. Unlike a MININEC calculation, NEC calculates both surface and space waves to wind up with a field-strength calculation, although the two will be coincident over perfect ground. Note finally the simplification of the ground-wave request to a single azimuth bearing. We might select periodic azimuth positions for a phased array with directional properties, where the positions correspond to bearings on which we would take physical measurements.

```

- - - RADIATED FIELDS NEAR GROUND - - -
- - - LOCATION - - -
RHO   PHI   Z
METERS DEGREES METERS
- - - E (THETA) - - -
MAG   PHASE
VOLTS/M DEGREES
- - - E (PHI) - - -
MAG   PHASE
VOLTS/M DEGREES
- - - E (RADIAL) - - -
MAG   PHASE
VOLTS/M DEGREES
1609.34   0.00   0.00   2.7520E-01   134.12   4.6094E-22   -108.70   0.0000E+00   0.00

```

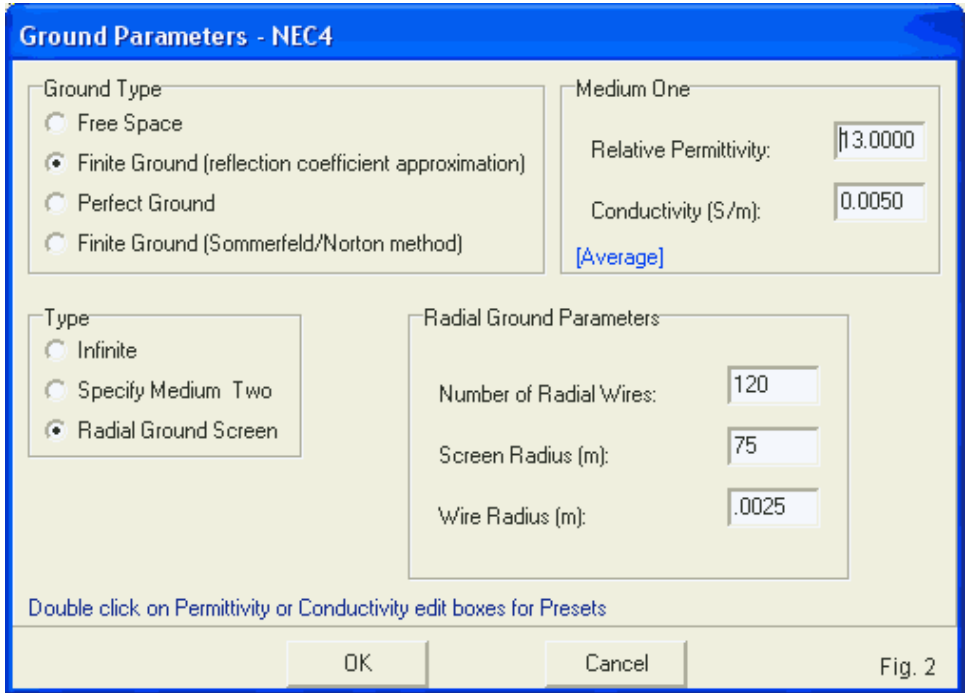
The field strength calculations are part of the final section of the NEC output report. From the entries for E(theta) and E(phi), we can recognize the vertical component of the field by its much higher value--as we would expect from a vertical monopole. In fact, as values drop below E-9 to E-10, the numerical value becomes unreliable. For example, had we used an azimuth specification of 0 to 360 degrees, the E(phi) values for zero and for 360 degrees might have differed, except for one property: both would be too small to be significant.

The E(theta) value is the field strength, but like all NEC output reports for voltage or current, the value is in peak Volts/meter. Applying the 0.7071 correction, we obtain 0.1956 V/m or (more commonly) 195.6 mV/m.

Suppose that we wish to obtain an approximation of the field strength over a soil quality other than perfect. For this task, we must revise the ground parameters in the model. Since we do not wish to model the buried radials, we must invoke the reflection coefficient approximation (RCA) system for ground calculations. The steps that we would take vary between NEC-2 and NEC-4. Let's begin with the NEC-4 procedure.

```
CM resonant monopole, RCA ave ground
CM NEC-4 procedures
CE
GW 1 41 0 0 234 0 0 0 0.74
GW 30901 1 9901.0000 9901.0000 9901.0000 9901.0001
9901.0001 9901.0001 .00001
GS 0 0 .3048
GE 1
GN 0 120 0 0 13.0000 0.0050 75 .0025
EX 0 30901 1 0 0.0 7.4507
NT 30901 1 1 41 0 0 0 1 0 0
FR 0 1 0 0 1 1
RP 0 1 361 1000 90 0 1 1
RP 1 1 1 0000 0 0 1.00000 1.00000 1609.344
EN
```

In NEC-4, we alter the type of ground that we wish and enter further data into the command. **Fig. 2** can help us sort out the line entries.



The upper portion of the help screen shows us the selection of the ground calculating system and the ground quality (average: conductivity = 0.005 S/m, permittivity = 13). The lower portion of the screen shows a special feature available with the RCA system, namely, the ability to specify the number of radials, their length, and the wire radius (the latter two in meters). A standard AM BC radial field uses 120 radials about 1/4-wavelength long. I have arbitrarily selected a wire radius of 2.5-mm (about 0.2" diameter) for each radial. The RCA calculating system is not as accurate as the

Sommerfeld-Norton (SN) system with a set of buried radials, but the model size and run time is much smaller with the RCA specification.

With the RCA ground system and no radial system specification, the feedpoint impedance of the monopole will differ from the value with a perfect ground. As we add radials, the source impedance levels off at the same value that we obtain for a perfect ground, as the extract from the model output file shows.

#### Input Impedance and VSWR

Frequency	Tag	Seg.	Real(Z)	Imag(Z)	Mag(Z)	Phase(Z)
1.000000	1	41	36.020	0.307	36.021	0.488

The RCA radial system affects only the region beneath the antenna, but not the region beyond. Since our field-strength distance is 1 mile from the antenna, we obtain a different value than we obtained over perfect ground.

```

- - - RADIATED FIELDS NEAR GROUND - - -
- - - LOCATION - - -      - - E (THETA) - -      - - E (PHI) - -      - - E (RADIAL) - -
RHO  PHI  Z              MAG  PHASE              MAG  PHASE              MAG  PHASE
METERS DEGREES METERS  VOLTS/M  DEGREES      VOLTS/M  DEGREES      VOLTS/M  DEGREES
1609.34  0.00  0.00  2.3839E-01  91.89  6.8932E-20  -28.12  2.4734E-02  -47.39

```

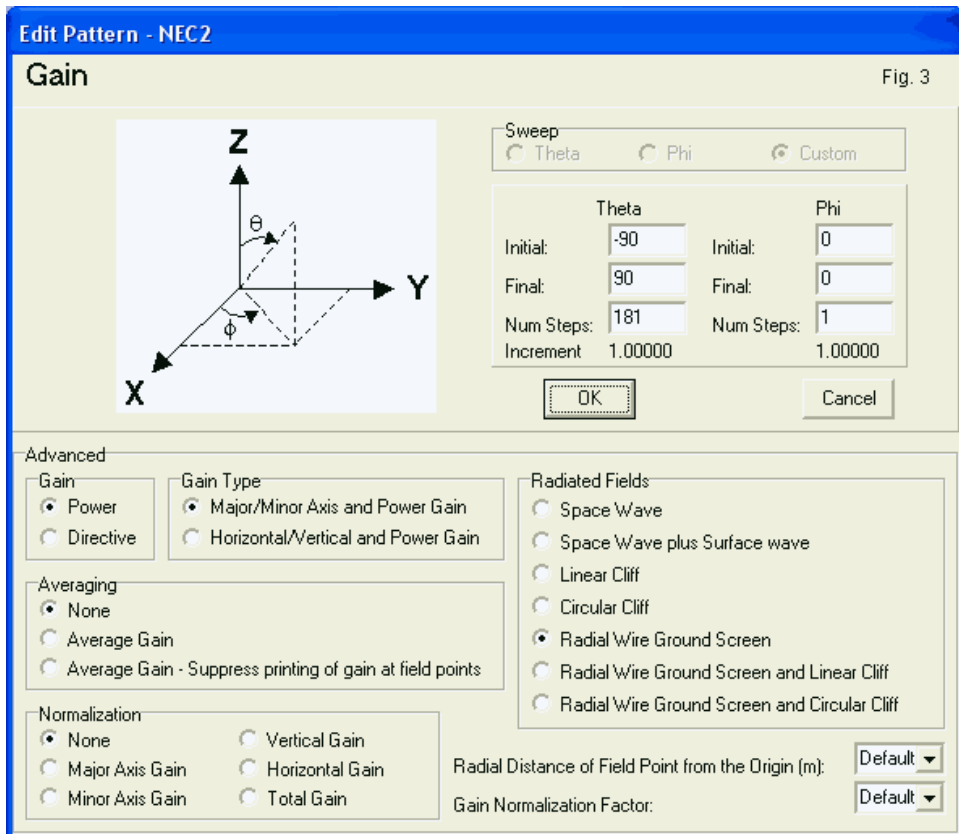
Once again, the E(theta) reading is in peak V/m. After translation, we arrive at 168.5 mV/m at a phase angle of 91.89 degrees.

In NEC-2, we must revise the set-up procedure to obtain a field-strength report. The GN command has the same appearance as it

did in the NEC-4 model. So too does the RP1 line. However, the RP0 command has suddenly turned into an RP4 command, as shown in the NEC-2 model below.

```
CM resonant monopole, RCA ave ground
CM NEC-2 model file
CE
GW 1 41 0 0 234 0 0 0 0.74
GW 30901 1 9901.0000 9901.0000 9901.0000 9901.0001
9901.0001 9901.0001 .00001
GS 0 0 .3048
GE 1
GN 0 120 0 0 13.0000 0.0050 75 .0025
EX 0 30901 1 0 0.0 7.4507
NT 30901 1 1 41 0 0 0 1 0 0
FR 0 1 0 0 1 1
RP 4 181 1 0000 -90 90 1.00000 1.00000
RP 1 1 1 0000 0 0 1.00000 1.00000 1609.344
EN
```

NEC-2 sorted among the various output options by assigning each one a different integer. The use of a radial field without a second medium happens to be option 4. Moreover, NEC-2 does not accept theta angles of 90 degrees (elevation angles of 0 degrees) over any real ground. Therefore, for utility, I changes the pattern request to a theta (elevation) pattern, as shown in **Fig. 3**. The help screen determines the RP option number from its entries and automatically translates the line into an RP4 request.



We could have reverted to (or added) an elevation (theta) pattern request anywhere along this progression. At this stage, the elevation patterns is useful as a reminder that the far-field is negligible at an elevation angle of zero degrees, as shown in **Fig. 4**.

Note the decrease in far-field gain from the perfect-ground value of about 5.2 dBi.

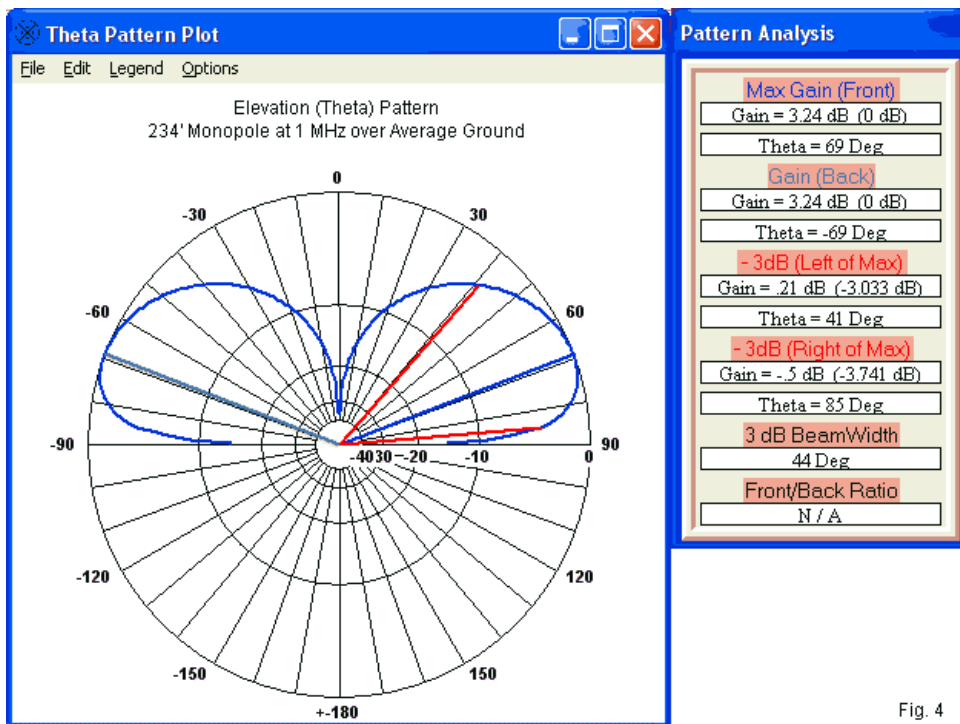


Fig. 4

The NEC-2 field-strength table is very close to being identical to the **NEC-4** version.

```

      - - - RADIATED FIELDS NEAR GROUND - - -
      - - - LOCATION - - -      - - E (THETA) - -      - - E (PHI) - -      - - E (RADIAL) - -
      RHO   PHI   Z           MAG   PHASE           MAG   PHASE           MAG   PHASE
      METERS DEGREES METERS   VOLTS/M DEGREES   VOLTS/M DEGREES   VOLTS/M DEGREES
1609.34   0.00   0.00       2.3753E-01  91.89   6.1979E-20  -78.41   2.4653E-02  -46.89

```

Translated to RMS terms, the E(theta) field strength is 167.9 mV/m at 91.89 degrees. The phase angle is the same, but the estimated field strength is about a half-millivolt less. Part of the reason for the different derives from the NEC-2 source impedance report:

#### Input Impedance and VSWR

Frequency	Tag	Seg.	Real(Z)	Imag(Z)	Mag(Z)	Phase(Z)
1.000000	1	41	36.028	0.339	36.029	0.538

Of course, the differences between the NEC-2 and NEC-4 outputs are less than significant and possibly even less than insignificant.

## Conclusion--So Far

Thus far, we have employed the standard recommended single-wire substitutions for a multi-face tower to arrive at some of the most used data in modeling AM BC towers. For clarity, we have used a resonant length for the tower model, which does not correspond to what the FCC considers to be a 90-degree tower. The simple monopole set up has allowed us to use both a perfect ground and an RCA ground with a radial screen to produce the data from the model. To this point, NEC has shown the ability to calculate as well as MININEC.

Still, we have just begun the journey into tower modeling. Suppose, for instance, that we wish to model the tower as a three-legged affair. The question for modelers who wish to be as economical as possible with their segments is whether we really need all that angular and cross bracing. NEC has both some promises and some pitfalls. In addition, we might ask whether the correlation between NEC and MININEC holds up for towers of other heights with significant reactance at the source segment. One might receive the impression that we are not close to the end of our journey.

## Chapter 132: AM BC Modeling with NEC

### 2. Quandaries: How Many Legs? How Good is Good?

In the preceding episode, we moved step-by-step through the process needed in NEC to obtain most of the basic information required for simple monopoles in AM BC service. For simplicity, we used the NAB-recommended substitute for the complex interlaced pieces of a physical tower: a single wire with a diameter that was 0.72 times the face width of a presumed triangular tower 2' across. The simplification was justified in that episode because we wanted to feature the steps in the process, not the geometry of the monopole tower.

In this set of notes, we shall consider in more detail the structure of towers, at least in the abstract. Most currently available new towers use a triangular structure, although many 4-sided towers still exist. We shall retain the presumed 24" spacing between vertical legs, even though 18" may be more common in practice. Our goal remains the illustration of modeling situations and techniques rather than a replication of actual engineering efforts.

In fact, for reference, we shall use one of the last of our models, a 234' tower composed of a single lossless wire that is 17.76" in diameter as a substitute for a 2' tower face. As the model listing shows, we have placed the antenna over perfect ground and requested both an elevation pattern and a ground wave reading for field strength at a design frequency of 1.0 MHz. The model uses a current source and includes the remote wire and network to achieve this goal. The source current in peak Amps is set for a

power level of 1 kilowatt. The only difference between this model and those in the preceding episode is that the new one grows from the ground upward. It uses 41 segments to assure that the source is as close as feasible to the actual ground level. In this and subsequent models, I shall use NEC-4, although applying NEC-2 to the models should produce reasonably consistent results.

```
CM resonant monopole, perfect ground
CM NAB substitute single-wire monopole
CE
GW 1 41 0 0 0 0 0 234 0.74
GW 30901 1 9901.0000 9901.0000 9901.0000 9901.0001
9901.0001 9901.0001 .00001
GS 0 0 .3048
GE 1 0 0
GN 1
EX 0 30901 1 0 0.0 7.4515
NT 30901 1 1 1 0 0 0 1 0 0
FR 0 1 0 0 1 1
RP 0 181 1 1000 -90 0 1.00000 1.00000
RP 1 1 1 0000 0 0 1.00000 1.00000 1609.344
EN
```

The following table summarizes the essential information in which we are interested in these notes. F-S indicates the field strength, and I have left the value in the NEC-report form of showing peak milliVolt/meter.

## Resonant Single-Wire Monopole Model Data

Impedance (Ohms)	Current (Apk)	Gain (dBi)	AGT	AGT-dB	F-S @ 1 mile
36.02 + j0.31	7.4515	5.15	1.999	0.00	275.2 mV/m @ -45.9 deg

The source impedance provides a means of correlating our standard model against what we obtain from succeeding models. The required current will reflect the same comparison from a different perspective. The combination of the gain and Average Gain Test (AGT) score, shown in both basic and dB form) will give us a measure of the model's adequacy as a model. (Note that for a monopole over perfect ground, an ideal AGT value is 2.000. Some programs such as EZNEC pre-convert this value to 1.000 so that results coincide with free-space applications of the AGT test.) The field strength reading provides an additional check on how severely a model may deviate from the standard form in terms of data that may be critical for some applications.

My reason for a somewhat elaborate set-up emerges from a collection of models that I have seen over the years. Many NEC modelers wish to model multi-legged towers as multi-legged geometry structures within the model. There are two general questions that such models pose. Are they necessary? Are they adequate? However, perhaps the most fundamental question is how we should source or feed multi-leg models.

### Feeding 3-Legged Towers

We shall begin with the simplest possible multi-leg model: three 2"-diameter legs 2' apart center-to-center. The tower height remains

234' for this and all succeeding models. The model omits all crosspieces. Hence, it requires attention to the feedpoint.

As the model shows, we use 3 separate source segments, one per leg on the lowest segment of that leg. We adjust the current so that the total power fed to the model--summing all three legs--is 1 kW. The source impedance requires a post-run calculation that essentially takes any one of the source impedance values and divides it by 3 to obtain the net source impedance. The technique is equivalent to a centered physical feedpoint with negligible distance between that point and each leg. It also presumes that the legs in operation have equal current levels at any height, a situation relatively assured by the actual cross pieces on a tower.

One significant reason for using the 3-source technique is to avoid a large collection of very short wires in the base region of the model. The shortest length that a NEC segment should be for accuracy in the reported data is 0.001-wavelength. At 1 MHz, that length is 11.803". Even though shorter segments may still meet segment-length-to-diameter ratio guidelines, their presence jeopardizes the trustworthiness of some results. The 3-source method (which would become a 4-source method for a square tower) avoids both the problem of very short segments and a companion problem of adjacent segments in the model having very different lengths.

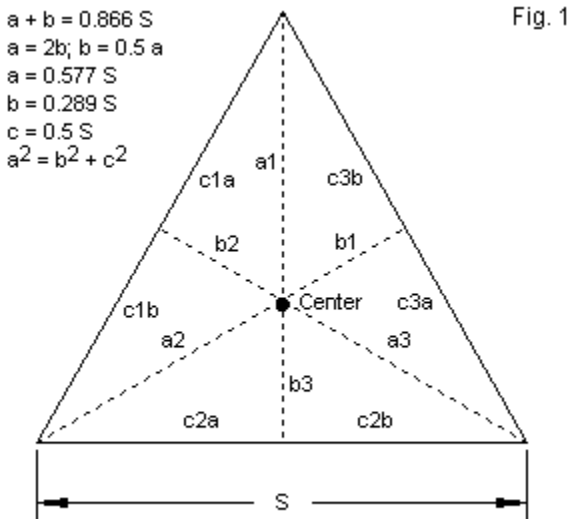
CM resonant 3-leg monopole, perfect ground

CM 3 sources

CE

```
GW 1 41 1.1547 0 0 1.1547 0 234 0.085
GW 2 41 -0.5774 1 0 -0.5774 1 234 0.085
GW 3 41 -0.5774 -1 0 -0.5774 -1 234 0.085
GW 30901 1 9901.0000 9901.0000 9901.0000 9901.0001
9901.0001 9901.0001 .00001
GW 30902 1 9902.0000 9902.0000 9902.0000 9902.0001
9902.0001 9902.0001 .00001
GW 30903 1 9903.0000 9903.0000 9903.0000 9903.0001
9903.0001 9903.0001 .00001
GS 0 0 .3048
GE 1
GN 1
EX 0 30901 1 0 0.0 2.4928
EX 0 30902 1 0 0.0 2.4928
EX 0 30903 1 0 0.0 2.4928
NT 30901 1 1 1 0 0 0 1 0 0
NT 30902 1 2 1 0 0 0 1 0 0
NT 30903 1 3 1 0 0 0 1 0 0
FR 0 1 0 0 1 1
RP 0 181 1 1000 -90 0 1.00000 1.00000
RP 1 1 1 0000 0 0 1.00000 1.00000 1609.344
EN
```

The three tower legs in the model are set in a triangular pattern so that the center of the 3 legs is at  $X=0$  and  $Y=0$  in the coordinate system. **Fig. 1** shows the handy relationships that make such arrangements routine.



Some Handy Equilateral Triangle Relationships

Of course, to feed the 3 legs with separate current sources, we require 3 separate remote wires and networks. The following data provide the results of our modeling exercise. The impedance value shown is the calculated value derived from the 3 reported values.

## Resonant 3-Leg, 3-Source Monopole Model Data

Impedance (Ohms)	Current (Apk)	Gain (dBi)	AGT	AGT-dB	F-S @ 1 mile
35.76 - j0.76	2.4928/leg	5.15	1.999	0.00	275.2 mV/m @ -45.8 deg

The impedance is within a quarter-Ohm of the single-wire standard model, and all other data are virtually identical.

If a modeler wishes to obtain a composite or net source impedance without the need for a post-run calculation, there is a straightforward technique to obtain it. Let's use the very same 3 tower legs. However, instead of placing current sources on the lowest segment of the legs, we shall add a remote wire that is far enough away not to interact with the basic structure. The one-segment wire will be short and thin and will act as the source segment plus a terminal point for transmission lines running to each of the 3 legs, more specifically, to the segments formerly used as the source points. The physically modeled distance between the new wire and the tower legs does not determine the electrical distance between the points. The TL control command allows the user to specify that distance. If we select a very short distance, such a 0.001', the impedance cannot undergo any significant transformation. In effect, we have created a short circuit between each leg and the new wire. Since TL constructs are not part of the model geometry, they do not enter the calculations for the output data except for the source information.

```
CM resonant 3-leg monopole, perfect ground
CM 1 source segment, 3 TLs
CE
GW 1 41 1.1547 0 0 1.1547 0 234 0.085
GW 2 41 -0.5774 1 0 -0.5774 1 234 0.085
GW 3 41 -0.5774 -1 0 -0.5774 -1 234 0.085
GW 4 1 5000 0 0.1 5000 0 1.1 0.005
GW 30901 1 9901.0000 9901.0000 9901.0000 9901.0001
9901.0001 9901.0001 .00001
GS 0 0 .3048
GE 1
GN 1
```

```

EX 0 30901 1 0 0.0 7.4783
NT 30901 1 4 1 0 0 0 1 0 0
TL 1 1 4 1 50 .0001 0 0 0 0 ! User Defined VF = 1
TL 2 1 4 1 50 .0001 0 0 0 0 ! User Defined VF = 1
TL 3 1 4 1 50 .0001 0 0 0 0 ! User Defined VF = 1
FR 0 1 0 0 1 1
RP 0 181 1 1000 -90 0 1 1
RP 1 1 1 0000 0 0 1.00000 1.00000 1609.344
EN

```

One difficulty with using the remote source wire is that visualization becomes difficult. **Fig. 2** shows that we will not be able to visually inspect the tower legs, even at the maximum limits of viewer magnification.

Fig. 2



Nevertheless, as shown in the data table, we are able to draw the desired information from the NEC output report and from program selections from that table. The current value is for the source segment and not for each leg. The current at each former source point on the tower legs is 2.4928 Apk, and the phase shift is only -0.007 degrees due to the use of the transmission-line connections.

## Resonant 3-Leg, 1-Source Monopole Model Data

Impedance (Ohms)	Current (Apk)	Gain (dBi)	AGT	AGT-dB	F-S @ 1 mile
35.76 - j0.76	7.4780	5.15	1.999	0.00	275.1 mV/m @ -45.8 deg

Since the legs are identical except for their position, we need not model all three. Instead, we may simplify the modeling by replicating 1 leg. Since we took the initial trouble to place the legs so that the coordinate center falls at the center of the triangle formed by the legs, we may simply replicate and rotate the first leg by 120 degrees. In the model, I have returned to the 3-source system to allow a visualization of the result.

CM resonant 3-leg monopole, perfect ground

CM 3 sources

CM GM for legs 2 and 3

CE

GW 1 41 1.1547 0 0 1.1547 0 234 0.085

GM 1 2 0 0 120 0 0 0

GW 30901 1 9901.0000 9901.0000 9901.0000 9901.0001  
9901.0001 9901.0001 .00001

GW 30902 1 9902.0000 9902.0000 9902.0000 9902.0001  
9902.0001 9902.0001 .00001

GW 30903 1 9903.0000 9903.0000 9903.0000 9903.0001  
9903.0001 9903.0001 .00001

GS 0 0 .3048

GE 1

GN 1

EX 0 30901 1 0 0.0 2.4928

EX 0 30902 1 0 0.0 2.4928

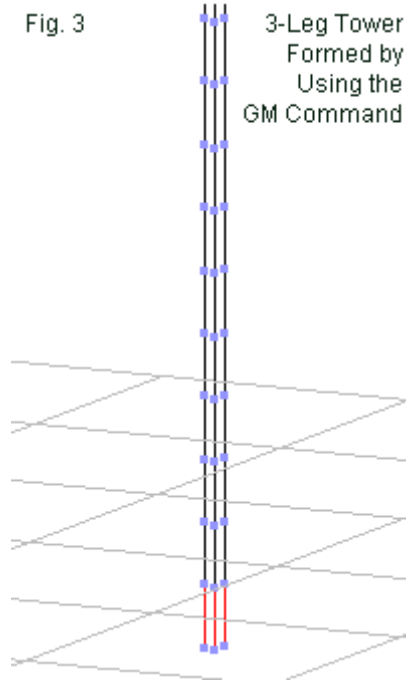
EX 0 30903 1 0 0.0 2.4928

NT 30901 1 1 1 0 0 0 1 0 0

NT 30902 1 2 1 0 0 0 1 0 0

NT 30903 1 3 1 0 0 0 1 0 0

```
FR 0 1 0 0 1 1
RP 0 181 1 1000 -90 0 1.00000 1.00000
RP 1 1 1 0000 0 0 1.00000 1.00000 1609.344
EN
```



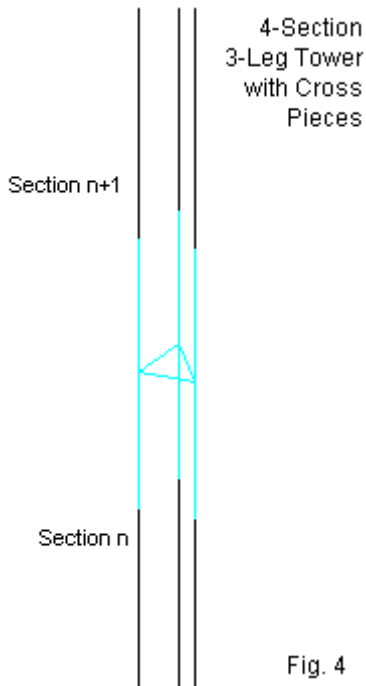
Since the GM command also increments the tag number by 1 for each added replication of the original wire, nothing else in the model requires change. In fact, the data for the model is identical to the data for the original 3-leg, 3-source model. Although the application of the GM command is fairly trivial in this application, it will play a more significant role in subsequent models. Our models,

whose primary use has been to illustrate methods of feeding multi-leg towers, have used a highly simplified structure. Many modelers wish to show all of the towers pieces. Even when we keep the segment length above the NEC minimum, we may easily have 2000 or more segments. Modeling those segments as individual GW entries can result in some very large model files.

## Modeling Tower Bits and Pieces

So far, we have looked at towers composed only of 3 legs and found them to yield results that are consistent with those produced by the NAB-recommended substitute single-wire tower model. However, many modelers wish to include all or some of the typical horizontal and sloping members that compose actual towers. Therefore, we should look in a progressive succession at constructing such models--and see what consequences emerge.

The first example is simple. We shall subdivide the 234' tower into 3 equal 58.5' sections. In addition to the vertical legs, we shall add a horizontal cross element at the top of each section, as shown in the partial model view in **Fig. 4**. For ease of viewing, we shall retain the 3-source method of feeding the tower, although the TL method of combining the sources into a single source always remains available.



Our first version of the model uses only wires (GW commands) to construct the tower.

```

CM resonant 3-leg monopole perfect ground
CM 3 sources
CM 4 sections with cross braces
CE
GW 1 10 1.1547 0 0 1.1547 0 58.5 0.085
GW 2 10 -0.5774 1 0 -0.5774 1 58.5 0.085
GW 3 10 -0.5774 -1 0 -0.5774 -1 58.5 0.085
GW 4 1 1.1547 0 58.5 -0.5774 1 58.5 0.085

```

```
GW 5 1 -0.5774 1 58.5 -0.5774 -1 58.5 0.085
GW 6 1 -0.5774 -1 58.5 1.1547 0 58.5 0.085
GW 7 10 1.1547 0 58.5 1.1547 0 117 0.085
GW 8 10 -0.5774 1 58.5 -0.5774 1 117 0.085
GW 9 10 -0.5774 -1 58.5 -0.5774 -1 117 0.085
GW 10 1 1.1547 0 117 -0.5774 1 117 0.085
GW 11 1 -0.5774 1 117 -0.5774 -1 117 0.085
GW 12 1 -0.5774 -1 117 1.1547 0 117 0.085
GW 13 10 1.1547 0 117 1.1547 0 175.5 0.085
GW 14 10 -0.5774 1 117 -0.5774 1 175.5 0.085
GW 15 10 -0.5774 -1 117 -0.5774 -1 175.5 0.085
GW 16 1 1.1547 0 175.5 -0.5774 1 175.5 0.085
GW 17 1 -0.5774 1 175.5 -0.5774 -1 175.5 0.085
GW 18 1 -0.5774 -1 175.5 1.1547 0 175.5 0.085
GW 19 10 1.1547 0 175.5 1.1547 0 234 0.085
GW 20 10 -0.5774 1 175.5 -0.5774 1 234 0.085
GW 21 10 -0.5774 -1 175.5 -0.5774 -1 234 0.085
GW 22 1 1.1547 0 234 -0.5774 1 234 0.085
GW 23 1 -0.5774 1 234 -0.5774 -1 234 0.085
GW 24 1 -0.5774 -1 234 1.1547 0 234 0.085
GW 30901 1 9901.0000 9901.0000 9901.0000 9901.0001
9901.0001 9901.0001 .00001
GW 30902 1 9902.0000 9902.0000 9902.0000 9902.0001
9902.0001 9902.0001 .00001
GW 30903 1 9903.0000 9903.0000 9903.0000 9903.0001
9903.0001 9903.0001 .00001
GS 0 0 .3048
GE 1
GN 1
EX 0 30901 1 0 0.0 2.479
EX 0 30902 1 0 0.0 2.479
EX 0 30903 1 0 0.0 2.479
NT 30901 1 1 1 0 0 0 1 0 0
NT 30902 1 2 1 0 0 0 1 0 0
NT 30903 1 3 1 0 0 0 1 0 0
```

```
FR 0 1 0 0 1 1
RP 0 181 1 1000 -90 0 1.00000 1.00000
RP 1 1 1 0000 0 0 1.00000 1.00000 1609.344
EN
```

Even with only 4 sections, the model file size has grown considerably. Since each of the 4 sections is identical, we can shorten the file by using the GM command after completing the lowest section with GW commands. We simply replicate the section three more times, translating each new section 58.5' higher (+Z) than the preceding one.

```
CM resonant 3-leg monopole perfect ground
CM 3 sources
CM 4 sections with cross braces
CE Section 1 = GW, Sections 2-4 = GM
CE
GW 1 10 1.1547 0 0 1.1547 0 58.5 0.085
GW 2 10 -0.5774 1 0 -0.5774 1 58.5 0.085
GW 3 10 -0.5774 -1 0 -0.5774 -1 58.5 0.085
GW 4 1 1.1547 0 58.5 -0.5774 1 58.5 0.085
GW 5 1 -0.5774 1 58.5 -0.5774 -1 58.5 0.085
GW 6 1 -0.5774 -1 58.5 1.1547 0 58.5 0.085
GM 6 3 0 0 0 0 0 58.5
GW 30901 1 9901.0000 9901.0000 9901.0000 9901.0001
9901.0001 9901.0001 .00001
GW 30902 1 9902.0000 9902.0000 9902.0000 9902.0001
9902.0001 9902.0001 .00001
GW 30903 1 9903.0000 9903.0000 9903.0000 9903.0001
9903.0001 9903.0001 .00001
GS 0 0 .3048
GE 1
GN 1
```

```

EX 0 30901 1 0 0.0 2.479
EX 0 30902 1 0 0.0 2.479
EX 0 30903 1 0 0.0 2.479
NT 30901 1 1 1 0 0 0 1 0 0
NT 30902 1 2 1 0 0 0 1 0 0
NT 30903 1 3 1 0 0 0 1 0 0
FR 0 1 0 0 1 1
RP 0 181 1 1000 -90 0 1.00000 1.00000
RP 1 1 1 0000 0 0 1.00000 1.00000 1609.344
EN

```

Both model files yield identical data output reports, summarized in the following table.

Resonant 3-Leg, 3-Source 4-Section (with Simple Cross Pieces) Monopole Model Data

Impedance (Ohms)	Current (Apk)	Gain (dBi)	AGT	AGT-dB	F-S @ 1 mile
36.16 + j1.09	2.479/leg	5.15	1.999	0.00	275.2 mV/m @ -45.8 deg

The impedance of the 4-section model is about as much higher than the single-wire version as the 3-leg versions without cross pieces were lower. Resistive values all fall within a 1-Ohm range, while reactive values have a 2-Ohm range. Otherwise, the data are identical. The reason for the lack of difference is the exceptionally low current carried by the cross members. The current magnitude is at least 6 orders of magnitude lower than the current in the vertical legs, making the cross members superfluous in this arrangement.

Towers usually also contain sloping elements. When modeling such arrangements, the lowest section should omit the sloping wires. The current division below the source at  $Z=0$  will lead to unusable values of impedance and other calculation inaccuracies.

As a first trial of adding sloping tower pieces, we shall retain the simple 4-section structure, with only horizontal cross pieces in the lowest section. Then we shall add sloping wires to the second section and replicate it twice more to reach the 234' top height. The model will prove instructive in several ways.

```

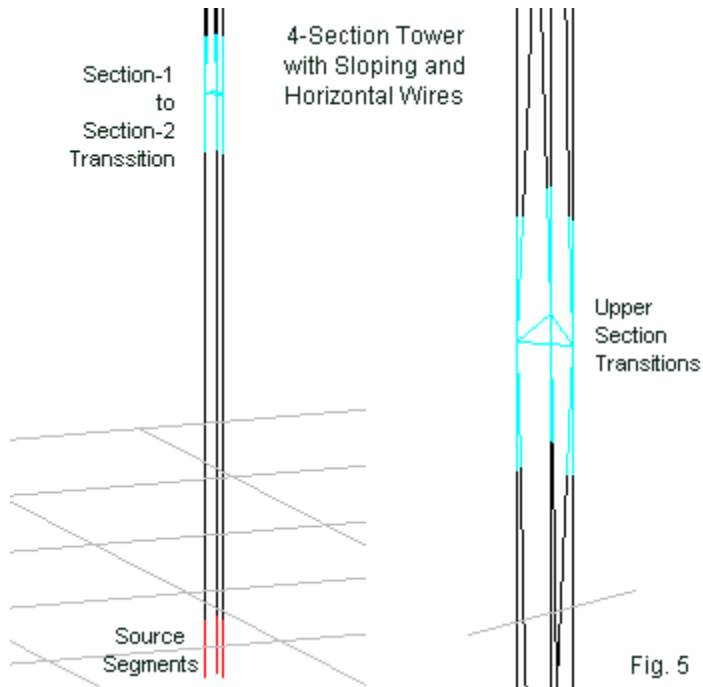
CM resonant 3-leg monopole perfect ground
CM 3 sources
CM 4 sections with cross braces
CE
GW 1 10 1.1547 0 0 1.1547 0 58.5 0.085
GW 2 10 -0.5774 1 0 -0.5774 1 58.5 0.085
GW 3 10 -0.5774 -1 0 -0.5774 -1 58.5 0.085
GW 4 1 1.1547 0 58.5 -0.5774 1 58.5 0.085
GW 5 1 -0.5774 1 58.5 -0.5774 -1 58.5 0.085
GW 6 1 -0.5774 -1 58.5 1.1547 0 58.5 0.085
GW 7 10 1.1547 0 58.5 1.1547 0 117 0.085
GW 8 10 -0.5774 1 58.5 -0.5774 1 117 0.085
GW 9 10 -0.5774 -1 58.5 -0.5774 -1 117 0.085
GW 10 1 1.1547 0 117 -0.5774 1 117 0.085
GW 11 1 -0.5774 1 117 -0.5774 -1 117 0.085
GW 12 1 -0.5774 -1 117 1.1547 0 117 0.085
GW 13 10 1.1547 0 58.5 -0.5774 1 117 0.085
GW 14 10 -0.5774 1 58.5 -0.5774 -1 117 0.085
GW 15 10 -0.5774 -1 58.5 1.1547 0 117 0.085
GM 1 2 0 0 0 0 0 58.5 71 15 10
GW 30901 1 9901.0000 9901.0000 9901.0000 9901.0001
9901.0001 9901.0001 .00001
GW 30902 1 9902.0000 9902.0000 9902.0000 9902.0001
9902.0001 9902.0001 .00001
GW 30903 1 9903.0000 9903.0000 9903.0000 9903.0001
9903.0001 9903.0001 .00001
GS 0 0 .3048
GE 1

```

```

GN 1
EX 0 30901 1 0 0.0 2.488
EX 0 30902 1 0 0.0 2.488
EX 0 30903 1 0 0.0 2.488
NT 30901 1 1 1 0 0 0 1 0 0
NT 30902 1 2 1 0 0 0 1 0 0
NT 30903 1 3 1 0 0 0 1 0 0
FR 0 1 0 0 1 1
RP 0 181 1 1000 -90 0 1.00000 1.00000
RP 1 1 1 0000 0 0 1.00000 1.00000 1609.344
EN

```



The ease of replicating upper sections that are identical to lower sections is clear from the GM command line entry. **Fig. 5** shows the lowest section and the beginning of the second section, with its added sloping wires. The right side of the figure shows a transition between upper sections in more detail. Initially, to avoid NEC's well-known accuracy slippage when we have angular junctions of wires with different diameters, I have modeled everything with 2" diameter (0.085' radius) wires.

Resonant 3-Leg, 3-Source 4-Section (with Sloping and Horizontal Cross Pieces) Monopole Model Data

Impedance (Ohms)	Current (Apk)	Gain (dBi)	AGT	AGT-dB	F-S @ 1 mile
35.90 + j7.77	2.047/leg	5.25	2.047	+0.10	278.5 mV/m @ -45.8 deg

The data departs noticeably from the data from preceding models. The reactive component of the source impedance has increased, as has the gain value and the field-strength report (still in peak mV/m for easy comparison with other data tables). The key variance in the data is the AGT score. Although a value of 2.047 seems only a small deviation from the ideal value of 2.000, it results in a 0.1-dB error in the gain report. It is not possible from the data stream to know whether the impedance report is reliable in comparison to the reports for the other models. The last statement, of course, rests on a presumption that the difference is sufficient to make a difference to a modeling task. For tasks in which the difference makes no differences, there would be no reason to resort to the more complex model.

One key reason for the variance in AGT scores is the very shallow angle of the sloping wires at the intersection with the vertical model wires. The two wires inter-penetrate in the region of current

sensitivity in the joining segments, although not enough to trigger NEC-4 warnings. To counter this problem, we need to better reflect reality and to use smaller tower sections.

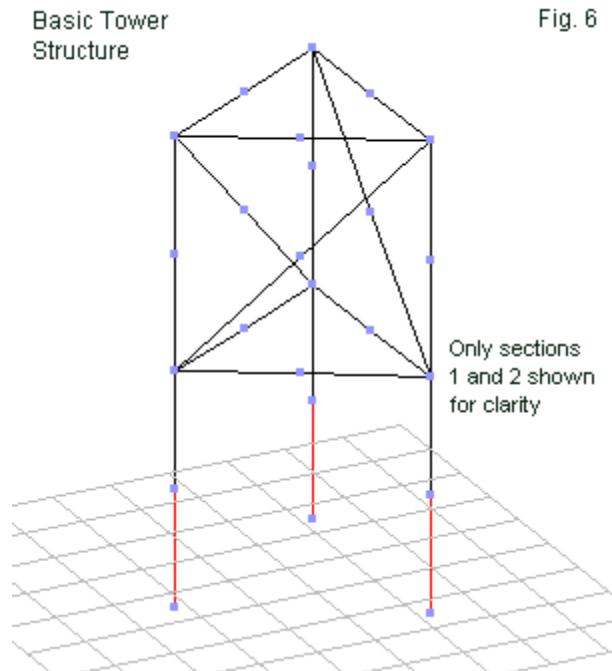


**Fig. 6** shows the outline of the lowest section without any sloping wires, along with the next section--prior to the use of the GM command to add 115 more 2' section to arrive at the 234' total tower height. Each 2' section, also 2' wide, uses 2 segments per wires to remain within the NEC minimum segment length. As well,

all wires are 0.17' in diameter, consistent with preceding models of multi-leg towers in this exercise set. The total model has the following lines.

```
CM resonant 3-leg monopole perfect ground
CM 3 sources
CM 117 sections with cross braces (diameter = to legs)
CE
GW 1 2 1.1547 0 0 1.1547 0 2 0.085
GW 2 2 -0.5774 1 0 -0.5774 1 2 0.085
GW 3 2 -0.5774 -1 0 -0.5774 -1 2 0.085
GW 4 2 1.1547 0 2 -0.5774 1 2 0.085
GW 5 2 -0.5774 1 2 -0.5774 -1 2 0.085
GW 6 2 -0.5774 -1 2 1.1547 0 2 0.085
GW 7 2 1.1547 0 2 1.1547 0 4 0.085
GW 8 2 -0.5774 1 2 -0.5774 1 4 0.085
GW 9 2 -0.5774 -1 2 -0.5774 -1 4 0.085
GW 10 2 1.1547 0 4 -0.5774 1 4 0.085
GW 11 2 -0.5774 1 4 -0.5774 -1 4 0.085
GW 12 2 -0.5774 -1 4 1.1547 0 4 0.085
GW 13 2 1.1547 0 2 -0.5774 1 4 0.085
GW 14 2 -0.5774 1 2 -0.5774 -1 4 0.085
GW 15 2 -0.5774 -1 2 1.1547 0 4 0.085
GM 9 115 0 0 0 0 2 7 1 15 2
GW 30901 1 9901.0000 9901.0000 9901.0000 9901.0001
9901.0001 9901.0001 .00001
GW 30902 1 9902.0000 9902.0000 9902.0000 9902.0001
9902.0001 9902.0001 .00001
GW 30903 1 9903.0000 9903.0000 9903.0000 9903.0001
9903.0001 9903.0001 .00001
GS 0 0 .3048
GE 1
GN 1
EX 0 30901 1 0 0.0 2.472
```

```

EX 0 30902 1 0 0.0 2.472
EX 0 30903 1 0 0.0 2.472
NT 30901 1 1 1 0 0 0 1 0 0
NT 30902 1 2 1 0 0 0 1 0 0
NT 30903 1 3 1 0 0 0 1 0 0
FR 0 1 0 0 1 1
RP 0 181 1 1000 -90 0 1.00000 1.00000
RP 1 1 1 0000 0 0 1.00000 1.00000 1609.344
EN

```

The model takes all reasonable precautions to arrive at a balance between reflecting a realistic physical structure and meeting modeling guidelines. The following table shows the data that emerges from the 1053-wire, 2103-segment model.

Resonant 3-Leg, 3-Source 117-Section (with Sloping and Horizontal Cross Pieces) Monopole Model Data

Impedance (Ohms)	Current (Apk)	Gain (dBi)	AGT	AGT-dB	F-S @ 1 mile
36.36 + j5.94	2.472/leg	5.21	2.028	+0.06	277.2 mV/m @ -46.5 deg

The AGT score, while more ideal than the preceding model, still departs from a perfect 2.000 value. The result is a gain value that is too high, and a corresponding field-strength value. The degree by which the model departs from the ideal is noticeable. Whether it is significant to a modeling task is a user-decision, largely created by the standards brought to the exercise. Again, if the differences are too small to make a difference to the enterprise, using the complex model loses its rationale.

To complete our sequence of hypothetical models, let's revise the complex model by showing one further modeler urge. The sloping and horizontal members of a tower generally are smaller in

diameter than the legs. Although it is a technical violation of recommended NEC practice to have angular junctions of wires with dissimilar diameters, we shall reduce the diameter values of these linking pieces to 1" (0.0425' radius). The visual appearance of the model does not change, but the changes are noticeable in the model file.

```
CM resonant 3-leg monopole perfect ground
CM 3 sources
CM 117 sections with cross braces (1/2-diameter of legs)
CE
GW 1 2 1.1547 0 0 1.1547 0 2 0.085
GW 2 2 -0.5774 1 0 -0.5774 1 2 0.085
GW 3 2 -0.5774 -1 0 -0.5774 -1 2 0.085
GW 4 2 1.1547 0 2 -0.5774 1 2 0.0425
GW 5 2 -0.5774 1 2 -0.5774 -1 2 0.0425
GW 6 2 -0.5774 -1 2 1.1547 0 2 0.0425
GW 7 2 1.1547 0 2 1.1547 0 4 0.085
GW 8 2 -0.5774 1 2 -0.5774 1 4 0.085
GW 9 2 -0.5774 -1 2 -0.5774 -1 4 0.085
GW 10 2 1.1547 0 4 -0.5774 1 4 0.0425
GW 11 2 -0.5774 1 4 -0.5774 -1 4 0.0425
GW 12 2 -0.5774 -1 4 1.1547 0 4 0.0425
GW 13 2 1.1547 0 2 -0.5774 1 4 0.0425
GW 14 2 -0.5774 1 2 -0.5774 -1 4 0.0425
GW 15 2 -0.5774 -1 2 1.1547 0 4 0.0425
GM 9 115 0 0 0 0 2 7 1 15 2
GW 30901 1 9901.0000 9901.0000 9901.0000 9901.0001
9901.0001 9901.0001 .00001
GW 30902 1 9902.0000 9902.0000 9902.0000 9902.0001
9902.0001 9902.0001 .00001
GW 30903 1 9903.0000 9903.0000 9903.0000 9903.0001
9903.0001 9903.0001 .00001
GS 0 0 .3048
```

```

GE 1
GN 1
EX 0 30901 1 0 0.0 2.4733
EX 0 30902 1 0 0.0 2.4733
EX 0 30903 1 0 0.0 2.4733
NT 30901 1 1 1 0 0 0 1 0 0
NT 30902 1 2 1 0 0 0 1 0 0
NT 30903 1 3 1 0 0 0 1 0 0
FR 0 1 0 0 1 1
RP 0 181 1 1000 -90 0 1.00000 1.00000
RP 1 1 1 0000 0 0 1.00000 1.00000 1609.344
EN

```

Resonant 3-Leg, 3-Source 117-Section (with Sloping and Horizontal Cross Pieces) Monopole Model Data

Impedance (Ohms)	Current (Apk)	Gain (dBi)	AGT	AGT-
dB F-S @ 1 mile				
36.33 + j6.02	2.4733/leg	5.21	2.029	
+0.06	277.3 mV/m @ -46.5 deg			

As the table shows, the numerical degradation of the model due to the changes is minuscule. In large measure, this small change is a function of the fact that vertical legs carry about 3 times the current of the sloping sections. Hence, they remain the dominant factors within the model, with the cross members having only a relatively small supporting role. Once more, if the numerical differences between the models are not significant to a modeling task, we lose any reason for constructing excessively complex tower models.

## Conclusion

Our set of exercise models has shown that we may construct straightforward multi-leg tower models in lieu of using the NAB-recommended substitute single-wire tower model. For models using a uniform diameter or face-width for the total height, the simple 3-leg models, even with periodic horizontal crosspieces, show a very good correlation to the single-wire model. The feeding or sourcing method is easy to implement, whether we employ separate sources for each tower leg or develop a composite source using near-zero-length transmission lines.

When we increased the complexity of the tower models to include both horizontal and sloping cross members, we encountered some interesting results that raise questions that one cannot answer from a perspective wholly within modeling. The complex models depart somewhat from ideal AGT scores. Although the scores are in many contexts perfectly acceptable, in the present comparative context, they show variations in the data reports. The AGT value allows only a correction of the raw gain report. However, variations in the impedance value, especially relative to the reactive component, are not directly correctable.

The quandary left behind by these results is whether to use the data from the complex model or to use the data from one of the simpler models with a virtually ideal AGT score. (The AGT scores may or may not be as good when using NEC-2.) The quandary only becomes one if the report differences are sufficiently large to make a difference to the larger task within which the model plays a role. If

the differences are not significant, then we have no reason to resort to excessively complex models of towers.

The correlations among impedance and other data values among the models are overall very tight. One may legitimately raise the question of whether the tight grouping of values is at least a partial function of the use of resonant tower sizes--234' at 1 MHz. A 90-degree tower for FCC is taller--about 273'. Many towers used in the AM BC service are considerable shorter. Before closing the book on tower modeling in NEC (with special reference to NEC-4), we should do a small survey of what happens when we have tower lengths with a considerable reactive component in their source impedance.

## Other Publications

We hope you've enjoyed this 6th in a series of volumes of the **Antenna Modeling Notes**. Volume 7 of this series is soon to follow. Together with existing volumes 1 through 6 of this series, you'll find many other very fine books and publications by the author L.B. Cebik, W4RNL and other fine authors in the **antenneX Online Magazine BookShelf** at the web site shown below.

---

**A Publication by  
antenneX Online Magazine  
<http://www.antennex.com/>  
POB 271229  
Corpus Christi, Texas 78427-1229  
USA**

**March 2010**

---

Copyright © 2010 by **antenneX Online Magazine**. All rights reserved. No part of this book may be reproduced or transmitted in any form, by any means (electronic, photocopying, recording, or otherwise) without the prior written permission of the publisher.

ISBN: 1-877992-57-7

---